THE UNIVERSITY OF QUEENSLAND

AUSTRALIA

New Insights into Copper-Mediated Polymerization and Polymer Topologies

Mikhail Gavrilov

Diploma in Chemistry

A thesis submitted for the degree of Doctor of Philosophy at

The University of Queensland in 2017

Australian Institute for Bioengineering and Nanotechnology

Abstract

Polymer science has developed new synthetic methods to create complex polymer architectures. The solution and bulk properties of these architectures are influenced by the structure and chemical composition of the original building blocks (e.g. monomers or reactive polymeric blocks). One of the greatest challenges to the field is characterization of these polymers with diverse structures and chemical compositions. Size exclusion chromatography (SEC) has been one of the most used characterization techniques to determine the molecular weight distribution (MWD) of polymers. The information obtained about the polymer from SEC is generally restricted to molecular weight averages and dispersity indexes. However, there is a wealth of valuable information that can be obtained from a deeper analysis of the SEC chromatograms. This information can provide insights into polymerization mechanisms, the amount of unreacted polymer in a coupling reaction, or even the amount of cyclic polymer formed during a ring-closure reaction.

The thesis first develops the theory to analyse the SEC chromatograms and provides a methodology to fit the MWDs with a log-normal distribution (LND) model based on a Gaussian function. The LND model was then used to analyse polymers made by a variant of copper-mediated 'living' radical polymerization (LRP) in water. This LRP technique is capable of producing hydrophilic polymers with both narrow MWDs and high chain-end functionality, but the chain-end halide groups were susceptible to hydrolysis upon purification attempts and, therefore, the polymers cannot be further used to create complex polymer architectures. To preserve high chain-end functionality, the terminal halide of the polymers was capped using in situ azidation at the end of aqueous copper-mediated LRP. The azide chain-end fidelity of the purified polymer was tested in a copper-catalyzed azide-alkyne cycloaddition (CuAAC) 'click' reaction. The LND model of MWDs of the resulting products gave an accurate determination of the end-group functionality and insight into the effectiveness of our new polymerization variant.

In the final stage of this thesis, the LND model was used to quantify the sequential polymerization of cyclic macromers through successive CuAAC 'click' reactions. The versatility of the LND model was further demonstrated by determining the multicyclic coil conformation as a function of the number of cyclic macromers in the polymer chain.

Declaration by author

This thesis is composed of my original work, and contains no material previously published or written by another person except where due reference has been made in the text. I have clearly stated the contribution by others to jointly-authored works that I have included in my thesis.

I have clearly stated the contribution of others to my thesis as a whole, including statistical assistance, survey design, data analysis, significant technical procedures, professional editorial advice, and any other original research work used or reported in my thesis. The content of my thesis is the result of work I have carried out since the commencement of my research higher degree candidature and does not include a substantial part of work that has been submitted to qualify for the award of any other degree or diploma in any university or other tertiary institution. I have clearly stated which parts of my thesis, if any, have been submitted to qualify for another award.

I acknowledge that an electronic copy of my thesis must be lodged with the University Library and, subject to the policy and procedures of The University of Queensland, the thesis be made available for research and study in accordance with the Copyright Act 1968 unless a period of embargo has been approved by the Dean of the Graduate School.

I acknowledge that copyright of all material contained in my thesis resides with the copyright holder(s) of that material. Where appropriate I have obtained copyright permission from the copyright holder to reproduce material in this thesis.

Publications during candidature

- Peer-reviewed papers

1. Monteiro, M. J.; Gavrilov, M., Characterization of hetero-block copolymers by the log-normal distribution model. *Polymer Chemistry* **2016,** *7* (17), 2992-3002.
2. Gavrilov, M.; Jia, Z.; Percec, V.; Monteiro, M. J., Quantitative end-group functionalization of PNIPAM from aqueous SET-LRP via in situ reduction of Cu(ii) with $NaBH_4$. *Polymer Chemistry* **2016,** *7* (29), 4802-4809.
3. Gavrilov, M.; Zerk, T. J.; Bernhardt, P. V.; Percec, V.; Monteiro, M. J., SET-LRP of NIPAM in water via in situ reduction of Cu(ii) to Cu(0) with $NaBH_4$. *Polymer Chemistry* **2016,** *7* (4), 933-939.
4. Gavrilov, M.; Monteiro, M. J., Derivation of the molecular weight distributions from size exclusion chromatography. *European Polymer Journal* **2015,** *65*, 191-196.
5. Sebakhy, K. O.; Gavrilov, M.; Valade, D.; Jia, Z.; Monteiro, M. J., Nanoparticles of Well-Defined 4-Arm Stars made using Nanoreactors in Water. *Macromolecular Rapid Communications* **2014,** *35* (2), 193-197.

Publications included in this thesis

Gavrilov, M.; Monteiro, M. J., Derivation of the molecular weight distributions from size exclusion chromatography. *European Polymer Journal* **2015,** *65*, 191-196. – Incorporated as Chapter 2.

Contributor	Statement of contribution
Mikhail Gavrilov (Candidate)	Analysis and data interpretation (40%) Designed experiments (40%) Drafting and writing (40%) Experiments (100%)
Michael Monteiro	Analysis and data interpretation (60%) Designed experiments (60%) Drafting and writing (60%)

Monteiro, M. J.; **Gavrilov, M.**, Characterization of hetero-block copolymers by the log-normal distribution model. *Polymer Chemistry* **2016,** *7* (17), 2992-3002. - Incorporated as Chapter 3.

Contributor	Statement of contribution
Mikhail Gavrilov (Candidate)	Analysis and data interpretation (40%) Designed experiments (40%) Drafting and writing (40%) Experiments (100%)
Michael Monteiro	Analysis and data interpretation (60%) Designed experiments (60%) Drafting and writing (60%)

Gavrilov, M.; Zerk, T. J.; Bernhardt, P. V.; Percec, V.; Monteiro, M. J., SET-LRP of NIPAM in water via in situ reduction of Cu(ii) to Cu(0) with $NaBH_4$. *Polymer Chemistry* **2016,** *7* (4), 933-939. - Incorporated as Chapter 4.

Contributor	Statement of contribution
Mikhail Gavrilov (Candidate)	Analysis and data interpretation (40%) Designed experiments (40%) Drafting and writing (40%) Experiments (90%)
Timothy Zerk	Analysis and data interpretation (5%) Experiments (10%)
Paul Bernhardt	Analysis and data interpretation (5%) Designed experiments (10%)
Virgil Percec	Analysis and data interpretation (10%) Designed experiments (10%)
Michael Monteiro	Analysis and data interpretation (40%) Designed experiments (40%) Drafting and writing (60%)

Gavrilov, M.; Jia, Z.; Percec, V.; Monteiro, M. J., Quantitative end-group functionalization of PNIPAM from aqueous SET-LRP via in situ reduction of Cu(ii) with $NaBH_4$. *Polymer Chemistry* **2016,** *7* (29), 4802-4809. - Incorporated as Chapter 5.

Contributor	Statement of contribution
Mikhail Gavrilov (Candidate)	Analysis and data interpretation (40%) Designed experiments (30%) Drafting and writing (45%) Experiments (100%)
Zhongfan Jia	Analysis and data interpretation (15%)

	Designed experiments (35%) Drafting and writing (10%)
Virgil Percec	Analysis and data interpretation (5%) Designed experiments (5%)
Michael Monteiro	Analysis and data interpretation (40%) Designed experiments (30%) Drafting and writing (45%)

Contributions by others to the thesis

The author acknowledges the following individuals who have contributed to this thesis:

Prof. Michael J. Monteiro for contributing to drafting and writing, data analysis and interpretation, design and conception of experiments.

Dr. Zhongfan Jia for contributing to data analysis and interpretation, design and conception of experiments.

Prof. Virgil Percec for contributing to data analysis and interpretation and design and conception of experiments.

Prof. Paul Bernhardt for contributing to data analysis and interpretation and design and conception of experiments.

Timothy Zerk for UV-vis experiments and data analysis and interpretation.

Statement of parts of the thesis submitted to qualify for the award of another degree

"None".

Acknowledgements

I primary want to acknowledge my supervisor Prof. Michael J. Monteiro, for his enormous support throughout my PhD candidature. Apart from his strong guidance of my research and funding of the first year of my PhD, he also helped me to develop personally by teaching me to communicate my data properly during both vis-à-vis and weekly group meetings, time management, to pay thorough attention to details and gently support people around me. I will do my best to make his time and effort investments worthy. If we imagine science as a coin with one of its side being theory, models and equations describing laws of nature then another side of the coin must be assigned to experiments, and their reflection of how precisely these models and equations embrace natural phenomena. Michael mostly helped me with first side of the coin — theory, and Dr. Zhongfan Jia was my guide on the other side. He navigated me through the experiment ”jungles” with his colossal “machete” of experience. You would not be reading this thesis without Zhongfan’s support because no matter how precise the models are, they cannot take into account every component of a natural phenomenon; there will always be some sort of simplification due to the limits of human knowledge, computational limits, etc. When theory and lab work meet sometimes they can contradict, and if you cannot resolve the problem, a PhD can get pretty stressful and it becomes crucial to keep a healthy working atmosphere in a group. All our group members were there for me, they managed to convert my PhD downs into ups. I would like to appreciate among them Valentin Bobrin, Faheem Solangi, Dr. Derong Lu, Dr. Pieter Derboven and Timothy Zerk for their friendship and help in the lab and Jennifer Schöning for her patient proofreading of my scribbles. I also thank my UQ colleagues for broadening the scope of my knowledge beyond chemistry.

As theory cannot be imagined without experiments, work should be alternated with rest. All my family, ASA social activities and multiple housemates kept me recharged, turned the PhD program into an enjoyable journey and helped balance my serotonin levels.

Finally I thank the University of Queensland for a UQI scholarship and access to state-of-the-art instruments.

Keywords

‘Living’ radical polymerization, LND simulation, ‘click’ chemistry, polymer end-group functionality, polymer synthesis, cyclic polymers

Australian and New Zealand Standard Research Classifications (ANZSRC)

ANZSRC code: 030301, Chemical Characterisation of Materials, 30 %
ANZSRC code: 030305, Polymerization Mechanisms, 20 %
ANZSRC code: 030306, Synthesis of Materials, 50 %

Fields of Research (FoR) Classification

FoR code: 0303, Macromolecular and Materials Chemistry, 80%
FoR code: 0305, Organic Chemistry, 20 %

Table of contents

Chapter 6

Synthesis of Densely Packed Multicyclic Polystyrene

List of Figures

List of Schemes

List of Tables

List of Abbreviations

AIBN – 2,2-Azobis(2-methylpropionitrile)

ATR-FTIR – Attenuated Total Reflectance – Fourier Transform Infra-Red

ATRP – Atom Transfer Radical Polymerization

BIB – 2-Bromoisobutyryl bromide

BPB – 2-Bromopropionyl bromide

Bpy – 2,2'-Bipyridine

$CHCl_3$ – Chloroform

CuAAC – Copper-Catalyzed Azide-Alkyne Cycloaddition

CuBr – Copper(I) bromide

$CuBr_2$ – Copper(II) bromide

Đ – Dispersity

DBU – 1,8-Diazabicycloundec-7-ene

DCM – Dichloromethane

DFT – Density Functional Theory

DMAc – *N,N*-Dimethylacrylamide

DMF – *N,N*-Dimethylformamide

DMSO – Dimethylsulfoxide

DPPA – Diphenylphosphoryl azide

DSC – Differential Scanning Calorimetry

EBiB – Ethyl α-bromoisobutyrate

EGF – End-Group Functionality

ESA-CF – Electrostatic Self-Assembly and Covalent Fixation

EtOAc – Ethyl Acetate

FRP – Free Radical Polymerization

GPC – Gel Permeation Chromatography

HF/DFT – Hartree-Fock Density Functional Theory

HPLC – High Performance Liquid Chromatography

ISET – Inner Sphere Electron Transfer

LCST – Lower Critical Solution Temperature

LND – Log-Normal Distribution

LRP – 'Living' Radical Polymerization

MA – Methyl acrylate

MALDI-ToF – Matrix-Assisted Laser Desorption Ionization – Time-of-Flight

MBP – Methyl-2-bromopropionate

Me_6TREN – Tris[2-(dimethylamino)ethyl]amine

MeOH – Methanol

$MgSO_4$ – Magnesium sulfate anhydrous

MMA – Methyl methacrylate

M_n – Number-average molecular weight

MRI – Magnetic Resonance Imaging

M_w – Weight-average molecular weight

MWCO – Molecular Weight Cut-Off

MWD – Molecular Weight Distribution

NaN_3 – Sodium azide

NIPAM – *N*-Isopropylacrylamide

NMP – Nitroxide-Mediated Radical Polymerization

NMR – Nuclear Magnetic Resonance

NPs – Nanoparticles

NRC – Nitroxide Radical Coupling

OSET – Outer Sphere Electron Transfer

PEG – Poly(ethylene glycol)

PMDETA – *N,N,N',N'',N''*-Pentamethyldiethylenetriamine

PNIPAm – Poly(N-isopropylacrylamide)

PREP-SEC – Preparative Size Exclusion Chromatography

PSTY – Polystyrene

P*t*-BA – Poly(*tert*-butyl acrylate)

RAFT – Reversible Addition-Fragmentation Chain Transfer

REMP – Ring Expansion Metathesis Polymerization

R_h – Hydrodynamic Radius

RI – Refractive Index

RT – Room Temperature

SEC – Size Exclusion Chromatography

SET – Single-Electron Transfer

SET-LRP – Single-Electron Transfer Living Radical Polymerization

STY – Styrene

^{t}BA – *tert*-Butyl acrylate

TEA – Triethylamine

T_g – Glass Transition Temperature

THF – Tetrahydrofuran

UV-Vis – Ultraviolet-Visible

Chapter 1

Introduction

1.1. 'Living' Radical Polymerization (LRP)

'Living' polymerization was first introduced by Szwarc in 1956 for the anionic polymerization of styrene, allowing polymers with low dispersity and near 100% end-group functionality (EGF).[1] The key to this 'livingness' is the elimination of termination reactions, such as proton transfer to carbanion and electron transfer from carbanion, by using non-acidic well-solvating reaction media (e.g. tetrahydrofuran). Although ionic polymerizations show 'living' behaviour and give almost uniform-sized polymers, the synthetic technique requires stringent conditions; such as low reaction temperatures, monomers capable of stabilizing propagating ions via charge delocalization, high purity of reagents and the elimination of water and oxygen, thus, limiting the applicability of ionic polymerization to well-equipped laboratories and restraining monomer choice.[2] Free radical polymerization (FRP) is the most widely used alternative as the process is relatively insensitive to impurities, can utilise a wider range of unsaturated monomers, and various synthetic conditions are available, such as bulk, emulsion and solution polymerization. However, for certain applications, such as generating polymers with narrow molecular weight distributions and high EGF, the traditional FRP process is insufficient.

The first work on radical polymerization that demonstrated controlled behaviour was published by Ferington and Tobolsky, who used dithiuram disulfides as initiators.[3] Although this technique showed a linear increase in molecular weight with conversion similar to LRP, the obtained polymers had broad molecular weight distributions due to high transfer constants. The development of nitroxide-mediated radical polymerization (NMP)[4-6] demonstrated that these issues can be overcome by reversibly capping propagating radicals with stable nitroxide radicals and, thus, NMP can be referred to as LRP. An alternative approach to reduce radical concentration by reversibly capping them was introduced by Sawamoto[7] and Matyjaszewski[8] in a concept known as atom transfer radical polymerization (ATRP). Using this technique, wide libraries of polymers with high chain-end fidelity and narrow molecular weight distributions (Đ<1.10) can be made under moderate experimental conditions.[9, 10] A wide range of monomers and end groups that can be made via LRP is broadened by reversible addition-fragmentation chain-transfer (RAFT) polymerization,[11] single-electron transfer living radical polymerization (SET-LRP)[12] and iodine transfer polymerization (ITP).[13] Reaction media properties, such as biocompatibility,[14, 15] ppm catalyst levels,[16] tolerance to

oxygen and moisture,[17] polymerization temperature[18-20] and basic/acidic conditions[21] can be varied to optimise reactions. High chain-end functionality of certain polymers made by LRP was confirmed by model studies and in experiments.[22, 23]

1.1.1. Atom Transfer Radical Polymerization (ATRP)

Ca. 20 million of the 50 million tons of synthetic polymers produced annually are made by FRP.[24] The technology is widespread, and such polymer properties as, for example, broad molecular weight distributions, play an important role in manufacturing. However, certain applications require uniform-sized polymers and high chain-end retention, for instance, conjugation chemistry[25, 26] and the synthesis of complex polymer architectures.[27, 28] For several decades the only available methodology to overcome limitations of FRP and make tailor made polymers, has been living ionic polymerization. ATRP, introduced independently by Sawamoto[7] and Matyjaszewski[8], has become the most widely used alternative of ionic polymerization because of its tolerance to traces of oxygen and moisture,[29] broader choice of monomers[9] and simple reaction setup. The polymers synthesized via ATRP have relatively high chain-end functionality[30] and low dispersity indices (Đ<1.2) due to fast polymerization initiation and the absence of chain-transfer reactions.

The key aspect of ATRP is the introduction of equilibrium dormant polymer chains – propagating radical species (Scheme 1.1).[31]

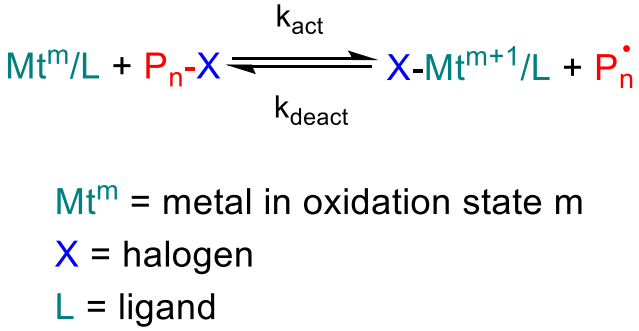

Scheme 1.1. The mechanism of the atom transfer radical polymerization process. Adapted with permission from[9]. Copyright 2012 American Chemical Society.

Activation of dormant species proceeds through homolytic cleavage of P-X bond via inner-sphere electron transfer,[32] where X is a halide and P is a propagating polymer chain. The activation step is catalysed by metal complex Mt^m/L, where Mt is presented by various transition metals, such as Cu,[33] Fe,[34] Co[35] and Mo[36], with *m* being their oxidation state and L a ligand. Activation results in the formation of carbon-centered radicals ($P_n^{\cdot}$) and halide coordinated metal complexes in a higher oxidation state ($X\text{-}Mt^{m+1}/L$). The deactivation step involves halide abstraction from the metal complex and its conjugation with the propagating radical. The activation-deactivation equilibrium is

shifted to the dormant species due to persistent radical effect (PRE)[37] responsible for the initial build-up of deactivating catalytic species, which results in low radical concentration and, therefore, significant suppression of radical termination.

The most commonly used and studied ATRP catalyst is $Cu^{I}X/L$, where X is bromide or chloride and L is a polydentate ligand, such as *N,N,N',N'',N''*-pentamethyldiethylenetriamine (PMDETA), 2,2'-bipyridine (bpy), tris[2-aminoethyl]amine (TREN) and tris[2-(dimethylamino)ethyl]amine (Me_6TREN). A vast diversity of monomers, solvents, polymer architectures and initiators can be used in ATRP and are reported elsewhere.[38] The latest developments in ATRP involve polymerization with low levels of catalyst (ppm levels),[16] activators regenerated by electron transfer (ARGET) ATRP,[39] photo-induced ATRP[40, 41] and emulsion ATRP.[42] The applications of ATRP made polymers include smart surfaces,[43, 44] bioconjugates,[45] analytical metal affinity columns[46] and micelles with low critical micelle concentration values.[47]

Alongside with its multiple advantages, ATRP has several limitations. The first and the most important issue is loss of polymerization control caused by unavoidable radical recombination due to the nature of the polymerization.[48] In order to avoid bimolecular termination monomer conversions cannot reach high levels. Also, if ATRP is carried out at elevated temperatures, β-H elimination can have the impact on chain-end functionality.[49] In addition, due to the use of bases in catalyst composition, acidic monomers cannot be polymerized using ATRP and group protection is necessary to overcome this problem.[50]

1.1.2. Single-Electron Transfer Living Radical Polymerization (SET-LRP)

Halogen abstraction from aryl halides catalyzed by zero-valent metal traces back to 1901AD, and is known as Ullmann coupling.[51] However, it took almost a century until zero-valent metal catalyzed polymerizations came to be widely used.[52] Cu/bpy and Cu_2O/Cu^0/bpy mixed catalysts were introduced by Percec et al. for the polymerization of butyl methacrylate initiated by sulfonyl chlorides.[53] Further elucidated mechanisms[54] suggested heterogeneous activation of alkyl halides with Cu^0 through outer-sphere electron transfer (OSET) process (Scheme 1.2).

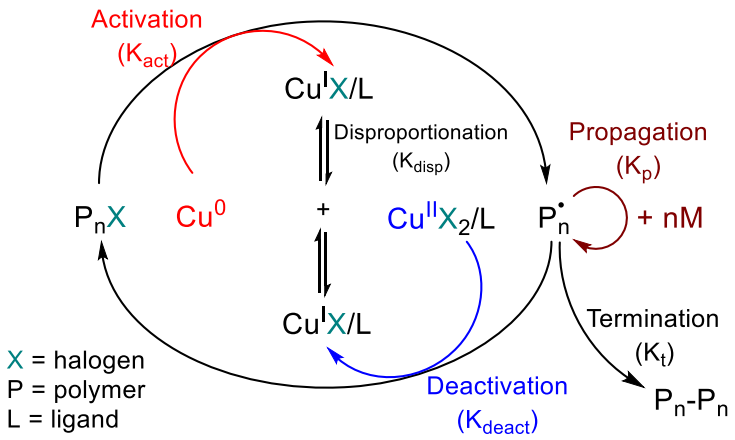

Scheme 1.2. The mechanism of the single-electron transfer living radical polymerization process. Adapted with permission from[55]. Copyright 2006 American Chemical Society.

Substantial amount of work was dedicated to elucidate the nature of electron transfer in the activation step. According to Marcus theory, electron transfer is a complex process and cannot be ascribed simply to either inner-sphere electron transfer (ISET) or OSET pathway.[56] In particular, reaction conditions such as temperature and solvent can alter the rate of electron transfer. Density Functional Theory (DFT) studies of heterolytic bond dissociation energies of a model initiator and dormant polymer species demonstrated that an effective electron donor like Cu^0 or Cu_2X can favour heterolytic bond dissociation over homolytic.[57] The termination step is believed to be significantly suppressed in SET-LRP due to the low mobility of propagating radicals on the copper surface.[23] Continuous regeneration of the activating metal species is achieved through carrying out polymerization in polar solvents (*vide infra*), which results in rapid disproportionation of $Cu^{I}X/L$ formed during the activation/deactivation step. Additionally, appropriate ligands, for example TREN or Me_6TREN, that preferentially stabilizing $Cu^{II}X_2/L$ over $Cu^{I}X/L$ must be used in order to achieve high disproportionation.[58] Reaction kinetics are consistent with Langmuir-Hinshelwood kinetics describing heterogeneous catalysis and the apparent rate constant of polymerization (k_p^{app}) is dependent on the halide, solvent concentration and catalyst surface area.[59-61]

The main advantages of SET-LRP over ATRP are the abilities to synthesize polymers with ultrahigh molecular weights,[55] near 100% polymer end-group functionality (EGF)[62] and in milder polymerization conditions.[63] High molecular weights are important for various industry applications, for instance resistance of a material to abrasion, low friction coefficients, etc. High chain-end fidelity is essential for conjugational chemistry (*vide infra*). Elevated reaction temperature results in β-scission of propagating radicals and, therefore, mild polymerization conditions are also critical for the synthesis of tailor-made polymers. Additionally, recent developments of aqueous SET-LRP introduced by Haddleton et al. in 2013 broadened the scope of

SET-LRP.[64] This includes SET-LRP in biological medium,[65] synthesis of bioconjugates[66] and biomimetic polymers.[67] SET-LRP in organic solvents has also been used in multiple studies including the development of nitroxide radical polymers,[68] stress-reactive materials,[69] Magnetic Resonanse Imaging (MRI) contrast agents[70] and oil-absorbents.[71]

In addition to these advantages SET-LRP is applicable for a broad range of monomers, such as acrylates, methacrylates, acrylamides, methacrylamides, vinyl halides, styrene and poly(acrylonitrile) (detailed lists of monomers shown elsewhere[72, 73]). The most commonly used initiators are methyl-2-bromopropionate (MBP)[74] and ethyl α-bromoisobutyrate (EBiB).[75] Chlorine α-haloester initiators are often used as an alternative to bromide ones;[76] the initiator choice can be further broadened by sulfonyl halides,[53] haloforms[77] and amide initiators.[78] In addition to a type of functionality the number of initiating groups can also vary. The initiators can be mono- bi- and multifunctional resulting in α,ω-telechelical, n-arm star and brush polymers respectively. A broad range of transition metals can activate dormant species in SET-LRP, such as iron,[79] nickel[80] and lanthanum,[81] but undoubtedly copper-based catalysts remain the most widely used in SET-LRP as they are cheap and easy to make. As a theoretical support Hartree-Fock DFT (HF/DFT) estimations of ionization potentials of various copper species showed that Cu(I) pseudohalides and Cu^0 facilitate OSET and are, therefore, the best catalysts for SET-LRP.[82] Indeed, Cu_2Se and Cu_2Te were successfully employed in SET-LRP of methyl methacrylate (MMA).[83] Nevertheless, Cu^0 remains the most widely used catalyst due to its cheapness and simplicity of removal. Different forms of Cu^0 can be used for SET-LRP, such as powder,[60] wire[84] and nascent nanoparticles.[85] The ligand, a necessary component for the deactivation step, is generally represented by TREN or Me_6TREN, which known to stabilize $Cu^{II}X_2$/L species over Cu^{I}X/L species. To ensure SET-LRP mechanism, polymerization must be carried out in highly polar solvents such as water,[64] dimethyl sulfoxide (DMSO),[85] alcohols[86] and ionic liquids,[87] as the high disproportionation constant of Cu^{I}X/L in these solvents ensures rapid regeneration of activation species.

1.1.3. Mechanistic Debate

Copper-mediated polymerization has been used for the synthesis of polymers with narrow molecular weight distribution and high end-group functionality for more than two decades. The nature of activating species in polar solvents has been the subject of intense discussions since the introduction of SET-LRP. There are two theories that explain activation step namely supplemental activator and reducing agent atom transfer radical polymerization (SARA-ATRP)[88] and single-electron transfer 'living' radical polymerization (SET-LRP).[12] According to SARA-ATRP activation follows homolytic cleavage of terminal halide catalyzed by Cu^{I}X/L species. Cu^0 formed

in situ via reduction or added prior to polymerization is necessary to trap traces of oxygen presented in reaction media and acts only as a supplementary activator. On the other hand, SET-LRP postulates that Cu^0 acts as primary activating species and Cu^I is not presented in reaction media when polymerization is carried out in solvents with high polarity. Even though the main aim of this thesis was not to answer whether one or another theory is correct, it is important to highlight the main arguments of both theories. The debates are mainly focused on the nature of electron transfer, comparison of activation constants for Cu^I and Cu^0 and disproportionation constants for various reaction media.

According to SARA-ATRP activation occurs though inner-sphere electron transfer (ISET)[32] which was supported by computational studies using Marcus theory. DFT calculations for Cu^I/TPMA complex showed that ISET is favoured by approximately 15 kcal/mol over outer-sphere electron transfer (OSET), which should result in 10^{10} rate enhancement of ATRP pathway over SET-LRP.[89] Stopped flow analysis demonstrated that activation of alkyl halides with Cu^IBr/Me_6TREN is an extremely rapid process and conversion of Cu^I species is complete within one second. For a typical polymerization in DMSO activation rate coefficient of methyl 2-bromopropionate by Cu^IBr/Me_6TREN was estimated to be 320 $M^{-1}s^{-1}$.[90] Additional experiments on the activation rates in aqueous phase via electrochemical methods showed that activation of 2-hydroxyethyl 2-bromoisobutyrate with Cu^I/TPMA is an extremely fast process with an activation rate constant $k_{a1} \geq 2.6 \times 10^6$ $M^{-1}s^{-1}$.[91] Finally, studies on the extent of disproportionation of Cu^IBr/Me_6TREN in typical SET-LRP media showed that if polymerization is carried out in DMSO the extent of disproportionation is only 0.2% with disproportionation equilibrium constant being of 2 M^{-1}. However, when polymerization is carried out in more polar aqueous solution, disproportionation equilibrium constant equals to 10^6-10^7.[92] It is important to mention that the amount of monomer and ligand can significantly affect solvent polarity and comproportionation can still occur under certain reaction conditions. For example, when 18 wt% OEOA in water was used to study comproportionation reaction between $CuBr_2$ and Cu^0 it was found that even though comproportionation rate was slow about 20% of $CuBr_2$ was converted to Cu^IBr in 300 min reaching near equilibrium concentration.[93] To sum up, the studies describe polymerization mechanism for certain reaction conditions. However copper-mediated polymerization is a multicomponent process, and for certain reaction conditions, e.g. ratio Cu(II):ligand, type of monomer, type of ligand, reaction temperature, etc., the aforementioned parameters can change substantially and, therefore reaction mechanism can differ.

First important change in reaction conditions that leads to high disproportionation equilibrium constants is changing the ratio between CuBr and Me_6TREN. Percec's group reported that the

extent of disproportionation reaches maximum when 0.5 equivalents of ligand to CuBr is used.[94] Indeed, in further studies on disproportionation of CuBr in water, Haddelton's group showed that disproportionation of CuBr/Me_6TREN is 100% if equimolar ratio between Me_6TREN and CuBr is used.[64] In the same publication, they optimized polymerization conditions to obtain polymers with low dispersity by using 0.5 equivalents of Me_6TREN, which is in accordance to Percec's results. Another important phenomenon that cannot be explained by ATRP mechanism is dependence of polymerization rate on copper particle size. Percec's group studied kinetics of copper-mediated polymerization for a range of particle size and found that polymerization rate is dependent on surface area of the catalyst and follows Langmuir-Hinshelwood kinetics.[60] In addition, activation of alkyl halides on copper surface explains such phenomena as extremely high chain-end retention at 100% monomer conversions and accumulation of polymer solely on copper surface.[23] Finally the OSET nature of electron transfer was supported by computational studies.[57] To conclude, copper-mediated polymerization mechanism in aqueous media is dependent upon many factors and for specific conditions SET-LRP mechanism gives thorough and sufficient explanation to the observed phenomena.

1.2. Chain-End Functionality

Chain-end functionality of the polymers made via copper-mediated LRP is often used for conjugational chemistry. Although the concept of living radical polymerization implies near 100% chain-end retention, in reality chain-end functionality of the polymers synthesized by ATRP decreases significantly with the increase in conversion.[95] This loss happens due to various reasons, including radical-radical termination, β-H elimination and side reactions between growing radicals and copper catalysts.[49] The presence of dead chain ends is detrimental as contaminated halide-functional polymers require additional purification steps. In contrast, SET-LRP is capable of producing polymers with near 100% chain-end functionality.[62] The SET-LRP mechanism includes the adsorption of propagating species onto a copper surface,[23] which hinders the movement of radicals[96] formed during activation step and, therefore, almost fully suppresses radical-radical termination. Thus, SET-LRP is a more desirable technique for the synthesis of highly functional polymers.

1.3. 'Click' Reactions

'Click' chemistry is a class of reactions designed to efficiently couple two molecules. The term 'click' was coined by Kolb, Finn and Sharpless who proposed a set of conditions that define a 'click' reaction.[97] The most important attributes of a 'click' reaction include high reaction yields,

high specificity, benign or easy to remove solvents, simple product isolation and available or easy to make starting materials. Although the requirements are stringent, there is a large library of reactions that meet these criteria.

Copper-catalyzed azide-alkyne cycloaddition (CuAAC) is undoubtedly the most studied and used 'click' reaction.[98] The reaction is orthogonal, gives near quantitative yields and can be performed in organic solvents and water making it a perfect tool not only to join two molecules together but also for combined chemistry and biology studies (*vide infra* for details). Another example of a widely used 'click' chemistry is thioetherifaction of alkyl halides introduced by Percec and co-workers in 2007.[77, 99] The reaction is advantageous for the synthesis of polymeric architectures for two main reasons. First, there is no need for any modifications of halide functional polymers synthesized by Cu-mediated LRP as the polymer can be used directly for a 'click' reaction after polymerization. Secondly, thiol-functional materials are cheap and multiple functionalities are commercially available. The scope of 'click' reactions is further extended by thiol-ene/yne reactions,[100] Diels-Alder addition,[101] strain promoted addition of aziridines and epoxydes,[102] oxime ligation,[103] and nitroxide radical coupling (NRC).[104, 105]

It is generally desirable for a 'click' reaction to require no catalyst, for example strained-promoted CuAAC[106] and Diels-Alder addition of triazolinediones.[107] However, often moderate stimulus is applied to stimulate the reaction; including physical processes such as irradiation[108] or mild heating.[109] Additionally, many types of 'click' reactions use a chemical catalyst. In that case certain techniques are used to simplify catalyst removal, for example immobilization of the catalyst on solid supports[110] or magnetic particles.[111]

Being an extremely powerful and at the same time simple instrument, 'click' chemistry is employed in multiple research areas. For example, fundamental studies in polymer science have used 'click' reactions for more than a decade to make a broad range of polymer structures and investigate their properties.[28, 112, 113] In addition, nanoparticles (NPs) modified or created using click chemistry are of great interest. Numerous instances of the synthesis of organic NPs[114] and modification of metals,[115] silica[116] and carbon[117] are reported; and the materials synthesized via 'click' reactions can be used as nanoreactors,[118] stabilizators of colloids[119] and sensors[120]. In addition to conventional 'click' chemistry, reversible reactions can be employed in self-healing or reshaping materials and are attracting growing attention.[121] Furthermore, two or more 'click' reactions can be performed orthogonally, thereby simplifying synthetic pathways.[122] Click chemistry is also widely used in biochemical and biological applications; main research trends include enzyme inhibition,[123] drug delivery,[124] modification of peptide properties,[125] drug

discovery,[126] biocompatibility of materials,[127] imaging agents,[128] antibacterial surfaces[129] and cell growth media.[130]

1.3.1. Copper-Catalyzed Azide-Alkyne Cycloaddition

The first work on 1,3-dipolar cycloaddition was published by Dimroth in 1902.[131] The mechanism of the reaction was proposed four decades later by Rolf Huisgen who studied the cycloaddition reaction to couple various organic molecules.[132] However, the yields of Huisgen reactions were not quantitative, and the reactions required elevated temperatures. These problems were later solved independently by Morten Meldal [98] and Barry Sharpless group,[133] by catalysing the reaction with Cu(I) complex. Since then CuAAC has become one of the most used 'click' reactions across multiple disciplines. The reaction gives near 100% yields, orthogonal, fast and if required copper catalyst can be eliminated using strain-promoted CuAAC or it can be easily removed. These features of the CuAAC meet all the criteria of 'click' chemistry and make the reaction highly desirable for conjugation purposes.

CuAAC mechanism suggested by Fokin group includes both single and bis-complex catalysis (Scheme 1.3).[134]

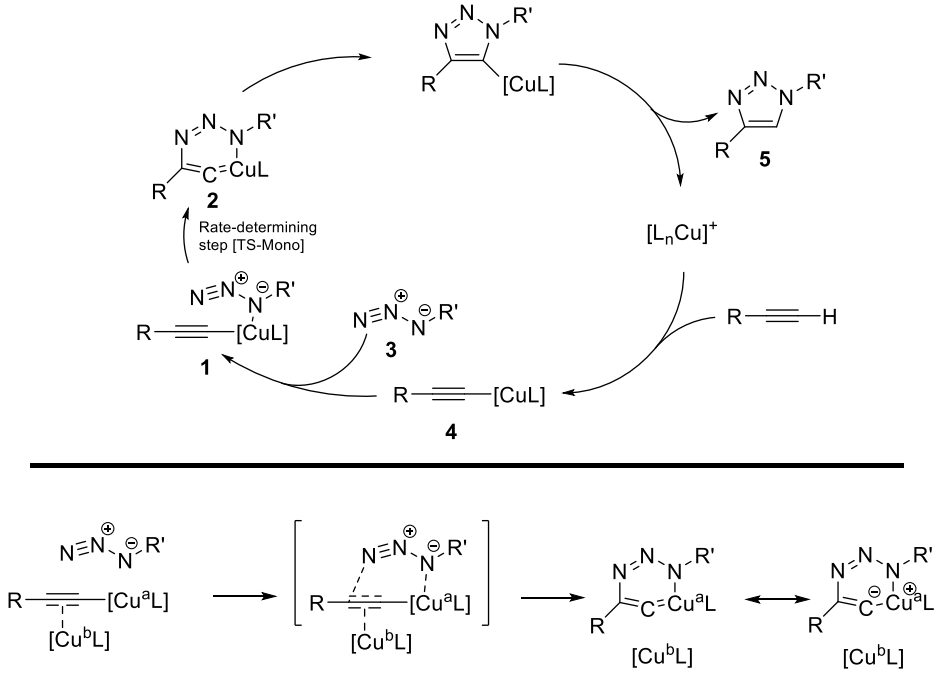

Scheme 1.3. The mechanism of copper-catalyzed azide-alkyne cycloaddition. Adapted with permission from[134]. Copyright 2007 American Chemical Society.

Coordination of copper complex to the π-orbitals of alkyne occurs in the first step. It is followed by the base catalyzed deprotonation of terminal hydrogen and the formation of copper acetylide **4**. It was suggested by the authors that the coordination of the second copper complex to the alkyne can

additionally stabilize the intermediate. In the next stage, azides coordinate the intermediate **1** and displaces labile ligand; copper-azyde-acetylide complex **2** formes and cyclization occurs. In the last step the cycloadduct is protonated and the copper complex detaches resulting in the final product **5**.

The mechanism of the reaction was revised by Bertrand's group in 2015 (Scheme 1.4) after the isolation of intermediate compounds.[135]

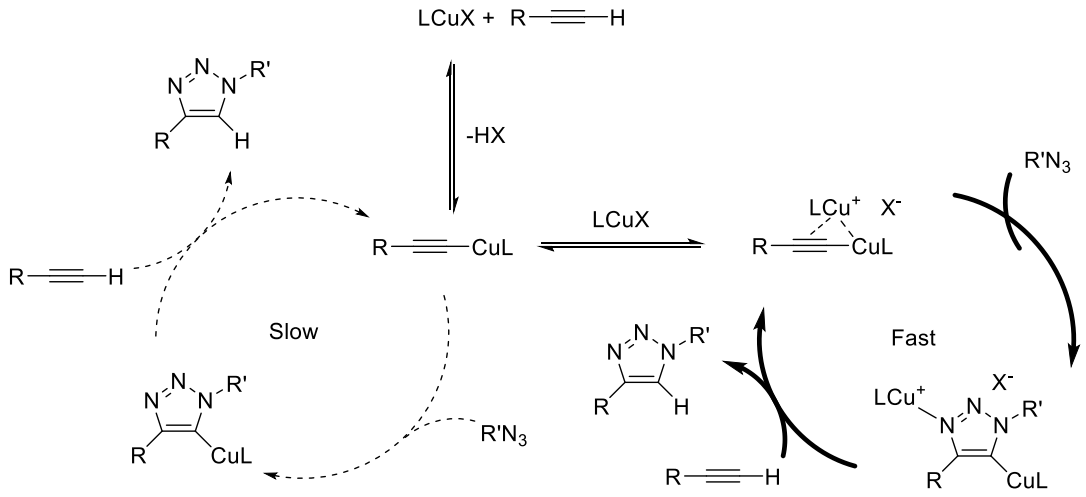

Scheme 1.4. Two-centered mechanism of copper-catalyzed azide-alkyne cycloaddition.[135]

It was found that both mono- and bis-copper acetylides are formed during CuAAC. The intermediates were purified and further used for the CuAAC with benzyl azide. The reaction rate of the bis(nuclear) complex pathway turned out to be 2 orders of magnitude higher than that of the mononuclear complex, meaning that both catalytic cycles are valid, but the pathway in which the coordination of two copper molecules occurs is more favourable. Bertrand group reported that the ligand also plays role in the mechanism, as no bis-copper complexes were observed for other ligands. This brings to conclusion that the CuAAC mechanism is a complex process and dependent on reaction conditions.

Many forms of copper catalyst can be used in CuAAC and depend on the requirements of the experiment. If the reaction is carried out in non-polar solvents, copper halide complexes with Cu(I) stabilizing ligands are generally used.[136] In cases of highly polar aqueous media, continuous regeneration of active copper species is achieved by using a mild reducing agent, for example sodium ascorbate.[137] It was also reported that certain water soluble ligands can significantly increase reaction rates.[138] However, for biological applications copper use is detrimental due to the formation of reactive oxygen species that damage biomaterials.[139] In order to address this issue and so create biocompatible 'click' reactions strain-promoted azide-alkyne cycloaddition is commonly used.[140] Because of its exceptional 'click' properties, CuAAC has found multiple scientific

applications, such as synthesis of polymer architectures,[27] nanoreactors,[141] catalysts,[142] surface functionalization,[143] drug delivery,[144] peptide modification[145] and imaging.[146]

1.4. Polymer Topologies

LRP and 'click' chemistry are two main instruments in the field of polymer topology, the former generates well-defined building blocks of narrow molecular weight distribution and high chain-end functionality, and the latter joins these blocks together. The main topologies synthesized using LRP and/or 'click' reactions are shown on Figure 1.1.

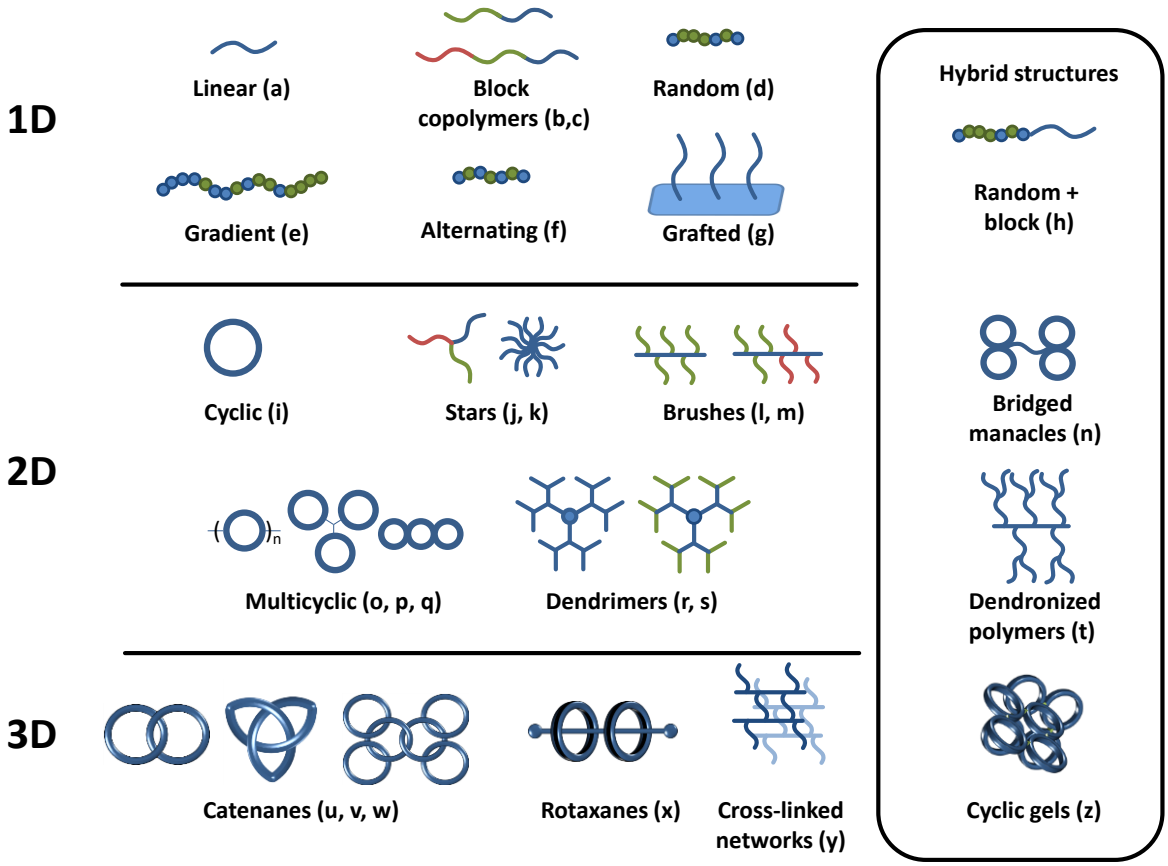

Figure 1.1. Topologies made via LRP and 'click' chemistry. (a),[147] (b),[70] (c),[148] (d),[149] (e),[150] (f),[151] (g),[152] (h),[153] (i),[154] (j),[155] (k),[156] (l),[157] (m),[158] (n),[159] (o),[160] (p),[113] (q),[161] (r),[162] (s),[112] (t),[28] (u),[163] (v),[164] (w),[165] (x),[166] (y),[167] (z).[168]

Specific properties of the polymer topologies have been employed in a wide range of applications. For example, semiconducting and solvent impermeable films were made using Grignard metathesis polymerization and thiol-ene reaction.[169] In another work, peptidomimetic dendrimers were synthesized using CuAAC; lysine (or MKF tripeptide) outer layer of these dendrimers was used to bind to the mammalian K^+ channels.[112] Finally, 3D adipose-derived stem cell growth media was made by using ATRP to synthesize hyperbranched triblock copolymer that

encapsulated stem cells via thiol-ene reactions between remaining alkene groups of copolymer and thiols of thio-modified hyaluronic acid.[170]

In addition to the spatial dimensions, temporal change of polymer topologies can be introduced, such structures can be considered to have 4D topologies. This time dependence can be triggered by one or more stimuli, for example electric or magnetic fields,[171, 172] temperature,[173] pH,[174] irradiation[175], ionic strength[176] and mechanical force.[177] These response polymer topologies can reversibly change their properties upon stimulus,[178] irreversibly degrade[177] or interchange in topologies.[121]

Although problem-solution approach is a pragmatic and reasonable way for the development of scientific areas, synthesis and investigation of fundamental properties of new materials remains of great interest, as often these studies give unforeseeable results which can lead to the development of completely new research areas.[179-181] From this point of view cyclic polymers represent an intriguing class of polymer topologies as such a small change of polymer structure as lack of chain ends results in significant alteration of polymer properties.

1.4.1. Cyclic Polymers

Cyclic polymers demonstrate different properties compared to their linear analogues: glass transition temperature,[182] intrinsic viscosity,[183] fluorescence,[184] self-assembly behaviour,[185] crystallization rates,[186] flow dynamics[187] and pharmacokinetics.[188] By introducing additional topological changes one could expect further alteration in polymer properties. Indeed, multicyclic polystyrene topologies made by Hossain et al. showed further increase in glass transition temperature (T_g) and decrease in hydrodynamic radius (R_h) and, therefore, intrinsic viscosity.[189] A variety of cyclic architectures and hybrids were obtained and studied over the last decade including polybridged cycles and spirocyclics;[160] trefoil rings;[190] manacles;[159] tadpoles;[191] brushed cycles;[192] linear chains with grafted cycles;[193] cyclic gels;[168] catenanes[194] and rotaxanes.[195] Cyclic polymers were theoretically predicted in 1950,[196] and the first cyclic structure for poly(dimethylsiloxane) was synthesized by Brown et al. a decade later.[197] There are two main strategies to synthesize a cyclic polymer: ring expansion and ring closure (Scheme 1.5).

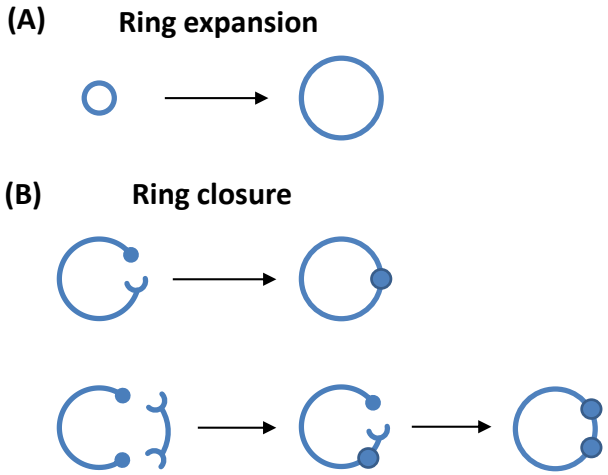

Scheme 1.5. Pathways for the synthesis of cyclic polymers. (A) Ring expansion. (B) Ring closure.

Ring expansion strategy is mainly carried out through ring expansion metathesis polymerization (REMP),[198] although other strategies are known.[199] The main advantage of REMP is that no linear chains or catenanes can form due to the polymerization mechanism. In addition, REMP gives cyclic polymers of high concentrations and any molecular weight. However, the method is inapplicable for the synthesis of various cyclic topologies, as REMP made polymers can have only two types of functionalities: double bonds of the cyclic core and side functionality of monomer residues. It is impossible to introduce other functionalities or control their positions within a cyclic molecule.

The ring-closure method allows tailor-made cyclic polymers to be made; type, position and number of functionalities can vary depending on the desired polymer architecture. This makes ring-closure strategy preferable for the synthesis of cyclic topologies. Ring closure can be carried out either via bi- or unimolecular approaches. Cyclic polystyrene synthesized via bimolecular approach was first made independently by Höcker,[200] Rempp[201] and Vollmert.[202] In their work, cyclization was performed by coupling polystyrene dianions with electrophilic p-xylene dihalides. However, the fraction of cyclic species was low (less than 50%), and stoichiometric ratios of reactants is necessary. To address the problems Tezuka et. al described a strategy called electrostatic self-assembly and covalent fixation (ESA-CF).[203] In this approach dicarboxylate end functionalities and cyclic ammonium counterions of polytetrahydrofuran were used to form ion-pair cyclic precursors. The heating of the formed complex results in selective ring-opening of cyclic ammonium end groups and subsequent covalent coupling with carboxylate moieties to give the final cyclic polymer. Although ESA-CF gives high yields of cyclic species, second order kinetics and high polymer dilution results in slow cyclization rates. An additional drawback is the necessity to use equimolar ratios of reagents. In contract unimolecular ring-closure approach uses intramolecular coupling of α,ω-telechelic polymers. The key to high purity cyclic polymer synthesis, using the ring-closure

approach, is to maximize the probability of intramolecular reactions and minimize that of intermolecular coupling. Two possible reaction pathways for a linear difunctional polymer synthesis are shown in Scheme 1.6 and follow the encountered-pair model (Scheme 1.6).

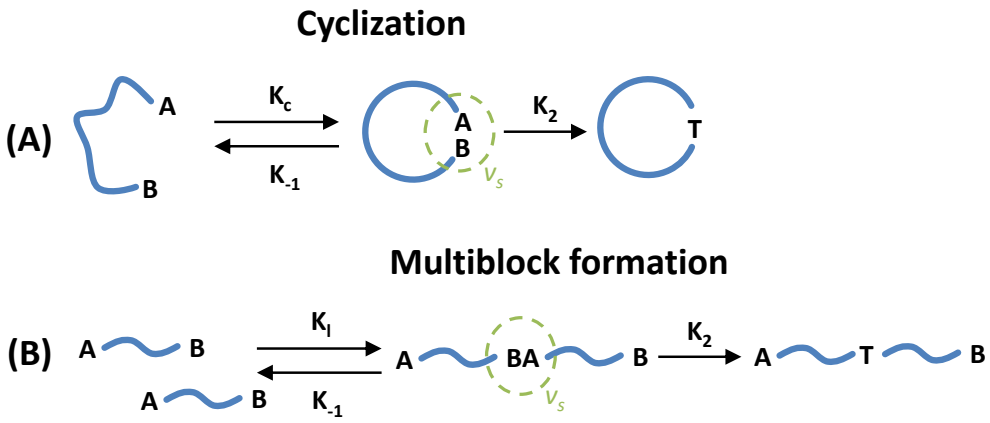

Scheme 1.6. Encounter pair model of a chemical reaction. (A) Intramolecular cyclization. (B) Linear multiblock formation. Adapted with permission from[154]. Copyright 2010 American Chemical Society.

The "encountered" control of the process allows one to calculate probabilities of two chain ends to be within capture volume v_s by using the Jacobson-Stockmayer equation[196] for type II condensation:

$$P_C = \left(\frac{3}{2\pi}\right)^{3/2} \frac{v_s}{<r^2>^{3/2}} \qquad (1.1)$$

$$P_L = 2N\frac{v_s}{V} = \frac{2N_A c}{M} v_s \qquad (1.2)$$

where P_C and P_L are the joining probabilities for two ends of one polymer and two ends of different polymer molecules correspondingly. $<r^2>$ is the mean square end-to-end distance of the chain, N is the number of polymer molecules in volume V, N_A is Avogadro's constant, c is the polymer concentration and M is the polymers molecular weight. The ratio between cyclic product and linear multiblocks is given by[204]:

$$\frac{P_C}{P_L} = \left(\frac{3}{2\pi<r^2>}\right)^{3/2} \frac{2000}{N_A[P]} = \frac{k_c}{k_l[P]} \qquad (1.3)$$

such that

$$\frac{k_c}{k_l} = \left(\frac{3}{2\pi<r^2>}\right)^{3/2} \frac{2000}{N_A} \qquad (1.4)$$

Square end-to-end distance $<r^2>$ for polystyrene in a good solvent is dependent on molecular weight[205]:

$$< r^2 >= 11.42 \times 10^{-18} M^{-1.17} \qquad (1.5)$$

Thus, one can predict cyclic polymer purity using equations 1.4 and 1.5. This theory was further developed by Monteiro group using kinetic simulations and cyclization experiments of polystyrene

via CuAAC.[206] The methodology gives quantitative data on cyclic polymer purity when reaction conditions are known and the data correlates well with experiments. Optimized reaction setup gives large scale, high purity cyclic polymers in within short periods of time.

1.5. Log-Normal Distribution Simulation

Central limit theorem of the probability theory postulates that when independent random variables add up, their sum approaches a normal distribution. As an inevitable consequence, Gaussian function appears throughout the Universe: from the realm of quantum mechanics[207] through human-size objects[208] and beyond galaxy scales.[209] Furthermore, the applications of the Gaussian function may spread beyond the known Universe: scientists use the distribution for higher dimensions[210] and Multiverse theory.[211] The sizes of polymer topologies fall into nanometer scales and the Gaussian function for a polymer chemist applies to log-normal distribution simulation of polymer molecular weight distributions.

Size Exclusion Chromatography (SEC) is an important tool for the characterization of polymer molecular weight distributions and purity analysis. For example, presence of low molecular weight components and bimolecular coupling on a polymer GPC curve is a direct indication of polymerization control loss. In addition, after the introduction of 'click' chemistry, GPC has also become an essential instrument for the characterization of polymeric architectures as the presence of unreacted polymer blocks gives information on coupling efficiency.[27, 161, 212] In order to correctly quantify the amount of polymer species in GPC samples, log-normal distribution (LND) simulation is used in which a GPC trace of a polymer is fitted by a Gaussian function:

$$f = \frac{1}{\sqrt{2\pi\sigma^2}} e^{\frac{-(x-\mu)^2}{2\sigma^2}} \qquad (1.6)$$

where μ is mean and σ is standard deviation. The pre-exponential factor of equation 1.6 is the height of the curve's peak, μ controls the position of the centre of the bell curve and σ determines the breadth of the function. The molecular weight distribution has a "bell" shape because of the nature of polymer chain conformation. When a polymer is in solution its confirmation can be assigned, under certain approximations, to that of an ideal chain. The total end-to-end vector $\vec{R}$ of the ideal chain consists of $\vec{r}_1$,...,$\vec{r}_N$ vectors corresponding to N individual monomers, each of length b. From the definition of a random walk, $\vec{r}_i$ vectors are independent random variables and, therefore, the resulting sum vector $\vec{R}$ follows central limit theorem and is distributed in 3D space according to the probability density function:[213]

$$P(\vec{R}) = \left(\frac{3}{2\pi N b^2}\right)^{3/2} e^{-\frac{3\vec{R}^2}{2Nb^2}} \qquad (1.7)$$

GPC separates polymer molecules according to their hydrodynamic radius (R_h) which differs from root-mean-square end-to-end distance $<\vec{R}^2>^{1/2}$ by a constant.[214, 215]

1.6. Objectives and Outlines of This Thesis

The main objective of this thesis was to study in details polymer molecular weight distributions and to apply the obtained knowledge in synthesis of polymers with high chain-end functionality and in polymer architectures. In addition, we developed a strategy for the synthesis of poly(N-isopropylacrylamide) (PNIPAM) with near 100% chain-end functionality using a new catalyst for aqueous SET-LRP coupled with in situ azidation of pendant halide. Being a thermoresponsive polymer, PNIPAM becomes hydrophobic when heated above lower critical solution temperature (LCST); making the polymer a potential candidate for various scientific applications.[216-218]

In Chapter 2 we derive equations for polymer molecular weight distributions and use the distributions to create log-normal distribution (LND) simulation method, which can be used for characterization of polymers obtained via wide range of processes, for example, 'living' radical polymerization, 'click' reactions and cyclization.

In Chapter 3 LND simulation was modified to characterize heteropolymer mixtures. The impact of d*n*/d*c* on the intensity of GPC traces of various polymers is taken into account and the efficiency of the methodology is demonstrated for the simulation of CuAAC between polystyrene (PSTY) and various polymers, such as poly(*tert*-butyl acrylate) (P*t*-BA), PNIPAM and polyethylene glycol (PEG).

In Chapter 4 we introduce a new catalytic system to carry out aqueous SET-LRP. The activating Cu^0 species form through the reduction of $CuBr_2$/Me_6TREN complex with sodium borohydride ($NaBH_4$). The reduction is quantitative and no Cu(I) species were detected before or after polymerizations which indicates that the reaction proceeds via a SET-LRP mechanism. The ratio between $NaBH_4$ and $CuBr_2$/Me_6TREN gives control over the polymerization rate. Polymers synthesized under optimized conditions have low dispersity (Đ<1.1) and high chain-end functionality (>95%).

Chapter 5 focuses on studies of in-situ azidation of PNIPAM synthesized via aqueous SET-LPR. Sodium azide (NaN_3) is added to the polymer directly after the end of polymerization, which overcomes the issue of hydrolysis of bromide chain ends in water and efficiently converts it to

azide. Subsequent ‘click’ of the purified PNIPAM azide using CuAAC shows extremely high chain-end retention (>97% for most polymers).

In Chapter 6 we synthesize densely packed multicyclic PSTY using copper-mediated LRP by sequential and one-pot synthetic approaches. The LND data obtained for the n-mers in sequential synthesis is used to determine the composition of a mixture of multicyclic species obtained in a one-pot synthesis demonstrating the versatility of the LND simulation. Glass transition temperature studies showed unusual properties of the multicyclic PSTY due to the entropy decrease.

1.7. References

1. Szwarc, M. *Nature* **1956,** 178, (4543), 1168-1169.
2. Morton, M.; Rembaum, A. A.; Hall, J. L. *Journal of Polymer Science Part A: General Papers* **1963,** 1, (1), 461-474.
3. Ferington, T. E.; Tobolsky, A. V. *Journal of the American Chemical Society* **1955,** 77, (17), 4510-4512.
4. Moad, G.; Rizzardo, E.; Solomon, D. H. *Macromolecules* **1982,** 15, (3), 909-914.
5. Solomon, D. H.; Rizzardo, E.; Cacioli, P. US Patent No. US4581429 A, **1986**.
6. Georges, M. K.; Veregin, R. P.; Kazmaier, P. M.; Hamer, G. K. *Macromolecules* **1993,** 26, (11), 2987-2988.
7. Kato, M.; Kamigaito, M.; Sawamoto, M.; Higashimura, T. *Macromolecules* **1995,** 28, (5), 1721-1723.
8. Wang, J.-S.; Matyjaszewski, K. *Journal of the American Chemical Society* **1995,** 117, (20), 5614-5615.
9. Matyjaszewski, K. *Macromolecules* **2012,** 45, (10), 4015-4039.
10. Kamigaito, M.; Ando, T.; Sawamoto, M. *Chemical Reviews* **2001,** 101, (12), 3689-3746.
11. Chiefari, J.; Chong, Y. K.; Ercole, F.; Krstina, J.; Jeffery, J.; Le, T. P. T.; Mayadunne, R. T. A.; Meijs, G. F.; Moad, C. L.; Moad, G.; Rizzardo, E.; Thang, S. H. *Macromolecules* **1998,** 31, (16), 5559-5562.
12. Percec, V.; Popov, A. V.; Ramirez-Castillo, E.; Monteiro, M.; Barboiu, B.; Weichold, O.; Asandei, A. D.; Mitchell, C. M. *Journal of the American Chemical Society* **2002,** 124, (18), 4940-4941.
13. Tatemoto, M.; Nakagawa, T. US Patent No. US4158678 A, **1979**.
14. Lele, B. S.; Murata, H.; Matyjaszewski, K.; Russell, A. J. *Biomacromolecules* **2005,** 6, (6), 3380-3387.
15. Bontempo, D.; Maynard, H. D. *Journal of the American Chemical Society* **2005,** 127, (18), 6508-6509.
16. Konkolewicz, D.; Magenau, A. J. D.; Averick, S. E.; Simakova, A.; He, H.; Matyjaszewski, K. *Macromolecules* **2012,** 45, (11), 4461-4468.
17. Jiang, X.; Rosen, B. M.; Percec, V. *Journal of Polymer Science Part A: Polymer Chemistry* **2010,** 48, (12), 2716-2721.
18. Convertine, A. J.; Ayres, N.; Scales, C. W.; Lowe, A. B.; McCormick, C. L. *Biomacromolecules* **2004,** 5, (4), 1177-1180.

19. Ding, W.; Lv, C.; Sun, Y.; Luan, H.; Yu, T.; Qu, G. *Polymer Bulletin* **2011,** 67, (8), 1499-1505.

20. Anastasaki, A.; Haddleton, A. J.; Zhang, Q.; Simula, A.; Droesbeke, M.; Wilson, P.; Haddleton, D. M. *Macromolecular Rapid Communications* **2014,** 35, (10), 965-970.

21. Chaduc, I.; Crepet, A.; Boyron, O.; Charleux, B.; D'Agosto, F.; Lansalot, M. *Macromolecules* **2013,** 46, (15), 6013-6023.

22. Zhong, M.; Matyjaszewski, K. *Macromolecules* **2011,** 44, (8), 2668-2677.

23. Samanta, S. R.; Nikolaou, V.; Keller, S.; Monteiro, M. J.; Wilson, D. A.; Haddleton, D. M.; Percec, V. *Polymer Chemistry* **2015,** 6, (11), 2084-2097.

24. Odian, G. G., *Principles of Polymerization*. Wiley-Interscience: 2004.

25. Ma, L.; Tu, C.; Le, P.; Chitoor, S.; Lim, S. J.; Zahid, M. U.; Teng, K. W.; Ge, P.; Selvin, P. R.; Smith, A. M. *Journal of the American Chemical Society* **2016,** 138, (10), 3382-3394.

26. Knall, A.-C.; Slugovc, C. *Chemical Society Reviews* **2013,** 42, (12), 5131-5142.

27. Jia, Z.; Lonsdale, D. E.; Kulis, J.; Monteiro, M. J. *ACS Macro Letters* **2012,** 1, (6), 780-783.

28. Amir, F.; Hossain, M. D.; Jia, Z.; Monteiro, M. J. *Polymer Chemistry* **2016,** 7, (43), 6598-6607.

29. Yang, Q.; Lalevée, J.; Poly, J. *Macromolecules* **2016,** 49, (20), 7653-7666.

30. Lamson, M.; Kopeć, M.; Ding, H.; Zhong, M.; Matyjaszewski, K. *Journal of Polymer Science Part A: Polymer Chemistry* **2016,** 54, (13), 1961-1968.

31. Tang, W.; Tsarevsky, N. V.; Matyjaszewski, K. *Journal of the American Chemical Society* **2006,** 128, (5), 1598-1604.

32. Matyjaszewski, K. *Macromolecular Symposia* **1998,** 134, (1), 105-118.

33. Kickelbick, G.; Paik, H.-j.; Matyjaszewski, K. *Macromolecules* **1999,** 32, (9), 2941-2947.

34. Xue, Z.; He, D.; Xie, X. *Polymer Chemistry* **2015,** 6, (10), 1660-1687.

35. Matsubara, K.; Matsumoto, M. *Journal of Polymer Science Part A: Polymer Chemistry* **2006,** 44, (13), 4222-4228.

36. Maria, S.; Biedroń, T.; Poli, R.; Kubisa, P. *Journal of Applied Polymer Science* **2007,** 105, (1), 278-281.

37. Fischer, H. *Chemical Reviews* **2001,** 101, (12), 3581-3610.

38. Matyjaszewski, K.; Xia, J. *Chemical Reviews* **2001,** 101, (9), 2921-2990.

39. Elsen, A. M.; Burdyńska, J.; Park, S.; Matyjaszewski, K. *ACS Macro Letters* **2013,** 2, (9), 822-825.

40. Konkolewicz, D.; Schröder, K.; Buback, J.; Bernhard, S.; Matyjaszewski, K. *ACS Macro Letters* **2012,** 1, (10), 1219-1223.

41. Pan, X.; Malhotra, N.; Simakova, A.; Wang, Z.; Konkolewicz, D.; Matyjaszewski, K. *Journal of the American Chemical Society* **2015,** 137, (49), 15430-15433.

42. Rusen, E.; Mocanu, A. *Colloid and Polymer Science* **2013,** 291, (9), 2253-2257.

43. Sun, N.; Meng, X.; Xiao, Z. *Ceramics International* **2015,** 41, (10, Part A), 13830-13835.

44. Shen, Y.; Li, G.; Ma, Y.; Yu, D.; Sun, J.; Li, Z. *Soft Matter* **2015,** 11, (38), 7502-7506.

45. Kang, T.-H.; Lee, H.-i. *Bulletin of the Korean Chemical Society* **2016**, n/a-n/a.

46. McCarthy, P.; Chattopadhyay, M.; Millhauser, G. L.; Tsarevsky, N. V.; Bombalski, L.; Matyjaszewski, K.; Shimmin, D.; Avdalovic, N.; Pohl, C. *Analytical biochemistry* **2007,** 366, (1), 1-8.

47. Lin, W.; Nie, S.; Xiong, D.; Guo, X.; Wang, J.; Zhang, L. *Nanoscale Research Letters* **2014,** 9, (1), 243-243.

48. Krys, P.; Wang, Y.; Matyjaszewski, K.; Harrisson, S. *Macromolecules* **2016,** 49, (8), 2977-2984.

49. Lutz, J.-F.; Matyjaszewski, K. *Macromolecular Chemistry and Physics* **2002,** 203, (10-11), 1385-1395.

50. Treat, N. D.; Ayres, N.; Boyes, S. G.; Brittain, W. J. *Macromolecules* **2006,** 39, (1), 26-29.

51. Ullmann, F.; Bielecki, J. *Berichte der Deutschen Chemischen Gesellschaft* **1901,** 34, (2), 2174-2185.

52. Wayland, B. B.; Poszmik, G.; Mukerjee, S. L.; Fryd, M. *Journal of the American Chemical Society* **1994,** 116, (17), 7943-7944.

53. Percec, V.; Barboiu, B.; van der Sluis, M. *Macromolecules* **1998,** 31, (12), 4053-4056.

54. Percec, V.; Popov, A. V.; Ramirez-Castillo, E.; Weichold, O. *Journal of Polymer Science Part A: Polymer Chemistry* **2003,** 41, (21), 3283-3299.

55. Percec, V.; Guliashvili, T.; Ladislaw, J. S.; Wistrand, A.; Stjerndahl, A.; Sienkowska, M. J.; Monteiro, M. J.; Sahoo, S. *Journal of the American Chemical Society* **2006,** 128, (43), 14156-14165.

56. Sutin, N. *Accounts of Chemical Research* **1982,** 15, (9), 275-282.

57. Guliashvili, T.; Percec, V. *Journal of Polymer Science Part A: Polymer Chemistry* **2007,** 45, (9), 1607-1618.

58. Rosen, B. M.; Percec, V. *Journal of Polymer Science Part A: Polymer Chemistry* **2007,** 45, (21), 4950-4964.

59. Egorov, A. M.; Matyukhova, S. A.; Anisimov, A. V. *International Journal of Chemical Kinetics* **2005,** 37, (8), 496-501.

60. Lligadas, G.; Rosen, B. M.; Bell, C. A.; Monteiro, M. J.; Percec, V. *Macromolecules* **2008,** 41, (22), 8365-8371.

61. Egorov, A. M.; Matyukhova, S. A. *International Journal of Chemical Kinetics* **2007,** 39, (10), 547-555.

62. Nguyen, N. H.; Levere, M. E.; Percec, V. *Journal of Polymer Science Part A: Polymer Chemistry* **2012,** 50, (5), 860-873.

63. Lligadas, G.; Percec, V. *Journal of Polymer Science Part A: Polymer Chemistry* **2008,** 46, (10), 3174-3181.

64. Zhang, Q.; Wilson, P.; Li, Z.; McHale, R.; Godfrey, J.; Anastasaki, A.; Waldron, C.; Haddleton, D. M. *Journal of the American Chemical Society* **2013,** 135, (19), 7355-7363.

65. Zhang, Q.; Li, Z.; Wilson, P.; Haddleton, D. M. *Chemical Communications* **2013,** 49, (59), 6608-6610.

66. Zhang, Q.; Li, M.; Zhu, C.; Nurumbetov, G.; Li, Z.; Wilson, P.; Kempe, K.; Haddleton, D. M. *Journal of the American Chemical Society* **2015,** 137, (29), 9344-9353.

67. Garcia, M.; Beecham, M. P.; Kempe, K.; Haddleton, D. M.; Khan, A.; Marsh, A. *European Polymer Journal* **2015,** 66, 444-451.

68. Bertrand, O.; Ernould, B.; Boujioui, F.; Vlad, A.; Gohy, J.-F. *Polymer Chemistry* **2015,** 6, (33), 6067-6072.

69. Kean, Z. S.; Black Ramirez, A. L.; Craig, S. L. *Journal of Polymer Science. Part B, Polymer physics* **2012,** 50, (17), 3481-3484.

70. Basuki, J. S.; Esser, L.; Duong, H. T. T.; Zhang, Q.; Wilson, P.; Whittaker, M. R.; Haddleton, D. M.; Boyer, C.; Davis, T. P. *Chemical Science* **2014,** 5, (2), 715-726.

71. Fan, L.; Chen, H.; Hao, Z.; Tan, Z. *Journal of Polymer Science Part A: Polymer Chemistry* **2013,** 51, (2), 457-462.

72. Anastasaki, A.; Nikolaou, V.; Nurumbetov, G.; Wilson, P.; Kempe, K.; Quinn, J. F.; Davis, T. P.; Whittaker, M. R.; Haddleton, D. M. *Chemical Reviews* **2016,** 116, (3), 835-877.

73. Anastasaki, A.; Nikolaou, V.; Haddleton, D. M. *Polymer Chemistry* **2016,** 7, (5), 1002-1026.

74. Nguyen, N. H.; Rosen, B. M.; Lligadas, G.; Percec, V. *Macromolecules* **2009,** 42, (7), 2379-2386.

75. Zhang, Q.; Anastasaki, A.; Li, G.-Z.; Haddleton, A. J.; Wilson, P.; Haddleton, D. M. *Polymer Chemistry* **2014,** 5, (12), 3876-3883.

76. Nguyen, N. H.; Rodriguez-Emmenegger, C.; Brynda, E.; Sedlakova, Z.; Percec, V. *Polymer Chemistry* **2013,** 4, (8), 2424-2427.

77. Lligadas, G.; Ladislaw, J. S.; Guliashvili, T.; Percec, V. *Journal of Polymer Science Part A: Polymer Chemistry* **2008,** 46, (1), 278-288.

78. Wright, P. M.; Mantovani, G.; Haddleton, D. M. *Journal of Polymer Science Part A: Polymer Chemistry* **2008,** 46, (22), 7376-7385.

79. Wang, G.-X.; Lu, M.; Hou, Z.-H.; Li, J.; Zhong, M.; Wu, H. *Journal of Polymer Science Part A: Polymer Chemistry* **2013,** 51, (13), 2919-2924.

80. Liu, X.-H.; Yu, Y.-H.; Jia, D.; Cheng, B.-W.; Zhang, F.-J.; Li, H.-N.; Chen, P.; Xie, S. *Journal of Polymer Science Part A: Polymer Chemistry* **2013,** 51, (7), 1559-1564.

81. Zhang, J.; Hao, Z.; Chen, H. *Journal of Polymer Science Part A: Polymer Chemistry* **2013,** 51, (16), 3323-3327.

82. Percec, V. WO Patent No. WO2008019100 A3, **2008**.

83. Grigoras, C.; Percec, V. *Journal of Polymer Science Part A: Polymer Chemistry* **2005,** 43, (2), 319-330.

84. Nguyen, N. H.; Percec, V. *Journal of Polymer Science Part A: Polymer Chemistry* **2011,** 49, (19), 4241-4252.

85. Jiang, X.; Rosen, B. M.; Percec, V. *Journal of Polymer Science Part A: Polymer Chemistry* **2010,** 48, (2), 403-409.

86. Waldron, C.; Zhang, Q.; Li, Z.; Nikolaou, V.; Nurumbetov, G.; Godfrey, J.; McHale, R.; Yilmaz, G.; Randev, R. K.; Girault, M.; McEwan, K.; Haddleton, D. M.; Droesbeke, M.; Haddleton, A. J.; Wilson, P.; Simula, A.; Collins, J.; Lloyd, D. J.; Burns, J. A.; Summers, C.; Houben, C.; Anastasaki, A.; Li, M.; Becer, C. R.; Kiviaho, J. K.; Risangud, N. *Polymer Chemistry* **2014,** 5, (1), 57-61.

87. Ma, J.; Chen, H.; Zhang, M.; Yu, M. *Journal of Polymer Science Part A: Polymer Chemistry* **2012,** 50, (3), 609-613.

88. Zhang, Y.; Wang, Y.; Matyjaszewski, K. *Macromolecules* **2011,** 44, (4), 683-685.

89. Lin, C. Y.; Coote, M. L.; Gennaro, A.; Matyjaszewski, K. *Journal of the American Chemical Society* **2008,** 130, (38), 12762-12774.

90. Peng, C.-H.; Zhong, M.; Wang, Y.; Kwak, Y.; Zhang, Y.; Zhu, W.; Tonge, M.; Buback, J.; Park, S.; Krys, P. *Macromolecules* **2013,** 46, (10), 3803-3815.

91. Bortolamei, N.; Isse, A. A.; Magenau, A. J.; Gennaro, A.; Matyjaszewski, K. *Angewandte Chemie* **2011,** 123, (48), 11593-11596.

92. Tsarevsky, N. V.; Braunecker, W. A.; Matyjaszewski, K. *Journal of Organometallic Chemistry* **2007,** 692, (15), 3212-3222.

93. Konkolewicz, D.; Krys, P.; Góis, J. R.; Mendonça, P. V.; Zhong, M.; Wang, Y.; Gennaro, A.; Isse, A. A.; Fantin, M.; Matyjaszewski, K. *Macromolecules* **2014,** 47, (2), 560-570.

94. Rosen, B. M.; Jiang, X.; Wilson, C. J.; Nguyen, N. H.; Monteiro, M. J.; Percec, V. *Journal of Polymer Science Part A: Polymer Chemistry* **2009,** 47, (21), 5606-5628.

95. Jakubowski, W.; Kirci-Denizli, B.; Gil, R. R.; Matyjaszewski, K. *Macromolecular Chemistry and Physics* **2008,** 209, (1), 32-39.

96. Raut, J. S.; Fichthorn, K. A. *The Journal of Chemical Physics* **1998,** 108, (4), 1626-1635.

97. Kolb, H. C.; Finn, M. G.; Sharpless, K. B. *Angewandte Chemie International Edition* **2001,** 40, (11), 2004-2021.

98. Tornøe, C. W.; Christensen, C.; Meldal, M. *The Journal of Organic Chemistry* **2002,** 67, (9), 3057-3064.

99. Lligadas, G.; Percec, V. *Journal of Polymer Science Part A: Polymer Chemistry* **2007,** 45, (20), 4684-4695.

100. Ionescu, M.; Radojčić, D.; Wan, X.; Petrović, Z. S.; Upshaw, T. A. *European Polymer Journal* **2015,** 67, 439-448.

101. Pramanik, N. B.; Nando, G. B.; Singha, N. K. *Polymer* **2015,** 69, 349-356.

102. Weseliński, Ł. J.; Grillo, M. J.; Tanasova, M. *Tetrahedron Letters* **2016,** 57, (40), 4477-4479.

103. Chelushkin, P. S.; Leko, M. V.; Dorosh, M. Y.; Burov, S. V. *Journal of Peptide Science* **2016**, n/a-n/a.

104. Cavallo, G.; Al Ouahabi, A.; Oswald, L.; Charles, L.; Lutz, J.-F. *Journal of the American Chemical Society* **2016,** 138, (30), 9417-9420.

105. Gandavarapu, N. R.; Azagarsamy, M. A.; Anseth, K. S. *Advanced Materials* **2014,** 26, (16), 2521-2526.

106. Ledin, P. A.; Kolishetti, N.; Boons, G.-J. *Macromolecules* **2013,** 46, (19), 7759-7768.

107. Roling, O.; De Bruycker, K.; Vonhören, B.; Stricker, L.; Körsgen, M.; Arlinghaus, H. F.; Ravoo, B. J.; Du Prez, F. E. *Angewandte Chemie* **2015,** 127, (44), 13319-13323.

108. Arumugam, S.; Popik, V. V. *The Journal of Organic Chemistry* **2014,** 79, (6), 2702-2708.

109. Garcia-Astrain, C.; Gandini, A.; Pena, C.; Algar, I.; Eceiza, A.; Corcuera, M.; Gabilondo, N. *RSC Advances* **2014,** 4, (67), 35578-35587.

110. Presolski, S. I.; Mamidyala, S. K.; Manzenrieder, F.; Finn, M. G. *ACS Combinatorial Science* **2012,** 14, (10), 527-530.

111. Zhang, Q.; Su, H.; Luo, J.; Wei, Y. *Catalysis Science & Technology* **2013,** 3, (1), 235-243.

112. Lu, D.; Hossain, M. D.; Jia, Z.; Monteiro, M. J. *Macromolecules* **2015,** 48, (6), 1688-1702.

113. Lonsdale, D. E.; Monteiro, M. J. *Chemical Communications* **2010,** 46, (42), 7945-7947.

114. Zhang, S.; Zhao, Y. *Macromolecules* **2010,** 43, (9), 4020-4022.

115. Brennan, J. L.; Hatzakis, N. S.; Tshikhudo, T. R.; Razumas, V.; Patkar, S.; Vind, J.; Svendsen, A.; Nolte, R. J. M.; Rowan, A. E.; Brust, M. *Bioconjugate Chemistry* **2006,** 17, (6), 1373-1375.

116. Li, Y.; Benicewicz, B. C. *Macromolecules* **2008,** 41, (21), 7986-7992.

117. Campidelli, S.; Ballesteros, B.; Filoramo, A.; Díaz, D. D.; de la Torre, G.; Torres, T.; Rahman, G. M. A.; Ehli, C.; Kiessling, D.; Werner, F.; Sgobba, V.; Guldi, D. M.; Cioffi, C.; Prato, M.; Bourgoin, J.-P. *Journal of the American Chemical Society* **2008,** 130, (34), 11503-11509.

118. van Dongen, S. F. M.; Nallani, M.; Schoffelen, S.; Cornelissen, J. J. L. M.; Nolte, R. J. M.; van Hest, J. C. M. *Macromolecular Rapid Communications* **2008,** 29, (4), 321-325.

119. Breed, D. R.; Thibault, R.; Xie, F.; Wang, Q.; Hawker, C. J.; Pine, D. J. *Langmuir* **2009,** 25, (8), 4370-4376.

120. Xu, X.; Daniel, W. L.; Wei, W.; Mirkin, C. A. *Small* **2010,** 6, (5), 623-626.

121. Billiet, S.; De Bruycker, K.; Driessen, F.; Goossens, H.; Van Speybroeck, V.; Winne, J. M.; Du Prez, F. E. *Nat Chem* **2014,** 6, (9), 815-821.

122. Jia, Z.; Bell, C. A.; Monteiro, M. J. *Chemical Communications* **2011,** 47, (14), 4165-4167.

123. Theeramunkong, S.; Galli, U.; Grolla, A. A.; Caldarelli, A.; Travelli, C.; Massarotti, A.; Troiani, M. P.; Alisi, M. A.; Orsomando, G.; Genazzani, A. A.; Tron, G. C. *MedChemComm* **2015,** 6, (10), 1891-1897.

124. Du, J.-Z.; Du, X.-J.; Mao, C.-Q.; Wang, J. *Journal of the American Chemical Society* **2011,** 133, (44), 17560-17563.

125. Horne, W. S.; Olsen, C. A.; Beierle, J. M.; Montero, A.; Ghadiri, M. R. *Angewandte Chemie International Edition* **2009,** 48, (26), 4718-4724.

126. Montagnat, O. D.; Lessene, G.; Hughes, A. B. *Tetrahedron Letters* **2006,** 47, (39), 6971-6974.

127. Bach, L. G.; Islam, M. R.; Lee, D. C.; Lim, K. T. *Applied Surface Science* **2013,** 283, 546-553.

128. Li, Z.-B.; Wu, Z.; Chen, K.; Chin, F. T.; Chen, X. *Bioconjugate Chemistry* **2007,** 18, (6), 1987-1994.

129. Ringot, C.; Sol, V.; Granet, R.; Krausz, P. *Materials Letters* **2009,** 63, (21), 1889-1891.

130. DeForest, C. A.; Polizzotti, B. D.; Anseth, K. S. *Nat Mater* **2009,** 8, (8), 659-664.

131. Dimroth, O. *Berichte der Deutschen Chemischen Gesellschaft* **1902,** 35, (1), 1029-1038.

132. Huisgen, R. *Angewandte Chemie International Edition in English* **1963,** 2, (10), 565-598.

133. Rostovtsev, V. V.; Green, L. G.; Fokin, V. V.; Sharpless, K. B. *Angewandte Chemie* **2002,** 114, (14), 2708-2711.

134. Ahlquist, M.; Fokin, V. V. *Organometallics* **2007,** 26, (18), 4389-4391.

135. Jin, L.; Tolentino, D. R.; Melaimi, M.; Bertrand, G. *Science Advances* **2015,** 1, (5).

136. Nurmi, L.; Lindqvist, J.; Randev, R.; Syrett, J.; Haddleton, D. M. *Chemical Communications* **2009**, (19), 2727-2729.

137. Tishinov, K.; Fei, N.; Gillingham, D. *Chemical Science* **2013,** 4, (12), 4401-4406.

138. Kumar, A.; Li, K.; Cai, C. *Chemical Communications* **2011,** 47, (11), 3186-3188.

139. Houghton, E. A.; Nicholas, K. M. *JBIC Journal of Biological Inorganic Chemistry* **2009,** 14, (2), 243-251.

140. Wendeln, C.; Singh, I.; Rinnen, S.; Schulz, C.; Arlinghaus, H. F.; Burley, G. A.; Ravoo, B. J. *Chemical Science* **2012,** 3, (8), 2479-2484.

141. Villalba, M.; Bossi, M.; Pozo, M. d.; Calvo, E. J. *Langmuir* **2016,** 32, (27), 6836-6842.

142. Fernandes, A. E.; Jonas, A. M.; Riant, O. *Tetrahedron* **2014,** 70, (9), 1709-1731.

143. Dordelmann, G.; Meinhardt, T.; Sowik, T.; Krueger, A.; Schatzschneider, U. *Chemical Communications* **2012,** 48, (94), 11528-11530.

144. Crescenzi, V.; Cornelio, L.; Di Meo, C.; Nardecchia, S.; Lamanna, R. *Biomacromolecules* **2007,** 8, (6), 1844-1850.

145. Rachel, N. M.; Pelletier, J. N. *Chemical Communications* **2016,** 52, (12), 2541-2544.

146. Iddon, L.; Leyton, J.; Indrevoll, B.; Glaser, M.; Robins, E. G.; George, A. J. T.; Cuthbertson, A.; Luthra, S. K.; Aboagye, E. O. *Bioorganic & Medicinal Chemistry Letters* **2011,** 21, (10), 3122-3127.

147. Wenn, B.; Conradi, M.; Carreiras, A. D.; Haddleton, D. M.; Junkers, T. *Polymer Chemistry* **2014,** 5, (8), 3053-3060.

148. Xuan, J.; Han, D.; Xia, H.; Zhao, Y. *Langmuir* **2014,** 30, (1), 410-417.

149. Li, X.; Jiang, Y.; Shuai, L.; Wang, L.; Meng, L.; Mu, X. *Journal of Materials Chemistry* **2012,** 22, (4), 1283-1289.

150. Zaremski, M. Y.; Kalugin, D. I.; Golubev, V. B. *Polymer Science Series A* **2009,** 51, (1), 103-122.

151. O'Shea, J.-P.; Solovyeva, V.; Guo, X.; Zhao, J.; Hadjichristidis, N.; Rodionov, V. O. *Polymer Chemistry* **2014,** 5, (3), 698-701.

152. Choi, J.; Hui, C. M.; Pietrasik, J.; Dong, H.; Matyjaszewski, K.; Bockstaller, M. R. *Soft Matter* **2012,** 8, (15), 4072-4082.

153. Truong, N. P.; Gu, W.; Prasadam, I.; Jia, Z.; Crawford, R.; Xiao, Y.; Monteiro, M. J. *Nature Communications* **2013,** 4, 1902.

154. Lonsdale, D. E.; Bell, C. A.; Monteiro, M. J. *Macromolecules* **2010,** 43, (7), 3331-3339.

155. Whittaker, M. R.; Urbani, C. N.; Monteiro, M. J. *Journal of the American Chemical Society* **2006,** 128, (35), 11360-11361.

156. Blencowe, A.; Tan, J. F.; Goh, T. K.; Qiao, G. G. *Polymer* **2009,** 50, (1), 5-32.

157. Neugebauer, D.; Zhang, Y.; Pakula, T.; Sheiko, S. S.; Matyjaszewski, K. *Macromolecules* **2003,** 36, (18), 6746-6755.

158. Zou, J.; Yu, Y.; Li, Y.; Ji, W.; Chen, C.-K.; Law, W.-C.; Prasad, P. N.; Cheng, C. *Biomaterials Science* **2015,** 3, (7), 1078-1084.

159. Tomikawa, Y.; Fukata, H.; Ko, Y. S.; Yamamoto, T.; Tezuka, Y. *Macromolecules* **2014,** 47, (23), 8214-8223.

160. Sugai, N.; Heguri, H.; Ohta, K.; Meng, Q.; Yamamoto, T.; Tezuka, Y. *Journal of the American Chemical Society* **2010,** 132, (42), 14790-14802.

161. Hossain, M. D.; Jia, Z.; Monteiro, M. J. *Macromolecules* **2014,** 47, (15), 4955-4970.

162. Hedrick, J. L.; Trollsås, M.; Hawker, C. J.; Atthoff, B.; Claesson, H.; Heise, A.; Miller, R. D.; Mecerreyes, D.; Jérôme, R.; Dubois, P. *Macromolecules* **1998,** 31, (25), 8691-8705.

163. Cao, P.-F.; Mangadlao, J. D.; de Leon, A.; Su, Z.; Advincula, R. C. *Macromolecules* **2015,** 48, (12), 3825-3833.

164. Barran, P. E.; Cole, H. L.; Goldup, S. M.; Leigh, D. A.; McGonigal, P. R.; Symes, M. D.; Wu, J.; Zengerle, M. *Angewandte Chemie International Edition* **2011,** 50, (51), 12280-12284.

165. Wang, K.; Yee, C.-C.; Au-Yeung, H. Y. *Chemical Science* **2016,** 7, (4), 2787-2792.

166. Mock, W. L.; Irra, T. A.; Wepsiec, J. P.; Adhya, M. *The Journal of Organic Chemistry* **1989,** 54, (22), 5302-5308.

167. Kharkar, P. M.; Rehmann, M. S.; Skeens, K. M.; Maverakis, E.; Kloxin, A. M. *ACS Biomaterials Science & Engineering* **2016,** 2, (2), 165-179.

168. Zhang, K.; Tew, G. N. *Reactive and Functional Polymers* **2014,** 80, 40-47.

169. Martin, K. L.; Nyquist, Y.; Burnett, E. K.; Briseno, A. L.; Carter, K. R. *ACS Applied Materials & Interfaces* **2016,** 8, (44), 30543-30551.

170. Hassan, W.; Dong, Y.; Wang, W. *Stem Cell Research & Therapy* **2013,** 4, (2), 32.

171. Yiming, L.; Kai Liang, R.; Hofmann, H. F.; Qiming, Z. *IEEE Transactions on Ultrasonics, Ferroelectrics, and Frequency Control* **2005,** 52, (12), 2411-2417.

172. Varga, Z.; Filipcsei, G.; Zrínyi, M. *Polymer* **2006,** 47, (1), 227-233.

173. Qiu, X.-P.; Winnik, F. M. *Macromolecular Symposia* **2009,** 278, (1), 10-13.

174. Murthy, N.; Robichaud, J. R.; Tirrell, D. A.; Stayton, P. S.; Hoffman, A. S. *Journal of Controlled Release* **1999,** 61, (1–2), 137-143.

175. Jiang, X.; Lavender, C. A.; Woodcock, J. W.; Zhao, B. *Macromolecules* **2008,** 41, (7), 2632-2643.

176. Xu, Y.; Bolisetty, S.; Drechsler, M.; Fang, B.; Yuan, J.; Ballauff, M.; Müller, A. H. E. *Polymer* **2008,** 49, (18), 3957-3964.

177. Sheiko, S. S.; Sun, F. C.; Randall, A.; Shirvanyants, D.; Rubinstein, M.; Lee, H.-i.; Matyjaszewski, K. *Nature* **2006,** 440, (7081), 191-194.

178. Zareie, H. M.; Volga Bulmus, E.; Gunning, A. P.; Hoffman, A. S.; Piskin, E.; Morris, V. J. *Polymer* **2000,** 41, (18), 6723-6727.

179. Mandelbrot, B. B.; Passoja, D. E.; Paullay, A. J. **1984**.

180. Planck, M. *Annalen der Physik* **1901,** 309, (3), 553-563.

181. Novoselov, K.; Geim, A. K.; Morozov, S.; Jiang, D.; Katsnelson, M.; Grigorieva, I.; Dubonos, S.; Firsov, A. *nature* **2005,** 438, (7065), 197-200.

182. Clarson, S. J.; Dodgson, K.; Semlyen, J. A. *Polymer* **1985,** 26, (6), 930-934.

183. Guo, L.; Zhang, D. *Journal of the American Chemical Society* **2009,** 131, (50), 18072-18074.

184. Zhu, X.; Zhou, N.; Zhang, Z.; Sun, B.; Yang, Y.; Zhu, J.; Zhu, X. *Angewandte Chemie International Edition* **2011,** 50, (29), 6615-6618.

185. Yamamoto, T.; Tezuka, Y. *Soft Matter* **2015,** 11, (38), 7458-7468.

186. Shin, E. J.; Jeong, W.; Brown, H. A.; Koo, B. J.; Hedrick, J. L.; Waymouth, R. M. *Macromolecules* **2011,** 44, (8), 2773-2779.

187. McLeish, T. *Science* **2002,** 297, (5589), 2005-2006.

188. Chen, B.; Jerger, K.; Fréchet, J. M. J.; Szoka Jr, F. C. *Journal of Controlled Release* **2009,** 140, (3), 203-209.

189. Hossain, M. D.; Lu, D.; Jia, Z.; Monteiro, M. J. *ACS Macro Letters* **2014,** 3, (12), 1254-1257.

190. Cao, P.-F.; Mangadlao, J.; Advincula, R. *Angewandte Chemie International Edition* **2015,** 54, (17), 5127-5131.

191. Dedeoglu, T.; Durmaz, H.; Hizal, G.; Tunca, U. *Journal of Polymer Science Part A: Polymer Chemistry* **2012,** 50, (10), 1917-1925.

192. Oike, H.; Uchibori, A.; Tsuchitani, A.; Kim, H.-K.; Tezuka, Y. *Macromolecules* **2004,** 37, (20), 7595-7601.

193. Li, M.; Liu, C.; Hong, C.-Y.; Pan, C.-Y. *Polymer* **2015,** 71, 23-30.

194. Bunha, A.; Tria, M. C.; Advincula, R. *Chemical Communications* **2011,** 47, (32), 9173-9175.

195. Harada, A.; Hashidzume, A.; Yamaguchi, H.; Takashima, Y. *Chemical Reviews* **2009,** 109, (11), 5974-6023.

196. Jacobson, H.; Stockmayer, W. H. *The Journal of Chemical Physics* **1950,** 18, (12), 1600-1606.

197. Brown, J. F.; Slusarczuk, G. M. J. *Journal of the American Chemical Society* **1965,** 87, (4), 931-932.

198. Boydston, A. J.; Xia, Y.; Kornfield, J. A.; Gorodetskaya, I. A.; Grubbs, R. H. *Journal of the American Chemical Society* **2008,** 130, (38), 12775-12782.

199. Kudo, H.; Sato, M.; Wakai, R.; Iwamoto, T.; Nishikubo, T. *Macromolecules* **2008,** 41, (3), 521-523.

200. Geiser, D.; Höcker, H. *Macromolecules* **1980,** 13, (3), 653-656.

201. Hild, G.; Kohler, A.; Rempp, P. *European Polymer Journal* **1980,** 16, (6), 525-527.

202. Vollmert, B.; Huang, J.-x. *Die Makromolekulare Chemie, Rapid Communications* **1980,** 1, (5), 333-339.

203. Oike, H.; Imaizumi, H.; Mouri, T.; Yoshioka, Y.; Uchibori, A.; Tezuka, Y. *Journal of the American Chemical Society* **2000,** 122, (40), 9592-9599.

204. Rique-Lurbet, L.; Schappacher, M.; Deffieux, A. *Macromolecules* **1994,** 27, (22), 6318-6324.

205. Roovers, J. *Polymer* **1979,** 20, (7), 843-849.

206. Lonsdale, D. E.; Monteiro, M. J. *Journal of Polymer Science Part A: Polymer Chemistry* **2010,** 48, (20), 4496-4503.

207. Huber, D.; Heller, E. J.; Littlejohn, R. G. *The Journal of Chemical Physics* **1988,** 89, (4), 2003-2014.

208. Flynn, J. R. *Psychological Bulletin* **1987,** 101, (2), 171-191.

209. Bardeen, J. M.; Bond, J.; Kaiser, N.; Szalay, A. *The Astrophysical Journal* **1986,** 304, 15-61.

210. Schrenk, K. J.; Araújo, N. A. M.; Herrmann, H. J. *Physical Review E* **2011,** 84, (4), 041136.

211. Raphael, B.; Ben, F. *Journal of High Energy Physics* **2007,** 2007, (06), 018.

212. Kulis, J.; Bell, C. A.; Micallef, A. S.; Jia, Z.; Monteiro, M. J. *Macromolecules* **2009,** 42, (21), 8218-8227.

213. Teraoka, I., Polymer solutions: an introduction to physical properties. 2002. Wiley-Interscience.

214. Kok, C. M.; Rudin, A. *Die Makromolekulare Chemie, Rapid Communications* **1981,** 2, (11), 655-659.

215. Hadziioannou, G.; Cotts, P. M.; ten Brinke, G.; Han, C. C.; Lutz, P.; Strazielle, C.; Rempp, P.; Kovacs, A. J. *Macromolecules* **1987,** 20, (3), 493-497.

216. Gibson, M. I.; O'Reilly, R. K. *Chemical society reviews* **2013,** 42, (17), 7204-7213.

217. Sudo, Y.; Sakai, H.; Nabae, Y.; Hayakawa, T.; Kakimoto, M.-a. *Polymer* **2015,** 70, 307-314.

218. Gui, R.; Wang, Y.; Sun, J. *Colloids and Surfaces B: Biointerfaces* **2014,** 116, 518-525.

Chapter 2

Derivation of the Molecular Weight Distributions from Size Exclusion Chromatography and Log-Normal Distribution Simulation

Size exclusion chromatography (SEC) is one of the most used analytical methods in chemistry to determine the molecular weight distribution of macromolecules, including natural and synthetic polymers. With the advent of 'living' radical polymerization, researchers now have the capability to produce polymers with a wide range of chemical compositions and architectures. In many cases, SEC is the only method available for analysis of the polymer. The shape of an SEC curve can give information on polymer purity. In this chapter, we provide a derivation of the three molecular weight distributions from the raw concentration detector response data and use obtained parameters in Log-Normal Distribution (LND) simulation of cyclic PSTY. The derivations of MWD parameters are given in an easy to follow procedure. A method is derived to determine the molecular weight averages from the SEC data. Two case studies are then provided to demonstrate the insight that SEC can provide into the types of polymer species, and unlock mechanistic information from the SEC traces that may otherwise be overlooked. An additional example of LND simulation demonstrates the utility of the method in determining polymer purity in mixtures of two or more polymer species.

2.1. Introduction

Polymer chemistry has evolved rapidly over the past few decades, especially with the discovery of 'living' radical polymerization (LRP)[1-5] to make polymer with narrow molecular weight distributions (MWDs) and near quantitative 'click' coupling reactions.[6-8] Synthesis of complex polymer architectures formed by coupling well-defined linear polymer building blocks together has led to the production of well-defined stars,[9] dendrimers,[10-13] hyperbranched polymers,[14] multiblock copolymers,[15] cyclic[16-19] and many other structures. Characterization of such complex structures becomes increasingly more difficult due the increase in molecular weight upon its formation, leading to less than accurate NMR or MALDI spectra. Size exclusion chromatography (SEC) then becomes the only remaining method for analysis. It should be noted that many early texts and publications use the notation 'gel permeation chromatography (GPC)'. For polymers made by LRP, most publications provide the number-average molecular weight (M_n) and the dispersity Đ as a function of conversion (see Fig. 2.1A).

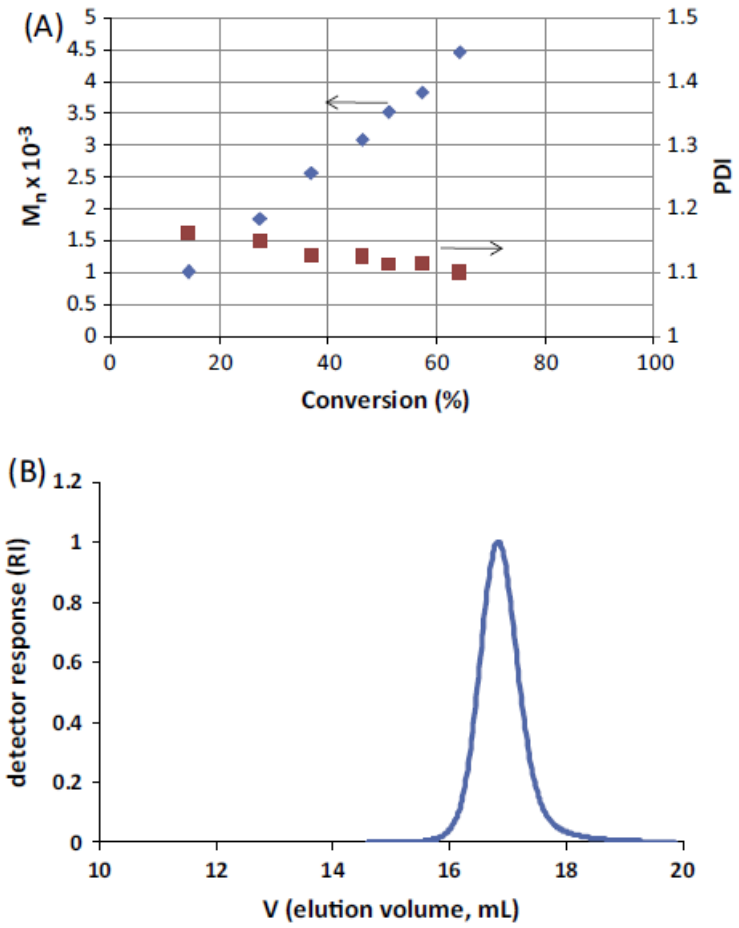

Figure 2.1. SEC data for the LRP of styrene. (A) M_n and Đ *vs* conversion, (B) an example of detector response (normalized) *vs* elution volume (*V*).

In addition, many publications illustrate the MWD using a plot of the normalized refractive index detector response (*RI*) *vs* elution volume (*V*) (Fig. 2.1B). This data is readily available from the SEC software. However, taken together the data is underutilized, and some meaningful insight into the formation of the product is overlooked. For, example it may be useful to determine the quantity of polymer species formed through side reactions (e.g. bimolecular radical termination and transfer reactions) and the polymer of interest in an LRP, or more importantly, if a macro chain transfer agent (CTA) is used, how much was consumed to make higher molecular weight or block copolymers.

In addition, chain ends of the linear polymers made by LRP are often used for further conjugational chemistry, e.g. cyclization reactions.[17, 19] For a cyclic polymer it is important to determine the amount of unreacted starting linear polymer or formed multiblock species as such impurities can significantly affect physical properties of the polymer.[20] This can be done using two parameter LND simulation through conversion of M_n and Đ derived from raw SEC response to

mean $\bar{M}$ and variance σ^2 of the Gaussian function respectively. The function can be used to separate broad or multimodal SEC distributions into individual polymer species.

The aim of this chapter was to present a clear and easy to follow guide for deriving the molecular weight distributions that provide a meaningful analysis of the polymer product and to use the obtained parameters for LND simulation of cyclic PSTY. The three most general MWDs were derived and presented so that researchers can easily and accurately produce any MWD from the raw *RI* detector response *vs V* data, and from this data determine the number average molecular weight (M_n), weight average molecular weight (M_w) and Đ. M_n and Đ were further used to calculate mean and variance of the Gaussian distribution. The importance of the Gaussian fit was demonstrated for the characterization of cyclic PSTY. This understanding will hopefully fully utilize the information obtained from the SEC instrument. In this work, only the refractive index detection was discussed for polystyrene (PSTY) as this is the simplest case for SEC; in addition, PSTY standards were used to calibrate the system. The nomenclature and derivations given by Shortt were closely followed,[21] and an example of scaling MWDs to conversion or weight for a LRP was also given. In addition, the effect of the calibration curve on the MWD was illustrated, especially where the slope of the calibration curve is non-linear which is required to convert the log-weight to a weight distribution.

2.1.1. Aim of the Chapter

The aim of the work in this chapter is to demonstrate the importance of proper interpretation of SEC data by deriving MWD parameters of polymers made by LRP taking into account the slope of the calibration curve. M_n, M_w and Đ were derived from raw GPC data and further used for LND simulation of cyclic polymers. It was shown that even seemingly insignificant changes in Gaussian shape can be caused by considerable amount of impurities. Therefore, we propose an easy-to-follow Gaussian simulation as a general analytical procedure for GPC data interpretation.

2.2. Experimental

2.2.1. Materials

The following solvents, materials and reagents were used as received unless otherwise stated: tetrahydrofuran (THF, HPLC grade, Lichrosolv, 99.8%), toluene (HPLC, LABSCAN, 99.8%), dichloromethane (DCM, Labscan, AR grade), N,N-dimethylformamide (DMF: Labscan, AR grade), dichloromethane (DCM, Labscan, AR grade), milli-Q water (Biolab, resistivity at 25 °C: 18.2 MΩ·cm), petroleum spirit (BR 40−60 °C, Univar, AR grade), ethyl acetate (EtOAc: ChemSupply, AR grade), anhydrous methanol (MeOH: Mallinckrodt, 99.9 %, HPLC grade), carbondisulfide

(Alrich, 99%), 1-butanethiol (Alrich, 99%), methyl bromopropionate (Alrich, 98%), triethylamine (TEA: Fluka, 98%), styrene (STY: Aldrich, >99%), DOWEX ion-exchange resin (Aldrich, 50WX8-200), anhydrous magnesium sulphate ($MgSO_4$: Scharlau, extra pure), silica gel 60 (230 – 400 mesh ATM (SDS)), TLC plates (silica gel 60 F254), activated basic alumina (Aldrich: Brockmann I, standard grade, ~ 150 mesh, 58 Å), 2,2-azobis(isobutyrylnitrile) (AIBN: Riedel-de Haën, 98 %) was recrystallized from methanol before use. 2-bromoisobutyryl bromide (BIB: Aldrich, 98 %), p-toluenesulfonyl chloride (Aldrich, ≥ 98 %), sodium azide (NaN_3: Aldrich, ≥ 99.5 %), 1,1,1-(trihydroxymethyl) ethane (Aldrich, 96%) sodium chloride (Univar, 99.9%), sodium hydride (Aldrich, 60 wt% in mineral oil), propargyl bromide (Aldrich, 80 wt % in toluene), triethylamine (TEA, Fluka, purum), *N,N,N',N',N''*-pentamethyldiethylenetriamine (PMDETA: Aldrich, 99 %), copper (II) bromide ($CuBr_2$: Aldrich, 99 %). Cu(I)Br and $CuBr_2$/PMDETA complexes were synthesized according to literature (see section 6.2.1).

2.2.2. Synthetic Procedures

2.2.2.1. Synthesis of Chain Transfer Agent, Methyl 2- (butylthiocarbonothioylthio) propanoate (MCEBTTC)

Carbondisulfide (3.1 mL, 0.051 mol) solution in dichloromethane (50 mL) was added dropwise to a stirred solution of 1- butanethiol (5 mL, 0.047 mol) and triethylamine (7.2 mL, 0.051 mol) in dichloromethane (25 mL) over a period of 30 min at 0 $^{\circ}$C under an argon atmosphere. The solution gradually turned yellow during the addition. After completing the addition, the solution was stirred at room temperature for 30 min. Methyl 2- bromopropionate (5.7 mL, 0.051 mol) in dichloromethane (25 mL) was then added dropwise over a period of 30 min and the solution stirred for 2 h. DCM was removed under nitrogen and the residue was dissolved in diethyl ether. The solution was washed with cold 10% HCl solution (3×50 mL) and then dried over anhydrous $MgSO_4$. Ether was removed under vacuum, and the residual yellow oil was purified by column chromatography (19:1 petroleum ether/ethyl acetate on silica, second band). ^{1}H NMR spectrum of MCEBTTC. ^{1}H NMR (300 MHz, $CDCl_3$): A) δ = 4.80 (quad, *J*= 7.4 Hz, 1H, CH), B) δ = 3.72 (s, 3H, CH_3), C) δ = 3.34 (tr, *J*= 7.4 Hz, 2H, CH_2), D) δ = 1.66 (quin, *J*= 7.4 Hz, 2H, CH_2), E) δ = 1.57 (d, *J*= 7.4 Hz, 3H, CH_3), F) δ = 1.40 (mult, *J*= 7.4 Hz, 2H, CH_2), G) δ = 0.90 (tr, *J*= 7.4 Hz, 3H, CH_3).

2.2.2.2. RAFT polymerization of styrene

Polymerization was carried out in a 10 mL dry Schlenk flask equipped with a magnetic stirrer. RAFT agent (0.158 g, $6.2 \cdot 10^{-4}$ mol) and AIBN (0.0103 g, $6.2 \cdot 10^{-5}$ mol) were dissolved in 1 mL of styrene. The mixture was transferred to a dry Schlenk flask with subsequent addition of 3.7 mL styrene to the reactor. The reaction mixture was purged with argon for 30 min and then heated to 80 °C and stirred for 7 h. To determine the molecular weights, dispersity of the polymers at different stages of synthesis and the conversion of the RAFT polymerization, the samples were withdrawn from reactor by syringe with one hour intervals and were analyzed by SEC. The polymer was purified 3 times by precipitation in methanol. The polymer was dried under high vacuum for 48 h at room temperature to give a yellow product.

*2.2.2.3. Synthesis of the initiator 3-hydroxy-2-methyl-2-((prop-2-yn-1-yloxy)methyl)propyl 2-bromo-2-methylpropanoate (**1**)*

The initiator **1** was synthesized according to the previously published literature.[22] B2-methyl-2-((prop-2-yn-1-yloxy)methyl)propane-1,3-diol (9.33 g, 0.059 mol) and TEA (5.97 g, 0.059 mol) were dissolved in 165 mL of dry THF and cooled to 0 °C in an ice-bath. To the solution, 2-bromoisobutyryl bromide (13.57 g, 0.059 mol) was added via dropping funnel over 30 min. Ice bath was removed and the reaction was allowed to stir overnight. Salts were removed by filtration. Crude product was concentrated, dried under high vacuum at RT and further purified by distillation under reduced pressure followed by column chromatography with EtOAc/petroleum spirit (4/1, v/v) as eluent. The fraction with R_f = 0.38 was collected and concentrated using rotary evaporator to obtain a colorless viscous liquid (11.9284 g, yield = 66 %). ^{1}H NMR ($CDCl_3$, 298K, 300 MHz); δ 4.19 (s, 2H; -C*H*$_2$-OC(=O)-), 4.15 (dd, 2H, *J*=4.05, 0.63 Hz; HC≡C-C***H*****$_2$**O-), 3.56 (d, 2H, *J*=1.23 Hz; HOC***H*****$_2$**-), 3.51 (s, 2H; HC≡C-CH$_2$OC***H*****$_2$**-), 2.44 (t, 1H, *J*=2.4 Hz; ***H***C≡C-CH2O-), 2.17 (b, 1H; *H*OCH$_2$-), 1.94 (s, 6H; methyl protons), 0.97 (s, 3H; methyl protons); ^{13}C NMR ($CDCl_3$, 298K, 400 MHz); 171.8, 79.3, 74.7, 73.6, 67.8, 66.8, 58.7, 55.8, 40.6, 30.8, 17.0.

Synthesis of cyclic PSTY

2.2.2.4. Synthesis of ≡(HO)-PSTY$_{30}$-Br

Styrene (20.75 g, 0.20 mol), PMDETA (0.340 mL, 1.63×10^{-3} mol), initiator **1** (1.0 g, 3.25×10^{-3} mol) were added to a 50 mL flask sealed with rubber septum and purged with argon for 30 min. A 50 mL Schlenk tube was charged with Cu(I)Br (0.234 g, 1.63 x 10^{-3} mol), Cu(II)Br$_2$/PMDETA complex (0.129 g, 3.25 x 10^{-4} mol) and magnetic stirrer, sealed with rubber septum and purged with

argon for 30 min. The solution was transferred to the Schlenk flask *via* cannula. The reaction vessel was placed in an oil bath at 80 °C and stirred for 6 h. The reaction was quenched by cooling to 0 °C, exposed to air, and diluted with THF (ca. 3 fold to the reaction mixture volume). The copper salts were removed by passage through an activated basic alumina column. The solution was concentrated by rotary evaporator and the polymer was recovered by precipitation into large volume of MeOH (20 fold excess to polymer solution) and then vacuum filtration. The polymer was dried *in vacuo* for 24 h at 25 °C and characterized by linear PSTY calibrated SEC (M_n = 3480 Đ = 1.05) and DMAc Triple Detection SEC (M_n = 3690, Đ = 1.02). The polymer was further characterized by ^{1}H NMR and MALDI-ToF.

2.2.2.5. Synthesis of ≡(HO)-PSTY$_{30}$-N$_3$

≡(HO)-PSTY$_{30}$-Br (8.66 g, 2.47 × 10^{-3} mol) was dissolved in 80 mL of DMF in a 100 mL reaction vessel equipped with magnetic stirrer. To this solution, NaN_3 (1.61 g, 2.47 × 10^{-2} mol) was added and the mixture stirred for 24 h at 25 °C. Product was precipitated into a mixture of methanol and water (95/5 v/v), filtered, washed exhaustively with MeOH and dried *in vacuo* for 24 h. Linear PSTY calibrated SEC (M_n = 3490, Đ = 1.088) and DMAc Triple Detection SEC (M_n = 3910, Đ = 1.03). The polymer was further characterized by ^{1}H NMR and MALDI-ToF.

2.2.2.6. Synthesis of c-PSTY$_{30}$-OH

A solution of ≡(HO)-PSTY$_{30}$-N$_3$ (2.0 g, 6.43 × 10^{-4} mol) in toluene (110 mL) was purged with argon for 90 min to remove oxygen. This polymer solution was added via argon feeding procedure[19], at a flow rate of 1.24 mL/min, to a deoxygenated solution of Cu(I)Br (4.61 g, 3.21 × 10^{-2} mol) and PMDETA (6.72 mL, 3.21 × 10^{-2} mol) in toluene (110 mL) at 25 °C. After the addition of the polymer solution the reaction mixture was stirred for 3 h. At the end of this period, toluene was evaporated. Polymer was dissolved in 200 mL of THF, and copper salts were removed by passage through activated neutral alumina column. To recover the polymer the column was washed with 200 mL of THF (4 times). THF was evaporated, and polymer was recovered by precipitation into MeOH (20 fold excess to polymer solution) and then by filtration. The polymer was dried *in vacuo* for 24 h at 25 °C. Linear PSTY calibrated SEC (M_n =2650, Đ = 1.305).

2.2.3. Analytical Methodologies

Size Exclusion Chromatography (SEC)

The polymers or polymer solutions were dissolved in tetrahydrofuran (THF) to a concentration of ca. 1 mg/mL and filtered through a 0.45 μm PTFE syringe filter prior to an injection. Analysis of the molecular weight distributions of the polymers was performed on a Waters 2695 separations module, fitted with a Waters 410 refractive index detector maintained at 35 °C, a Waters 996 photodiode array detector, and two Ultrastyragel linear columns (7.8 x 300 mm) arranged in series. The columns maintained at 40 °C for all analyses are capable of separating polymers in the molecular weight range of 500 – 4 million g/mol with high resolution. All samples were eluted at a flow rate of 1.0 mL/min. Narrow molecular weight PSTY standards ($Đ \leq 1.1$) ranging from 500 to 2 million g/mol were used for calibration. Data acquisition was performed using Empower software, and molecular weights were calculated relative to polystyrene standards.

^{1}H Nuclear Magnetic Resonance (NMR)

All NMR spectra were recorded using one of the following spectrometers: Bruker DRX 500, 400 or 300 MHz at 25 °C using an external lock ($CDCl_3$) and referenced to the residual non-deuterated solvent ($CHCl_3$). DOSY experiments were performed to acquire spectra presented herein by increasing the pulse gradient from 2 to 95 % of the maximum gradient strength and increasing gradient pulse length (*p30*) from 1 ms to 2 ms, using 32 to 256 scans.

Attenuated Total Reflectance Fourier Transform Spectroscopy (ATR-FTIR)

ATR-FTIR spectra were obtained using a single, horizontal bounce, diamond ATR accessory on a Nicolet Nexus 870 FT-IR. Spectra were recorded between 4000 and 500 cm^{-1} for 64 scans at 4 cm^{-1} resolution with an OPD velocity of 0.6289 cm/s. Solids were pressed directly onto the diamond internal reflection element of the ATR without further sample preparation.

Matrix-Assisted Laser Desorption Ionization – Time-of-Flight (MALDI-ToF) Mass Spectrometry

MALDI-ToF MS spectra were obtained using a Bruker MALDI-ToF autoflex III smartbeam equipped with a nitrogen laser (337 nm, 200 Hz maximum firing rate) with a mass range of 600 – 400,000 Da. All spectra were recorded in either reflectron (1500 – 5000 Da) or linear mode (5000 – 400,000 Da) using trans-2-[3-(4-*tert*-butylphenyl)-2-methyl-propenylidene] malononitrile (DCTB; 20 mg/mL in THF) as the matrix and $Ag(CF_3COO)$ (2 mg/mL in THF) as the cation source. The polymers were dissolved to a concentration of 1mg/mL. The matrix (20 μL), $Ag(CF_3COO)$ (2 μL) and polymer (20 μL) solutions were mixed together and spotted on the target plate via drying droplet method. Ca. 5000 shots randomly distributed over a sample spot were averaged.

Absolute Molecular Weight Determination by DMAc Triple Detection SEC

10-20 mg polymer samples were prepared in HPLC grade N,N-dimethylacetamide (DMAc, containing 0.03 wt % LiCl) and passed through a 0.45 µm PTFE filter membrane prior to injection. Analysis of the molecular weight distributions of the polymers were determined using a Polymer Laboratories GPC50 Plus equipped with differential refractive index detector. DMAc + 0.03 wt % LiCl was used as eluent at a flow rate of 1.0 mL/min. Separations were achieved using two PLGel Mixed B (7.8 x 300 mm) SEC columns connected in series and held at a constant temperature of 50 °C.

2.3. Results and Discussion

2.3.1. Derivation of the Molecular Weight Distributions

Size exclusion chromatography (SEC) separates random coil polymer chains based on their hydrodynamic volume (V_h) in a good solvent.[23, 24] An equation has been derived to determine V_h from the intrinsic viscosity (valid as the concentration of polymer approaches zero).

$$[\eta] = \frac{2.5 N_A V_h}{M} \qquad 2.1$$

where N_A is Avogadro's number, $[\eta]$ is the intrinsic viscosity and M is the viscosity-average molecular weight of the polymer. This equation is derived for a chain that is nondraining, and is valid for long flexible and coiled chains. In an SEC system, the polymer is considered quite dilute as it is eluted, and thus Eq. (2.1) can be used. Therefore, one should not overload the SEC columns with a high concentration of polymer. An empirical relationship between intrinsic viscosity and M is the well-known Mark–Houwink–Sakurada (MHS) relationship[25]:

$$[\eta] = KM^a \qquad 2.2$$

where K and a are constants that are fixed for a particular solvent–polymer type at a particular temperature. For solvents where the polymer in the solvent are under theta conditions, a is equal to 0.5. Under theta conditions, excluded volume expansion of the polymer coils is negligible. In other words, the coil behaves in an unperturbed state in which the coil is neither expanded nor contracted. This behaviour is equivalent to the polymer coil in its bulk state (i.e. without solvent). In a good solvent, the coils expand and the parameter a may increase up to 0.8 depending upon the solvent–polymer combination. Eq. (2.3) is derived by combining Eqs. (2.1) and (2.2), allowing V_h to be determined directly from known values of K and a.[26]

$$V_h = \frac{KM^{a+1}}{2.5 N_A} \qquad 2.3$$

It can be seen from Fig. 2.2A that the hydrodynamic diameter (D_h; where $V_h = 4/3\pi r_h^3$) in a theta solvent (curve a; $a = 0.5$) increased as a function of $M^{0.5}$.

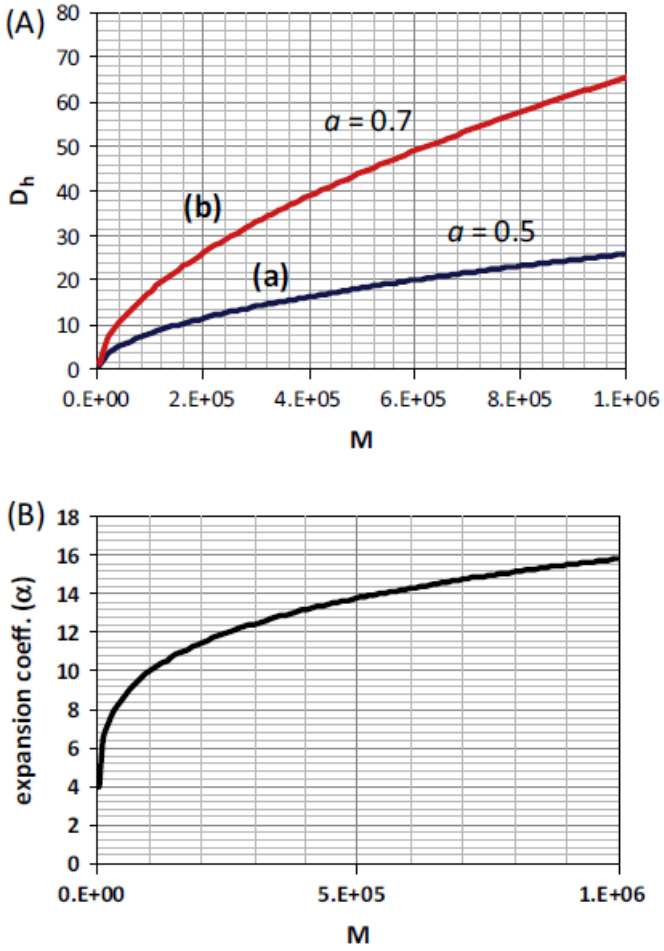

Figure 2.2. Calculation of hydrodynamic volume using Eq. (2.3). (A) D_h *vs* molecular weight (M) using K = 0.0141 (for THF) and a = 0.5 (curve a, theta solvent) and a = 0.7 (curve b, THF), (B) the expansion coefficient (α) calculated from $V_{\text{h,good solvent}}/V_{\text{h,theta solvent}}$ (i.e. where a = 0.7 and 0.5, respectively).

At low molecular weights between 14 and 55 k, D_h increased from 5 to 10 nm, whereas at high molecular weights (500–1000 k) the size increased from 30 to 45 nm. When the polymer is dissolved in a good solvent (e.g. polystyrene in THF; a = 0.7), D_h was much greater than the coil diameter under theta conditions as shown by curve b. A molecular weight of 100 k produced a D_h of 30 nm that could be increased to 100 nm at 800 k. Fig. 2.2B shows that the expansion coefficient ($\alpha = V_{\text{h,good solvent}}/V_{\text{h,theta solvent}}$) can increase as much as ten-fold at a molecular weight of 100 k. This showed that single polymer chains can swell in size well into the nano-sized domain. Note that charged polymers in water extend well beyond the Gaussian chain conformation due to charge repulsion from the side groups, invalidating the use of Eq. (2.3) in this case.

Injection of a polymer distribution on an SEC column will result in first the elution of the highest molecular weight polymer (i.e. with the largest D_h) followed by elution of the smaller polymer species until finally the smallest polymer molecular weight from the distribution has been eluted. A

typical example of a distribution is given in Fig. 2.1B, in which the mass was found using an *RI* detector. The mass in grams at each elution volume slice (i.e. ΔV) can be determined directly from the response of the concentration *RI* detector, and is a fraction of the initial mass of total polymer injected onto the column. A UV detector can also be used as a concentration detector but only where the polymer chain has the same UV chromophore evenly distributed along its backbone. A polymer (e.g. poly(methyl acrylate)) without a UV chromophore along it backbone but with a single chromophore at the chain-end will produce a very different distribution from the UV detector compared to that observed from the *RI* detector, and will lead to unsatisfactory results.

The elution volume (V_i) can be converted to molecular weight (M_i) by using a calibration curve consisting of polymer standards with known molecular weights. These polymer standards have quite a narrow MWD, and in general consist of PSTY standards made by ionic living polymerization, ranging in molecular weight from 600 to 2 million. A typical calibration plot is given in Fig. 2.3A, in which a calibration curve between the *V* and log*M* can be determined using a linear or odd number polynomial.

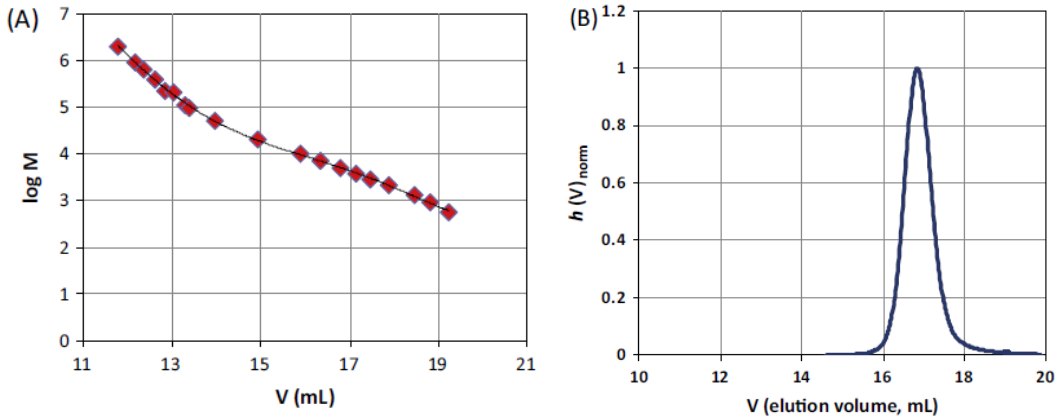

Figure 2.3. (A) Calibration curve log*M vs* elution volume *V* (see supplementary Excel file of the publication based on this chapter for coefficients of this calibration curve), (B) typical RI detector response, *h(V) vs V*.

The linear relationship between *V* and log*M* stems from the equilibrium concentrations of the polymer coil inside and outside the column beads, resulting in *V* varying exponentially with the diameter of the coil or, alternatively, *V* varies linearly with log diameter.

Let *h(V)* be the detector response from, for example, the *RI*, where *h*(*V*)*dV* is proportional to the mass of sample eluted from *V* to *dV*. If we normalize the detector response as follows:

$$h(V)_{norm} = \frac{h(V)}{\int h(V)dv} \qquad 2.4$$

Then $h(V)_{norm}$ in Eq. (2.4) is the weight fraction of polymer at *V* (Fig. 2.3B). If we let *F*(*V*) be the cumulative weight fraction at *V* then

$$h(V)_{norm} = \frac{dF(V)}{dV} \qquad 2.5$$

That is, $h(V)$ is the slope of the curve of cumulative weight fraction *vs V*. The 'differential log molecular weight distribution', *x(M),* is given by

$$x(M) = -\frac{dF(V)}{dlogM} \qquad 2.6$$

We use this distribution as log$M$ is a function of V determined from the calibration curve. Most SEC software packages use $dw(M)/d(\log M)$ instead of *x(M)*. Using the chain rule we obtain

$$x(M) = -\frac{dF(V)}{dV}\frac{dV}{d(logM)} \qquad 2.7$$

and from Eq. (2.5), we obtain Eq. (2.8), the 'differential log molecular weight distribution'.

$$x(M) = -\frac{dV}{d(logM)}\frac{hV}{\int h(V)dv} \qquad 2.8$$

where $d(\log M)/dV$ is the slope of the calibration curve, which is negative. This distribution most closely resembles the distribution of the raw $h(V)_{norm}$ *vs V* data, but accounts for the slope in the calibration curve. If the calibration curve is linear then the difference between *x(M) vs* log$M$ and $h(V)_{norm}$ *vs V* distribution curves will be a constant over the MWD; however, if a non-linear calibration curve is used the change could change significant as a function of M especially close to the exclusion limits of the SEC columns. Note, that all modern SEC software packages take the slope of the calibration curve into account. The area between logM_i and log(M_i + ΔM) from a *x(M) vs* log$M$ curve is equal to the weight fraction of polymer.

The most useful distribution is the 'weight distribution' or *w(M) vs M*; where *w(M)* is the weight fraction at M, not to be confused with *W(M)* which is the cumulative weight fraction. This distribution is quite useful as it allows us to scale the distributions to the amount of polymer in a reaction or polymerization, and thus compare polymer distributions as a function of, for example, conversion. To convert a 'differential log molecular weight distribution' to a 'weight distribution' we use the following relationship (see Fig. 2.4)

$$x(M) = \frac{dW(M)}{d(logM)} \qquad 2.9$$

$$= \frac{M}{log_{10}e}\frac{dW(M)}{dM} \qquad 2.10$$

$$= \frac{M}{log_{10}e}w(M) \qquad 2.11$$

such that

$$w(M) = \frac{log_{10}e}{M}x(M) \qquad 2.12$$

where log10e = 0.443429448, and the *w(M)* distribution shifts the distribution to lower molecular weights. The 'number distribution' is the mole fraction of polymer molecules *n(M) vs M*. The number distribution, *n(M),* can be easily determined from Eq. (2.13).

$$n(M) = \frac{w(M)}{M} \qquad 2.13$$

Fig. 2.4 shows the three distributions, and that as we move from *x(M)* to *w(M)* to *n(M)* the distribution shifts to lower molecular weights.

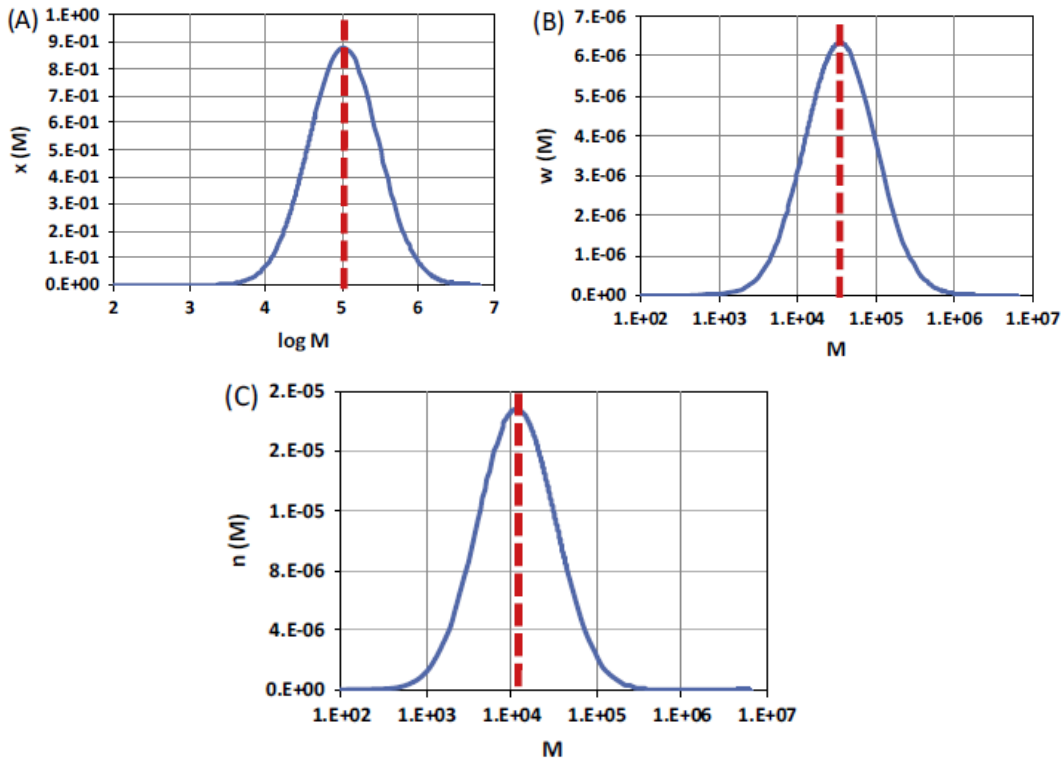

Figure 2.4. Three molecular weight distributions determined from equations above. (A) log-weight distribution, *x(M)*, (B) weight distribution, *w(M)*; and (C) number distribution, *n(M)*.

The number distribution is useful if one wants to determine the number of moles of polymer chains remaining after a polymerization; for example, the moles of MacroCTA consumed during an LRP. Care should be taken when using the number distribution as small baseline errors or small spurious peaks in the low molecular weight region will be amplified, leading to a gross misrepresentation of the true distribution. Due to the normalization of the *x(M)* distribution the following relations therefore hold:

$$\int x(M)d(logM) = 1 \qquad 2.14$$

$$\int w(M)dM = 1 \qquad 2.15$$

This means that the areas under the *x(M) vs* log*M* and *w(M) vs M* curves equal 1.

It is useful at this stage to describe the average molecular weight of a polymer sample. The most common way to assess the average molecular weight and the broadness of the MWD is to use the number-average molecular weight (M_n), weight-average molecular weight (M_w), and the dispersity ($Đ = M_w/M_n$). The dispersity gives a measure of the broadness of the MWD; if the Đ is 1 then all the

polymer chains have identical chain length, and Đ values greater than 1 represents an increase in the breadth of the distribution. Therefore, polymers made by LRP with Đ values close to 1 are considered to have a narrow MWD. In the case of conventional free-radical polymerizations, the Đ values are greater than 1 depending on the mode of termination. If termination is dominated by combination, the Đ is close to 1.5; whereas, if termination is dominated by disproportionation the Đ is close to 2. The addition of a chain transfer agent (e.g. mercaptans) will produce a Đ of 2.

We next use the method of moments to calculate M_n and M_w. The moment for each distribution is given by the generalized equation

$$\mu_i = \sum_{r=0}^{\infty} (M_r)^i n_r \qquad 2.16$$

where n_r is the number moles per unit volume with molecular weight M_r. For an unnormalized number distribution we obtain M_n from the ratio of the first moment to the zeroth moment.

$$M_n = \frac{\mu_1}{\mu_0} \qquad 2.17$$

$$= \frac{\int n(M) M dM}{\int n(M) dM} \qquad 2.18$$

and from Eq. (2.13)

$$M_n = \frac{\int w(M) dM}{\int n(M) dM} \qquad 2.19$$

and from Eq. (2.15) for a normalized distribution

$$M_n = \frac{1}{\int n(M) dM} \qquad 2.20$$

$$= \frac{1}{\int \frac{w(M)}{M} dM} \qquad 2.21$$

The weight-average molecular weight can be determined from an unnormalized distribution as follows

$$M_w = \frac{\mu_2}{\mu_1} \qquad 2.22$$

$$= \frac{\int n(M) M^2 dM}{\int n(M) M dM} \qquad 2.23$$

$$= \frac{\int w(M) M dM}{\int w(M) dM} \qquad 2.24$$

and from Eq. (2.15) for a normalized distribution

$$M_w = \int w(M) M dM \qquad 2.25$$

Therefore, we can obtain both the M_n and M_w from the areas under the respective distributions.

Next we use an example of an LRP of styrene using a polystyrene MacroCTA to illustrate the difference between the raw *RI* and the *w(M)* distributions. There is a linear increase in the M_n *vs* conversion and the Đ at each conversion is close to 1.1, similar to the data presented in Fig. 2.1A.

The SEC traces in many publications are illustrated in Fig. 2.5A, in which the normalized *RI* detector response is plotted against elution volume.

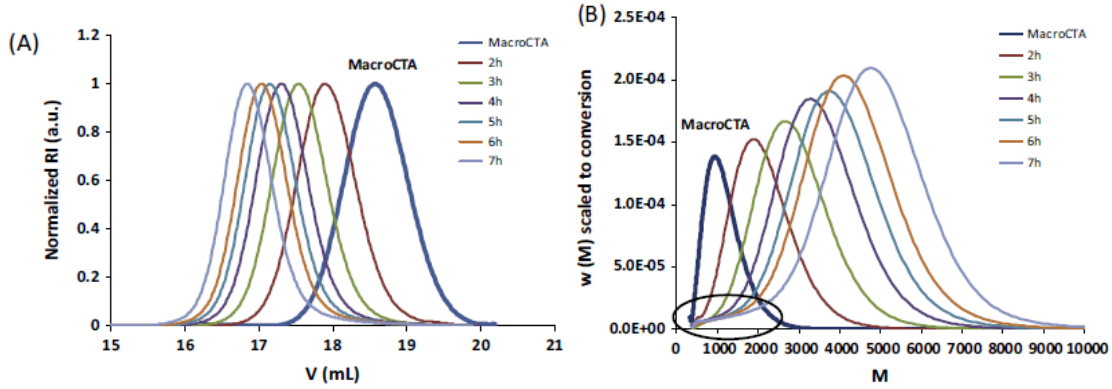

Figure 2.5. LRP of styrene as a function of time (or conversion) using a MacroCTA (dark blue curve). (A) $h(V)_{norm}$ *vs V*, and (B) weight distributions of those in (A) scaled to conversion using Eq. (2.27); *w(M) vs M*. (For interpretation of the references to colour in this figure legend, the reader is referred to the web version of the publication based on this chapter).

One can see that the initial MacroCTA elutes at ~18.6 mL (dark blue curve), and as monomer is polymerized onto the MacroCTA the distribution shifts to a lower elution volume. Looking at such a distribution it would seem acceptable to suggest that all MacroCTA is consumed during the polymerization. We can now use the method above to convert the raw normalized *RI vs V* data to a weight distribution (*w(M)*). In addition we can scale the *w(M)* to conversion or the weight of polymer in the polymerization mixture at time, *t*. Let the mass of MacroCTA be denoted as massMacroCTA and the initial mass of monomer as masso,mon, then the total weight of polymer at conversion *x* is given by the following relationship.

$$mass_{total} = mass_{MacroCTA} + xmass_{0,mon} \qquad 2.26$$

Therefore, the weight distribution can be scaled at each conversion at time *t* according to

$$w(M)_{scaled} = mass_{total}\, w(M)_{norm} \qquad 2.27$$

In Fig. 2.5B, we have set the area under the MacroCTA trace to be equal to 1, and scaled the other SEC traces over time according to their conversion at *x*. It is important to use the normalized weight distribution ($w(M)_{norm}$) in which the area under all SEC traces equals 1. From the *w(M)* distribution we can see that the MWD increased with time (or conversion) and the maximum peak molecular weight also increased with time. It is also observed that the breadth of the distribution increased with the increase in molecular weight even though the Đ values are similar for each distribution, decreasing from 1.16 at low conversion to 1.10 at high conversion (i.e. after a polymerization time of 7 h). The Đ is not a statistical value for the breadth of the distribution. More

interesting is the observation that not all the MacroCTA is consumed during the polymerization. Even at the highest conversion, there is still overlap over the original MacroCTA SEC trace. This suggests that this residual polymer consists of dead polymer, presumably formed through bimolecular radical termination in the making of the MacroCTA.

The example calculation given in the supplementary Excel file of the publication based on this chapter is for a bimodal distribution, in which each separate distribution has a low Đ value. It can be found that the areas under the *x(M)* and *w(M)* distributions are equal to 1. The reason why we used a bimodal distribution was to highlight the change in relative heights going from *x(M)* to *w(M)* to *n(M)*. The higher MWD decreases in height relative to the lower MWD, in which the higher MWD is not observable in the *n(M)* distribution. Even though the two MWDs are individually narrow (i.e. low Đ values), the overall M_n and Đ is a combination of both MWDs.

2.3.2. Log-Normal Distribution Simulation of Cyclic PSTY

The ring-closure method is a commonly used technique to obtain cyclic polymers.[16, 27] MWD distribution of a cyclic polymer shifts to a low molecular weight region because of introduced topological constrains resulting in a more compact molecule conformation. According to literature, the ratio between number-average molecular weight of cyclic ($M_{n,cyc}$) and that of linear ($M_{n,lin}$) polymers is close to 0.75,[19, 28] however, due to such difficulties as dead chain ends of polymers made via LRP and possible multiblock formation, it is a challenge to obtain 100% cyclic structures via the ring-closure method. As the impurities that may be present after cyclization can significantly alter polymer properties it is important to correctly determine their quantity in polymer mixture. LND simulation of SEC traces is commonly used to determine polymer species in a mixture of polymers. The Gaussian function of a number distribution is a two parameter function represented by the following equation:

$$n(M) = \frac{\exp\left(-(\bar{M}-M)^2\right)/2\sigma^2}{(2\pi\sigma^2)^{1/2}} \qquad 2.28$$

where mean $\bar{M}$ defines the position of the function's center and variance σ^2 controls the width of the function. M_n and Đ values of a polymer MWD obtained from SEC are used to calculate mean $\bar{M}$ and variance σ^2 of the Gaussian function as follows:

$$\bar{M} = \sqrt{M_n M_w} \qquad 2.29$$

$$\sigma^2 = (\ln(Đ))^2 \qquad 2.29$$

Thus, if M_n and Đ values of individual polymer MWDs are known, it is possible to determine the amount of each species in a mixture. A model example of such analysis to determine the purity of a

cyclic PSTY made via ring-closure method is given on Fig 2.6 and reaction scheme is given on Scheme 2.1.

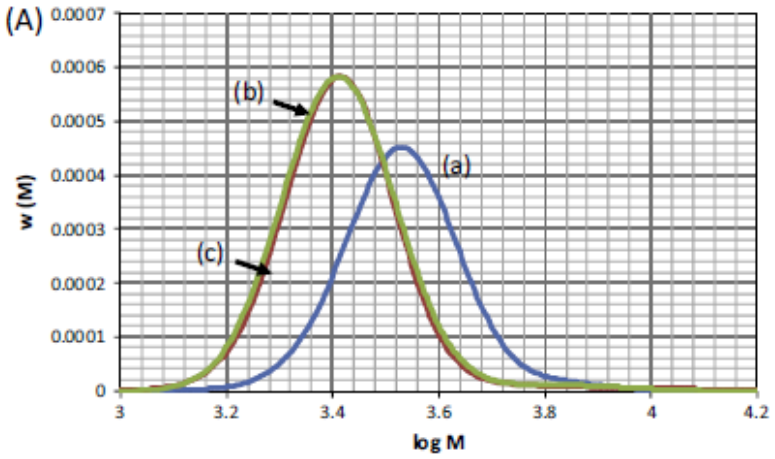

Figure 2.6. (A) Cyclization of ≡–$PSTY_n$–N_3 to c-$PSTY_n$. curve a (blue line): experimental SEC distribution for ≡–$PSTY_n$–N_3 (M_n = 3490, Đ = 1.088); curve b (green line): experimental SEC distribution after cyclization (c-PSTY, M_n = 2650, Đ = 1.305); curve c (red line): log-normal model fit to c-PSTY using 3 distributions (Dist 1: c-PSTY, M_n = 2650, Đ = 1.062, 94.3 wt%; Dist 2: M_n = 3490, Đ = 1.062, 0 wt%; Dist 3: linear terminated product, M_n = 6980, Đ = 1.062, 5.7 wt%).[29]

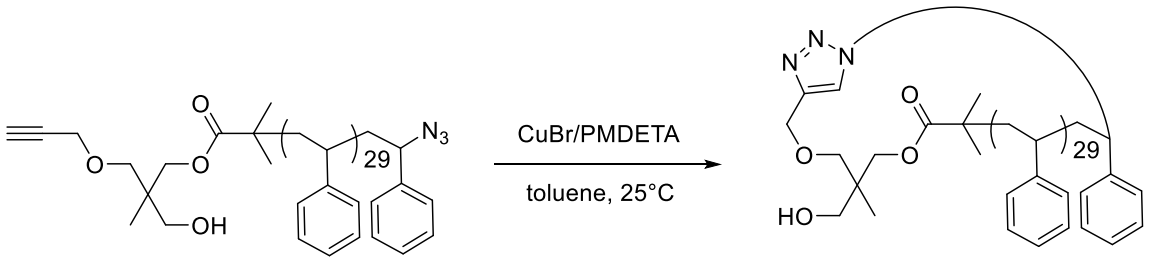

Scheme 2.1. Cyclization of PSTY using ring-closure method.

We used a copper catalyzed azyde-alkyne cycloaddition (CuAAC) reaction, as CuAAC is a well-known 'click' reaction that gives near quantitative yields. Cyclization resulted in a significant shift of the curve's peak to a low molecular weight region according to the refractive index response of SEC (RI-SEC) in accordance to literature. LND simulation of linear ≡–$PSTY_n$–N_3 ($M_{n,RI}$ = 3490, $Đ_{RI}$ = 1.088) showed that the seemingly symmetrical MWD actually contained a 5.7 wt% doubled molecular weight impurity. This could be caused by radical-radical termination due to the radical nature of the polymerization used (atom transfer radical polymerization) or by Glazer coupling[30] in the presence of oxygen. For the cyclization reaction the log-normal fitted $M_{n,cyc}/M_{n,lin}$ ratio (M_h) of 0.76 was close to that of theory ($M_{h,theory}$ = 0.75) indicating efficient cyclization. The resulting distribution had higher Đ because of high molecular weight tailing which was attributed to multiblock formation and bimolecular termination residue from ATRP. LND simulation of crude

cyclic PSTY showed that the MWD contained 94.3 wt% of cPSTY and ca. 0% of starting linear polymer. For this project, it was not necessary to further purify cPSTY from the residual 5.7 wt% high molecular weight polymer; however, it can be easily done using preparative SEC (see Chapter 6).

2.4. Conclusion

In conclusion, we have derived the molecular weight distributions from the raw *RI* detector response *vs* elution volume distribution. The three most general MWDs, including the differential log weight, weight and number distributions were presented using an easy to follow procedure. We highlighted the care required to convert the *RI vs V* distribution to *x(M)*, in which the slope of the calibration curve is included. If this slope is not included then gross errors in the *x(M)*, *w(M)* and *n(M)* distributions and errors in determining M_n, M_w and Đ will occur. Most, if not all, modern software packages correctly take the slope into account. A LRP case study was given to further highlight the usefulness of the *w(M)* distribution to account for conversion, and show that this distribution allowed us to show that not all MacroCTA was consumed during the polymerization. We have also included an Excel file with an example of converting the raw *RI* detector response *vs V* to the three molecular weight distributions. In addition, the derived MWD parameters were used in an LND simulation of a cyclization reaction to determine the purity of cyclic PSTY. This method can determine precise compositions of polymer mixtures containing more than one polymer species if their M_ns and Đs are known. Hopefully, this study will allow researchers to fully utilize the information from the SEC traces to derive mechanistic information that may otherwise be overlooked.

2.5. References

1. Solomon, D. H.; Rizzardo, E.; Cacioli, P. US Patent No. US4581429 A, **1986**.
2. Percec, V.; Guliashvili, T.; Ladislaw, J. S.; Wistrand, A.; Stjerndahl, A.; Sienkowska, M. J.; Monteiro, M. J.; Sahoo, S. *Journal of the American Chemical Society* **2006,** 128, (43), 14156-14165.
3. Le, T.; Moad, G.; Rizzardo, E.; Thang, S. In *WO 9801478, 1998*, Chem. Abstr, 1998; 1998; p 115390.
4. Wang, J.-S.; Matyjaszewski, K. *Journal of the American Chemical Society* **1995,** 117, (20), 5614-5615.
5. Kato, M.; Kamigaito, M.; Sawamoto, M.; Higashimura, T. *Macromolecules* **1995,** 28, (5), 1721-1723.
6. Kolb, H. C.; Finn, M. G.; Sharpless, K. B. *Angewandte Chemie International Edition* **2001,** 40, (11), 2004-2021.
7. Lutz, J.-F.; Börner, H. G.; Weichenhan, K. *Macromolecules* **2006,** 39, (19), 6376-6383.
8. Lutz, J.-F. *Angewandte Chemie International Edition* **2007,** 46, (7), 1018-1025.
9. Lammens, M.; Fournier, D.; Fijten, M. W. M.; Hoogenboom, R.; Prez, F. D. *Macromolecular Rapid Communications* **2009,** 30, (23), 2049-2055.
10. Whittaker, M. R.; Urbani, C. N.; Monteiro, M. J. *Journal of the American Chemical Society* **2006,** 128, (35), 11360-11361.
11. Urbani, C. N.; Bell, C. A.; Lonsdale, D. E.; Whittaker, M. R.; Monteiro, M. J. *Macromolecules* **2007,** 40, (19), 7056-7059.
12. Urbani, C. N.; Lonsdale, D. E.; Bell, C. A.; Whittaker, M. R.; Monteiro, M. J. *Journal of Polymer Science Part A: Polymer Chemistry* **2008,** 46, (5), 1533-1547.
13. Urbani, C. N.; Bell, C. A.; Whittaker, M. R.; Monteiro, M. J. *Macromolecules* **2008,** 41, (4), 1057-1060.
14. Konkolewicz, D.; Monteiro, M. J.; Perrier, S. *Macromolecules* **2011,** 44, (18), 7067-7087.
15. Hu, D.; Zheng, S. *European Polymer Journal* **2009,** 45, (12), 3326-3338.
16. Laurent, B. A.; Grayson, S. M. *Journal of the American Chemical Society* **2006,** 128, (13), 4238-4239.
17. Lonsdale, D. E.; Bell, C. A.; Monteiro, M. J. *Macromolecules* **2010,** 43, (7), 3331-3339.
18. Lonsdale, D. E.; Monteiro, M. J. *Chemical Communications* **2010,** 46, (42), 7945-7947.
19. Hossain, M. D.; Jia, Z.; Monteiro, M. J. *Macromolecules* **2014,** 47, (15), 4955-4970.

20. Kapnistos, M.; Lang, M.; Vlassopoulos, D.; Pyckhout-Hintzen, W.; Richter, D.; Cho, D.; Chang, T.; Rubinstein, M. *Nat Mater* **2008,** 7, (12), 997-1002.

21. Shortt, D. W. *Journal of Liquid Chromatography* **1993,** 16, (16), 3371-3391.

22. Jia, Z.; Lonsdale, D. E.; Kulis, J.; Monteiro, M. J. *ACS Macro Letters* **2012,** 1, (6), 780-783.

23. Young, R. J.; Lovell, P. A., *Introduction to Polymers*. CRC press: 2011.

24. Sperling, L. H., *Introduction to physical Polymer Science*. John Wiley & Sons: 2005.

25. Flory, P. J., *Principles of Polymer Chemistry*. Cornell University Press: 1953.

26. Gruendling, T.; Junkers, T.; Guilhaus, M.; Barner-Kowollik, C. *Macromolecular Chemistry and Physics* **2010,** 211, (5), 520-528.

27. Vollmert, B.; Huang, J.-x. *Die Makromolekulare Chemie, Rapid Communications* **1980,** 1, (5), 333-339.

28. Roovers, J.; Toporowski, P. *Macromolecules* **1983,** 16, (6), 843-849.

29. Monteiro, M. J. *European Polymer Journal* **2015,** 65, (0), 197-201.

30. Duxbury, C. J.; Cummins, D.; Heise, A. *Journal of Polymer Science Part A: Polymer Chemistry* **2009,** 47, (15), 3795-3802.

Chapter 3

Characterization of Hetero-Block Copolymers by the Log-Normal Distribution Model

In the previous chapter we described LND simulation to characterize MWDs of pure polymers and mixtures of homopolymers. However, often polymeric architectures consist of heterepolymers and the characterization of composition of such structures is difficult with conventional methods (e.g. NMR and MALDI-ToF). In many cases the only method left to characterize the heteropolymer structure is via size exclusion chromatography (SEC). An issue with SEC is that polymers with different chemical compositions have different responses from the SEC concentration detectors (e.g. refractive index) due to the dependence of the response from d*n*/d*c* values. In this chapter, we modify LND simulation from chapter 1 in order to be able to characterize heteropolymer mixtures. We derive equations that allow conversion of the true weight fraction (w_p) of a homopolymer or block to what would be determined directly from the refractive index (*RI*) detector of SEC (w_p^{app}) by using the individual polymer's refractive index increment (d*n*/d*c*)[1, 2] values from literature. The method was evaluated by characterization of mixtures of different homopolymers of known concentrations. The importance of taking d*n*/d*c* into account when characterizing polymers was exemplified in the evaluation of coupling efficiencies of heteropolymers. The modified log-normal distribution model allowed an excellent fit to all the RI-SEC chromatograms, and further allowed accurate determination of 'click' or coupling efficiencies of various homopolymers.

3.1. Introduction

'Living' radical polymerization[3-7] allows the production of polymer with high chain-end functionality that can be further coupled using 'click' reactions[8] to create complex polymer structures with desired architecture and composition. The types of complex structures range from block copolymers,[9] stars,[10], hyperbranched polymers[11] to dendrimers[12-15]. In recent years, cyclic polymer building blocks have also been used to create complex structures.[16-21] An issue with producing such polymer complexity is that characterization becomes difficult especially due to the increase in molecular weight upon their formation. Conventional analysis techniques (e.g. NMR, elemental analysis, mass spectroscopy) that provide near unambiguous elucidation of small molecules or oligomers fail for accurate characterization of polymers due to: (i) the low concentrations of chain-end functionality compared to the backbone monomer units, and (ii) the distribution of chain lengths in a polymer sample. The

latter allows only averages to be given with any confidence. With low molecular weight (oligomeric) polymers, NMR is routinely used to determine chain-end functionality and number-average molecular weight (M_n). MALDI-ToF can also be a powerful method to determine chain-end functionality and with caution molecular weight distributions (MWDs). Deciphering random copolymers or multiple monomers incorporated into the polymer by these methods, however, becomes extremely difficult. In the case of MALDI-ToF, this is further complicated by the ability of various polymer chains to fly in the instrument, making quantitative analysis difficult.

Polymer chemists are therefore left to characterize their polymers by size exclusion chromatography (SEC), in which polymer chains are separated through a column based on their hydrodynamic size. This coil size depends on the molecular weight and polymer composition.

3.1.1. Aim of the Chapter

The aim of this chapter is to provide an accurate method using SEC to determine the coupling efficiency for block copolymers of different compositions coupled together via 'click' reactions through the modified log-normal distribution model[22, 23]. The method allows quantification of unreacted polymer species and thus provides a means for obtaining the coupling or 'click' efficiency. This method can be extended to more complex polymer architectures (e.g. stars or dendrimers) with different arm chemical compositions. To the best of our knowledge no work was published on the correct characterization of heteropolymer blends.

3.2. Experimental

3.2.1. Materials

The following solvents, materials and reagents were used as received unless otherwise stated: tetrahydrofuran (THF, HPLC grade, Lichrosolv, 99.8%), toluene (HPLC, LABSCAN, 99.8%), dichloromethane (DCM, Labscan, AR grade), N,N-dimethylformamide (DMF: Labscan, AR grade), methanol (Univar, AR grade). sodium azide (NaN_3: Aldrich, ≥ 99.5 %), activated basic alumina (Aldrich: Brockmann I, standard grade, ~ 150 mesh, 58 Å), anhydrous magnesium sulphate ($MgSO_4$: Scharlau, extra pure), *N,N,N',N',N''*-pentamethyldiethylenetriamine (PMDETA: Aldrich, 99 %), cuprous bromide (Cu(I)Br, Aldrich, 99.999%), ethyl-2-bromoisobutyrate (EBiB, Aldrich, 98 %).

3.2.2. Synthetic Procedures

3.2.2.1. Synthesis of (2,2,5-trimethyl-1,3-dioxan-5-yl)methyl 2-bromo-2-methylpropanoate)

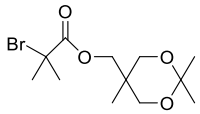

(2,2,5-trimethyl-1,3-dioxan-5-yl)methanol (2.0 g, 1.25 × 10^{-2} mol), synthesized following Jia et al.,[24] was dissolved in 28 mL of DCM, and placed to a 50 mL Schlenk flask equipped with a magnetic stirrer. TEA (1.91 mL, 1.37 x 10^{-2} mol) was added. The flask was placed into an ice-bath and solution kept stirred for 10 min. α-bromoisobutyryl bromide (1.53 g, 1.37 × 10^{-2} mol) was dissolved in 2 mL of DCM and added to the Schlenk flask via syringe over 15 min. The solution kept stirred overnight. TEA salt was filtered out, solvent was removed by rotary evaporation and crude product was purified by column chromatography (ethyl acetate to petroleum spirit ratio was 1:2, R_f of product = 0.37) to give 3.03g of pure product (yield = 78%). ^{1}H NMR ($CDCl_3$, 298K, 500 MHz); δ (ppm) 4.26 (s, 2H, -CO-O-CH_2-C), 3.67 (q, 4H, J = 15Hz, -O-CH_2-C), 1.94 (s, 6H, methyl protons), 1.42 (d, 2H, J = 16.3 Hz, methyl protons), 0.91 (s, 3H, methyl protons). ^{13}C NMR ($CDCl_3$, 298K, 500 MHz) δ (ppm): 171.7, 98.3, 68.3, 66.3, 55.9, 34.2, 31.0, 27.1, 20.5, 17.8.

3.2.2.2. Synthesis of SET-LRP initiator 3-hydroxy-2-(hydroxymethyl)-2-methylpropyl 2-bromo-2-methylpropanoate

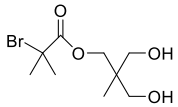

(2,2,5-trimethyl-1,3-dioxan-5-yl)methyl 2-bromo-2-methylpropanoate (3 g, 9.7 × 10^{-3} mol) was dissolved in 30 mL of methanol, and DOWEX (1.5 g) was added to the solution. Reaction mixture was kept stirred overnight. TLC was checked after that. As some unreacted dioxane was still in the system the solution was filtered and 0.77g of DOWEX resin added and the solution allowed stirring for additional 8 h. DOWEX was filtered and the solution was concentrated to give white crystals of pure product. Yield: 97%. ^{1}H NMR ($CDCl_3$, 298K, 500 MHz); δ (ppm) 4.27 (s, 2H, -CO-O-CH_2-C), 3.61 (d, 4H, J = 4.2Hz, -C-CH_2-OH), 2.53 (b, 2.26, hydroxyl protons), 1.95 (s, 6H, methyl protons), 0.90 (s, 3H, methyl protons). ^{13}C NMR ($CDCl_3$, 298K, 500 MHz) δ (ppm): 172.8, 68.3, 68.0, 56.1, 41.5, 31.1, 17.1.

*3.2.2.3. Synthesis of MBP-PSTY$_{175}$-Br (**1**)*

Styrene (20 mL, 0.174 mol), PMDETA (0.035 mL, 1.77 × 10^{-4} mol), methyl 2-bromopropionate (0.113 mL, 6.77 × 10^{-4} mol) and Cu(II)Br_2/ PMDETA complex (0.014 g, 3.4 × 10^{-5} mol) were added to a Schlenk flask and purged with argon for 60 min with vigorous stirring. Cu(I)Br (0.030 g, 2.08 × 10^{-4} mol) was added under a positive argon flow and the contents bubbled with argon for 10 more min. The reaction vessel was then sealed, placed in an oil bath at 80 °C. The reaction was terminated by quenching in ice followed by exposure to air. The contents were diluted with dichloromethane and passed through activated basic alumina. The solvent was removed under reduced pressure and the residue dissolved in a minimal amount of dichloromethane. The polymer was precipitated in 10 fold excess of MeOH. The resulting white precipitate was collected by vacuum filtration and dried under vacuum ($M_{n,RI}$ = 18405, $M_{p,RI}$ = 19560, Đ = 1.06).

Synthesis of BiB-PSTY$_{33}$-Alk (5)

3.2.2.4. Synthesis of BiB-PSTY$_{33}$-Br

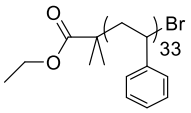

Styrene (16.36 g, 0.157 mol), PMDETA (0.387 mL, 1.9 × 10^{-3} mol), ethyl-2-bromoisobutyrate (EBiB) (0.376 mL, 2.56 × 10^{-3} mol) were added to a 20 mL glass vial sealed with rubber septum and sparged with Ar for 30 min. Cu(II)Br_2/PMDETA complex (0.254 g, 6.41 × 10^{-4} mol) and Cu(I)Br (0.276 g, 1.92× 10^{-3} mol) were added to a 50mL Schlenk flask and purged with argon for 30. The solution of monomer, ligand and initiator was cannula transferred to the Schlenk flask. The reaction mixture was allowed to stir at 80 °C for 7h 30 min. The reaction was quenched in ice followed by exposure to air. The contents were diluted with THF and passed through activated neutral alumina. The solvent was removed under reduced pressure and the residue dissolved in a minimal amount of acetone. The polymer was precipitated in 20× volume of MeOH. The resulting white precipitate was collected by vacuum filtration and dried under vacuum ($M_{n,\ THF\ RI}$ = 3535, $Đ_{\ THF\ RI}$ = 1.11, $M_{n,\ TD\ DMAc}$ = 4554, $Đ_{\ TD\ DMAc}$ = 1.05)

3.2.2.5. Synthesis of BiB-PSTY$_{33}$-N$_3$

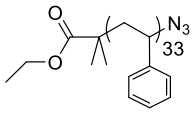

BiB-$PSTY_{33}$-Br (5.0 g, 1.43×10^{-3} mol), NaN_3 (0.929 g, 1.43×10^{-2} mol) were dissolved in 40 mL of DMF in a 50 mL flask equipped with magnetic stirrer. The flask was sealed and the reaction was allowed to stir at 25°C for 24h. NaBr was filtered out and polymer was purified via precipitation in 20 fold excess of methanol-water mixture (95:5 v/v.) and recovered by vacuum filtration. The residual solvent was removed in vacuo for 24h to give white powder ($M_{n, THF RI}$ = 3555, $Đ_{n, THF RI}$ = 1.11, $M_{n, TD DMAc}$ = 4393, $Đ_{TD DMAc}$ = 1.04)

*3.2.2.6. Synthesis of BiB-$PSTY_{33}$-Alk (**5**)*

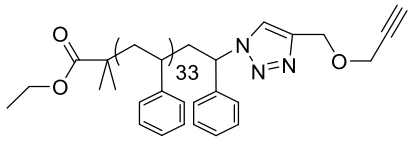

To a 20 mL Schlenk tube equipped with magnetic stirrer CuBr (4.9 mg, 3.40×10^{-5} mol) was added, the flask was sealed with rubber septum and purged with Ar for 30 min. At the same time BiB-PS_{33}-N_3 (0.6 g, 1.7×10^{-4} mol), PMDETA (7.2 µL, 3.4×10^{-5} mol), propargyl ether (0.88 mL, 1.7×10^{-4} mol) and dry toluene (6 mL) were added to a 10 mL glass vial, sealed, purged with Ar for 30 min at 0°C and then cannula transferred to the Schlenk tube. The reaction mixture was allowed to stir for 1 h at 25 °C. The solvent was removed by blow dry, polymer was redissolved in THF and passed through activated alumina column to remove copper complex. Solvent was evaporated; double molecular weight shoulder was removed by preparative GPC. THF was evaporated, polymer was recovered by precipitation in methanol (20 fold), filtration and removal of the residual solvent in vacuo for 24 h to give white powder ($M_{n, THF RI}$ = 3485, $Đ_{n, THF RI}$ = 1.08, $M_{n, TD DMAc}$ = 4221, $Đ_{TD DMAc}$ = 1.02)

*3.2.2.7. Synthesis of BiB-$PSTY_{30}$-Br (**10**)*

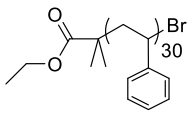

Styrene (18.0 mL, 0.157 mol), PMDETA (0.387 mL, 1.9×10^{-3} mol), ethyl-2-bromoisobutyrate (EBiB) (0.376 mL, 2.56×10^{-3} mol) were added to a 20 mL glass vial sealed with rubber septum and sparged with Ar for 30 min. Cu(II)Br_2/PMDETA complex (0.254 g, 6.41×10^{-4} mol) and Cu(I)Br (0.276 g, 1.92×10^{-3} mol) were added to a 50mL Schlenk flask and purged with argon for 30. The solution of monomer, ligand and initiator was cannula transferred to the Schlenk flask. The reaction mixture was allowed to stir at 80 °C for 7 h. The reaction was quenched in ice followed by exposure to air. The contents

were diluted with THF and passed through activated neutral alumina. The solvent was removed under reduced pressure and the residue dissolved in a minimal amount of acetone. The polymer was precipitated in 20× volume of MeOH. The resulting white precipitate was collected by vacuum filtration and dried under vacuum ($M_{n,\ THF\ RI}$ = 3341, $Đ_{THF\ RI}$ = 1.07).

Single Electron Transfer-Living Radical Polymerization (SET-LRP)

Synthesis of Pt-BA$_{43}$-≡ (3)

3.2.2.8. Synthesis of Pt-BA$_{43}$-Br

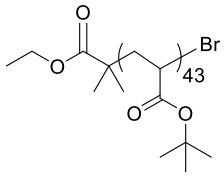

Tert-Butyl Acrylate (^{t}BA) (9.84 g, 0.076 mol), Me_6TREN (0.308 mL, 1.15 × 10^{-3} mol), Cu(II)Br_2/Me_6TREN (0.105 g, 2.3 × 10^{-4} mol), ethyl 2-bromo-2-methylpropionate (0.226 mL, 1.54 × 10^{-3} mol), DMSO (0.7 mL) and acetone (8 mL) were added to a 25 mL Schlenk flask equipped with a magnetic stirrer. The reaction mixture was cooled down to 0 °C and purged with argon for 30 min to remove oxygen. Cu(0) (0.074 g, 1.15 × 10^{-3} mol) was then carefully added to the solution under an argon blanket. The reaction mixture was further degassed for 5 min at 0 °C and then placed into a temperature controlled water bath at 22 °C for 50 min. The reaction was quenched by cooling in liquid nitrogen, exposure to air, and dilution with DCM (ca. 3 fold to the reaction mixture volume). The copper salts were removed by passage through an activated basic alumina column. The solution was concentrated by rotary evaporator and the polymer was precipitated into cold MeOH/water mixture (40:60 v/v, 20 fold excess to polymer solution) twice. The polymer (viscous glassy solid) was dried in vacuo for 24 h at 25 °C obtained as white powder ($M_{n,RI}$ = 5950, $M_{p,RI}$ = 6150, Đ = 1.05).

3.2.2.9. Synthesis of Pt-BA$_{43}$-N$_3$

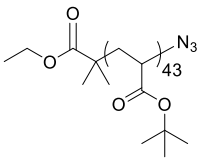

Pt-BA_{43}-Br (3.8 g, 6.22 × 10^{-4} mol) was dissolved in 25 mL of DMF in a 50 mL reaction vessel equipped with magnetic stirrer. To this solution NaN_3 (0.61 g, 9.34 × 10^{-3} mol) was

added and the mixture stirred overnight at 25 °C. The polymer solution was concentrated by airflow to approximately a third of the original volume and precipitated into cold MeOH/water mixture (20:80 v/v, ca. 10 fold excess to polymer solution) from DMF. All liquid was decanted and the polymer (viscous solid) was then dried in vacuo for 24 h at 25 °C. ($M_{n,RI}$ = 6030, $M_{p,RI}$ = 6180, Đ = 1.06).

*3.2.2.10. Synthesis of Pt-BA$_{43}$-≡ **(3)***

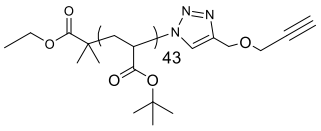

Propargyl ether (0.462 g, 4.91 × 10^{-3} mol), PMDETA (5.1 µL, 2.46 × 10^{-5} mol), P*t*-BA$_{43}$-N$_3$ (1 g, 1.63 × 10^{-4} mol) and toluene (5 mL) were added to a 20 mL vial and purged with argon for 30 min, degassed solution was transferred into a Schlenk tube containing CuBr (3.5 mg, 2.46 × 10^{-5} mol) and Cu wire under a positive argon flow. The reaction vessel was then sealed, placed in an oil bath at 25 °C and the reaction mixture stirred for 30 min. The reaction contents were diluted with dichloromethane and passed through activated basic alumina. The solvent was removed under reduced pressure and the residue dissolved in a minimal amount of acetone. The polymer was precipitated in cold MeOH/water mixture (20:80 v/v, ~10 fold excess to polymer solution). The resulting white precipitate was collected by vacuum filtration and dried under high vacuum. The resultant crude polymer was then further purified by preparative SEC to remove high molecular weight impurities. The resultant polymer was then re-precipitated from THF into cold MeOH/water mixture (20:80 v/v, ~10 fold excess to polymer solution), filtered and dried under high vacuum obtained as white powder ($M_{n,RI}$ = 5930, $M_{p,RI}$ = 6110, Đ = 1.05).

Aqueous SET-LRP

Synthesis of PNIPAM$_{37}$-≡ (2)

3.2.2.11. Synthesis of PNIPAM$_{37}$-N$_3$

To a 100 mL Schlenk flask equipped with magnetic stirrer, $CuBr_2$ (0.132 g, 5.94 × 10^{-4} mol), Milli-Q water (28.4 mL), Me_6TREN (0.238 mL, 8.92 × 10^{-4} mol), NIPAm (3.36 g, 0.297 mol), and initiator 3-hydroxy-2-(hydroxymethyl)-2-methylpropyl 2-bromo-2-methylpropanoate (0.2 g, 7.43 × 10^{-4} mol) were added. The tube was sealed with rubber septum and bubbled with argon for 30 min. After that, the tube was immersed in an ice-bath

and bubbled with argon for another 30 min. Meanwhile, $NaBH_4$ and Milli-Q water were sealed in 20 mL vial and purged with argon for 60 min. Degassed Milli-Q water (5.6 mL) was transferred into the vial containing $NaBH_4$ (5.6 mg, 1.486×10^{-4} mol) to form 1 mg mL^{-1} stock solution. The stock solution was added into the Schlenk tube to initiate the SET-LRP. A mixture of NaN_3 (1.93 g, 0.0297 mol) and mili-Q water (19.2 mL) was purged by argon for 60 min. After 60 min, the SER-LRP was quenched by adding the degassed NaN_3 solution into the Schlenk flask above via syringe, and kept stirring for 24 h. The reaction mixture was then recovered by freezer dry directly, redissolved in DCM followed by passage through activated basic alumina to remove copper salts. The solution was concentrated, and precipitated in 10 × volume of Et_2O. The white precipitate was collected by vacuum filtration and dried under high vacuum obtained as white powder. ($M_{n,RI}$ = 2200, $M_{p,RI}$ = 2410, Đ = 1.10; $M_{n,TD}$ = 4050, $M_{p,TD}$ = 4180, Đ = 1.02).

*3.2.2.12. Synthesis of PNIPAM$_{37}$-≡ **(2)***

Propargyl ether (1.85 g, 1.98×10^{-2} mol), PMDETA (13 µL, 6.17×10^{-5} mol), PNIPAM$_{37}$-N_3 (1 g, 2.46×10^{-4} mol) and DMF (8 mL) were added to a 20 mL vial and purged with argon for 60 min, degassed solution was transferred into a Schlenk tube containing Cu(I)Br (8.8 mg, 6.17×10^{-5} mol) and Cu wire under a positive argon flow. The reaction vessel was then sealed, placed in an oil bath at 25 °C and the reaction mixture stirred for 30 min. The reaction contents were diluted with DCM and passed through activated basic alumina. The solvent was removed under reduced pressure and the residue dissolved in a minimal amount of DCM. The solution was dialysis against with MeOH for 2 days to remove unreacted propargyl ether. The polymer was precipitated in 10 × volume of Et_2O. The white precipitate was collected by vacuum filtration and dried under high vacuum obtained as white powder ($M_{n,RI}$ = 2650, $M_{p,RI}$ = 2820, Đ = 1.09; $M_{n,TD}$ = 4230 , $M_{p,TD}$ = 4290, Đ = 1.02).

*3.2.2.13. Synthesis of PNIPAM$_{35}$-N_3 **(6)***

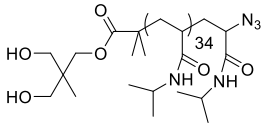

To a 20 mL Schlenk tube equipped with magnetic stirrer $CuBr_2$ (16.6 mg, 7.43×10^{-5} mol) and $NaBH_4$ (0.7 mg, 1.86×10^{-5} mol) were added. Sodium borohydrate was measured on the balance with 0.001 mg error. The flask was sealed with rubber septum and purged with Ar for 30 min. To a 5 mL glass vial Me_6TREN (19.9 µL, 7.43×10^{-5} mol) and mili-Q water (1

mL) were added; the vial was sealed and the solution was bubbled with Ar for 30 min. The solution was then cannula transferred to the Schlenk tube, the tube was placed in an ice-bath and reduction of Cu^{II} was carried out for 30 min. At the same time NIPAM (0.63g, 5.57×10^{-3} mol) and the initiator 3-hydroxy-2-(hydroxymethyl)-2-methylpropyl 2-bromo-2-methylpropanoate (25mg, 9.29×10^{-5} mol) were dissolved in water (3.48 mL) in a 20 mL glass vial, sealed and bubbled with Ar for 30 min at 0 °C. The solution was then cannula transferred to the Schlenk tube. The reaction was allowed to stir at 0°C for 2 h. 20-fold excess of NaN_3 (0.12 g, 1.86×10^{-3} mol) was added to Schlenk tubes, the solution was allowed to stir overnight. Polymer was purified via dialysis against 1 L mili-Q water with 3.5 kDa MWCO membrane (Thermo Fisher). Solvent was changed 5 times every 2 h. Pure polymer was recovered by freeze dry to give white powder ($M_{n,\ THF\ RI}$ = 4474, $Đ_{THF\ RI}$ = 1.06, $M_{n,\ TD\ DMAc}$ = 4474, $Đ_{TD\ DMAc}$ = 1.004).

*3.2.2.14. Synthesis of $PNIPAM_{25}$-N_3 (**9**)*

To a 20 mL Schlenk tube equipped with magnetic stirrer, $CuBr_2$ (16.6 mg, 7.43×10^{-5} mol) and $NaBH_4$ (0.68 mg, 1.85×10^{-5} mol) were added. Sodium borohydride was weighed with a precision of ±0.001 mg. The flask was sealed with a rubber septum and purged with Ar for 30 min. To a 5 mL glass vial, Me_6TREN (19.9 μL, 7.43×10^{-5} mol) and milli-Q water (1 mL) were added; the vial sealed and the solution purged with Ar for 30 min. The solution was cannula transferred to the Schlenk tube and placed in an ice-bath where the reduction of Cu^{II} was allowed to proceed for 30 min. Another mixture of NIPAM (0.21 g, 1.86×10^{-3} mol) and initiator 3-hydroxy-2-(hydroxymethyl)-2-methylpropyl 2-bromo-2-methylpropanoate (25.0 mg, 9.29×10^{-5} mol) were dissolved in water (2.48 mL) in a 20 mL glass vial, sealed, purged with Ar for 30 min at 0 °C, and then cannula transferred to the Schlenk tube. The reaction mixture was allowed to stir at 0 °C for 100 min. 20 fold excess of NaN_3 (0.12g, 1.86×10^{-3} mol) was added to Schlenk tube, the solution was allowed to stir overnight. Polymer was purified via dialysis against 1L mili-Q water with 3.5kDa MWCO membrane (Thermo Fisher). Solvent was changed 5 times every 2 h. Pure polymer was recovered by freeze dry to give white powder ($M_{n,\ THF\ RI}$ = 1140, $Đ_{THF\ RI}$ = 1.15).

Functionalization of PEG

*3.2.2.15. Synthesis of MeO-PEG_{52}-≡ (**4**)*

Sodium hydride (0.15 g, 3.75×10^{-3} mol, 60 % in mineral oil) was added to 30 mL of dry THF under argon and cooled to 0 °C. To this suspension, MeO-PEG_{52}-OH (M_n = 2000, Sigma, 5.00 g, 2.50×10^{-3} mol) was added portionwise and stirred until dissolved before

propargyl bromide (1.39 mL, 1.25 × 10^{-2} mol, 80 % in toluene) was added directly. The solution was stirred at 0 °C for 30 min then R.T. for 24 h after which saturated NH_4Cl solution (10 mL) was slowly added to quench the reaction. The solution was then extracted with DCM (50 mL) and the organic phase was then washed with brine (3 × 50 mL). The organic phase was collected, dried with anhydrous $MgSO_4$, filtered and taken to dryness. The light brown solid was redissolved in a minimum volume of DCM and precipitated (twice) into diethyl ether. The solid was then collected by vacuum filtration, washed with diethyl ether, collected and dried under high vacuum obtained as white powder ($M_{n,RI}$ = 2780, $M_{p,RI}$ = 2870, Đ = 1.04, $M_{n,TD}$ = 2200, $M_{p,TD}$ =2390, Đ = 1.04).

Synthesis of MeO-PEG$_{31}$-N$_3$ (7)

3.2.2.16. Synthesis of MeO-PEG$_{31}$-OTs

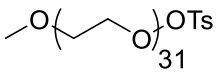

Dry polyethylene glycol monomethyl ether (M_n = 1500, Sigma, 20.00 g, 1.00 × 10^{-2} mol) was dissolved in pyridine (15 mL) with stirring, under Ar bubbling at 25 °C. The contents were cooled in an ice bath and tosyl chloride (4.28 g, 2.25 × 10^{-1} mol) was added with small portions under positive argon flow. The reaction contents were allowed to stir overnight at room temperature. The contents turned an orange color. After stirring, the reaction mixture was diluted with cold water and extracted with DCM (3 times). The organic phases were washed with cold 6 M HCl (×2), dried with Na_2SO_4 anhydrous and filtered. The solvent was reduced in volume by rotary evaporator and the polymer solution precipitated into 10× volume of diethyl ether. The white, waxy solid was recovered by vacuum filtration and dried in vacuo for 12 h.

3.2.2.17. Synthesis of MeO-PEG$_{31}$-N$_3$ (7)

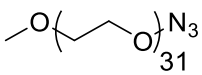

NaN_3 (1.63 g, 2.5 × 10^{-2} mol), MeO-PEG_{31}-OTs (M_n = 2000, 5 g, 2.50 × 10^{-3} mol) and DMF (25 mL) were added to a 50 mL Schlenk flask. The reaction mixture was stirred for 24 h at 25 °C. Then the reaction mixture was poured into a brine solution and polymer was extracted with dichloromethane (3 times). The organic layer was dried with Na_2SO_4 and filtered. The solvent was removed by rotary evaporation. The residue was dissolved in dichloromethane and precipitated into diethyl ether (10 fold). The white precipitate was

recovered via vacuum filtration and dried under vacuum to give faint yellow powder ($M_{n,\ RI,\ THF}$ = 2827, Đ = 1.05, $M_{n,\ TD\ DMAc}$ = 1878, $Đ_{\ TD\ DMAc}$ = 1.009).

*3.2.2.18. MeO-PEG$_{34}$-OH **(12)***

The polymer (M_n = 1500) was purchased from Sigma.

CuAAC 'Click' Reactions

*3.2.2.19. Synthesis of BiB-PSTY$_{33}$-PNIPAM$_{35}$ **(8)***

To a 5 mL Schlenk tube equipped with magnetic stirrer CuBr (4.12 mg, 2.87 × 10^{-5} mol) was added, the flask was sealed with rubber septum and purged with Ar for 30 min. At the same time BiB-PSTY$_{33}$-Alk (**5**) (50.1 mg, 1.44 × 10^{-5} mol), PNIPAM$_{35}$-N$_3$ (**6**) (84.9 mg 1.87 × 10^{-5} mol) and PMDETA (6.01 μL, 2.87 × 10^{-5} mol) were dissolved in 0.7 mL DMF in a 5 mL glass vial, sealed, purged with Ar for 30 min and then cannula transferred to the Schlenk tube. The reaction mixture was allowed to stir for 2 h at room temperature. DMF was removed by blow dry. Polymers were purified using preparative SEC, recovered by precipitation into methanol and dried in vacuo for 24 h.

*3.2.2.20. Synthesis of BiB-PSTY$_{33}$-PEG$_{31}$ **(11)***

To a 5 mL Schlenk tube equipped with magnetic stirrer CuBr (4.13 mg, 2.87 × 10^{-5} mol) was added, the flask was sealed with rubber septum and purged with Ar for 30 min. At the same time BiB-PS$_{33}$-Alk (**5**) (50.1 mg, 1.44 × 10^{-5} mol), MeO-PEG$_{31}$-N$_3$ (**7**) (26.9 mg 1.87 × 10^{-5} mol) and PMDETA (6.01 μL, 2.87 × 10^{-5} mol), were dissolved in 0.7 mL DMF in a 5 mL glass vial, sealed, purged with Ar for 30 min and then cannula transferred to the Schlenk tube. The reaction mixture was allowed to stir for 2 h at room temperature. DMF was removed by blow dry. Polymers were purified using preparative SEC, recovered by precipitation into methanol and dried in vacuo for 24 h.

3.2.3. Analytical Methodologies

^{1}H Nuclear Magnetic Resonance Spectroscopy (NMR)

All NMR spectra were recorded on a Bruker DRX 500 MHz spectrometer at 25 °C using an external lock ($CDCl_3$) and referenced to the residual non-deuterated solvent ($CHCl_3$).

Size Exclusion Chromatography (SEC)

The polymers or polymer solutions were dissolved in tetrahydrofuran (THF) to a concentration of ca. 1 mg/mL and filtered through a 0.45 μm PTFE syringe filter prior to an injection. Analysis of the molecular weight distributions of the polymers was performed on a Waters 2695 separations module, fitted with a Waters 410 refractive index detector maintained at 35 °C, a Waters 996 photodiode array detector, and two Ultrastyragel linear columns (7.8 x 300 mm) arranged in series. The columns maintained at 40 °C for all analyses are capable of separating polymers in the molecular weight range of 500 – 4 million g/mol with high resolution. All samples were eluted at a flow rate of 1.0 mL/min. Narrow molecular weight PSTY standards ($Đ \leq 1.1$) ranging from 500 to 2 million g/mol were used for calibration. Data acquisition was performed using Empower software, and molecular weights were calculated relative to polystyrene standards.

Absolute Molecular Weight Determination by DMAc Triple Detection SEC

Approximately 10 mg polymer samples were prepared in HPLC grade N,N-dimethylacetamide (DMAc, containing 0.03 wt % LiCl) and passed through a 0.45 μm PTFE syringe filter prior to injection. Analysis of the molecular weight distributions of the polymers were determined using a Polymer Laboratories GPC50 Plus equipped with differential refractive index detector. DMAc + 0.03 wt % LiCl was used as eluent at a flow rate of 1.0 mL/min. Separations were achieved using two PLGel Mixed B (7.8 × 300 mm) SEC columns connected in series and held at a constant temperature of 50 °C.

Matrix-Assisted Laser Desorption Ionization - Time-of-Flight (MALDI-ToF) Mass Spectrometry.

MALDI-ToF MS spectra were obtained using a Bruker MALDI-ToF autoflex III smartbeam with accessible mass range of 600 – 400,000 Da. Ions were accelerated with a nitrogen laser (337 nm, 200 Hz maximum firing rate). All spectra were recorded in either reflectron (1500 – 5000 Da) or linear mode (5000 – 400,000 Da) using trans-2-[3-(4-*tert*-butylphenyl)-2-methyl-propenylidene] malononitrile (DCTB; 20 mg/mL in THF) as the matrix and Na(CF_3COO) (2 mg/mL in THF) as the cation source. The polymers were dissolved to a concentration of 1mg/mL. The matrix (20 μL), Ag(CF_3COO) (2 μL) and polymer (20 μL) solutions were mixed together and spotted on the target plate via ‘dried droplet’ method.

3.3. Results and Discussion

The refractive index detector response ($h(V)$) at elution volume (V) is directly proportional to the concentration of a homopolymer (g/mL) according to the following relationship:

$$h(V) = K \cdot C(V) \cdot dn/dc \qquad (3.1)$$

where K is the apparatus sensitivity constant, $C(V)$ is the concentration (g/mL) at elution volume, V, and dn/dc is the refractive index increment of the polymer. Normalizing the detector response as follows[25, 26]:

$$h(V)_{norm} = \frac{h(V)}{\int h(V)dV} \qquad (3.2)$$

gives the weight fraction of polymer at V as $h(V)_{norm}$, and the area under the whole distribution is therefore 1. It can be shown that for the weight distribution ($w(M)$), the area under the curve is also 1 (the use of the weight distribution becomes important latter when fitting the distribution to the log-normal distribution model). The area (A) under the unnormalized elution volume is given by

$$A = K \cdot C_{Tot} \cdot {}^{dn}/_{dc} \qquad (3.3)$$

where C_{Tot} is the total concentration (g/mL) for the distribution injected into the SEC system.

3.3.1. Mixing two homopolymers

In the first case, we will derive equations for analyzing a mixture of two different homopolymers, A and B, injected into the SEC by *RI* with different dn/dc values. Should the dn/dc value of polymer A be substantially greater than that of B, it would be expected if A and B were mixed at an equal weight fraction (w_p) of 0.5 that the $w(M)$ distribution would give the apparent weight fraction of polymer A ($w_{p,A}^{app}$) to be substantially greater than B. The weight distribution is used throughout this paper since the weight of the polymer (i.e. reactants and products) in the reaction does not change. We do not recommend the use of the number distribution ($n(M)$) for two reasons: (1) the distribution is susceptible to baseline correction leading to large errors (where $n(M) = w(M)/M$), and (2) the coupling efficiency for a 'click' reaction requires knowledge of the moles of both the reactants and products at the end of the reaction, which makes analysis difficult especially when the reactant and product distributions have significant overlap.

One can derive the relationship between w_p and $w_{p,A}^{app}$ as follows. The true weight fraction of polymer A can be determined by[27]

$$w_{p,A} = \frac{C_A}{C_{Tot}} \tag{3.4}$$

or

$$C_A = w_{p,A} C_{Tot} \tag{3.5}$$

where $C_{Tot} = C_A + C_B$

The apparent molecular weight of polymer A ($w_{p,A}^{app}$) from the *w(M)* distribution can be determined from the area of the distribution.

$$w_{p,A}^{app} = \frac{A_A}{A_{Tot}} \tag{3.6}$$

substituting Eq. 3.3 into 3.6 gives

$$w_{p,A}^{app} = \frac{KC_A\left(dn/dc\right)_A}{KC_A\left(dn/dc\right)_A + KC_B\left(dn/dc\right)_B} \tag{3.7}$$

$$w_{p,A}^{app} = \frac{C_A\left(dn/dc\right)_A}{C_A\left(dn/dc\right)_A + C_B\left(dn/dc\right)_B} \tag{3.8}$$

Substitution of Eq. 3.5 into 3.8 gives

$$w_{p,A}^{app} = \frac{w_{p,A}C_{Tot}\left(dn/dc\right)_A}{w_{p,A}C_{Tot}\left(dn/dc\right)_A + w_{p,B}C_{Tot}\left(dn/dc\right)_B} \tag{3.9}$$

such that

$$w_{p,A}^{app} = \frac{w_{p,A}\left(dn/dc\right)_A}{w_{p,A}\left(dn/dc\right)_A + w_{p,B}\left(dn/dc\right)_B} \tag{3.10}$$

or the more generalized form for a mixture of multiple homopolymers

$$w_{p,j}^{app} = \frac{w_{p,j}\left(dn/dc\right)_j}{\sum_i w_{p,i}\left(dn/dc\right)_i} \tag{3.11}$$

where the sum of $w_{p,i} = 1$.

3.3.2. Log-Normal Distribution Model

The most commonly used methods to simulate the SEC distribution of polymer made by LRP are the Gaussian and Poisson distributions. Both methods have limitations as previously described.[23] Therefore, to simulate the weight distribution (i.e. *w(M) vs M*) for

the mixture of two homopolymers, we recommend the log-normal distribution model[23]. It is assumed with this model that the weight distribution is symmetrical about the median on a ln *M* abscissa (i.e. x-axis), resulting in the following equation:

$$w(ln\ M) = \frac{exp(-(ln\ M - ln\ \overline{M})^2/2\sigma^2}{(2\pi\sigma^2)^{0.5}} \qquad (3.12)$$

or

$$w(M) = \frac{exp(-(ln\ M - ln\ \overline{M})^2/2\sigma^2}{M(2\pi\sigma^2)^{0.5}} \qquad (3.13)$$

The median $\overline{M}$ is related to the M_n and the weight-average molecular weight (M_w) by the following equations.

$$M_n = \overline{M} exp(-\sigma^2/2) \qquad (3.14)$$

$$M_w = \overline{M} exp(\sigma^2/2) \qquad (3.15)$$

$$PDI = \frac{M_w}{M_n} = exp(\sigma^2) \qquad (3.16)$$

and, from equations 3.14 and 3.15, we obtain

$$\overline{M} = (M_n M_w)^{0.5} \qquad (3.17)$$

The maximum (i.e. peak maximum) of the distributions are located at

$$M_{p,w} = \frac{{M_n}^{3/2}}{{M_w}^{1/2}} \qquad (3.18)$$

$$M_{p,n} = \frac{{M_n}^{5/2}}{{M_w}^{3/2}} \qquad (3.19)$$

where $M_{p,w}$ and $M_{p,n}$ are the peak maximums for the weight and number distributions, respectively.

To produce a weight distribution for one polymer, the M_n and M_w (or Đ) values are substituted into Equations 3.16 and 3.17 to obtain the two parameters $\overline{M}$ and σ required for Equation 3.13. The area under the *w(M)* distribution should equal 1. If one is dealing with two polymer distributions, A and B, the total distribution $w(M)_{tot}$ is the weighted sum of each distributions at *M* according to the Equation 3.20.

$$w(M)_{tot} = w_{p,A}^{app} w(M)_A + w_{p,B}^{app} w(M)_B \qquad (3.20)$$

where $w_{p,A}^{app}$ and $w_{p,B}^{app}$ are the weight fraction of polymers A and B, respectively, from Equation 3.10. The more generalized equation for a mixture of multiple homopolymers is given by

$$w(M)_{tot} = \sum_i w_{p,i}^{app}\, w(M)_i \qquad (3.21)$$

where *i* represents polymer *i* and the sum of $w_{p,i}^{app} = 1$.

3.3.3. Simulating the SEC Molecular Weight Distribution with the Log-Normal Distribution Model

Four polymers (**1**-**4** in Table 3.1) of different compositions and molecular weights were prepared by atom transfer radical polymerization (ATRP), aqueous SET-LRP,[28] or functionalization of the chain end (i.e. PEG).

Table 3.1. Size exclusion chromatography (SEC) data for all polymers using *RI* detection and polystyrene calibration curve.

Polymer	M_n	M_p	Đ
1. MBP-PSTY$_{175}$-Br	18405	19560	1.06
2. (OH)$_2$PNIPAM$_{37}$-≡	2650	2820	1.09
3. P*t*-BA$_{43}$-≡	5930	6110	1.05
4. MeO-PEG$_{52}$-≡	2780	2870	1.04
5. BiB-PSTY$_{33}$-≡	3485	3576	1.08
6. (OH)$_2$PNIPAM$_{35}$-N$_3$	2303	2521	1.11
7. MeO-PEG$_{31}$-N$_3$	2827	2707	1.05
8. BiB-PSTY$_{33}$-PNIPAM$_{35}$-(OH)$_2$	6850	7062	1.04
9. (OH)$_2$PNIPAM$_{25}$-N$_3$	1140	1295	1.15
10. BiB-PSTY$_{30}$-Br	3341	3438	1.07
11. BiB-PSTY$_{33}$-PEG$_{31}$-OMe	6763	6914	1.03
12. MeO-PEG$_{34}$-OH	1426	1522	1.08

The individual polymers were fit such that half the height and half the width of the *w(M)* distribution gave an excellent fit with the log-normal distribution model, and the M_n and Đ values used in the fit were given in Table 3.2.

Table 3.2. Fitting parameters for the molecular weight distributions of polymer using the log-normal distribution (LND) model.

Polymer	M_n	$M_{p,w}$	Đ	σ^2	$\overline{M}$	d*n*/d*c*[b]
1. MBP-PSTY$_{175}$-Br	16603	16281	1.04	0.039	16932	0.185
2. (OH)$_2$PNIPAM$_{37}$-≡	2939	2835	1.075	0.072	3047	0.09
3. P*t*-BA$_{43}$-≡	6245	6127	1.039	0.038	6366	0.049
4. MeO-PEG$_{52}$-≡	2743	2688	1.041	0.040	2799	0.078
5. BiB-PSTY$_{33}$-≡	3540	3436	1.062	0.060	3649	0.185
6. (OH)$_2$PNIPAM$_{35}$-N$_3$	2443	2355	1.077	0.074	2536	0.09
7. MeO-PEG$_{31}$-N$_3$	2660	2604	1.044	0.043	2718	0.078
8.BiB-PSTY$_{33}$-PNIPAM$_{35}$-(OH)$_2$	6995	6886	1.032	0.031	7106	0.159
9. (OH)$_2$PNIPAM$_{25}$-N$_3$	1242	1185	1.10	0.095	1303	0.09
10. BiB-PSTY$_{30}$-Br	3350	3238	1.07	0.067	3465	0.185
11. BiB-PSTY$_{33}$-PEG$_{31}$-OMe	6815	6722	1.028	0.027	6910	0.148
12. MeO-PEG$_{34}$-OH	1480	1432	1.069	0.066	1530	0.078

[a]Experimental SEC *w(M) vs M* traces were fit using the LND model using a fitted $M_{p,w}$ and Đ.

[b]d*n*/d*c* values taken from literature.[1, 2]

The SEC chromatogram (*w(M) vs* log *M*) from mixing polystyrene (PSTY with 175 styrene units, **1**) with poly(t-butylacrylate) (P*t*-BA with 43 NIPAM units, **3**) at a $w_{p,PSTY}$ of 0.5 gave a bimodal weight distribution, in which the low MWD corresponded to P*t*-BA$_{43}$ and the high MWD to PSTY$_{175}$ (see Figure 3.1A). The normalized area under the distribution (i.e. *w(M) vs* M) for PSTY (1) was 0.81 and for P*t*-BA (3) was 0.19. This result suggests that according to Eq. 3.3 the d*n*/d*c* value for PSTY was approximately 3.8 times greater than that for P*t*-BA, which was close to that found in literature (d*n*/dc_{PSTY} = 0.185 and $dn/dc_{\mathrm{P}t\mathrm{BA}}$ = 0.049).[1] Using the log-normal distribution model above, we simulated the bimodal distribution in Figure 3.1A for the mixture PSTY$_{175}$ (**1**) and P*t*-BA$_{43}$ (**3**). Each *w(M) vs* M was simulated using the M_n and Đ values (in Table 3.2) to obtain σ^2 and $\overline{M}$ for use in Equation 3.13. The true weight fraction was 0.5 and together with the literature d*n*/d*c* values above, $w_{p,A}^{app}$ and $w_{p,B}^{app}$ were obtained from Equation 3.10. These apparent weight fractions were then used in Equation 3.20 for each *w(M)* distribution to produce a cumulative distribution (see dashed curve in Figure 3.1A).

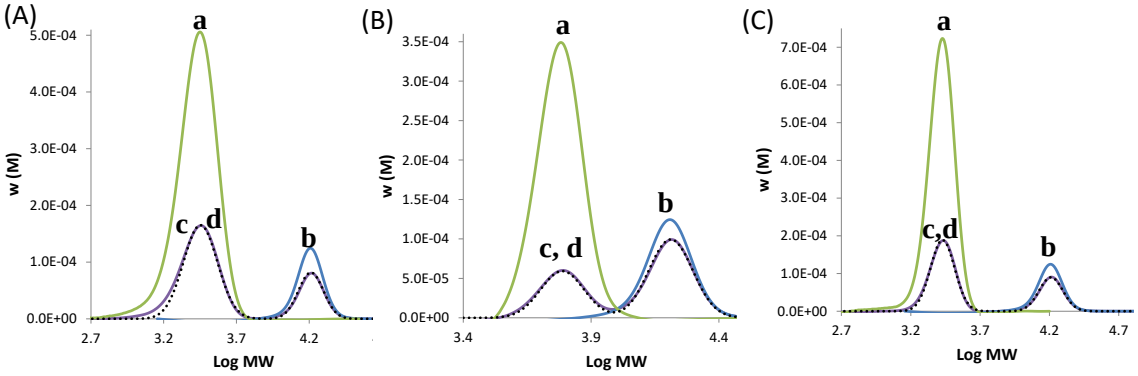

Figure 3.1. SEC traces and LND simulations of mixtures of polymers with different d*n*/d*c* values. SEC analysis is based on a polystyrene calibration curve. (A) Curve a (green line) $(OH)_2$PNIPAM$_{37}$-≡ (**2**), curve b (blue line) MBP-PSTY$_{175}$-Br (**1**), curve c (purple line) mixture of **2** and **1,** and curve d (dotted line) LND simulation of curve c. (B) Curve a (green line) Pt-BA$_{43}$-≡ (**3**), curve b (blue line) MBP-PSTY$_{175}$-Br (**1**), curve c (purple line) mixture of **1** and **3,** and curve d (dotted line) LND simulation of curve c. (C) Curve a (green line) MeO-PEG$_{52}$-≡ (**4**), curve b (blue line) MBP-PSTY$_{175}$-Br (**1**), curve c (purple line) mixture of **4** and **1,** and curve d (dotted line) LND simulation of curve c.

The simulated fit to the experimental data was excellent. The same approach was used for the mixture of PSTY$_{175}$ (**1**) and PEG$_{52}$ (**4**, d*n*/dc_{PEG} = 0.078) at a $w_{p,A}$ = 0.5 (Figure 3.1B). Again the simulation of the experimental *w(M)* was excellent. For the mixture of PSTY$_{175}$ (**1**) and PNIPAM$_{37}$ (**2**) at a $w_{p,A}$ = 0.5, we had to use the d*n*/dc_{PNIPAM} = 0.09 to obtain an excellent fit to the experimental SEC *w(M)* distribution (Figure 3.1C), since the literature value of 0.107 did not give a satisfactory fit due to different measurement conditions. The value of 0.09 was used in subsequent simulations, and all fits were found to be excellent (*vide infra*).

3.3.4. Mixing two homopolymers and their block copolymer

The next case study represents mixing two homopolymers, each a different polymer, with its block copolymer. This is a more complicated case since the block will have a d*n*/d*c* that is a weighted average of the homopolymers,[27, 29] A and B (i.e. $X_{p,A}$ and $X_{P,B}$, respectively), within the block, AB, according to equation 3.22:

$$dn/dc_{AB} = X_{p,A}dn/dc_A + X_{p,B}dn/dc_B \qquad (3.22)$$

Two block copolymers were synthesized through the CuAAC 'click' reaction of the homopolymers. The resultant crude block copolymer was then purified from its residual homopolymer reactants by preparative SEC (Figure 3.2). The first block copolymer, BiB-P(STY$_{33}$-b-NIPAM$_{35}$)-$(OH)_2$ (**8**) was synthesized by coupling polymers BiB-PSTY$_{33}$-≡ (**5**, 1 eq.) and $(HO)_2$-PNIPAM$_{35}$-N_3 (**6,** 1.3 eq.) in the presence of CuBr/PMDETA in DMF at

room temperature for 2 h (Scheme 3.1A). The SEC chromatogram based on RI detection using a PSTY calibration curve was given by curve a in Figure 3.2A. Due to the excess **6**, a low molecular weight shoulder was observed. The MWD for the block copolymer was purified by preparative SEC (curve b) and fit with a log-normal distribution (curve c, dashed line) using the molecular weight parameters in Table 3.2. Similarly, the second block, BiB-P(STY_{33}-b-EG_{31})-OMe (**11**) was formed by coupling BiB-$PSTY_{33}$-≡ (**5**, 1 eq.) with MeO-PEG_{31}-N_3 (**7,** 1.3 eq.) (Scheme 3.1B). Again, a low MWD was observed from unreacted **7**, which was subsequently removed by preparative SEC (Figure 3.2B).

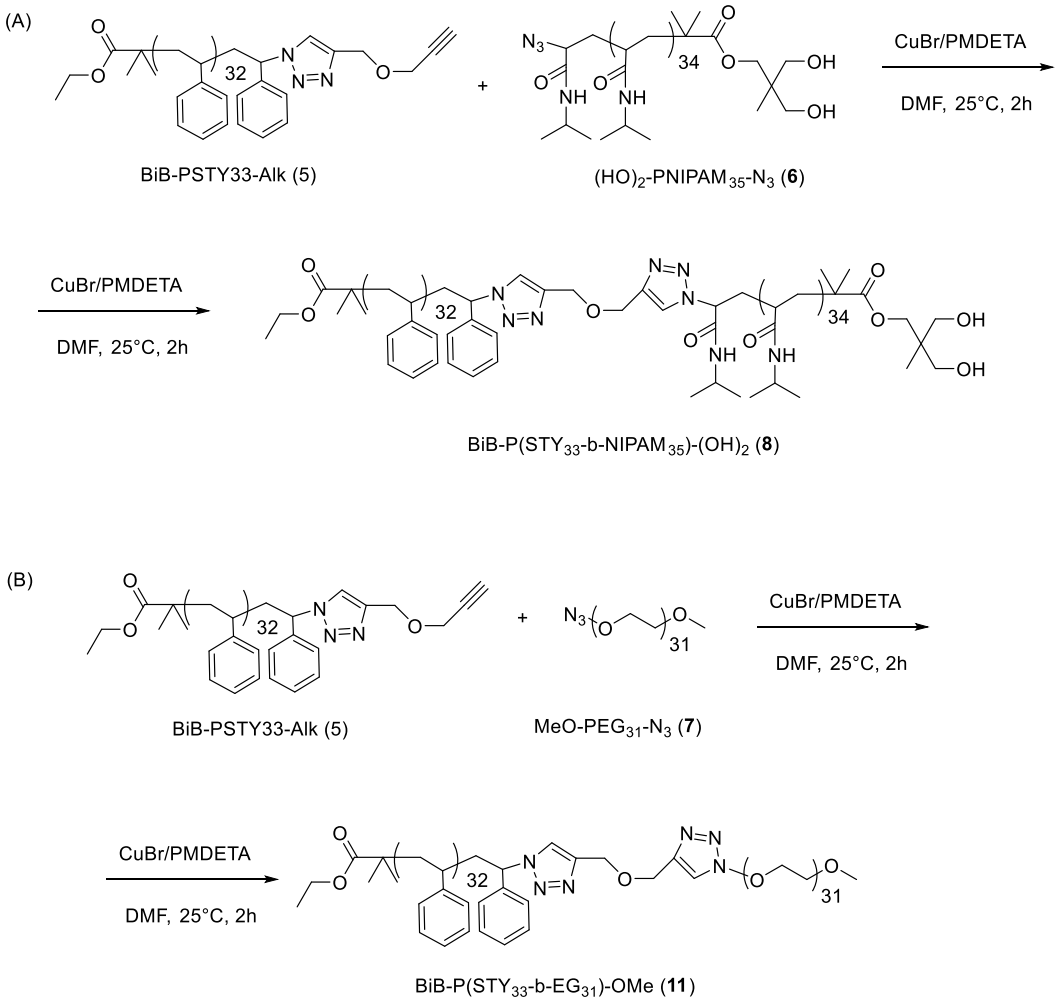

Scheme 3.1. CuAAC 'Click' reaction between polymers with different dn/dc ratios. (A) Synthesis of BiB-P(STY_{33}-b-$NIPAM_{35}$)-$(OH)_2$ (**8**). (B) Synthesis of BiB-P(STY_{33}-b-EG_{31})-OMe (**11**). Reaction conditions: DMF at 25°C for 2h.

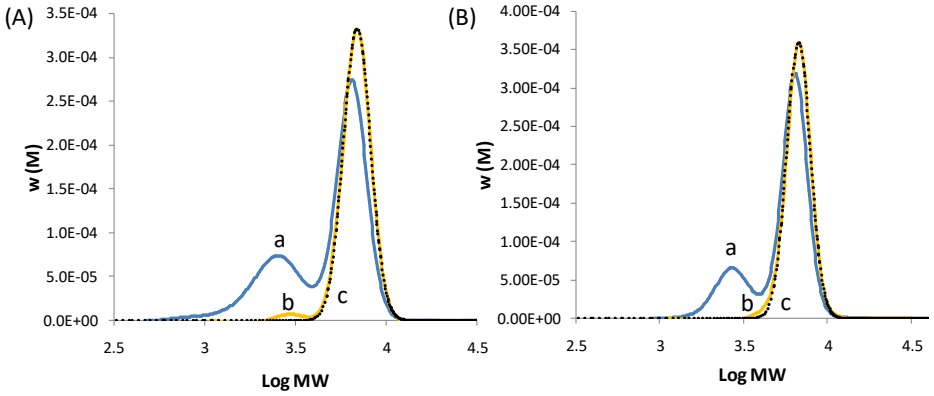

Figure 3.2. SEC traces and LND simulation of crude and purified block copolymers synthesized by CuAAC 'click' reaction. SEC analysis is based on polystyrene calibration curve. (A) Curve a (blue line) crude BiB-P(STY_{33}-b-$NIPAM_{35}$)-$(OH)_2$ (**8**), curve b (yellow line) **8** purified after preparative SEC, curve C (dotted line) LND simulation of purified **8**. (B) Curve a (blue line) BiB-P(STY_{33}-b-EG_{31})-OMe (**11**), curve b (yellow line) **11** purified after preparative SEC, curve C (dotted line) LND simulation of purified **11**.

Mixing three different polymers of equal mass and injecting this mixture into the SEC system was given in Figure 3.3, in which two polymers were different homopolymer and the third was the block copolymer of the two. As there was substantial overlap of the MWDs from the two original homopolymers used in the synthesis of the block, we used homopolymers with very different molecular weights to demonstrate the accuracy of our technique. Figure 3.3A showed the SEC (RI dection using PSTY calibration) for a mixture of equal amounts of BiB-$PSTY_{30}$-Br (**10**, 1 wt eq.), $(HO)_2$-$PNIPAM_{25}$-N_3 (**9,** 1 wt eq.) and BiB-P(STY_{33}-b-$NIPAM_{35}$)-$(OH)_2$ (**8**, 1 wt eq).

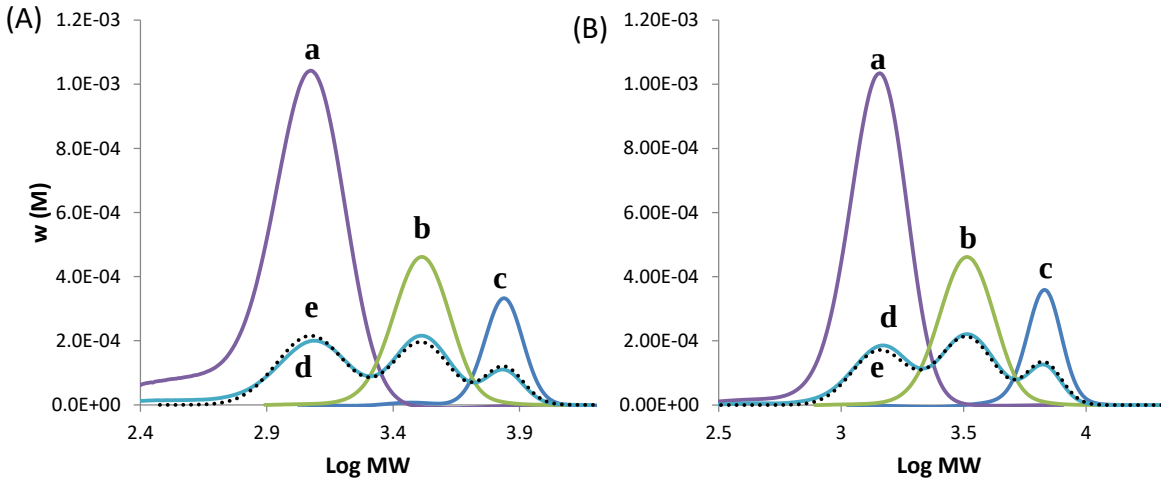

Figure 3.3. SEC traces and LND simulation of a mixture of two homopolymers and its block copolymer. SEC analysis is based on polystyrene calibration curve. (A) Curve a (purple line) $(OH)_2$-$PNIPAM_{25}$-N_3 (9), curve b (green line) BiB-$PSTY_{30}$-Br (10), curve c (dark blue line) BiB-P(STY_{33}-b-$NIPAM_{35}$)-$(OH)_2$ (**8**) purified by preparative SEC, curve d

(blue line) mixture of **10**, **9** and **8** pure, curve e (dotted line) LND simulation of curve d. (B) Curve a (purple line) MeO-PEG_{34}-OH (**12**), curve b (green line) BiB-$PSTY_{30}$-Br (**10**), curve c (dark blue line) BiB-P(STY_{33}-b-EG_{31})-OMe (**11**) purified by preparative SEC, curve d (blue line) mixture of **10**, **12** and **11** pure, curve e (dotted line) LND simulation of curve d.

The MWDs of all three polymers were well resolved (curve d in Figure 3.3A). The $dn/dc_{\mathbf{8}}$ was determined from Equation 3.22 (see Table 3.2), and used with the dn/dc values for PSTY and PNIPAM to calculate $w_{p,\mathbf{10}}^{app}$, $w_{p,\mathbf{9}}^{app}$ and $w_{p,\mathbf{8}}^{app}$. These values were then used in the log-normal distribution model (Equation 3.21) to produce a cumulative MWD (i.e. *w(M) vs M*) as showed by curve e (dashed line). The fit using these dn/dc values was excellent. Figure 3.3B showed the SEC for a mixture of BiB-$PSTY_{30}$-Br (**10**, 1 wt eq.), MeO-PEG_{34}-OH (**12,** 1 wt eq.) and BiB-P(STY_{33}-b-EG_{31})-OMe (**11**, 1 wt eq). Curve d showed that the MWDs were well resolved, and the fit (curve e, dashed line) using the same procedure above was again excellent for a different polymer system.

3.3.5. CuAAC 'click' reaction of two homopolymers; determination of coupling efficiency

The CuAAC 'click' reaction between BiB-$PSTY_{33}$-≡ (**5**, 1 eq., 50 mg) and $(HO)_2$-$PNIPAM_{35}$-N_3 (**6,** 1.3 eq., 84.7 mg) in the presence of CuBr/PMDETA was carried out in DMF at room temperature for 2 h. The moles of each polymer reactant were determined using the molecular weight from ^{1}H NMR. At the start of the reaction (i.e. 0 min, before addition of catalyst) the mixture of **5** and **6** gave a monomodal distribution as shown in Figure 3.4A with a low Đ of 1.14.

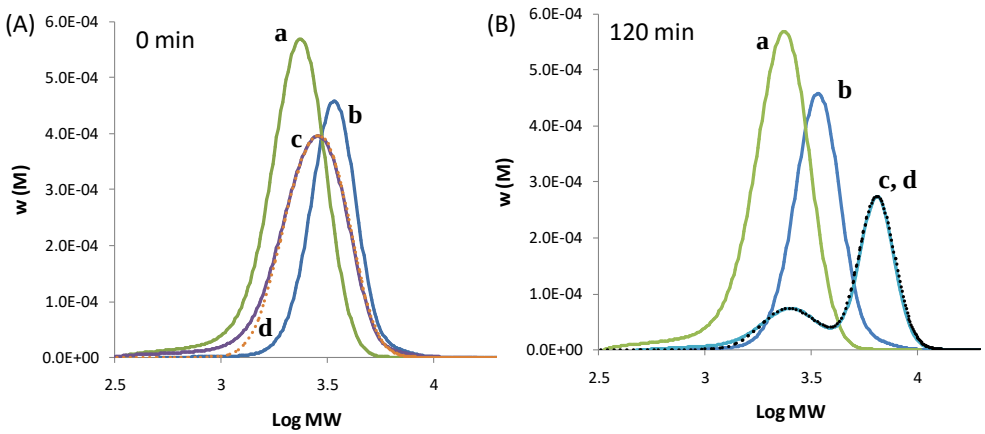

Figure 3.4. SEC traces and LND simulation for the CuAAC 'click' reaction between BiB-$PSTY_{33}$-≡ (**5**, 1 eq., 50 mg) and $(HO)_2$-$PNIPAM_{35}$-N_3 (**6,** 1.3 eq., 84.7 mg) catalyzed by CuBr/PMDETA in DMF at room temperature for 2 h. (A)

curve a is polymer **6**, curve b is polymer **5**, curve c is a mixture of **5** and **6** at 0 min reaction time, and curve d LND fit to curve c. (B); curve a is polymer **6**, curve b is polymer **5**, curve c after 120 min reaction time, and curve d is the LND fit to curve c.

This is quite typical of a mixture of two distributions that overlap.[23] The $w_{p,\mathbf{5}}$ and $w_{p,\mathbf{6}}$ are 0.37 and 0.63, respectively, which after using equation 3.10 and the d*n*/d*c* values in Table 3.2 gives values for $w_{p,\mathbf{5}}^{app}$ and $w_{p,\mathbf{6}}^{app}$ of 0.55 and 0.45, respectively. The log-normal distribution model using these values gave an excellent fit to the *w(M)* distribution for the mixture of **5** and **6** (dashed line, curve d in Figure 3.4A). After 120 min of reaction time, a high molecular weight peak was observed (curve c in Figure 3.4B) due to the formation of the product P(STY_{33}-b-$NIPAM_{35}$)-$(OH)_2$ (**8**). As we have discussed above, the very different d*n*/d*c* values will give an error in calculating the 'click' or coupling efficiency by SEC. The $w_{p,\mathbf{5}}^{app}$, $w_{p,\mathbf{6}}^{app}$ and $w_{p,\mathbf{8}}^{app}$ found by fitting the log-normal distribution model (curve d in Figure 3.4B) was 0.045, 0.105 and 0.85, respectively. The apparent 'click' efficiency was close to 99.4 % taking into account the excess (1.3 eq.) of **6**. The true 'click' efficiency for the coupling of **5** to **6** was then calculated using these apparent weight fractions in Equation 3.23 to determine the true weight fraction of each polymer species.

$$w_{p,j} = \frac{w_{p,j}^{app}/\left(dn/dc\right)_j}{\sum_i w_{p,i}^{app}/\left(dn/dc\right)_i} \qquad (3.23)$$

where the sum of $w_{p,i}^{app} = 1$. The $w_{p,\mathbf{5}}$, $w_{p,\mathbf{6}}$ and $w_{p,\mathbf{8}}$ from Equation 3.23 was 0.034, 0.162 and 0.805, respectively. Using these values gave a true 'click' efficiency of 94.1%, which is much lower than the apparent 'click' efficiency due to the very different d*n*/d*c* values of each polymer species. The CuAAC 'click' reaction BiB-$PSTY_{33}$-≡ (**5**, 1 eq., 50 mg) with MeO-PEG_{31}-N_3 (**7,** 1.3 eq., 26.9 mg) produced BiB-P(STY_{33}-b-EG_{31})-OMe (**11**). At the start of the reaction (i.e. 0 min) a monomodal *w(M)* distribution was found consisting of the two polymer reactants, **5** and **7**, as shown in Figure 3.5A. The true $w_{p,\mathbf{5}}$ and $w_{p,7}$ were 0.65 and 0.35, respectively. Using these and the d*n*/d*c* values from Table 3.1 for PSTY and PEG, we determined from Equation 3.10 that $w_{p,\mathbf{5}}^{app}$ and $w_{p,7}^{app}$ were 0.84 and 0.16, respectively. Again after using these values in the log-normal distribution model gave an gave an excellent fit to the *w(M)* distribution for the mixture of **5** and **7** (dashed line, curve d in Figure 3.5A).

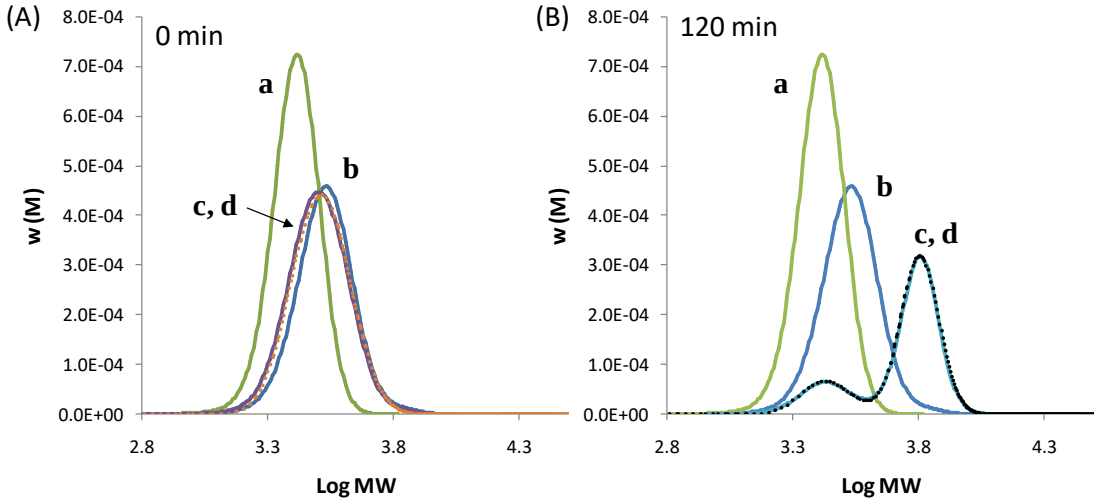

Figure 3.5. SEC traces and LND simulation for the CuAAC 'click' reaction between BiB-PSTY$_{33}$-≡ (**5**, 1 eq., 50 mg) and MeO-PEG$_{31}$-N$_3$ (**7,** 1.3 eq., 26.9 mg) catalyzed by CuBr/PMDETA in DMF at room temperature for 2 h. (A) curve a is polymer **7**, curve b is polymer **5**, curve c is a mixture of **5** and **7** at 0 min reaction time, and curve d LND fit to curve c. (B); curve a is polymer **7**, curve b is polymer **5**, curve c after 120 min reaction time, and curve d is the LND fit to curve c.

In this case, the very low d*n*/d*c* of PEG will underestimate its contribution to the mixture on the *w(M)* SEC trace. After 120 min of the CuAAC reaction, a high molecular weight peak corresponding to product 11 was observed (curve c in Figure 3.5B). There was also a low molecular weight peak due to a mixture of the starting reagents **5** and **7**, since an excess of **7** was used in the reaction. Similar to the procedure above, the apparent weight fractions of all polymer species was obtained by fitting curve c with the log-normal distribution model. The $w_{p,\mathbf{5}}^{app}$, $w_{p,\mathbf{7}}^{app}$ and $w_{p,\mathbf{11}}^{app}$ were 0.033, 0.079 and 0.888, respectively; and when substituted into Equation 23 gave the true weight fractions for $w_{p,\mathbf{5}}$, $w_{p,\mathbf{7}}$ and $w_{p,\mathbf{11}}$ as 0.023, 0.152 and 0.827, respectively. The apparent 'click' efficiency was close to 96.6 % that decreased to 89.9% for the true 'click' efficiency.

3.4. Conclusion

In this chapter, we demonstrated a method to simulate MWDs of polymers with different chemical compositions. We derived equations that allow conversion of the true weight fraction (w_p) of a homopolymer or block to what would be determined directly from the RI-SEC (w_p^{app}) by using the different polymer's d*n*/d*c* values. Including these values into the log-normal distribution model, we accurately fit all distributions and obtain the true coupling efficiencies for a 'click' reaction that without such a consideration could under- or

overestimate the 'click' efficiency. The method described here allows effective use of the SEC to provide quantitative characterization of many complex polymer systems.

3.5. References

1. Durmaz, H.; Dag, A.; Hizal, G.; Tunca, U. *J Polym Sci Pol Chem* **2011,** 49, (5), 1195-1200.
2. Ganachaud, F.; Monteiro, M. J.; Gilbert, R. G.; Dourges, M. A.; Thang, S. H.; Rizzardo, E. *Macromolecules* **2000,** 33, (18), 6738-6745.
3. Solomon, D. H.; Rizzardo, E.; Cacioli, P. 1986.
4. Kato, M.; Kamigaito, M.; Sawamoto, M.; Higashimura, T. *Macromolecules* **1995,** 28, (5), 1721-1723.
5. Wang, J. S.; Matyjaszewski, K. *Journal of the American Chemical Society* **1995,** 117, (20), 5614-5615.
6. Le, T. P.; Moad, G.; Rizzardo, E.; Thang, S. H.
7. Percec, V.; Guliashvili, T.; Ladislaw, J. S.; Wistrand, A.; Stjerndahl, A.; Sienkowska, M. J.; Monteiro, M. J.; Sahoo, S. *Journal of the American Chemical Society* **2006,** 128, (43), 14156-14165.
8. Iha, R. K.; Wooley, K. L.; Nystrom, A. M.; Burke, D. J.; Kade, M. J.; Hawker, C. J. *Chem. Rev. (Washington, DC, U. S.)* **2009,** 109, (11), 5620-5686.
9. Hu, D.; Zheng, S. X. *Eur Polym J* **2009,** 45, (12), 3326-3338.
10. Lammens, M.; Fournier, D.; Fijten, M. W. M.; Hoogenboom, R.; Du Prez, F. *Macromolecular Rapid Communications* **2009,** 30, (23), 2049-2055.
11. Konkolewicz, D.; Monteiro, M. J.; Petrie, S. *Macromolecules* **2011,** 44, (18), 7067-7087.
12. Whittaker, M. R.; Urbani, C. N.; Monteiro, M. J. *Journal of the American Chemical Society* **2006,** 128, (35), 11360-11361.
13. Urbani, C. N.; Bell, C. A.; Lonsdale, D. E.; Whittaker, M. R.; Monteiro, M. J. *Macromolecules* **2007,** 40, (19), 7056-7059.
14. Urbani, C. N.; Bell, C. A.; Whittaker, M. R.; Monteiro, M. J. *Macromolecules* **2008,** 41, (4), 1057-1060.
15. Urbani, C. N.; Lonsdale, D. E.; Bell, C. A.; Whittaker, M. R.; Monteiro, M. J. *J Polym Sci Pol Chem* **2008,** 46, (5), 1533-1547.
16. Laurent, B. A.; Grayson, S. M. *Journal of the American Chemical Society* **2006,** 128, (13), 4238-4239.
17. Lonsdale, D. E.; Bell, C. A.; Monteiro, M. J. *Macromolecules* **2010,** 43, (7), 3331-3339.
18. Lonsdale, D. E.; Monteiro, M. J. *Chemical Communications* **2010,** 46, (42), 7945-7947.
19. Hossain, M. D.; Jia, Z. F.; Monteiro, M. J. *Macromolecules* **2014,** 47, (15), 4955-4970.

20. Hossain, M. D.; Valade, D.; Jia, Z. F.; Monteiro, M. J. *Polymer Chemistry* **2012,** 3, (10), 2986-2995.

21. Hossain, M. D.; Lu, D. R.; Jia, Z. F.; Monteiro, M. J. *Acs Macro Lett* **2014,** 3, (12), 1254-1257.

22. Peebles, L. H., *Molecular Weight Distributions in Polymers*. Wiley-Interscience: New York, 1971.

23. Monteiro, M. J. *Eur Polym J* **2015,** 65, 197-201.

24. Jia, Z.; Lonsdale, D. E.; Kulis, J.; Monteiro, M. J. *ACS Macro Letters* **2012,** 1, (6), 780-783.

25. Gavrilov, M.; Monteiro, M. J. *Eur Polym J* **2015,** 65, 191-196.

26. Shortt, D. W. *Journal of Liquid Chromatography* **1993,** 16, (16), 3371-3391.

27. Tsitsilianis, C.; Chaumont, P.; Rempp, P. *Makromol Chem* **1990,** 191, (10), 2319-2328.

28. Gavrilov, M.; Zerk, T. J.; Bernhardt, P. V.; Percec, V.; Monteiro, M. J. *Polymer Chemistry* DOI: 10.1039/c5py01855b.

29. Tuzar, Z.; Kratochv.P. *J Polym Sci Pol Lett* **1969,** 7, (12PB), 825-&.

Chapter 4

SET-LRP of NIPAM in Water via in situ Reduction of Cu(II) to Cu(0) with $NaBH_4$

In the previous chapters we demonstrated the capability of the LND simulation to precisely determine weight fractions of polymer species in both homopolymer and heteropolymer mixtures. The polymers used in the previous chapter were made using Cu-mediated 'living' radical polymerization, in particular single-electron transfer 'living' radical polymerization (SET-LRP). In conventional SET-LRP the ratio activator/deactivator is controlled altering ratio Cu(0)/ligand or Cu(0)/$CuBr_2$. In this chapter we introduce the direct and quantitative reduction of the air-stable Cu(II)Br_2/Me_6TREN to Cu(0) by $NaBH_4$ represents for SET-LRP of NIPAM. By changing the stoichiometry of $NaBH_4$ to Cu(II)Br_2, any desired ratio of Cu(II)Br_2 to Cu(0) could be obtained with no evidence of Cu(I) species. This quantitative reduction to Cu(0) in combination with rapid disproportionation of Cu(I)Br/Me_6TREN in water resulted in activation by Cu(0) initially and during the polymerization. Polymerizations of NIPAM produced polymer within minutes and with controlled and narrow molecular weight distributions in agreement with ideal 'living' radical behavior. The direct in situ thio-bromo 'click' reaction produce polymers with stable chain-end functionality, eliminating the concern of hydrolysis of the halide end-group (i.e. Br). It was found that the end-group functionality was greater than 95%, and for the very rapid polymerizations close to 100%.

4.1. Introduction

Copper-mediated 'living' radical polymerization (LRP), including ATRP[1-3] and single electron transfer-living radical polymerization (SET-LRP)[4-7], is a powerful and widely used technique for the production of polymers with control over molecular weight, molecular weight distribution (MWD) and chain-end functionality.[8-10] Attention has recently shifted to the synthesis of hydrophilic polymers by copper-mediated LRP directly in water with efforts to study mechanistic aspects in water.[11-13] Aqueous SET-LRP has been successfully used to produce water-soluble polymers with narrow MWDs and high chain-end functionality rapidly under mild conditions.[8-10, 14-17] The aqueous synthesis of these polymers needs to be fast to reduce side reactions and maintain near perfect end-group functionality. The proposed activation catalyst, Cu(0), is generated in situ through the rapid disproportionation of Cu(I) species in water that concomitantly forms the deactivating species Cu(II) in equal

amounts to Cu(0) (Scheme 4.1A)[14, 17, 18]. Because of the low solubility of Cu(I) halides in water, N-donor ligands such as tris(2-(dimethylamino)ethyl)amine (Me_6TREN) are used to solubilize the Cu(I),[19] and drive the equilibrium to the right to reach 100% disproportionation.[14, 20]

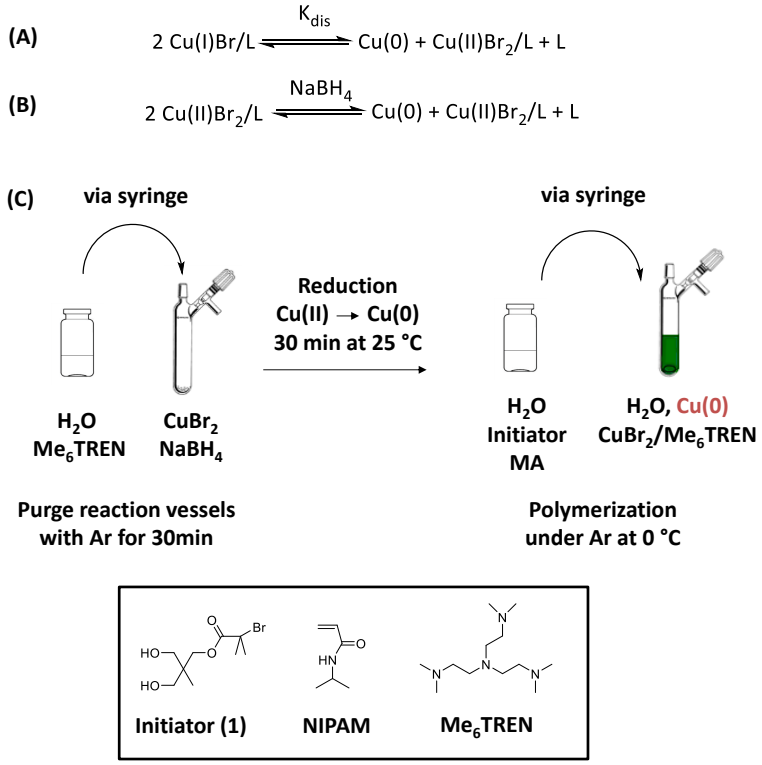

Scheme 4.1. (A) Mechanism for disproportionation, (B) reduction of Cu(II) with the reducing agent, NaBH4, and (C) schematic representation of the polymerization procedure with the pre-reduction of Cu(II) for the polymerizations.

In this chapter we demonstrate an alternative and highly effective way to generate Cu(0) directly from Cu(II)Br_2/Me_6TREN using the strong reducing agent, $NaBH_4$,[21, 22] in water (Scheme 4.1B). The advantage of using $NaBH_4$ is the stoichiometric production of Cu(0), allowing pre-defined ratios of Cu(0) activator to Cu(II) deactivator. With the desired Cu(0) to Cu(II) ratio, we polymerized N-isopropylacrylamide (NIPAM) in water to determine the level of control over the MWD and chain-end functionality using this new methodology. A major issue with aqueous polymerizations with amide-based polymers is that the halide end-groups can undergo hydrolysis to form -OH groups during polymerization, post-purification and isolation.[23] We used the thio-bromo 'click' reaction [8-10, 24, 25] in the polymerization mixture to cap the chain end-groups to overcome these issues. This procedure has the potential for coupling water-soluble polymers to a wide range of biomolecules or for generating complex polymer architectures (e.g. stars, dendrimers and sequence control brushes).[24-29]

4.1.1. Aim of the Chapter

In this chapter we introduce a new way to generate precise ratio activator/deactivator via the reduction of $CuBr_2$/Me_6TREN with $NaBH_4$. The method showed that no Cu(I) species form after the reduction and no comproportionation of copper species occurred after SET-LRP is complete according to UV-vis measurements. The catalytic system was successfully employed in SET-LRP of NIPAM and the synthesized polymers showed narrow molecular weight distributions and low dispersity.

4.2. Experimental

4.2.1. Materials

The following solvents, materials and reagents were used as received unless otherwise stated: tetrahydrofuran (THF, HPLC grade, Lichrosolv, 99.8%), toluene (HPLC, LABSCAN, 99.8%), dichloromethane (DCM, Labscan, AR grade), N,N-dimethylformamide (DMF: Labscan, AR grade), milli-Q water (Biolab, resistivity at 25 °C: 18.2 MΩ·cm), methanol (Univar, AR grade). N-isopropylacrylamide (NIPAM, Aldrich, 97 %) was recrystallized from n-hexane/toluene (9/1, v/v), sodium azide (NaN_3: Aldrich, ≥ 99.5 %), DOWEX ion-exchange resin (Aldrich, 50WX8-200), activated basic alumina (Aldrich: Brockmann I, standard grade, ~ 150 mesh, 58 Å), anhydrous magnesium sulphate ($MgSO_4$: Scharlau, extra pure) silica gel 60 (230-400 mesh) ATM (SDS), TLC plates (silica gel 60 F254), 2-bromoisobutyryl bromide (BIB: Aldrich, 98%), triethylamine (TEA, Fluka, purum), copper (II) bromide ($CuBr_2$: Aldrich, 99), thiophenol (Aldrich, 97%), sodium borohydride (Aldrich, 99%), and tris(2-(dimethylamino)ethyl)amine (Me_6TREN) was synthesized as previously described using the method of Ciampolini and Nardi.[30]

4.2.2. Synthetic Procedures

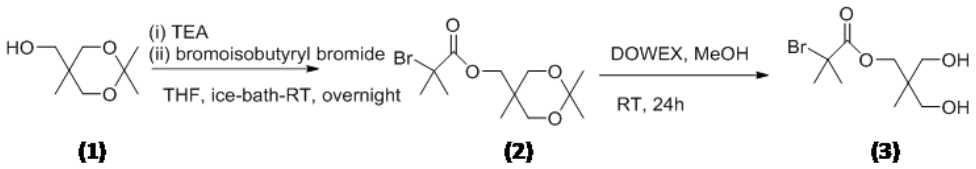

Scheme 4.2. Synthesis of water-soluble initiator for NIPAM polymerization in water.

*4.2.2.1. Synthesis of (2,2,5-trimethyl-1,3-dioxan-5-yl)methyl 2-bromo-2-methylpropanoate (**2**)*

(2,2,5-Trimethyl-1,3-dioxan-5-yl)methanol (***1***) (2.0 g, 1.25 x 10^{-2} mol), synthesized following the procedure by Jia et al.[31], was dissolved in 28 mL of DCM and placed in a 50 mL Schlenk flask equipped with a magnetic stirrer. TEA (1.91 mL, 1.37 x 10^{-2} mol) was then added. The flask was placed into an ice-bath and stirred for 10 min. α-Bromoisobutyryl bromide (1.53 g, 1.37 x 10^{-2} mol) was dissolved in 2 mL of DCM and added to the Schlenk flask via syringe over 15 min, and the solution stirred overnight. The TEA salt was filtered out, the solvent was removed by rotary evaporation and the crude product was purified by column chromatography (ethyl acetate to petroleum spirit ratio was 1:2, R_f of product = 0.37) to give 3.03 g of pure product (***2***) (yield = 78%). ^{1}H NMR ($CDCl_3$, 298K, 500 MHz); δ (ppm) 4.26 (s, 2H, -CO-O-CH_2-C), 3.67 (q, 4H, J = 15Hz, -O-CH_2-C), 1.94 (s, 6H, methyl protons), 1.42 (d, 2H, *J* = 16.3 Hz, methyl protons), 0.91 (s, 3H, methyl protons). ^{13}C NMR ($CDCl_3$, 298K, 500 MHz) δ (ppm): 171.7, 98.3, 68.3, 66.3, 55.9, 34.2, 31.0, 27.1, 20.5, 17.8.

*4.2.2.2. Synthesis of initiator 3-hydroxy-2-(hydroxymethyl)-2-methylpropyl 2-bromo-2-methylpropanoate (**3**)*

(2,2,5-Trimethyl-1,3-dioxan-5-yl)methyl 2-bromo-2-methylpropanoate (***2***) (3 g, 9.7 x 10) was dissolved in 30 mL of methanol, and DOWEX (1.5 g) was added to the solution. The reaction mixture was stirred overnight, and the conversion was monitored by TLC. As some unreacted dioxane was still in the system the solution was filtered, 0.77g of DOWEX resin was added and the solution was stirred for additional 8 h. DOWEX was removed by filtration and the solution was concentrated to give white crystals of pure product. Yield: 97%, mp = 65.5 °C. ^{1}H NMR ($CDCl_3$, 298K, 500 MHz); δ (ppm) 4.27 (s, 2H, -CO-O-CH_2-C), 3.61 (d, 4H, *J* = 4.2Hz, -C-CH_2-OH), 2.53 (b, 2.26, hydroxyl protons), 1.95 (s, 6H, methyl protons), 0.90 (s, 3H, methyl protons). ^{13}C NMR ($CDCl_3$, 298K, 500 MHz) δ (ppm): 172.8, 68.3, 68.0, 56.1, 41.5, 31.1, 17.1.

4.2.2.3. General procedure for SET-LRP in water

To a 20 mL Schlenk tube equipped with magnetic stirrer, $CuBr_2$ and $NaBH_4$ were added. Sodium borohydride was weighed with a precision of ±0.001mg. The flask was sealed with a rubber septum and purged with Ar for 30 min. To a 5 mL glass vial, Me_6TREN and milli-Q water (1 mL) were added; the vial sealed and the solution purged with Ar for 30 min. The solution was cannula transferred to the Schlenk tube and placed in an ice-bath where the reduction of Cu^{II} was allowed to proceed for 30 min. Another mixture of NIPAM and the initiator were dissolved in water (2.48 mL) in a 20 mL glass vial, sealed, purged with Ar for 30 min at 0 °C, and then cannula transferred to the Schlenk tube. The reaction mixture was allowed to stir at 0 °C. Samples for THF RI GPC were dissolved in THF, passed through activated neutral alumina and filtered using a 0.45 μL membrane. Samples for ^1H NMR were dissolved in D_2O and used directly.

4.2.2.4. General procedure for thio-bromo 'click' reaction

A polymer sample for thio-bromo 'click' reaction was taken from the polymerization mixture and added to a 10-fold excess of thiophenol in a 1.5 mL GPC vial equipped with a magnetic stirrer. TEA (10 equivalents) in 0.3 mL of acetonitrile were then added, the vial was capped and the reaction was stirred for 3 h. 10 μL of the reaction solution was directly mixed with 20 μL of DCTB matrix (20 mg/mL in THF) and 2 μL of Na^+ salt (1 mg/mL in THF) for analysis by MALDI-ToF spectrometry.

4.2.2.5. Synthesis of $[Cu^{II}(Me_6TREN)Br]Br$ for glovebox experiments

The synthesis of this compound was conducted in an identical manner to that previously reported by our laboratory.[32] Anal. Calc. For $C_{12}H_{30}N_4CuBr_2$ (453.75 $gmol^{-1}$): C, 31.8; H, 6.7; N, 12.3. Found: C, 31.9; H, 6.7; N, 12.3.

4.2.2.6. Glovebox Reduction of $[Cu^{II}(Me_6TREN)Br]Br$

Unless otherwise stated, all manipulations were performed inside a Nitrogen glovebox containing < 10 ppm O_2. All solutions were distilled, degassed and stored in the glovebox for a minimum of 24 h before being used.

To five identical cuvettes each containing 3.0 mL of a 5.0 mM solution of $[Cu^{II}(Me_6TEN)Br]Br$ in H_2O (34 mg in 0.015 L) were added varied portions of a 0.20 M stock solution of $NaBH_4$ in dry ethanol (38 mg in 5.0 mL). Upon addition of the relevant molar equivalents of reducing agent, each cuvette was sealed with a gas-tight lid and

vigorously mixed for two minutes. Immediate reduction of Cu^{II} to Cu^{0} was observed by the formation of bronze/grey particles. Once the relevant concentration of reducing agent was added, the solutions were allowed to stand for 30 min during which sedimentation of the particles occurred yielding solutions with less intense blue color (including solutions with imperceptible color after addition of greater than equimolar $NaBH_4$ *vs* Cu^{II}).

The spectrophotometer was standardized against distilled water and the spectrum of each cuvette recorded. In order to determine the presence of copper(I) species, a sealed oxygen balloon/syringe was introduced into the glovebox and bubbled into the relevant cuvette for ca. 60 seconds without disturbing the precipitate. The spectrum was immediately re-measured, all other conditions being constant to the previous measurements, and differences between the absorbance at 850 nm were used in conjunction with Beers law to determine changes in the concentration of copper(II).

4.2.3. Analytical Methodologies

^{1}H Nuclear Magnetic Resonance Spectroscopy (NMR)

All NMR spectra were recorded on a Bruker DRX 500 MHz spectrometer at 25 °C using an external lock ($CDCl_3$) and referenced to the residual non-deuterated solvent ($CHCl_3$). Conversion was determined by ^{1}H NMR by adding 5-6 drops of the polymerization mixture into 0.7 mL of D_2O.

Size Exclusion Chromatography (SEC)

The polymers or polymer solutions were dissolved in tetrahydrofuran (THF) to a concentration of ca. 1 mg/mL and filtered through a 0.45 µm PTFE syringe filter prior to an injection. Analysis of the molecular weight distributions of the polymers was performed on a Waters 2695 separations module, fitted with a Waters 410 refractive index detector maintained at 35 °C, a Waters 996 photodiode array detector, and two Ultrastyragel linear columns (7.8 x 300 mm) arranged in series. The columns maintained at 40 °C for all analyses are capable of separating polymers in the molecular weight range of 500 – 4 million g/mol with high resolution. All samples were eluted at a flow rate of 1.0 mL/min. Narrow molecular weight PSTY standards ($Đ \leq 1.1$) ranging from 500 to $2x10^{6}$ g/mol were used for calibration. Data acquisition was performed using Empower software, and molecular weights were calculated relative to polystyrene standards. MWDs from kinetic

experiments were determined by adding 5-6 drops of polymer mixture to 1.3 mL of THF, filtered and injected onto the SEC system.

Matrix-Assisted Laser Desorption Ionization – Time-of-Flight (MALDI-ToF) Mass Spectrometry

MALDI-ToF MS spectra were obtained using a Bruker MALDI-ToF autoflex III smartbeam with accessible mass range of 600 – 400,000 Da. Ions were accelerated with a nitrogen laser (337 nm, 200 Hz maximum firing rate). All spectra were recorded in either reflectron (1500 – 5000 Da) or linear mode (5000 – 400,000 Da) using trans-2-[3-(4-*tert*-butylphenyl)-2-methyl-propenylidene] malononitrile (DCTB; 20 mg/mL in THF) as the matrix and Na(CF_3COO) (2 mg/mL in THF) as the cation source. The polymers were dissolved to a concentration of 1 mg/mL in THF. The matrix (20 μL), Ag(CF_3COO) (2 μL) and polymer (20 μL) solutions were mixed together and spotted on the target plate via a 'dried droplet' method.

UV-vis Spectroscopy

UV-vis studies were all conducted within a glove box using an Ocean Optics DT-MINI-2-GS UV-VIS-NIR light source. Identical 4.0 mL quartz cuvettes were used. Given that this is a single beam instrument, a reference spectrum was collected prior to the experiment using a cuvette which contained only the relevant solvent.

4.3. Results and Discussion

The mechanism of SET-LRP relies on the in situ disproportionation of Cu(I) to Cu(0) and Cu(II) to continuously produce high levels of deactivator during the polymerization, a 'self-regulated' system.[5, 6, 8-10] Recent work by Haddleton and coworkers[14, 15, 17, 18] used the rapid and complete disproportionation process of Cu(I)Br/Me_6TREN in water to generate the Cu(0) and Cu(II)Br_2/Me_6TREN species in equal concentrations. A water-solution containing monomer and initiator was then added, resulting in rapid polymerization and excellent control of the MWD. This pre-mixture has been used successfully to polymerize many monomer systems. The difficulty with using Cu(I) is its facile oxidation to Cu(II) in the presence of air, requiring careful elimination of oxygen prior to and during disproportionation of the pre-mixture. Here, we propose directly generating Cu(0) from the air stable Cu(II) species using the reducing agent $NaBH_4$.

A nitrogen glovebox containing less than 10 ppm of O_2 was used to monitor the reduction of Cu(II)Br in the presence of $NaBH_4$ in water using a UV-vis spectrometer within the

glovebox. All the solutions were stored in the glovebox for a minimum of 24 h prior to being mixed. Figure 4.1A showed the UV-vis spectra from 500-900 nm at different ratios of Cu(II)Br_2/Me_6TREN to $NaBH_4$. The addition of $NaBH_4$ resulted in the reduction of absorbance in the spectrum, supporting the reduction of Cu(II) species. The mixture immediately changed from aqua to dark green accompanied by formation of bronze/grey particles, indicating generation of Cu(0) and loss of Cu(II). After 30 min, once the solid particles settled yielding a light blue solution, the concentration of Cu(II) was determined from the absorbance at 850 nm. With the increasing ratio of $NaBH_4$, the reduction of Cu(II) was quantitative according to available analytical methods (Figure 4.1B, experimental *vs* theoretically predicted). To test whether Cu(II) was fully reduced to Cu(0) with $NaBH_4$, we added oxygen to the mixture after 30 min and found no change in the UV-vis spectrum for $NaBH_4$ to Cu(II) ratios of 0.21 and 0.67 (see Figure 4.1A). These findings provide strong support for the quantitative reduction according to available analytical methods of Cu(II) to Cu(0) relative to the added equivalents of $NaBH_4$ with no evidence of Cu(I) species in solution.

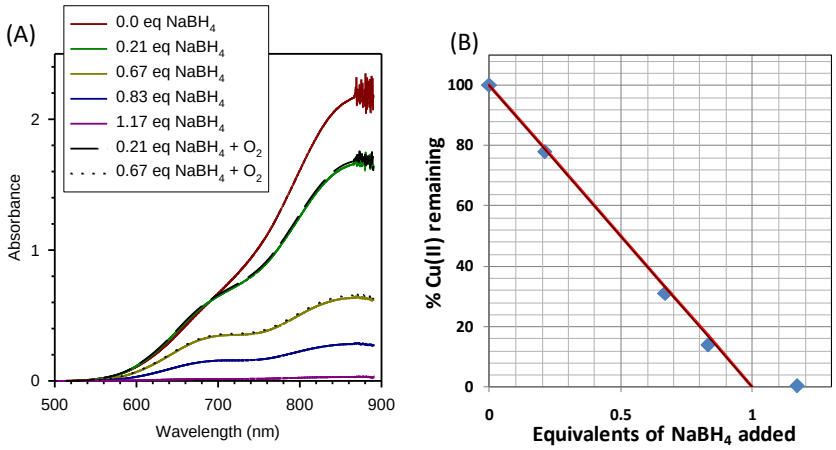

Figure 4.1. (A) UV-vis spectra of 5 mM [Cu^{II}(Me_6TREN)Br]Br in H_2O upon $NaBH_4$ addition (measured in the 500-900 nm range), and (B) percentage of remaining Cu(II) calculated from Beers law at 850 nm. Red line denotes theoretical loss of Cu(II) to quantitative conversion to Cu(0) only via the $NaBH_4$ reduction method.

The NIPAM polymerizations utilized the in situ production of Cu(0) with $NaBH_4$. The Cu(II)Br_2/Me_6TREN complex was made in situ through the addition of an aqueous solution of Me_6TREN to a solid mixture of $CuBr_2$ and $NaBH_4$, bypassing the pre-formation of the copper/ligand complex as described in the reduction experiments above. It should be noted that the polymerization data was similar for the pre-made (data not shown) as compared to the in situ made complex (*vide infra*). During storage in water, $NaBH_4$ slowly self-

hydrolyses to hydrogen gas and basic hydrated metaborate, resulting in gas evolution and a pH increase, in which this hydrolysis can be slowed at high pH.[33] Therefore, we added Me_6TREN in water (pH >8) to solid $CuBr_2$ and $NaBH_4$, resulting in much faster reduction of $CuBr_2/Me_6TREN$ (Scheme 4.1B) relative to $NaBH_4$ hydrolysis. The halide initiator (**3**) was synthesized in a 97% yield with two -OH groups to make it water soluble.

The first set of NIPAM polymerizations was carried out using a $[Cu(II)]_0/[NaBH_4]_0$ ratio of 0.8/0.2 and targeting varying degrees of polymerization from 20 to 50 (see Scheme 4.1C for polymerization procedure). All reactant concentrations were kept constant except for the monomer concentration. There was a relatively linear increase in conversion with time for all four polymerizations (Figure 4.2A).

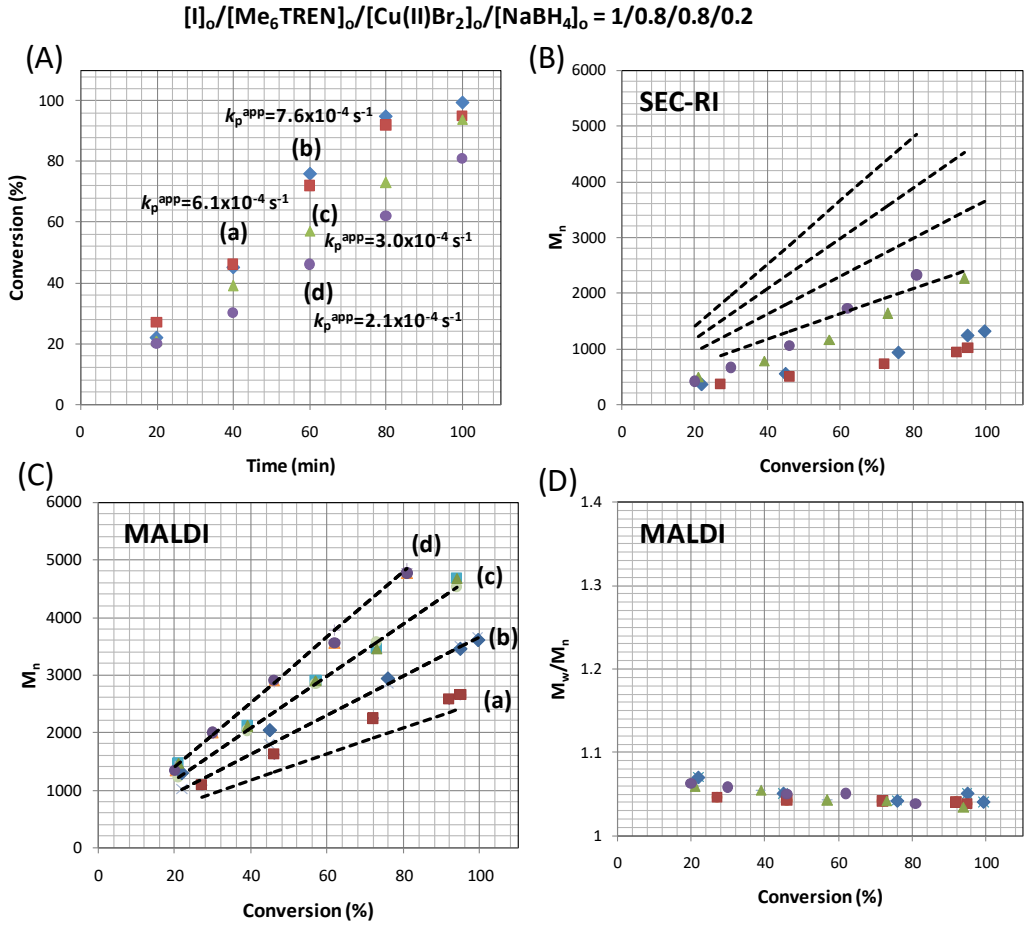

Figure 4.2. Aqueous SET-LRP of NIPAM catalyzed by the in situ generation of Cu(0) from $NaBH_4$ by varying $[NIPAM]_0/[I]_0$ from (a) 20/1 ■, (b) 30/1 ♦, (c) 40/1 ▲, (d) 50/1 ●. (A) Kinetic plots using the procedure given in Scheme 4.1C, (B) M_n determined from SEC using RI and polystyrene standards (dashed lines represent theoretical M_n values), (C) M_n determined by MALDI-ToF (dashed lines represent theoretical M_n values), and (D) M_w/M_n. Reaction conditions: $[I]_0/[Me_6TREN]_0/[Cu(II)Br_2]_0/[NaBH_4]_0$ = 1/0.8/0.8/0.2. [I] = 0.0267 M in 3.48 mL of water.

The rate of polymerization decreased with an increase in monomer concentration due to the lowering of the propagation rate coefficient (k_p) as a function of [NIPAM]. Within the NIPAM concentration range used here, it was found that k_p decreased by a factor of 4 with increasing [NIPAM].[34] The k_p^{app} ($=k_p[P^{\cdot}]$) determined from the first order rate equation for the highest $[NIPAM]_0$ (1.33 M) was approximately half that at the lowest $[NIPAM]_0$ used (i.e. 0.534 M) in agreement with the reducing k_p value.

The number-average molecular weight (M_n) determined by size exclusion chromatography (SEC) using polystyrene (PSTY) standards with conversion (Figure 4.2B) was significantly lower than $M_{n,theory}$ (dashed lines) for all four polymerizations. This resulted from the different hydrodynamic volumes of PNIPAM as compared to those of PSTY. The literature Mark-Houwink (M-H) K and a values for PNIPAM gave poor agreement with either $M_{n,theory}$ or $M_{n,MALDI}$ determined from the MALDI distributions (see Figure 4.3 and Appendix). The reason for this was that the experimental molecular weights were all close to the exclusion limit of the SEC columns. The $M_{n,MALDI}$ was in excellent agreement with $M_{n,theory}$ (Figure 4.2C). Calculation of new M-H parameters (K = 1.087 x 10^{-4} mL/g; a = 1.335) from the correlation between SEC-RI and MALDI M_n's allowed us to overlay the SEC traces with the MALDI distributions as shown in Figure 4.3 (and also in Appendix) even though the a value (>1) was physically unrealistic. Therefore, the dispersity (Đ) was determined from the MALDI distributions. The dispersity values for the four polymerizations ($[Cu(II)]_0/[NaBH_4]_0$ = 0.8/0.2) were all well below 1.1, indicating the formation of polymers with very narrow molecular weight distributions (Figure 4.2D). The data supported the 'living' radical behaviour in our polymerizations. The data also supported that our new method for the reduction of $Cu(II)Br_2$ with $NaBH_4$ in combination with rapid disproportionation of $Cu(I)Br/Me_6TREN$ in water generated activation by Cu(0) and eliminated any activation by Cu(I).

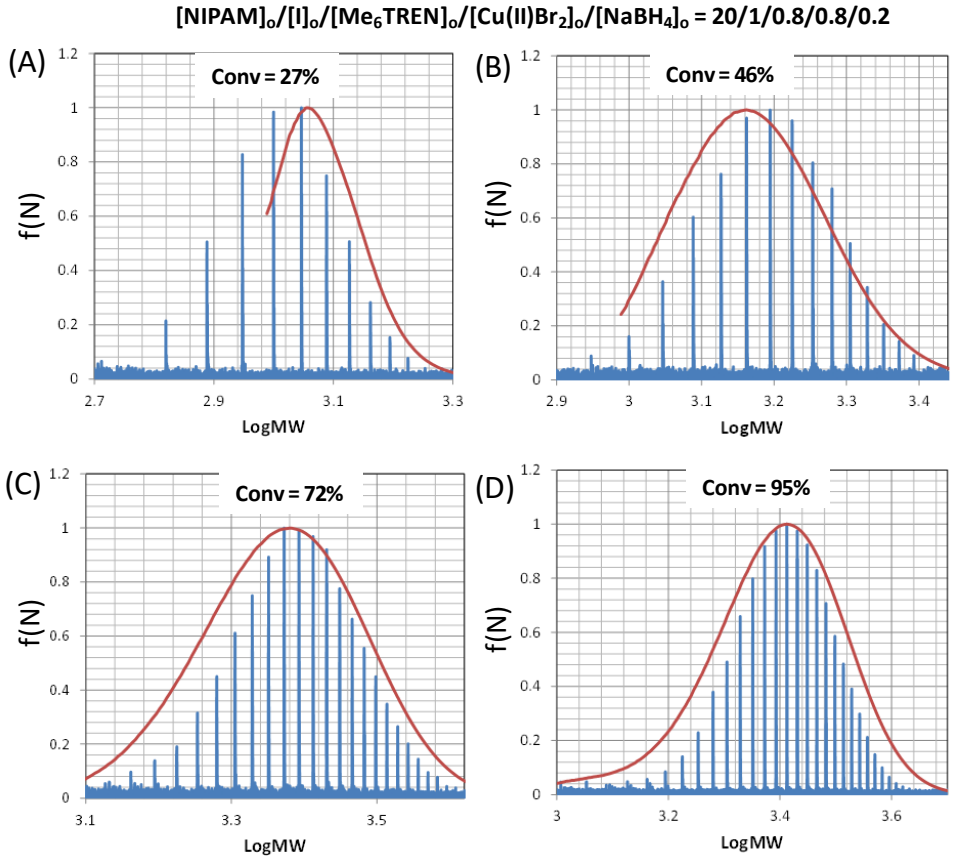

Figure 4.3. MALDI-ToF and SEC (RI using polystyrene standards, red line) for the aqueous SET-LRP of NIPAM over the conversion range. Reaction conditions: $[NIPAM]_0/[I]_0/[Me_6TREN]_0/[Cu(II)Br_2]_0/[NaBH_4]_0$ = 20/1/0.8/0.8/0.2. [I] = 0.0267 M in 3.48 mL of water.

One of the most important aspects of LRP is the production of polymer chains with high chain-end functionality. SET-LRP has been a demonstrated technique to produce chains with near 100% end-group fidelity.[8-10] The problem with water-based polymerizations, however, is the rapid hydrolysis of the -Br groups.[23] Attempts to purify the polymers after the polymerizations produced mainly -OH groups (data not shown). We therefore in situ reacted the -Br end-groups with thiophenol using the established thio-bromo 'click' reaction,[8, 24, 25] eliminating exposure of the polymer halide end-groups to hydrolysis. The MALDI showed that the thio-bromo reaction at different conversions was near quantitative for the $[NIPAM]_0/[I]_0/[Me_6TREN]_0/[Cu(II)Br_2]_0/[NaBH_4]_0$ = 20/1/0.8/0.8/0.2 polymerization (Figure 4.4).

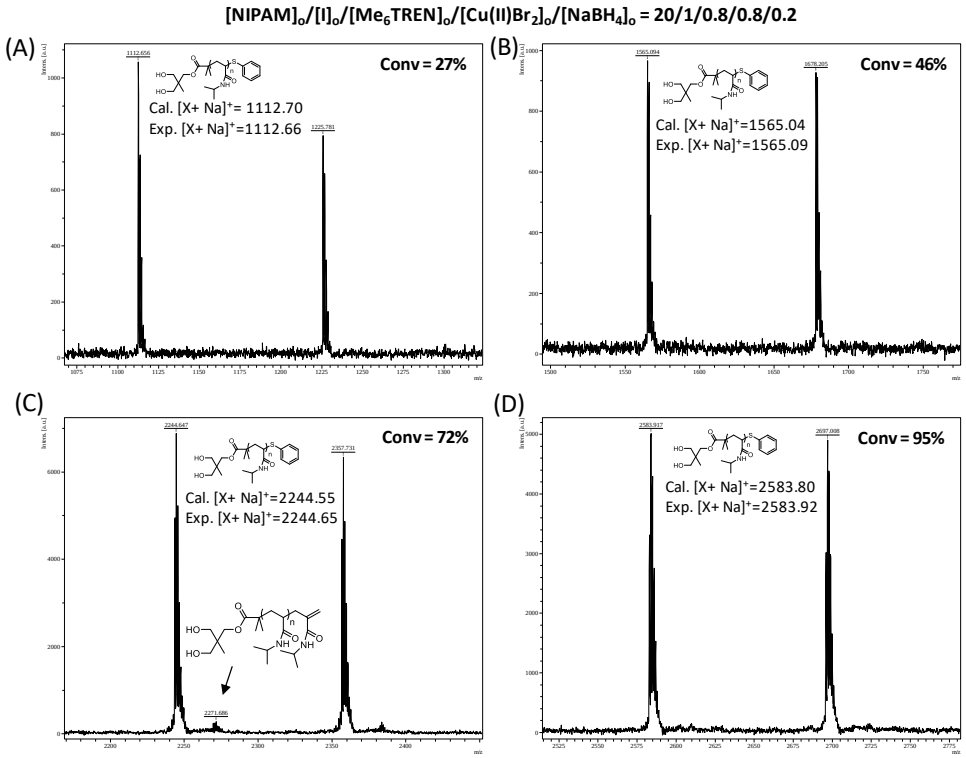

Figure 4.4. MALDI-ToF for the aqueous SET-LRP of NIPAM over the conversion range. Reaction conditions: $[NIPAM]_0/[I]_0/[Me_6TREN]_0/[Cu(II)Br_2]_0/[NaBH_4]_0$ = 20/1/0.8/0.8/0.2. [I] = 0.0267 M in 3.48 mL of water.

There was no evidence of termination products from radical-radical coupling even up to 95% conversion. The Appendix has MALDI data for all other polymerizations. The four polymerizations at a $[Cu(II)Br_2]_0/[NaBH_4]_0$ ratio of 0.8/0.2 gave close to 100% chain-end functionality up to 60% conversion independent of the $[NIPAM]_0$ (Figure 4.5).

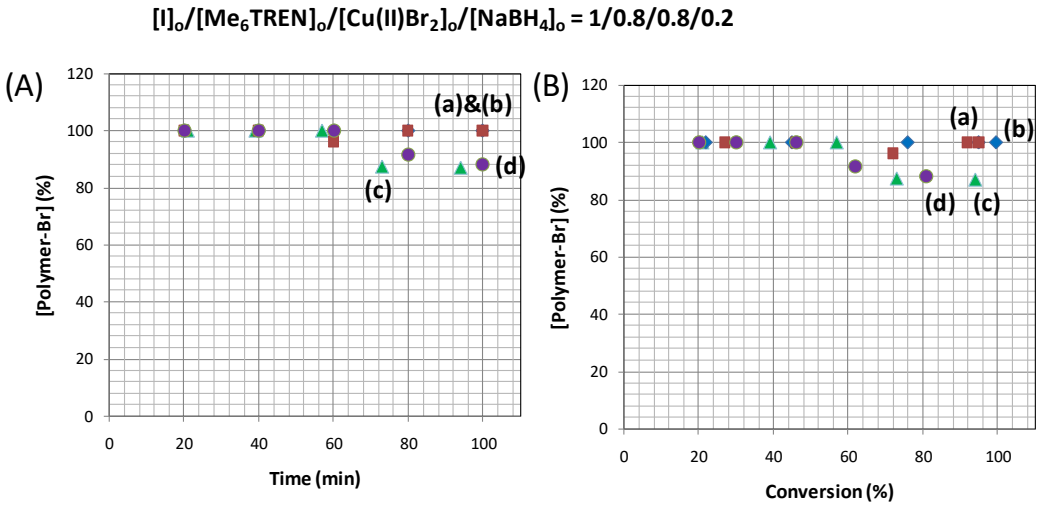

Figure 4.5. Chain-end functionality after in situ thio-bromo reaction from aqueous SET-LRP of NIPAM; varying $[NIPAM]_0/[I]_0$ from (a) 20/1■, (b) 30/1 ♦, (c) 40/1 ▲, (d) 50/1●.

At conversions greater than 60%, the end-group functionality was maintained close to 100% for the two lowest NIPAM concentrations (i.e. $[NIPAM]_0/[I]_0$ = 20 and 30), but at $[NIPAM]_0/[I]_0$ greater than 30 there was some loss of end-group functionality. Since the latter polymerizations were slower due to the lower k_p at higher $[NIPAM]_0$ there would be a greater chance of other competing side reactions (e.g. transfer to monomer). Most peaks from these side reactions were assigned to either the internal (i.e. I-$NIPAM_n$-$CH{=}CH(CONHCH(CH_3)_2)$) or external double bonds on the chain-ends (i.e. I-$NIPAM_n$-$CH(CONHCH(CH_3)_2){=}CH_2$) (see Appendix). The external double bond occurs through a backbiting mechanism induced by the MALDI spectrometer.[35, 36] We next wanted to investigate the effect of increasing the ratio of $[NaBH_4]_0$ to $[Cu(II)]_0$. This should produce a higher ratio of the activating Cu(0) to the deactivating Cu(II) at the start of the polymerization. Increasing the ratio of $NaBH_4$ generated a rapid rate of polymerization (Figure 4.6A), in which close to 100% conversion was observed when the $[Cu(II)]_0/[NaBH_4]_0$ was 0.8/0.6 and 0.8/0.8.

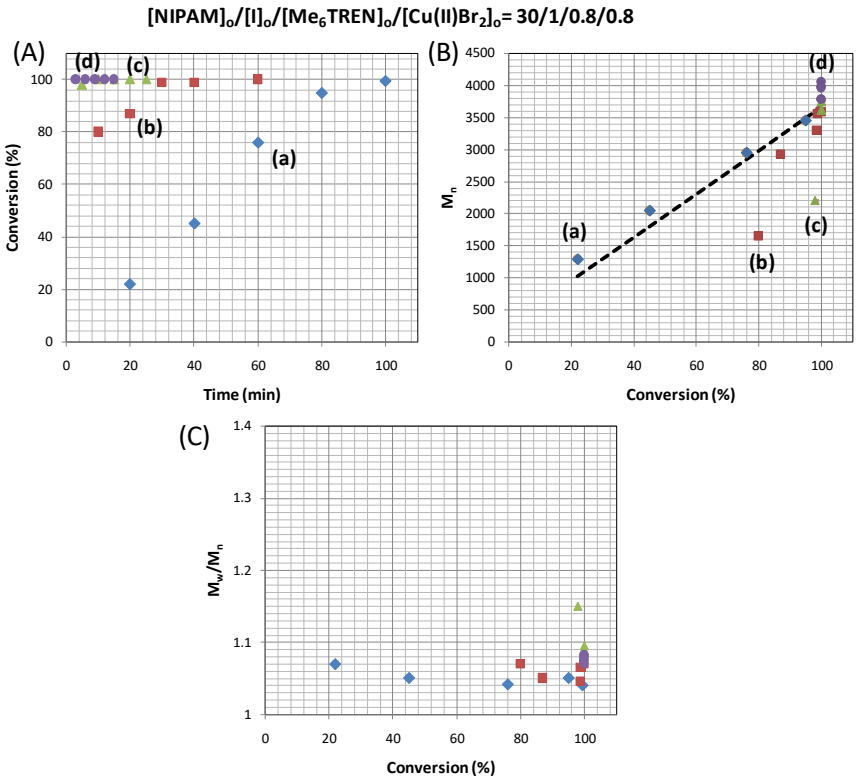

Figure 4.6. Aqueous SET-LRP of NIPAM catalyzed by the in situ generation of Cu(0) from $NaBH_4$ at $[NIPAM]_0/[I]_0$ = 30 and varying $[CuBr_2]_0/[NaBH_4]_0$ from (a) 0.8/0.2 ♦, (b) 0.8/0.4 ■, (c) 0.8/0.6 ▲, (d) 0.8/0.8 ●. (A) Kinetic plots using the procedure given in Scheme 4.1C, (B) M_n determined from SEC using RI and polystyrene standards (dashed lines represent theoretical M_n values), (C) M_n determined by MALDI-ToF (dashed lines represent theoretical M_n values), and (D) M_w/M_n. Reaction conditions: $[NIPAM]_0/[I]_0/[Me_6TREN]_0/[Cu(II)Br_2]_0$ = 30/1/0.8/0.8. [I] = 0.0267 M in 3.48 mL of water.

The $M_{n,MALDI}$ was close to $M_{n,Theory}$ except for two data points (Figure 4.6B), and the dispersity index values were lower than 1.1 (Figure 4.6C). Even though the polymerization for the highest $[NaBH_4]_0$ of 0.8 reached 100% conversion in less than 3 min, control over the MWD was excellent. In addition, we found that the chain-end functionality was close to 100% for all polymerizations, even up to conversions close to 95% (Figure 4.7).

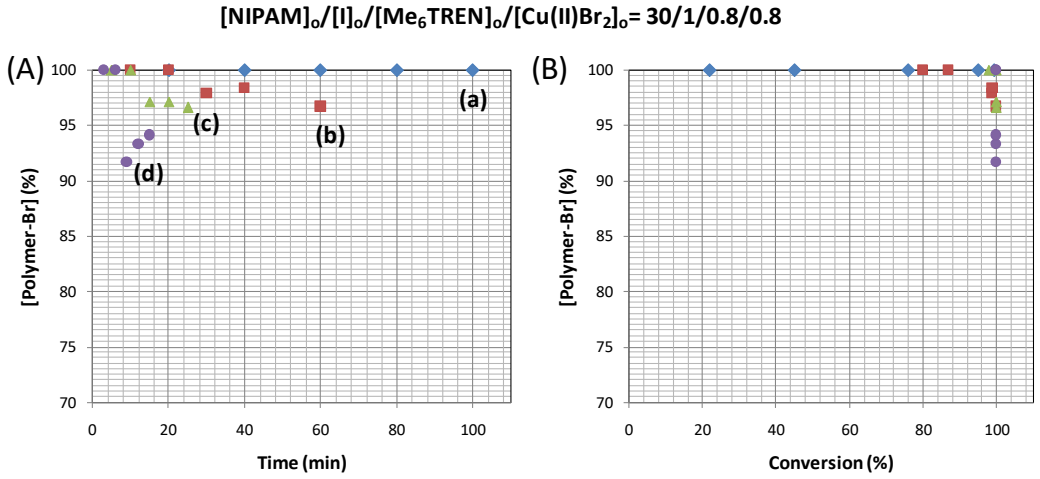

Figure 4.7. Chain-end functionality after the in situ thio-bromo reaction after the aqueous SET-LRP of NIPAM at $[NIPAM]_0/[I]_0$ = 30 and varying $[CuBr_2]_0/[NaBH_4]_0$ from (a) 0.8/0.2 ♦, (b) 0.8/0.4 ■, (c) 0.8/0.6 ▲, (d) 0.8/0.8 ●.

The conversion measure by ^{1}H NMR showed no difference if MEHQ inhibitor was added immediately after sampling (see Figure A4.19 in Appendix), confirming the accuracy of conversion determination by ^{1}H NMR analysis. We further carried out UV-vis experiments to determine the concentration of Cu(I) at the end of the polymerization (see Figure A4.21 in Appendix). The data showed that after opening and bubbling the polymerization mixture with air there was no change in the UV-vis spectra for two polymerizations, supporting the case that Cu(I) is not present at detectable levels at the start and during the polymerization.

4.4. Conclusion

In summary we introduced direct reduction of the air stable $Cu(II)Br_2/Me_6TREN$ complex to Cu(0) with $NaBH_4$ which represented a new methodology to produce the activating Cu(0) in water without the aid of disproportionation. Glovebox experiments showed quantitative reduction according to available analytical methods of Cu(II) to Cu(0) with added equivalents of $NaBH_4$, as no change in Cu(II) concentration was observed with the addition of oxygen after reduction. This reduction method allowed desired stoichiometric ratios of Cu(0)/Cu(II) to be produced at the initial stage of polymerization by adding the appropriate equivalents of $NaBH_4$ to Cu(II). The water-based polymerization of NIPAM at different

ratios of $[Cu(0)]_0/[Cu(II)Br_2]_0$ produced polymers with controlled rates of polymerizations and MWDs. The M_n's gave excellent correlation to $M_{n.theory}$ and polymers with dispersities lower than 1.1, demonstrated ideal 'living' radical behaviour. The concern of hydrolysis of the halide (-Br) end-group was eliminated by capping the chain-ends using the extremely rapid thio-bromo 'click' reaction directly in the polymerization mixture. This allowed determination of the end-group functionality as a function of conversion with the end-group functionality greater than 95% in most cases, and for the fast polymerizations (with a high $[Cu(0)]_0/[Cu(II)Br_2]_0$ ratio) end-group functionality was close to 100%. Our new method in combination with the rapid disproportionation reaction in water clearly demonstrated that activation could only occur via Cu(0), eliminating activation by Cu(I) species.

4.5. References

1. Wang, J. S.; Matyjaszewski, K. *J Am Chem Soc* **1995,** 117, (20), 5614-5615.

2. Matyjaszewski, K. *Macromolecules* **2012,** 45, (10), 4015-4039.

3. Kato, M.; Kamigaito, M.; Sawamoto, M.; Higashimura, T. *Macromolecules* **1995,** 28, (5), 1721-1723.

4. Percec, V.; Popov, A. V.; Ramirez-Castillo, E.; Monteiro, M.; Barboiu, B.; Weichold, O.; Asandei, A. D.; Mitchell, C. M. *J Am Chem Soc* **2002,** 124, (18), 4940-4941.

5. Percec, V.; Guliashvili, T.; Ladislaw, J. S.; Wistrand, A.; Stjerndahl, A.; Sienkowska, M. J.; Monteiro, M. J.; Sahoo, S. *J Am Chem Soc* **2006,** 128, (43), 14156-14165.

6. Rosen, B. M.; Percec, V. *Chem Rev* **2009,** 109, (11), 5069-5119.

7. Zhang, N.; Samanta, S. R.; Rosen, B. M.; Percec, V. *Chem Rev* **2014,** 114, (11), 5848-5958.

8. Lligadas, G.; Percec, V. *J Polym Sci Pol Chem* **2007,** 45, (20), 4684-4695.

9. Nguyen, N. H.; Levere, M. E.; Kulis, J.; Monteiro, M. J.; Percec, V. *Macromolecules* **2012,** 45, (11), 4606-4622.

10. Nguyen, N. H.; Levere, M. E.; Percec, V. *J Polym Sci Pol Chem* **2012,** 50, (5), 860-873.

11. Konkolewicz, D.; Wang, Y.; Krys, P.; Zhong, M. J.; Isse, A. A.; Gennaro, A.; Matyjaszewski, K. *Polym Chem-Uk* **2014,** 5, (15), 4396-4417.

12. Konkolewicz, D.; Krys, P.; Gois, J. R.; Mendonca, P. V.; Zhong, M. J.; Wang, Y.; Gennaro, A.; Isse, A. A.; Fantin, M.; Matyjaszewski, K. *Macromolecules* **2014,** 47, (2), 560-570.

13. Asubaie, F.; Anastasaki, A.; Nikolaou, V.; Simula, A.; Nurumbetov, G.; Wilson, P.; Kempe, K.; Haddleton, D. M. *Macromolecules* **2015,** 48, (18), 6421-6432.

14. Zhang, Q.; Wilson, P.; Li, Z. D.; McHale, R.; Godfrey, J.; Anastasaki, A.; Waldron, C.; Haddleton, D. M. *J Am Chem Soc* **2013,** 135, (19), 7355-7363.

15. Waldron, C.; Zhang, Q.; Li, Z. D.; Nikolaou, V.; Nurumbetov, G.; Godfrey, J.; McHale, R.; Yilmaz, G.; Randev, R. K.; Girault, M.; McEwan, K.; Haddleton, D. M.; Droesbeke, M.; Haddleton, A. J.; Wilson, P.; Simula, A.; Collins, J.; Lloyd, D. J.; Burns, J. A.; Summers, C.; Houben, C.; Anastasaki, A.; Li, M. X.; Becer, C. R.; Kiviaho, J. K.; Risangud, N. *Polym Chem-Uk* **2014,** 5, (1), 57-61.

16. Alsubaie, F.; Anastasaki, A.; Wilson, P.; Haddleton, D. M. *Polym Chem-Uk* **2015,** 6, (3), 406-417.

17. Samanta, S. R.; Nikolaou, V.; Keller, S.; Monteiro, M. J.; Wilson, D. A.; Haddleton, D. M.; Percec, V. *Polym Chem-Uk* **2015,** 6, (11), 2084-2097.

18. Nguyen, N. H.; Rosen, B. M.; Percec, V. *J Polym Sci Pol Chem* **2010,** 48, (8), 1752-1763.

19. Navon, N.; Cohen, H.; Paoletti, P.; Valtancoli, B.; Bencini, A.; Meyerstein, D. *Ind Eng Chem Res* **2000,** 39, (10), 3536-3540.

20. Rosen, B. M.; Jiang, X.; Wilson, C. J.; Nguyen, N. H.; Monteiro, M. J.; Percec, V. *J Polym Sci Pol Chem* **2009,** 47, (21), 5606-5628.

21. Liu, Q. M.; Zhou, D. B.; Yamamoto, Y.; Ichino, R.; Okido, M. *T Nonferr Metal Soc* **2012,** 22, (1), 117-123.

22. Jia, B. Q.; Mei, Y.; Cheng, L.; Zhou, J. P.; Zhang, L. N. *Acs Appl Mater Inter* **2012,** 4, (6), 2897-2902.

23. Rademacher, J. T.; Baum, R.; Pallack, M. E.; Brittain, W. J.; Simonsick, W. J. *Macromolecules* **2000,** 33, (2), 284-288.

24. Rosen, B. M.; Lligadas, G.; Hahn, C.; Percec, V. *J Polym Sci Pol Chem* **2009,** 47, (15), 3940-3948.

25. Rosen, B. M.; Lligadas, G.; Hahn, C.; Percec, V. *J Polym Sci Pol Chem* **2009,** 47, (15), 3931-3939.

26. Liu, Z. Z.; Zhu, S. J.; Li, Y. J.; Li, Y. S.; Shi, P.; Huang, Z.; Huang, X. Y. *Polym Chem-Uk* **2015,** 6, (2), 311-321.

27. Lu, G. L.; Li, Y. J.; Gao, H. S.; Guo, H.; Zheng, X. L.; Huang, X. Y. *J Polym Sci Pol Chem* **2013,** 51, (5), 1099-1106.

28. Li, Y. J.; Lu, G. L.; Dai, B.; Xu, C. X.; Huang, X. Y. *J Polym Sci Pol Chem* **2013,** 51, (9), 1942-1949.

29. Lu, G. L.; Li, Y. J.; Guo, H.; Du, W. Y.; Huang, X. Y. *Polym Chem-Uk* **2013,** 4, (10), 3132-3139.

30. Ciampoli.M; Nardi, N. *Inorg Chem* **1966,** 5, (1), 41-&.

31. Jia, Z. F.; Lonsdale, D. E.; Kulis, J.; Monteiro, M. J. *Acs Macro Lett* **2012,** 1, (6), 780-783.

32. Bell, C. A.; Bernhardt, P. V.; Monteiro, M. J. *J Am Chem Soc* **2011,** 133, (31), 11944-11947.

33. Retnamma, R.; Novais, A. Q.; Rangel, C. M. *Int J Hydrogen Energ* **2011,** 36, (16), 9772-9790.

34. Ganachaud, F.; Balic, R.; Monteiro, M. J.; Gilbert, R. G. *Macromolecules* **2000,** 33, (23), 8589-8596.

35. Gies, A. P.; Vergne, M. J.; Orndorff, R. L.; Hercules, D. M. *Macromolecules* **2007,** 40, (21), 7493-7504.

36. Ladaviere, C.; Lacroix-Desmazes, P.; Delolme, F. *Macromolecules* **2009,** 42, (1), 70-84.

Chapter 5

Quantitative End-Group Functionalization of PNIPAM from Aqueous SET-LRP via in situ Reduction of Cu(II) with $NaBH_4$

In the previous chapter we introduced a new method to control polymerization rate of aqueous single-electron transfer 'living' radical polymerization (SET-LRP) using a new method to reduce Cu(II) directly and quantitatively to Cu(0) with no trace of Cu(I). Although the method gives poly(*N*-isopropylacrylamide) (PNIPAM) with low dispersity (Đ), the major issue with the technique is the hydrolysis of the halide chain-end which has restricted the use of the polymer from further 'click' reactions. In this chapter we examined the kinetics of hydrolysis of halide chain end of PNIPAM. It was found that hydrolysis followed a pseudo first order loss rate, reaching near completion after ~15 h. The hydrolysis rate was not influenced by either molecular weight or the amount of Cu(0) or Cu(II) in the system. To overcome the issues of hydrolysis, we introduce an aqueous-phase in situ azidation, which usually is a slow process (from 10-24 h) in organic solvents, but when carried out in aqueous phase, it quantitatively converts the halide end-groups to azides within 30 s. This allowed the polymer to be purified and further coupled to an alkyne PNIPAM with greater than 97% coupling efficiency. Our work provides a direct and quantitative method to produce polymers made in water with stable 'click' functional end-groups, expanding the use of such polymers in the construction of more complex polymer architectures.

5.1. Introduction

Cu(0) catalyzed single-electron transfer 'living' radical polymerization (SET-LRP)[1, 2] provides one of the most efficient polymerization methods to rapidly produce well-defined polymer chains from polar monomers, including acrylates, methacrylates, acrylamides, methacrylamides, acrylonitrile, methacrylonitrile, vinyl chloride and other monomers.[1-11] Control over the molecular weight distribution (MWD) and the rate of polymerization for SET-LRP is controlled through a self-regulated process[2, 12] driven by the disproportionation of Cu(I) to Cu(II) and Cu(0) in polar protic and aprotic solvents, water and their corresponding mixtures. Ligands stabilize the Cu(II) complex and further drive the equilibrium towards disproportionation.[13] The halide end-groups of the polymer provide a versatile synthetic handle for the direct coupling to nitroxide radicals (denoted as SET-NRC[14-16]) or further chemical modification using electrophilic,[17] nucleophilic[18] and radical transformations[19]. The ability to use 'click' chemistry via either direct coupling (e.g. thio-

bromo reaction[20, 21]) or direct transformation of the halide to an azide group for use in the CuAAC reaction makes copper-catalyzed polymerizations[2, 22, 23] one of the most used methods to create complex polymer architectures.[20, 24, 25]

Aqueous SET-LRP has recently emerged as a powerful technique to produce water-soluble polymers directly in water with narrow MWDs and near perfect halide end-group retention under mild polymerization conditions at the end of the polymerization. Haddleton and coworkers[8, 26-28] utilized the rapid and quantitative disproportionation of Cu(I) in water to produce equal amounts of Cu(0) and Cu(II). The addition of monomer in water into this solution rapidly produced water soluble polymers with excellent control over the MWD. Recently, an alternative (SET-LRP/$NaBH_4$) method was used to generate pre-defined stoichiometric ratios of Cu(0) to Cu(II) in water and alcohol-water mixtures through the quantitative in situ reduction of Cu(II) to Cu(0) with $NaBH_4$.[29, 30] No evidence for Cu(I) was found after reduction in water,[29] suggesting activation via Cu(0) and the ability to regulate the ratio of Cu(0):Cu(II). The latter allows fine control over the rate of polymerization and MWD with near perfect end-group retention. These two aqueous phase methods will not only expand the monomer types by SET-LRP but allow polymerizations from biomolecule initiators directly in water at ambient temperatures without concern for denaturation or degradation of the biomolecule.

One major issue with polymers made directly in water is the loss of halide end-groups post-purification or storage in water through hydrolysis to the corresponding –OH group.[31-33] Copper species can further facilitate the homolytic cleavage or removal of the halide end-groups.[28] Loss of halide functionality will therefore limit the subsequent use of polymers made in water.

Here, we report the influence of hydrolysis on the halide end-group of poly(*N*-isopropylacrylamide) (PNIPAM) made by the SET-LRP/$NaBH_4$ method in water (Scheme 5.1). This polymerization method allows us to determine the influence of copper species on end-group removal versus hydrolysis by water. The polymers, made under different polymerization conditions by varying either the [Cu(II)]/[$NaBH_4$] or [NIPAM]/[Initiator], were left in water and then coupled through the thio-bromo ‘click’ reaction to measure the amount of hydrolysis. Our main goal was to produce a polymer with chain-ends that could be isolated and stored for further coupling reactions. To achieve this, we carried out an in situ azidation of the halide groups in the reaction mixture immediately after completion of the polymerization, providing a fast one-pot transformation methodology. The purified PNIPAM-N_3 polymers were then coupled with alkyne functional PNIPAM to determine

both the end-group functionality and the azide reactivity, and have the potential for further use as building blocks to create complex polymer architectures.

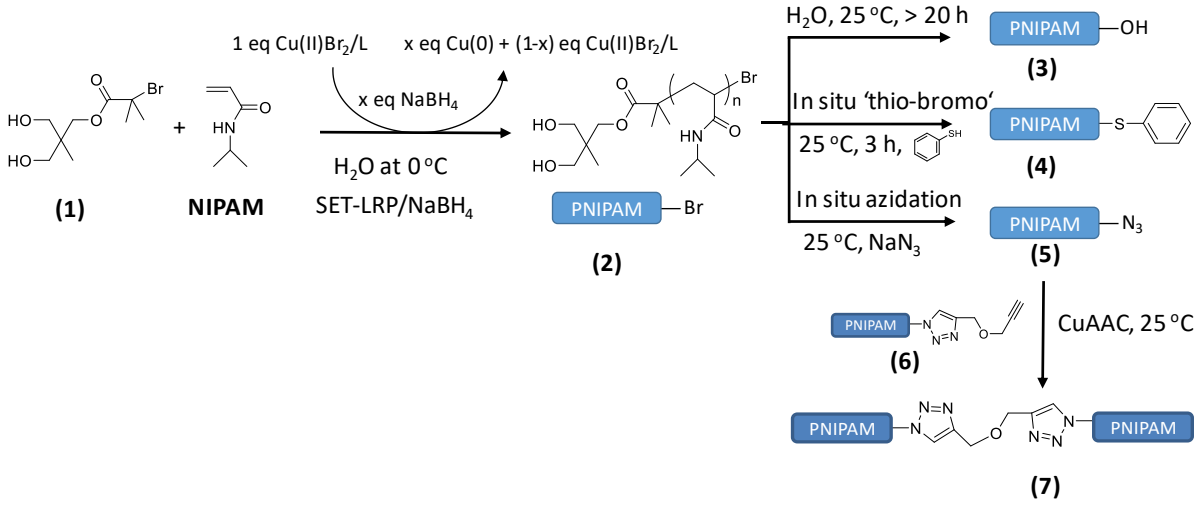

Scheme 5.1. Methods to functionalize PNIPAM chain end-groups using the 'click' reactions, 'thio-bromo' and CuAAC

Aim of the Chapter

The aim of the chapter was to study the rate of chain-end hydrolysis of PNIPAM made via aqueous SET-LRP. In order to eliminate the loss of chain-end functionality we introduced aqueous azidation directly after polymerization by simply adding sodium azide to the polymerization mixture. This technique gives polymer with nearly 100% azide functionality which is often used for conjugations.

5.2. Experimental

5.2.1. Materials

The following solvents were used as received: acetone (Chem-Supply, AR), ethyl acetate (EtOAc: ChemSupply, AR grade), N,N-dimethylacetamide (DMAc: Aldrich, HPLC grade), petroleum spirit (BR 40−60 °C, Univar, AR grade), diethyl ether (Merck, GR grade), tetrahydrofuran (THF, HPLC grade, Lichrosolv, 99.8%), dichloromethane (DCM, Labscan, AR grade), N,N-dimethylformamide (DMF: Labscan, AR grade), milli-Q water (Biolab, resistivity at 25 °C: 18.2 MΩ·cm), methanol (Univar, AR grade). The following reagents were used as received unless otherwise stated: N-isopropylacrylamide (NIPAM, Aldrich, 97 %) was recrystallized from n-hexane/toluene (9/1, v/v), sodium azide (NaN_3: Aldrich, ≥ 99.5 %), DOWEX ion-exchange resin (Aldrich, 50WX8-200), activated basic alumina (Aldrich: Brockmann I, standard grade, ~ 150 mesh, 58 Å), anhydrous magnesium sulphate ($MgSO_4$:

Scharlau, extra pure), silica gel 60 (230-400 mesh) ATM (SDS), TLC plates (silica gel 60 F254), 2-bromoisobutyryl bromide (BIB: Aldrich, 98%), triethylamine (TEA, Fluka, purum), *N,N,N',N',N''*-pentamethyldiethylenetriamine (PMDETA: Aldrich, 99 %), copper (II) bromide (Cu(II)Br_2: Aldrich, 99%), thiophenol (Aldrich, 97%), cuprous bromide (Cu(I)Br, Aldrich, 99.999%), propargyl ether (Sigma, 98%), sodium borohydride (Aldrich, 99%), 1,1,1-(trihydroxymethyl) ethane (Aldrich, 96%), *p*-toluenesulfonylchloride (Aldrich, ≥ 98 %). The following ligands and initiators were synthesized according to the literature[34]: tris(2-(dimethylamino)ethyl)amine (Me_6TREN), 3-hydroxy-2-(hydroxymethyl)-2-methylpropyl 2-bromo-2-methylpropanoate (water-soluble initiator)[29].

5.2.2. Synthetic Procedures

5.2.2.1. Aqueous SET-LRP

The synthetic procedures have been previously described (Scheme 5.2).[29] Below is an example of a typical aqueous SET-LRP/$NaBH_4$.

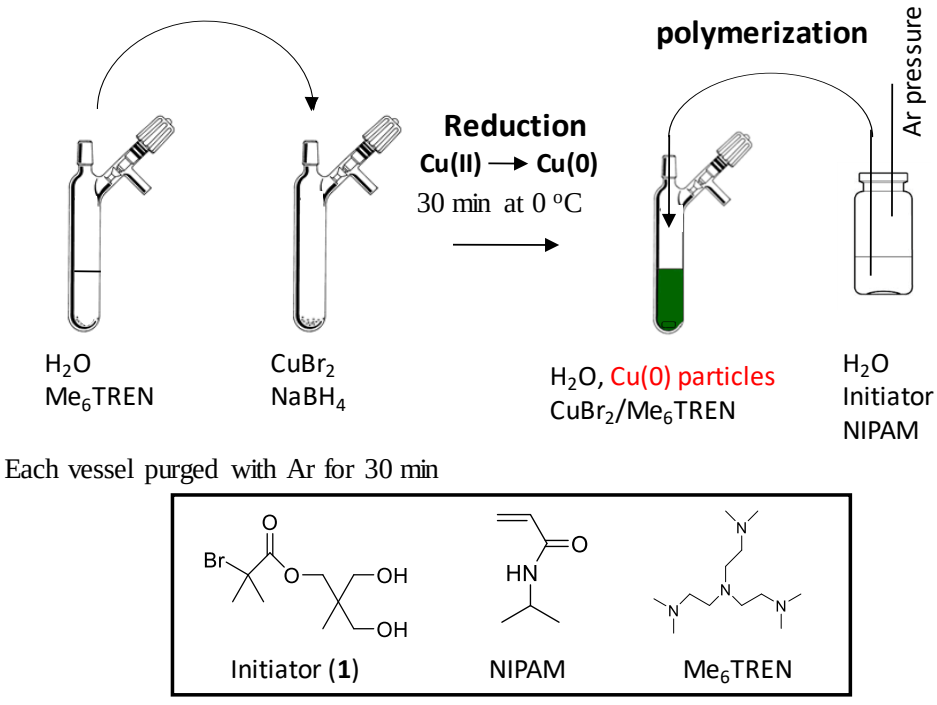

Scheme 5.2. Procedure for the in situ reduction of Cu(II)Br_2 with $NaBH_4$

Table 5.1. Polymerization molar ratios of reactants for the SET-LRP/$NaBH_4$ polymerization at 0 °C to make polymer **2**. [I] = 0.0267 M in 3.48 mL of water.

Polymerization	$[NIPAM]_0$	$[I]_0$	$[Me_6TREN]_0$	$[Cu(II)Br_2]_0$	$[NaBH_4]_0$
a	20	1	0.8	0.8	0.2
b	30	1	0.8	0.8	0.2
c	40	1	0.8	0.8	0.2
d	50	1	0.8	0.8	0.2
e	30	1	0.8	0.8	0.4
f	30	1	0.8	0.8	0.6
g	30	1	0.8	0.8	0.8
h	90	1	0.8	0.8	0.2

5.2.2.2. Typical polymerization to synthesize $(HO)_2$-$PNIPAM_{22}$-Br (2a)

To a 20 mL Schlenk tube equipped with magnetic stirrer, $Cu(II)Br_2$ (16.6 mg, 7.43×10^{-5} mol) and $NaBH_4$ (0.7 mg, 1.85×10^{-5} mol) were added. Sodium borohydride was weighed with a precision of ±0.001mg. The flask was sealed with a rubber septum and purged with Ar for 30 min. To a 5 mL glass vial, Me_6TREN (19.9 μL, 7.43×10^{-5} mol) and Milli-Q water (1 mL) were added; the vial sealed and the solution purged with Ar for 30 min. This solution was cannula transferred to the $Cu(II)Br_2/NaBH_4$ Schlenk tube and placed in an ice-bath where the reduction of Cu^{II} was allowed to proceed for 30 min. Another mixture of NIPAM (0.21 g, 1.85×10^{-3} mol) and the initiator (3-hydroxy-2-(hydroxymethyl)-2-methylpropyl 2-bromo-2-methylpropanoate; 0.025 g, 9.29×10^{-5} mol) were dissolved in Milli-Q water (2.48 mL) in a 20 mL glass vial, sealed, purged with Ar for 30 min at 0 °C, and then cannula transferred to the polymerization Schlenk tube. The polymerization was carried out at 0 °C. Samples for THF RI GPC were dissolved in THF, passed through activated neutral alumina and filtered using a 0.45 μL membrane filter. Conversion was measured by ^1H NMR by dissolving the polymerization mixture in D_2O.

5.2.2.3. Hydrolysis experiments of $(HO)_2$-$PNIPAM_n$-Br

Immediately after polymerization using the SET-LRP/$NaBH_4$ method, the polymer was kept in the polymerization mixture under argon and warmed to 25 °C. Samples of ~ 100 μL for the thio-bromo 'click' reaction were taken at various time intervals, injected into a solution of thiophenol (~20 eq, 5.5 μL, 5.3×10^{-5}mol) and acetonitrile (0.1 mL), and then TEA (20 eq, 7.4 μL, 5.3×10^{-5} mol) was added and left to react for 3 h at 25 ^oC. 10 μL of the reaction

solution was directly mixed with 20 µL of DCTB matrix (20 mg/mL in THF) and 2 µL of Na^+ salt (1 mg/mL in THF) for analysis by MALDI-ToF spectrometry. MALDI-ToF was used to determine the end-group functionality ratio between –Br and –OH end-groups on the polymer.

5.2.2.4. Thio-bromo 'click' reaction

A typical thio-bromo 'click' reaction of $(HO)_2$-PNIPAM$_{22}$-Br (**2a**) to form $(HO)_2$-PNIPAM$_{22}$-S-Ph (**4a**): The polymer solution (1.74 mL, ~105 mg of polymer, ~4.67×10^{-5} mol) at the end of the polymerization was added to a 5 mL vial containing deoxygenated acetonitrile (1.74 mL) and 50 eq of thiophenol (0.24 mL, 2.3×10^{-3}mol). Then TEA (50 eq, 0.325 mL, 2.3×10^{-3}mol) was added, the vial was sealed and the reaction stirred for 3 h at 25 °C. The polymer was purified by dialysis using a mixture of methanol/water (90:10 v/v, 1L bottle, changing solvent 5 to 6 times), the solvent removed and the polymer then dried under vacuum for 24 h. ^{1}H NMR was then used to determine both the end-group functionality and number-average molecular weight (M_n).

5.2.2.5. In situ azidation

Typical synthesis of $(HO)_2$-PNIPAM$_{22}$-N_3 (**5a**): At the completion of the polymerization, ~20 eq of NaN_3 (120 mg, 1.86×10^{-3} mol) was added to a polymerization mixture, warmed to 25 °C, and then left to stir overnight. The polymer was purified by dialysis using Milli-Q water (MWCO = 3,000 Da) in a 1 L flask with the water being changed every 2 h, a process repeated 5 times. The polymer solution was freeze-dried for 24 h to give a white powder ($M_{n,RI}$ = 940, $M_{p,RI}$ = 1047, Đ = 1.15).

*5.2.2.6. Synthesis of $(HO)_2$-PNPIPAM$_{117}$-≡ (**6**)*

Polymer **6** was formed through the CuAAC reaction of **5h** with propagyl ether. The procedure was as follows: Cu(I)Br (1.7 mg, 1.2×10^{-5} mol) was placed in a 5 mL Schlenk tube, sealed and purged with Ar for 30 min. PMDETA (2.5 µL, 1.2×10^{-5} mol), $(HO)_2$PNIPAM$_{117}$-N_3 (**4h**) (0.6 g, 6.0×10^{-5} mol) and propargyl ether (0.308 mL, 3.0×10^{-3} mol) were dissolved in DMF (6 mL) in a 20 mL glass vial, sealed and purged with Ar for 30 min in an ice-bath. This solution was then cannula transferred to the Schlenk tube, and reaction was complete after 1 h. The reaction mixture was diluted in acetone, passed through a basic alumina column to remove the copper complex, and the solvent removed by rotary evaporation and with a further blow drying with an air flow. The polymer was recovered by

precipitation into diethyl ether (×3 times) and dried *in vacuo* for 12 h to give white powder (0.5g, 83% yield, $M_{n,RI}$ = 7030, $M_{p,RI}$ = 7240, Đ = 1.07).

5.2.2.7. CuAAC 'click' reaction

The CuAAC reaction between polymer **6** and **5(a-g)** provided a quantitative method to determine the end-group functionality after azidation. The polymers **5a**-**5g** were first purified by dialysis then recovered by freeze-drying before the CuAAC reaction. A typical procedure is given for the synthesis of $(HO)_2$-PNIPAM$_{22}$-b-PNIPAM$_{117}(OH)_2$ (**7a**): Cu(I)Br (2.0 mg, 1.39×10^{-5}mol) was placed in a 5 mL Schlenk tube, sealed and purged with Ar for 30 min. PMDETA (2.92 μL, 1.39×10^{-5} mol), $(HO)_2$PNIPAM$_{22}$-N_3 (**5a**) (8.0 mg, 2.79×10^{-6} mol) and $(HO)_2$PNIPAM$_{117}$-≡ (**6**) (59.2 mg, 4.19×10^{-6} mol) were dissolved in DMF (0.7 mL) in a 5 mL glass vial, sealed and purged with Ar for 30 min. This solution was then cannula transferred to the Schlenk tube, and the reaction was left for 3 h at 25 °C. DMF was removed by blow drying, and copper salts were removed by passing the polymer solution in THF through activated neutral alumina.

5.2.3. Analytical Methodologies

^{1}H Nuclear Magnetic Resonance Spectroscopy (NMR)

All NMR spectra were recorded on a Bruker DRX 400 MHz spectrometer at 25 °C using either $CDCl_3$ or D_2O/DMSO-d_6 mixture as solvent as specified.

Size Exclusion Chromatography (SEC)

The polymers or polymer solutions were dissolved in tetrahydrofuran (THF) to a concentration of ca. 1 mg/mL and filtered through a 0.45 μm PTFE syringe filter prior to an injection. Analysis of the molecular weight distributions of the polymers was performed on a Waters 2695 separations module, fitted with a Waters 410 refractive index detector maintained at 35 °C, a Waters 996 photodiode array detector, and two Ultrastyragel linear columns (7.8 x 300 mm) arranged in series. The columns maintained at 40 °C for all analyses are capable of separating polymers in the molecular weight range of 500 – 4 million g/mol with high resolution. All samples were eluted at a flow rate of 1.0 mL/min. Narrow molecular weight PSTY standards (Đ ≤ 1.1) ranging from 500 to 2 million g/mol were used for calibration. Data acquisition was performed using Empower software, and molecular weights were calculated relative to polystyrene standards.

Matrix-Assisted Laser Desorption Ionization–Time-of-Flight (MALDI-ToF) Mass Spectrometry

MALDI-ToF MS spectra were obtained using a Bruker MALDI-ToF autoflex III smart beam with accessible mass range of 600 – 400,000 Da. Ions were accelerated with a nitrogen laser (337 nm, pulse frequency: 200 Hz). All spectra were recorded in either reflectron (1500 – 5000 Da) or linear mode (5000 – 400,000 Da) using trans-2-[3-(4-*tert*-butylphenyl)-2-methyl-propenylidene] malononitrile (DCTB; 20 mg/mL in THF) as the matrix and Na(CF_3COO) (2 mg/mL in THF) as the cation source. The polymers were dissolved to a concentration of 1mg/mL. The matrix (20 μL), Ag(CF_3COO) (2 μL) and polymer (20 μL) solutions were mixed together and spotted on the target plate via 'dried droplet' method. Ca. 5000 shots randomly distributed over a MALDI spot were averaged for each sample.

Absolute Molecular Weight Determination by DMAc Triple Detection SEC

Absolute molecular weights of polymers were determined using a Polymer Laboratories GPC50 Plus equipped with dual angle laser light scattering detector, viscometer, and differential refractive index detector. HPLC grade *N*,*N*-dimethylacetamide (DMAc, containing 0.03 wt % LiCl) was used as the eluent at a flow rate of 1.0 mL min^{-1}. Separations were achieved using two PLGel Mixed B (7.8 x 300 mm) SEC columns connected in series and held at a constant temperature of 50 ^oC. The triple detection system was calibrated using a 2 mg mL^{-1} PSTY standard (Polymer Laboratories: M_w = 110 K, d*n*/d*c* = 0.16 mL g^{-1} and IV = 0.5809). Samples of known concentration were freshly prepared in DMAc + 0.03 wt % LiCl and passed through a 0.45 μm PTFE syringe filter prior to injection. The absolute molecular weights and d*n*/d*c* values were determined using Polymer Laboratories Multi Cirrus software based on the quantitative mass recovery technique.

LND Model Simulation

We used a log-normal distribution (LND) model based on a Gaussian function to fit the experimental MWD.[35] One can simulate the molecular weight distributions, and in particular the weight distribution, with a log-normal distribution (see ref[35] for more details) using the following equations:

$$w(M) = \frac{\exp(-(\ln M - \ln \overline{M})^2 / 2\sigma^2)}{M(2\pi\sigma^2)^{0.5}} \qquad (5.1)$$

where

$$\overline{M} = (M_n M_w)^{0.5} \quad (5.2)$$

and

$$\sigma^2 = \ln(PDI) \quad (5.3)$$

where equation 5.1 is the Gaussian distribution function of *w(M)* (the weight distribution of the SEC trace), M_n is the number-average molecular weight, M_w is the weight-average molecular weight, and the dispersity Đ = M_w/M_n.[36]

5.3. Results and Discussion

The aqueous SET-LRP of NIPAM in water via the in situ quantitative reduction of Cu(II)Br_2 with $NaBH_4$ to generate Cu(0) has previously been reported.[29] The end-group functionality (EGF) was determined from MALDI-ToF by adding thiophenol, a known 'click' reaction (see Experimental section for details), to rapidly and quantitatively cap the halide groups. The EGF during the polymerization remained near perfect up to ~50% conversion (after ~1 h) when $[Cu(II)Br_2]_0$ /$[NaBH_4]_0$ was 0.8/0.2. Beyond this time, loss of EGF due to the longer polymerization time was a result from the lowering of the propagation rate coefficient (k_p) with increasing [NIPAM][37]. Surprisingly, the EGF at the lower $[NIPAM]_0/[I]_0$ = 30 showed that the amount of Cu(0) activator had little or no influence on the EGF, which was near prefect upto ~80% conversion even when all Cu(II) was reduced to Cu(0).[29]

In this work, we wanted to investigate the influence of hydrolysis or copper-mediated hydrolysis on the EGF of PNIPAM-Br (Scheme 5.1). Polymer **2b** was left in water at 25 °C immediately after full conversion (denoted as time = 0 h). The OH EGF resulting from hydrolysis increased to 50% after ~ 9 h with a further increase to 90% after ~12 h under argon (Figure 5.1A). The MALDI-ToF showed no formation of the hydrolysis product (i.e. PNIPAM-OH) after 2 h (Figure 5.1C), but after 11 h the amount of hydrolysis product was greater than of the thio-bromo product (Figure 5.1D). The rate of hydrolysis followed a pseudo first order rate loss that was independent on the presence of air and the amount of Cu(0) or Cu(II) in the system (when compare to hydrolysis of **2g**) as shown in Figure 5.1A. The apparent rate constant (*k*') for all the hydrolysis rates were found to be the same within experimental error (using a 95% confidence interval), suggesting that copper-mediated hydrolysis has little or no influence on the loss of halide end-groups. The effect of pH is

known to affect the hydrolysis rate, and as shown in Figure 5.1B for **2b,** only at a pH of 10 was there a statistically significant increase in hydrolysis rate by a factor of 1.5.

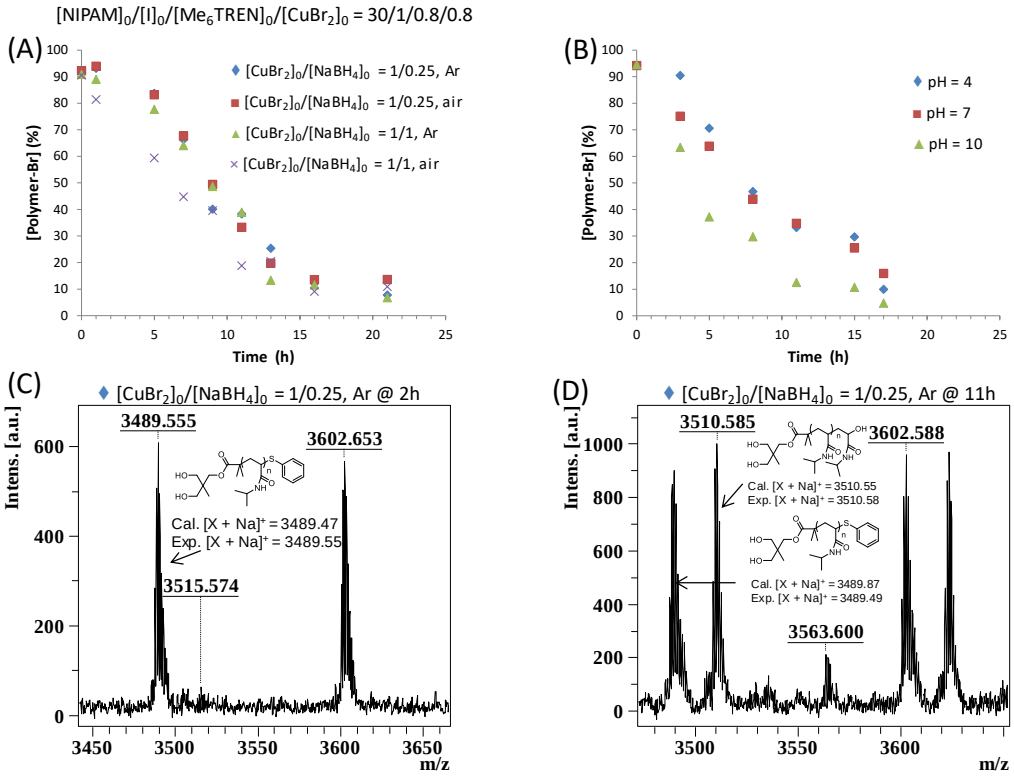

Figure 5.1. Hydrolysis experiments for polymer 2 in the polymerization water mixture at 25 °C. (A) Kinetic experiments for **2b** and **2g** in the presence or absence of air, (B) Influence of pH on kinetics, (C) MALDI-ToF of **2b** after 2 h under Ar, and (D) MALDI-ToF of **2b** after 11 h under Ar.

Most literature procedures for the reaction of –Br polymer end-groups with NaN_3 to produce an azide end-group use organic solvents (e.g. DMF) and takes between 12 to 24 h.[24, 38-40] This is due to the low solubility of NaN_3. For example, in DMF the solubility is 4.9 mg/mL at 95 °C) and by changing the solvent to DMSO at this temperature not only did the solubility increase to 52 mg/mL but there was a dramatic increase in the rate of azidation.[40] At first sight, from the hydrolysis data above, significant hydrolysis in water of PNIPAM-Br should occur prior to formation of azide end-groups. The in situ addition of NaN_3 (~20 eq to halide end-group) in water immediately after the polymerization for azidation of **2a** reached ~92% EGF after only 30 s measured by MALDI-ToF (Figure 5.2A), and the EGF did not change after 10 min (see Figure A5.2 in Appendix).

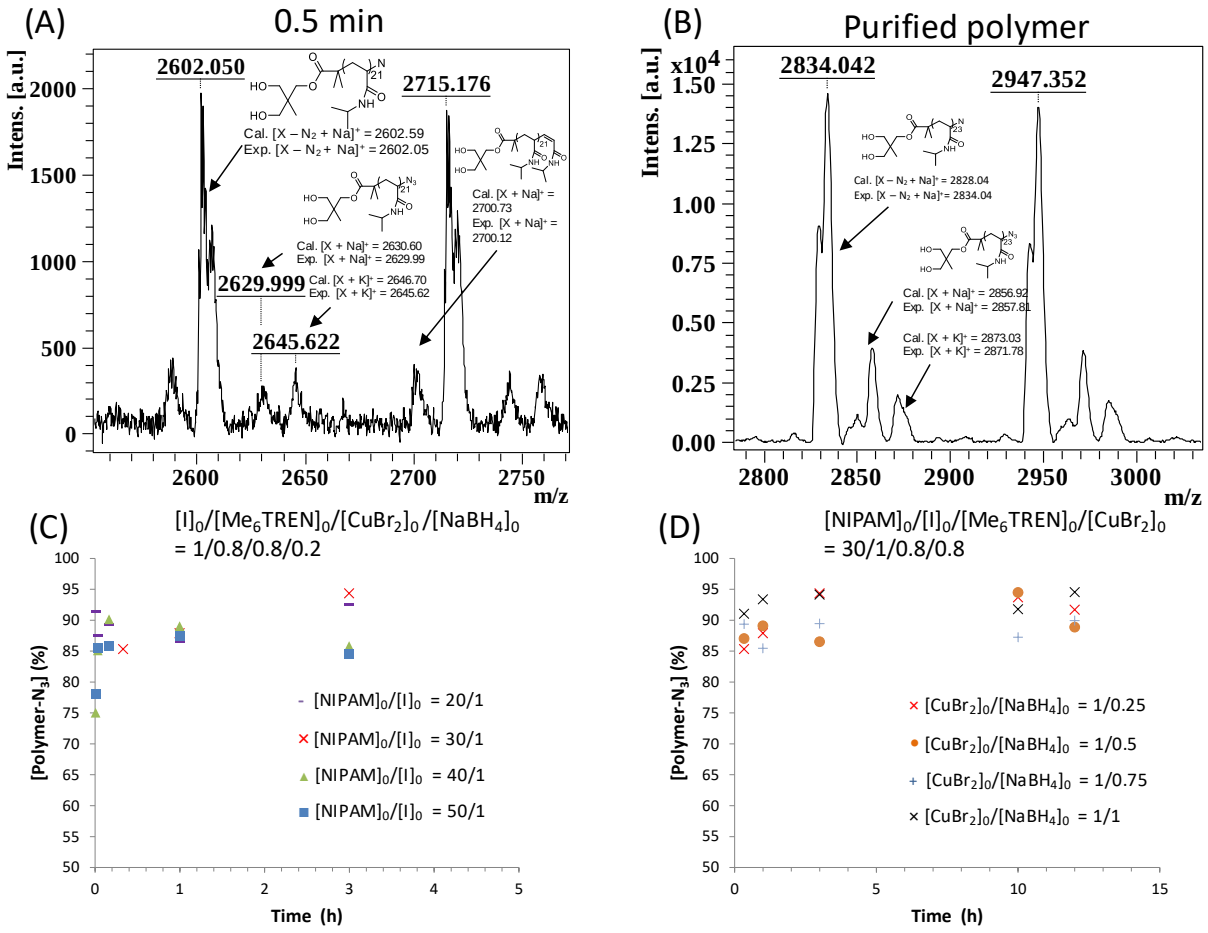

Figure 5.2. Kinetics for the in situ azidation of **2** in water at 25 °C. (A) MALDI-ToF of **2a** after 0.5 min at 25 °C, (B) MALDI-ToF of purified 5**a**, (C) Kinetic azidation experiments for **2a-d**, and (D) Kinetic azidation experiments for **2b** and **2e-g**.

The reason for this enhanced rate in water results from the high solubility of NaN_3 and the greater ion-pair separation that facilitates nucleophilic attack. To our knowledge, this the first example for rapid azidation of polymer chains in water.

After 24 h of reaction and then purification by dialysis, the EGF of **5a** (purified) increased to ~98% EGF (Figure 5.2B). The molecular weight peaks were assigned to two major species consistent with that found in the literature;[38, 41, 42] the first, the azide end-group with its parent polymer ($[X + Na]^+$) and in-source expulsion of N_2 ($[X - N_2 + Na]^+$ and $[X - N_2 + K]^+$)[41], and the second, an internal double bond found from fragmentation of the halide end-group ($[X\text{-}Br – HBr + Na]^+$)[42]. The accuracy of the EGF determinations is subject to a large uncertainty due to the large signal to noise ratio found in the spectra and could underestimate the EGF. Figure 5.2C showed that the EGF was greater than 85% after ~1 h for azidation of polymers **2a**, **2b**, **2c** and **2d** with no change in EGF after 12 h. It was found that the EGF was independent with an increase in molecular weight. A similar trend was

found for the in situ azidation of **2e**, **2f** and **2g** (Figure 5.2D). This data suggested that azidation was both rapid and highly efficient in water for PNIPAM, an unexpected result. The EGF for nearly all polymers after 24 h reaction and dialysis gave high EGFs for polymer **5**(**a-g**, purified) greater than 95% (Table 5.2). These results are similar for the in situ thio-bromo 'click' reaction of **2** to produce **4** with the EGF in most cases greater than 93 % (Table 5.2).

Table 5.2. Size exclusion chromatography (SEC) and ^{1}H NMR data for polymer **5**, and the end group functionality (EGF) after thio-bromo of **2** to form **4** determined by MALDI-ToF, after azidation of **2** to form **5** determined by MALDI-ToF, and the EGF determined by the LND model from the CuAAC 'click' reaction of **5** with **6**.

Polymer ($PNIPAM_n$-N_3)	SEC (RI)[a]		SEC (Absolute)[b]		M_n (NMR)[c]	EGF % thio-bromo[d]	EGF % NaN_3	EGF % CuAAC with **6**[e]
	M_n	Đ	M_n	Đ				
5a	930	1.15	3060	1.02	2720	100	92.5	98.7
5b	1480	1.14	4430	1.01	4410	93.7	94.3	>99
5c	2130	1.12	5510	1.06	5660	92.8	85.8	98.1
5d	2780	1.11	5920	1.02	6900	88.0	84.5	97.3
5e	2110	1.14	5770	1.02	3730	93.7	86.5	97.7
5f	2260	1.19	4870	1.03	4410	93.4	89.4	95.4
5g	1970	1.28	5370	1.01	4750	93.4	94.1	97.6

[a] SEC (RI) based on a PSTY calibration curve, [b] DMAc + 0.03 wt.% LiCl, [c] M_n calculated from integration following equation: $M_n = 231.25 + (I_{4.0\ ppm} - 3)*113.15$. [d] In-situ 'thio-bromo' reaction of **2**, [e]CuBr/PMDETA in DMF for 24 h at 25°C.

Since the MALDI-ToF provide large uncertainty in the EGF values, the azide functional polymers **5**(**a-g**, purified) were reacted with an alkyne functional PNIPAM (**6**) using the CuAAC 'click' reaction to further determine the azide EGF. The molar ratio of **6** used in the reaction was 1.5 times greater than **5** to drive the reaction towards the product. It also allowed us to use SEC to determine the loss of **5** since the molecular weight distribution of **5** was both much lower and importantly well separated from that of **6**. We further used the log-normal distribution (LND) model[35, 36] to simulate the molecular weight distribution of the final 'click' product. Figure 5.3A shows the CuAAC reaction between **5a** and **6** catalyzed by CuBr and PMDETA ligand in DMF. After 180 min, the SEC chromatogram (curve d) showed trace amounts of starting polymer **5a** (curve a). The LND model showed that the crude CuAAC products consisted of 0.14 wt% of **5a**, 8.6 wt% of **6**, 65.7 wt% of **7**

and 25.6 wt% of the Glazer (alkyne-alkyne) coupling product (see Table A5.1 in Appendix). Using this data, the CuAAC coupling efficiency was determined to be 98.7%, suggesting a much higher azide EGF than found from MALDI-ToF. Similar SEC traces were also observed for the reactions of **6** with **5b**, **5c** and **5d** (Figure 5.3) and with **5e**, **5f** and **5g** (Figure A5.1 in Appendix). The CuAAC 'click' efficiencies for nearly all of the reactions were greater than 97%, again suggesting that the azide EGF was high and much higher than that found by MALDI-ToF (Table 5.2). The results demonstrated that the in situ azidation was rapid and produced a high azide EGF in water overcoming the issues found from loss of end groups through hydrolysis. This was further confirmed from the very high coupling efficiency found from the CuAAC 'click' reaction of the purified PNIPAM-N_3 (**5**) with a PNIPAM alkyne modified chain-end (**6**). The results also demonstrate that we can isolate the PNIPAM-N_3 from the water solution, purify as a solid and reuse it in further CuAAC reactions.

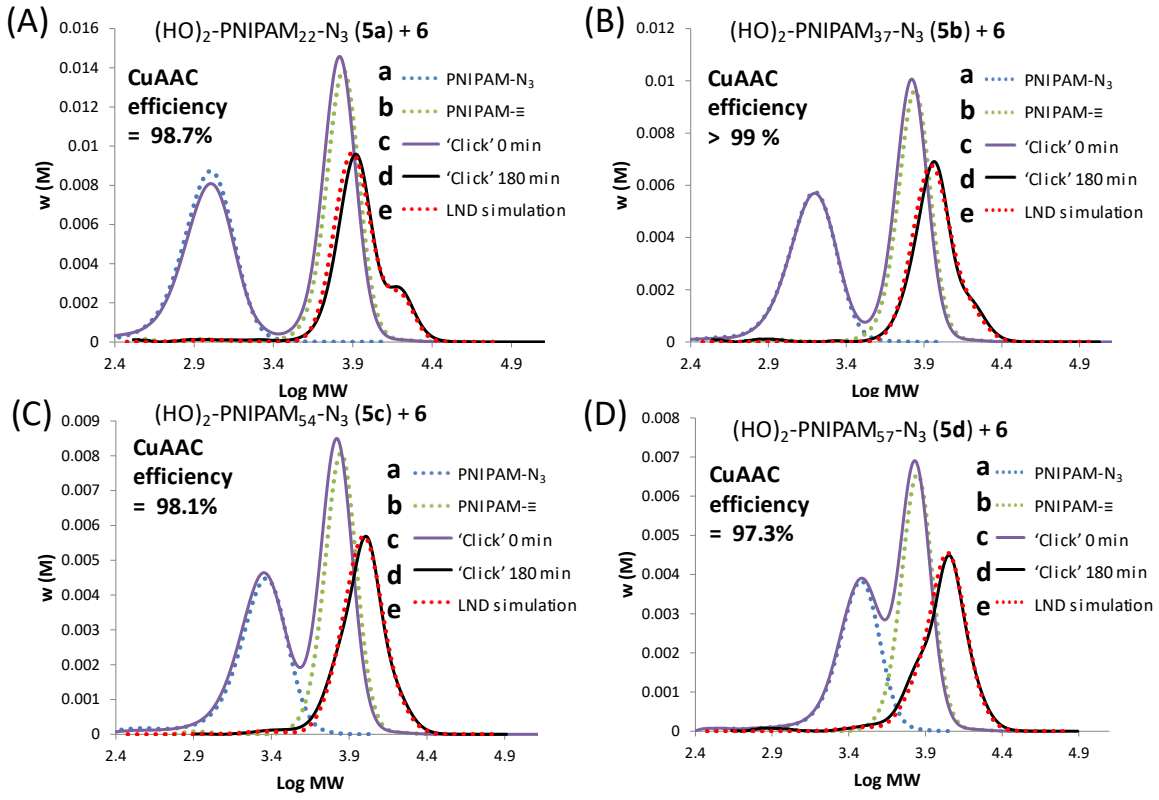

Figure 5.3. Size exclusion chromatograms for the CuAAC 'click' reaction between **5** and **6**. (A) Polymer **5a** + **6**, (B) Polymer **5b** + **6**, (C) Polymer **5c** + **6**, (D) Polymer **5d** + **6**. Curves (a) **5**, (b) **6**, (c) at time = 0 min for CuAAC, (d) at time = 180 min for CuAAC, and (e) LND model simulation of curve d.

5.4. Conclusion

Hydrolysis of halide polymer chain-ends in water has limited the use of many water-based synthesized polymer in the construction of more complex polymer architectures. In this work, we find that hydrolysis reached 50% after ~8 h and near complete hydrolysis after 15 h. The thio-bromo ‘click’ reaction of PNIPAM-Br with a small thiol molecule was rapid. It was found that the in situ azidation of the PNIPAM-Br chain ends in water was also rapid, reaching near full completion within 30 s due to the increased solubility of NaN_3. This allowed PNIPAM-N_3 chains to be purified and further coupled to alkyne functional polymers with coupling efficiencies greater than 97%, thereby overcoming the major issues of hydrolysis and extending the use of such polymers made in water for further possible orthogonal ‘click’ reactions.

5.5. References

1. Percec, V.; Popov, A. V.; Ramirez-Castillo, E.; Monteiro, M.; Barboiu, B.; Weichold, O.; Asandei, A. D.; Mitchell, C. M. *J Am Chem Soc* **2002,** 124, (18), 4940-4941.

2. Percec, V.; Guliashvili, T.; Ladislaw, J. S.; Wistrand, A.; Stjerndahl, A.; Sienkowska, M. J.; Monteiro, M. J.; Sahoo, S. *J Am Chem Soc* **2006,** 128, (43), 14156-14165.

3. Samanta, S. R.; Levere, M. E.; Percec, V. *Polym Chem-Uk* **2013,** 4, (11), 3212-3224.

4. Samanta, S. R.; Anastasaki, A.; Waldron, C.; Haddleton, D. M.; Percec, V. *Polym Chem-Uk* **2013,** 4, (22), 5555-5562.

5. Nguyen, N. H.; Leng, X. F.; Sun, H. J.; Percec, V. *J Polym Sci Pol Chem* **2013,** 51, (15), 3110-3122.

6. Soeriyadi, A. H.; Boyer, C.; Nystrom, F.; Zetterlund, P. B.; Whittaker, M. R. *J Am Chem Soc* **2011,** 133, (29), 11128-11131.

7. Nguyen, N. H.; Rosen, B. M.; Percec, V. *J Polym Sci Pol Chem* **2010,** 48, (8), 1752-1763.

8. Zhang, Q.; Wilson, P.; Li, Z. D.; McHale, R.; Godfrey, J.; Anastasaki, A.; Waldron, C.; Haddleton, D. M. *J Am Chem Soc* **2013,** 135, (19), 7355-7363.

9. Zhang, Q.; Wilson, P.; Anastasaki, A.; McHale, R.; Haddleton, D. M. *Acs Macro Letters* **2014,** 3, (5), 491-495.

10. Zhang, Q.; Li, Z. D.; Wilson, P.; Haddleton, D. M. *Chem Commun* **2013,** 49, (59), 6608-6610.

11. Waldron, C.; Anastasaki, A.; McHale, R.; Wilson, P.; Li, Z. D.; Smith, T.; Haddleton, D. M. *Polym Chem-Uk* **2014,** 5, (3), 892-898.

12. Urbani, C. N.; Bell, C. A.; Lonsdale, D.; Whittaker, M. R.; Monteiro, M. J. *Macromolecules* **2007,** 41, (1), 76-86.

13. Rosen, B. M.; Jiang, X.; Wilson, C. J.; Nguyen, N. H.; Monteiro, M. J.; Percec, V. *J Polym Sci Pol Chem* **2009,** 47, (21), 5606-5628.

14. Kulis, J.; Jia, Z. F.; Monteiro, M. J. *Macromolecules* **2012,** 45, (15), 5956-5966.

15. Kulis, J.; Bell, C. A.; Micallef, A. S.; Jia, Z. F.; Monteiro, M. J. *Macromolecules* **2009,** 42, (21), 8218-8227.

16. Jia, Z. F.; Bell, C. A.; Monteiro, M. J. *Chem Commun* **2011,** 47, (14), 4165-4167.

17. Nakagawa, Y.; Gaynor, S. G.; Matyjaszewski, K. *Abstr Pap Am Chem S* **1996,** 211, 89-Poly.

18. Matyjaszewski, K.; Nakagawa, Y.; Gaynor, S. G. *Macromol Rapid Comm* **1997,** 18, (12), 1057-1066.

19. Coessens, V.; Matyjaszewski, K. *Macromol Rapid Comm* **1999,** 20, (2), 66-70.

20. Rosen, B. M.; Lligadas, G.; Hahn, C.; Percec, V. *J Polym Sci Pol Chem* **2009,** 47, (15), 3931-3939.

21. Rosen, B. M.; Lligadas, G.; Hahn, C.; Percec, V. *J Polym Sci Pol Chem* **2009,** 47, (15), 3940-3948.

22. Wang, J. S.; Matyjaszewski, K. *J Am Chem Soc* **1995,** 117, (20), 5614-5615.

23. Matyjaszewski, K. *Macromolecules* **2012,** 45, (10), 4015-4039.

24. Whittaker, M. R.; Urbani, C. N.; Monteiro, M. J. *J Am Chem Soc* **2006,** 128, (35), 11360-11361.

25. Antoni, P.; Robb, M. J.; Campos, L.; Montanez, M.; Hult, A.; Malmstrom, E.; Malkoch, M.; Hawker, C. J. *Macromolecules* **2010,** 43, (16), 6625-6631.

26. Waldron, C.; Zhang, Q.; Li, Z. D.; Nikolaou, V.; Nurumbetov, G.; Godfrey, J.; McHale, R.; Yilmaz, G.; Randev, R. K.; Girault, M.; McEwan, K.; Haddleton, D. M.; Droesbeke, M.; Haddleton, A. J.; Wilson, P.; Simula, A.; Collins, J.; Lloyd, D. J.; Burns, J. A.; Summers, C.; Houben, C.; Anastasaki, A.; Li, M. X.; Becer, C. R.; Kiviaho, J. K.; Risangud, N. *Polym Chem-Uk* **2014,** 5, (1), 57-61.

27. Samanta, S. R.; Nikolaou, V.; Keller, S.; Monteiro, M. J.; Wilson, D. A.; Haddleton, D. M.; Percec, V. *Polym Chem-Uk* **2015,** 6, (11), 2084-2097.

28. Zhang, Q.; Wilson, P.; Li, Z.; McHale, R.; Godfrey, J.; Anastasaki, A.; Waldron, C.; Haddleton, D. M. *Journal of the American Chemical Society* **2013,** 135, (19), 7355-7363.

29. Gavrilov, M.; Zerk, T. J.; Bernhardt, P. V.; Percec, V.; Monteiro, M. J. *Polym Chem-Uk* **2016,** 7, (4), 933-939.

30. Enayati, M.; Jezorek, R. L.; Monteiro, M. J.; Percec, V. *Polym Chem-Uk* **2016,** 7, 3608-3621.

31. Rademacher, J. T.; Baum, R.; Pallack, M. E.; Brittain, W. J.; Simonsick, W. J. *Macromolecules* **2000,** 33, (2), 284-288.

32. Teodorescu, M.; Matyjaszewski, K. *Macromolecules* **1999,** 32, (15), 4826-4831.

33. Teodorescu, M.; Matyjaszewski, K. *Macromol Rapid Comm* **2000,** 21, (4), 190-194.

34. Ciampoli.M; Nardi, N. *Inorganic Chemistry* **1966,** 5, (1), 41-&.

35. Monteiro, M. J. *Eur Polym J* **2015,** 65, 197-201.

36. Gavrilov, M.; Monteiro, M. J. *Eur Polym J* **2015,** 65, 191-196.

37. Ganachaud, F.; Balic, R.; Monteiro, M. J.; Gilbert, R. G. *Macromolecules* **2000,** 33, (23), 8589-8596.

38. Lu, D. R.; Hossain, M. D.; Jia, Z. F.; Monteiro, M. J. *Macromolecules* **2015,** 48, (6), 1688-1702.

39. Liu, J.; Gan, Z. *Macromol. Biosci*, **2014,** 14, 699-708.

40. Barbieri, U.; Polacco, G.; Paesano, E. *Prop. Explos., Pyrotech.* **2006,** 31, (5), 369-375.

41. Li, Y. J.; Hoskins, J. N.; Sreerama, S. G.; Grayson, S. M. *Macromolecules* **2010,** 43, (14), 6225-6228.

42. Ladaviere, C.; Lacroix-Desmazes, P.; Delolme, F. *Macromolecules* **2009,** 42, (1), 70-84.

Chapter 6

Synthesis of Densely Packed Multicyclic Polystyrene

In this chapter an oligomer of cyclic polystyrene (PSTY) blocks was synthesized using copper-catalyzed azide-alkyne cycloaddition (CuAAC) 'click' chemistry via two synthetic routes. In the first approach the oligomer was synthesized by adding each cyclic polystyrene block stepwise. In the second route feeding synthesis of the oligomer was developed allowing for a mixture of oligomers of up to 56 cyclic units. The position of functionalities in the cyclic units was designed to create topological constraints for attaching each subsequent unit, resulting in a densely packed polymer formation. Differential scanning calorimetry (DSC) showed that glass transition temperature (T_g) of the oligomers exceeds that of polystyrene of infinite molecular weight (T_g^{∞}) starting from 6 kDa PSTY and reaches the plateau of 384 K at 63 kDa oligomer. Such high values are attributed to the lack of chain ends and multiple knots within the polymer molecules and thus, a decrease in conformational entropy. Log-normal distribution (LND) simulation showed that the ratio between apparent and actual M_n does not change when the number of cyclic blocks exceeds 10 units, which asserts the formation of a stable and compact polymer structure.

6.1. Introduction

Cyclic polymers exhibit different diffusion and viscoelastic properties compared to their linear analogues.[1-4] This is due to the lower degree of freedom from a lack of chain-ends, and thus a more compact conformation resulting in a hydrodynamic radius ratio for polystyrene cyclic to linear ($g_h = R_{h,c}/R_{h,l}$) of ~0.89 under theta solvent conditions[5], and ~0.84 in a good solvent.[6] These ratios, determined from quasi-elastic light scattering, are relatively constant over a wide range of molecular weights. This more compact cyclic topology can also be observed from the lower apparent number-average molecular weight ($M_{n,cyc}$) compared to the absolute M_n ($M_{n,abs}$) of linear analogues from size exclusion chromatography (SEC) using linear polystyrene standards as the calibration curve. The ratio of $M_{n,cyc}/M_{n,abs}$ (denoted here as M_h) was found to be close to 0.75,[7] corresponding to a value of g_h close to 0.85 in THF calculated from Eq. 6.2. This value of g_h is close to that found experimentally (*vide supra*).

The hydrodynamic volume can be determined from SEC using the following equation:

$$V_{h,SEC}^3 = \frac{2KM_n^{a+1}}{5\pi N_A} \qquad (6.1)$$

where K = 0.0141 cm^3 g^{-1}, a = 0.7 (in a good solvent), N_A is Avogadro's number and M_n is the number-average molecular weight found using a linear PSTY calibration curve. The K and a values

used in this work were determined by light scattering[8] for molecular weights ranging from 13,000 to 2.2×10^6, which was in the range of molecular weights studied here. The relationship between g_h and the ratio of $M_{n,cyc}/M_{n,abs}$ can be determined using Eq 6.1, and is given as follows:

$$g_h = \left(\frac{M_{n,cyc}}{M_{n,abs}}\right)^{1.7/3} \quad (6.2)$$

Synthetic cyclic polymers can be made either via the ring-closure or the ring expansion methods.[9-11] The ring-expansion method provides a unique synthetic strategy to produce high molecular weight cyclic chains without linear polymer impurities, but control over the molecular weight distribution (MWD) is limited resulting in broad MWDs.[12] In comparison, the ring-closure method can produce low molecular weight cyclics with narrow distributions, but the cyclic product contains a small amount of linear impurity.[13, 14] These linear impurities have been found to influence the viscoelastic properties.[15] Pioneering works on the synthesis of cyclic polymers using ring-closure method reported high amount of linear impurities.[16-18] An improved ring-closure method was introduced by Laurent and Grayson in 2006, in which the ends of heterodifunctional polystyrene were coupled using copper-catalyzed azide-alkyne cycloaddition (CuAAC) 'click' chemistry, showed much higher content of cyclic product.[10] Nevertheless, cyclic polystyrene obtained in the aforementioned work still contained linear impurities, and subsequent studies published by Monteiro group showed that linear starting material and multiblocks can be efficiently removed from the cyclic product through preparative size exclusion chromatography (SEC) and purity of cyclic product can be quantified using the log-normal distribution (LND) fitting of a polymer MWDs.[19, 20] The main advantage of the ring-closure method is the ability to synthesize a wide range of cyclic polymer compositions and topologies.[7, 21-25] However, the ring-closure method may produce knot impurities during the coupling of the chain-ends; a polymer with $M_n = 1\times10^6$ has a 15% chance to form a knot.[26] The nature and number of knots within a ring should in principle have a profound influence on the physical properties of the polymer within a melt. It should be noted that the molecular weights of polymers usually used in the ring closure method are less than 20 kDa, with little or no likelihood of knot formation in a good solvent. In addition, ring-closure at these low molecular weights is usually carried out under dilute conditions, eliminating the possibility of other structures including catenated ring formation.

Cyclic peptides are widespread in nature[27, 28] as this topology makes them resistant to enzymatic proteolysis.[29] In addition, many of these cyclic peptides contain disulfide linkages or knots that act to further compact the topology and even change the peptide's shape. These knots increase the stability, alter binding affinity, and thus can improve pharmacokinetic properties of candidate cyclic peptide drugs.[30] Similarly, DNA is organized into loop structures along a central backbone structure

using knots. This compact structure seems to play a dominant role in establishing chromosome territories within the nucleus.[31]

We have recently shown that by introducing knots into a cyclic polystyrene structure, the compactness of the coil increased which correlated with an increase in the glass transition temperature (T_g).[32] This increase in T_g results from the loss of entropy due to both the cyclic nature and the number and type of knot. In this work, we aimed to produce compact spherical multicyclic polymers through coupling cyclic polystyrene monomers, and studying their compactness in solution via SEC and LND simulation and at theta conditions via DSC. The nature of the linkage between cyclic monomers (see Scheme 6.1) should result in more compact topologies compared to spiro and other cyclic topologies. An understanding of the solution and bulk properties of our multicyclic structures could illuminate how conformational change and polymer molecular weight influences the compactness of the polymer coil.

6.1.1. Aim of the Chapter

In this chapter we use Cu mediated LRP and CuAAC 'click' chemistry to synthesize new compact multicyclic topologies. The novelty of this work was to introduce topological constraints into the multicyclic PSTY and to study if these constraints impede the growth of the architecture. The properties of the multicyclic PSTY were characterized via LND simulation and DSC.

6.2. Experimental

6.2.1. Materials

The following solvents were used as received: diethyl ether (Et_2O, Labscan, AR grade), tetrahydrofuran (THF, HPLC grade, Lichrosolv, 99.8%), toluene (HPLC, LABSCAN, 99.8%), dimethyl sulfoxide (DMSO, LABSCAN, 99.8%), dichloromethane (DCM, Labscan, AR grade), N,N-dimethylformamide (DMF: Labscan, AR grade), methanol (Univar, AR grade).

The following reagents were used as received: 1,8-diazabicyclo[5.4.0]undec-7-ene (DBU, Aldrich, 98%), diphenyl phosphoryl azide (DPPA, Aldrich, 97%), DOWEX ion-exchange resin (Aldrich, 50WX8-200), activated basic alumina (Aldrich: Brockmann I, standard grade, ~ 150 mesh, 58 Å), anhydrous magnesium sulfate ($MgSO_4$: Scharlau, extra pure), silica gel 60 (230-400 mesh ATM (SDS)), p-toluenesulfonyl chloride (Aldrich, ≥ 98 %), sodium azide (NaN_3: Aldrich, ≥ 99.5 %), 1,1,1-(trihydroxymethyl) ethane (Aldrich, 96%) TLC plates (silica gel 60 F254), methyl 3,5-dihydroxybenzoate (Aldrich, 97%), 2-bromoisobutyryl bromide (BIB: Aldrich, 98 %), 2-bromopropionyl bromide (BPB: Aldrich, 98 %), sodium chloride (Univar, 99.9%), sodium hydride

(Aldrich, 60 wt% in mineral oil), propargyl bromide (Aldrich, 80 wt % in toluene), triethylamine (TEA, Fluka, purum), *N,N,N',N'',N''*-pentamethyldiethylenetriamine (PMDETA: Aldrich, 99 %), copper (II) bromide ($CuBr_2$: Aldrich, 99 %). Cu(I)Br and $CuBr_2$/PMDETA complexes were synthesized according to literature procedure.[33]

6.2.2. Synthetic Procedures

*6.2.2.1. Synthesis of the initiator 3-hydroxy-2-methyl-2-((prop-2-yn-1-yloxy)methyl)propyl 2-bromo-2-methylpropanoate (**1**)*

The initiator **1** was synthesized according to the previously published literature.[34] 2-methyl-2-((prop-2-yn-1-yloxy)methyl)propane-1,3-diol (9.33 g, 0.059 mol) and TEA (5.97 g, 0.059 mol) were dissolved in 165 mL of dry THF and cooled to 0 °C in an ice-bath. To the above solution, 2-bromoisobutyryl bromide (13.57 g, 0.059 mol) was added dropwise over 30 min. The reaction was allowed to slowly warm up to RT and then stirred overnight. The reaction mixture was filtered to remove salts, concentrated and dried under high vacuum at RT. The brown crude product was first purified by distillation under reduced pressure, followed by column chromatography with EtOAc/petroleum spirit (4/1, v/v) as eluent. The fraction with R_f as 0.38 was collected and concentrated to obtain a colorless viscous liquid (11.9284 g, yield = 66 %). ^{1}H NMR ($CDCl_3$, 298K, 300 MHz); δ 4.19 (s, 2H; -C*H*$_2$-OC(=O)-), 4.15 (dd, 2H, *J*=4.05, 0.63 Hz; HC≡C-C***H*****$_2$**O-), 3.56 (d, 2H, *J*=1.23 Hz; HOC***H*****$_2$**-), 3.51 (s, 2H; HC≡C-CH$_2$OC***H*****$_2$**-), 2.44 (t, 1H, *J*=2.4 Hz; ***H***C≡C-CH2O-), 2.17 (b, 1H; *H*OCH$_2$-), 1.94 (s, 6H; methyl protons), 0.97 (s, 3H; methyl protons); ^{13}C NMR ($CDCl_3$, 298K, 400 MHz); 171.8, 79.3, 74.7, 73.6, 67.8, 66.8, 58.7, 55.8, 40.6, 30.8, 17.0.

6.2.2.2. Synthesis of methyl 3,5-bis(ethynyloxy)benzoate

Methyl 3,5-bis(ethynyloxy)benzoate (13.44 g, 0.078 mol) was dissolved in 480 mL acetone in a 500 mL two-neck round bottom flask. The flask was flushed with argon and K_2CO_3 (44.19 g, 0.312 mol) was added, followed by the addition of propargyl bromide (80 wt % in toluene) (28.71 g, 0.257 mol). The contents were then placed in an oil bath at 78 ºC and refluxed for 24 h. After cooling, the contents were filtered to yield a golden yellow solution which was blown dry with N_2 flow. The residue was dissolved in DCM and extracted with H_2O (x 2), the organics dried with Mg_2SO_4 and solvent removed under vacuum. The purified product was obtained by a recrystallization from boiling MeOH to yield a pale yellow coloured crystalline solid (16.27 g, yield = 83 %).

^{1}H NMR ($CDCl_3$, 298K, 400 MHz); δ 7.29 (d, 2H, *J*=2.40, phenyl protons), 6.81 (t, 1H, *J*=2.4 Hz; phenyl proton), 4.71 (d, 4H, *J*=2.4 Hz; *H*C≡C**H$_2$**-), 3.90 (s, 2H; methyl protons), 2.54 (t, 1H *J*=2.4 Hz; ***H***C≡CH_2-); ^{13}C NMR ($CDCl_3$, 298K, 400 MHz); 166.4, 158.5, 132.1, 108.8, 107.5, 77.9, 75.9, 56.1, 52.3.

*6.2.2.3. Synthesis of (3,5-bis(prop-2-yn-1-yloxy)phenyl)methanol (**16**)*

Methyl 3,5-bis(ethynyloxy)benzoate (1.6748 g, 6.85 x 10^{-3} mol) was dissolved in 30 mL of dry THF in a 100 mL Schlenk flask under argon and cooled in an ice bath. $LiAlH_4$ (0.39 g, 1.00 x 10^{-2} mol) was then added portion wise with a spatula under a positive argon flow. Gas evolution was observed during the addition of $LiAlH_4$. After complete addition the reaction was stirred at 25 °C for 24 h. Complete disappearance of starting material was confirmed by TLC (R_f of the product in pure EtOAc = 0.8). $LiAlH_4$ was quenched via the careful addition of wet Na_2SO_4 followed by addition of 5 drops of water. The contents were then filtered and the remaining Li gel washed with THF (x 4) and filtered. The solvent was removed under vacuum to yield a yellow solid which was recrystallised from hot toluene with a small addition of hexane. The pure product was obtained as a white crystalline solid (1.035 g, yield = 70 %).

^{1}H NMR ($CDCl_3$, 298K, 400 MHz); δ 6.61 (d, 2H, *J*=1.8, phenyl protons), 6.53 (t, 1H, *J*=1.92 Hz; phenyl proton), 4.69 (d, 4H, *J*=2 Hz; *H*C≡C**H$_2$**-), 4.63 (d, 2H; C**H$_2$**-OH), 2.51 (t, 2H *J*=1.88 Hz; ***H***C≡CH_2-), 1.77 (t, 1H, *J*=14.69 Hz; -O**H**), ^{13}C NMR ($CDCl_3$, 298K, 400 MHz); 159.0, 143.7, 106.3, 101.6, 78.5, 75.8, 65.3, 56.0.

Synthesis of c-PSTY derivatives (Sequential synthesis of oligomer of cyclic PSTY blocks)

*6.2.2.4. Synthesis of ≡(HO)-PSTY$_{30}$-Br (**2**)*

Styrene (20.75 g, 0.20 mol), PMDETA (0.340 mL, 1.63 × 10^{-3} mol), initiator **1** (1.0 g, 3.25 × 10^{-3} mol) were added to a 50 mL flask sealed with rubber septum and purged with argon for 30 min. A 50 mL Schlenk tube was charged with Cu(I)Br (0.234 g, 1.63 x 10^{-3} mol), Cu(II)Br_2/PMDETA complex (0.129 g, 3.25 x 10^{-4} mol) and magnetic stirrer, sealed with rubber septum and purged with argon for 30 min. The solution was transferred to the Schlenk flask *via* cannula. The reaction vessel was placed in an oil bath at 80 ºC and stirred for 6h. The reaction was quenched by cooling to 0 °C, exposed to air, and diluted with THF (ca. 3 fold to the reaction mixture volume). The copper salts were removed by passage through an activated basic alumina column. The solution was concentrated by rotary evaporator and the polymer was recovered by precipitation into large volume

of MeOH (20 fold excess to polymer solution) and then vacuum filtration. The polymer was dried *in vacuo* for 24 h at 25 °C and characterized by linear PSTY calibrated SEC (M_n = 3480 Đ = 1.05) and DMAc Triple Detection SEC (M_n = 3690, Đ = 1.02). The polymer was further characterized by ^{1}H NMR and MALDI-ToF.

*6.2.2.5. Synthesis of ≡(HO)-PSTY$_{30}$-N$_3$ (**3**)*

≡(HO)-PSTY$_{30}$-Br **2** (8.66 g, 2.47 × 10^{-3} mol) was dissolved in 80 mL of DMF in a 100 mL reaction vessel equipped with magnetic stirrer. To this solution, NaN_3 (1.61 g, 2.47 × 10^{-2} mol) was added and the mixture stirred for 24 h at 25 °C. Product was precipitated into a mixture of methanol and water (95/5 v/v%), filtered, washed exhaustively with MeOH and dried *in vacuo* for 24 h. Linear PSTY calibrated SEC (M_n = 3550, Đ = 1.08) and DMAc Triple Detection SEC (M_n = 3910, Đ = 1.03). The polymer was further characterized by ^{1}H NMR and MALDI-ToF.

*6.2.2.6. Synthesis of c-PSTY$_{30}$-OH (**4**)*

A solution of ≡(HO)-PSTY$_{30}$-N$_3$ **3** (2.0 g, 6.43 × 10^{-4} mol) in toluene (110 mL) was purged with argon for 90 min to remove oxygen. This polymer solution was added via argon feeding procedure[7], at a flow rate of 1.24 mL/min, to a deoxygenated solution of Cu(I)Br (4.61 g, 3.21 × 10^{-2} mol) and PMDETA (6.72 mL, 3.21 × 10^{-2} mol) in toluene (110 mL) at 25 °C. After the addition of the polymer solution the reaction mixture was stirred for 3 h. At the end of this period, toluene was evaporated. Polymer was dissolved in 200 mL of THF, and copper salts were removed by passage through activated neutral alumina column. To recover the polymer the column was washed with 200 mL of THF (4 times). THF was evaporated, and polymer was recovered by precipitation into MeOH (20 fold excess to polymer solution) and then by filtration. The polymer was dried *in vacuo* for 24 h at 25 °C. (Purity by log-normal distribution simulation = 71 %). In order to analyse the polymer, 100 mg of the crude product was fractionated by preparative SEC and fractions combined and precipitated in MeOH. Linear PSTY calibrated SEC (M_n =2730, Đ = 1.05) and DMAc Triple Detection SEC (M_n = 3740, Đ = 1.01). The polymer was further characterized by ^{1}H NMR and MALDI-ToF.

*6.2.2.7. Synthesis of c-PSTY$_{30}$-Br (**5**)*

c-PSTY$_{30}$-OH **4** (1.54 g, 4.4 x 10^{-4} mol), TEA (0.61 mL, 4.4 x 10^{-3} mol) and 65 mL of dry THF were added under an argon blanket to a dry 100 mL Schlenk flask that had been purged with argon. The reaction was then cooled on ice. To this stirred mixture, a solution of BPB (0.46 mL, 4.4 x 10^{-3} mol) in dry THF (5 mL) was added drop-wise under argon via an air-tight syringe over 30 min.

After stirring the reaction mixture for 56 h at RT, the polymer was precipitated in MeOH and filtered. The polymer was dried for 24 h *in vacuo* at 25 °C. In order to analyse the polymer 100 mg of the crude product was fractionated by preparative SEC and fractions combined and precipitated in MeOH. Linear PSTY calibrated SEC (M_n = 2760, Đ = 1.05). The polymer was further characterized by ^{1}H NMR and MALDI-ToF spectroscopy.

*6.2.2.8. Synthesis of c-PSTY$_{30}$-N$_3$ (**6**)*

c-PSTY$_{30}$-Br, **5** (1.5 g, 4.28 x 10^{-4} mol) was dissolved in 15 mL of DMF. To this solution, NaN_3 (0.278 g, 4.28 x 10^{-3} mol) was added and the mixture stirred for 24 h at 25 ºC. The polymer solution was precipitated into MeOH/H_2O (95/5 v/v%) (20 fold excess to polymer solution) from DMF, recovered by vacuum filtration and washed exhaustively with MeOH. The polymer was dried *in vacuo* for 24 h at 25 ºC. The crude product was fractionated by preparative SEC and fractions combined and precipitated in MeOH. Linear PSTY calibrated SEC (M_n = 2780, Đ = 1.05) and DMAc Triple Detection SEC (M_n = 3790, Đ = 1.01). The polymer was further characterized by ^{1}H NMR and MALDI-ToF.

*6.2.2.9. Synthesis of c-PSTY$_{30}$-(≡)OH (**7**)*

A 20 mL Schlenk flask was charged with CuBr (1.62×10^{-2} g, 1.12×10^{-4} mol). c-PSTY$_{30}$-N_3 **6** (0.3 g, 6.63×10^{-5} mol), (3,5-bis(prop-2-yn-1-yloxy)phenyl)methanol (0.287 g, 1.33×10^{-3} mol) and PMDETA (2.35×10^{-2} mL, 1.12×10^{-4} mol) were dissolved in a mixture of DMSO (0.3 mL) and toluene (3 mL), sealed in a 20 mL glass vial and bubbled with Ar for 30 min. The solution was cannula transferred to the Schlenk flask, placed into a water bath at 25°C for 1 h. The reaction was quenched by dilution with THF (ca. 3 fold to the reaction mixture volume) and the copper salts removed by passage through an activated neutral alumina column. The solution was concentrated by rotary evaporator and the polymer recovered by precipitation into MeOH (20 fold excess to polymer solution) and vacuum filtration. The product was also purified by preparative SEC to remove the minimal amount of 2-arm PSTY formed. The polymer was dried *in vacuo* for 24 h at 25 °C. Linear PSTY calibrated SEC (M_n = 2920, Đ = 1.05) and DMAc Triple Detection SEC (M_n = 4010, Đ = 1.01). The polymer was further characterized by ^{1}H NMR and MALDI-ToF.

*6.2.2.10. Synthesis of c-PSTY$_2$-OH Oligomer (**8**)*

c-PSTY-(≡)OH **7** (M_n = 2930, Đ = 1.07) (0.20 g, 5.22×10^{-5} mol), c-PSTY-N_3 **6** (M_n = 2780, Đ = 1.05) (0.19 g, 5.22×10^{-5} mol) and PMDETA (1.6×10^{-2} mL, 7.82×10^{-5} mol) were placed in a Schlenk flask and dissolved in toluene (4 mL). Oxygen was removed from the solution by purging

with argon (30 min). CuBr (0.011 g, 7.82×10^{-5} mol) was added under a positive argon flow and the reaction vessel was sealed and placed in a water bath at 25 ºC with stirring for 1 h. The contents were diluted with THF and passed through activated neutral alumina. The solvent was removed under reduced pressure to yield a residue. The crude product was fractionated by preparative SEC, to remove starting mono-cyclic polymer, and fractions combined and precipitated into MeOH. Linear PSTY calibrated SEC (M_n = 5880, Đ = 1.05) and Triple Detection SEC (M_n = 7880, Đ = 1.003). The polymer was further characterized by ^{1}H NMR and MALDI-ToF.

*6.2.2.11. Synthesis of c-PSTY$_2$-N$_3$ Oligomer (**9**)*

c-PSTY$_2$-OH **8** (0.186 g, 2.48×10^{-5} mol), DPPA (0.021 mL, 9.92 x 10^{-5} mol) and DBU (0.015 mL, 9.92×10^{-5} mol) were dissolved in dry toluene (2 mL) at 0 ºC under argon and placed to a 20 mL Schlenk flask. The flask was wrapped with aluminium foil to avoid light and the solution stirred for 24 h. After stirring the toluene was evaporated via nitrogen flow and the contents dissolved in minimal amount of THF, then precipitated into MeOH/H_2O (95/5 v/v%) (20 fold excess to polymer solution) and recovered via vacuum filtration. Linear PSTY calibrated SEC (M_n = 5980, Đ = 1.03) and Triple Detection SEC (M_n = 8010, Đ = 1.02). The polymer was further characterized by ^{1}H NMR and MALDI-ToF.

*6.2.2.12. Synthesis of c-PSTY$_3$OH Oligomer (**10**)*

(c-PSTY)$_2$-N$_3$ **9** (0.164 g, 2.08×10^{-5} mol), c-PSTY-(≡)OH **7** (M_n = 2920, Đ = 1.05) (0.085 g, 2.21×10^{-5} mol) and PMDETA (6.5×10^{-3} g, 3.12×10^{-5} mol) were placed in a Schlenk flask and dissolved in toluene (2.4 mL). Oxygen was removed from the solution by purging with argon (30 min). CuBr (4.48×10^{-3} g, 3.12×10^{-5} mol) was added under a positive argon flow and the reaction vessel was sealed and placed in a water bath at 25 ºC with stirring for 30 min. The contents were diluted with THF and passed through activated neutral alumina. The solvent was removed under reduced pressure to yield a residue. The crude product was fractionated by preparative SEC and fractions combined and precipitated into MeOH. Linear PSTY calibrated SEC (M_n = 8480, Đ = 1.03) and DMAc Triple Detection SEC (M_n = 12490, Đ = 1.003).

*6.2.2.13. Synthesis of c-PSTY$_3$-N$_3$ Oligomer (**11**)*

c-PSTY$_3$-OH **10** (0.087 g, 7.42×10^{-6} mol), DPPA (0.016 mL, 7.41×10^{-5} mol) and DBU (0.011 mL, 7.41×10^{-5} mol) were added to dry toluene (1 mL) at 0 ºC under argon. The flask was wrapped with aluminium foil to avoid light and the solution stirred for 24 h. After stirring the toluene was evaporated via nitrogen flow and the contents dissolved in minimal amount of THF, then

precipitated into MeOH/H_2O (95/5 v/v%) (20 fold excess to polymer solution) and recovered via vacuum filtration. Linear PSTY calibrated SEC (M_n = 8550, Đ = 1.04) and Triple Detection SEC (M_n = 12320, Đ = 1.01).

*6.2.2.14. Synthesis of c-PSTY$_4$-OH Oligomer (**12**)*

c-PSTY$_3$-N$_3$ **11** (0.055 g, 4.68 × 10^{-6} mol), c-PSTY-(≡)OH **7** (M_n = 2920, Đ = 1.05) (0.020 g, 5.20 × 10^{-6} mol) and PMDETA (4.9 × 10^{-3} mL, 2.34 × 10^{-5} mol) were placed in a Schlenk flask and dissolved in toluene (0.7 mL). Oxygen was removed from the solution by purging with argon (30 min). CuBr (3.3 × 10^{-3} g, 2.3 × 10^{-5} mol) was added under a positive argon flow and the reaction vessel was sealed and placed in a water bath at 25 ºC with stirring for 30 min. The contents were diluted with THF and passed through activated neutral alumina. The solvent was removed under reduced pressure to yield a residue. The crude product was fractionated by preparative SEC and fractions combined and precipitated into MeOH. Linear PSTY calibrated SEC (M_n = 10650, Đ = 1.03) and DMAc Triple Detection SEC (M_n = 16845, Đ = 1.001).

*6.2.2.15. Synthesis of c-PSTY$_4$-N$_3$ Oligomer (**13**)*

c-PSTY$_4$-OH **12** (0.030 g, 1.92 × 10^{-6} mol), DPPA (8.0×10^{-3} mL, 3.84 × 10^{-5} mol) and DBU (5.7 × 10^{-3} mL, 3.84 × 10^{-5} mol) were added to dry toluene (0.4 mL) at 0 ºC under argon. The flask was wrapped in aluminium foil to avoid light and the solution stirred for 24 h. After stirring the toluene was evaporated via nitrogen flow and the contents dissolved in minimal amount of THF, then precipitated into MeOH (20 fold excess to polymer solution) and recovered via vacuum filtration. Linear PSTY calibrated SEC (M_n = 10720, Đ = 1.02) and Triple Detection SEC (M_n = 15970, Đ = 1.01).

*6.2.2.16. Synthesis of c-PSTY$_5$-OH Oligomer (**14**)*

c-PSTY$_4$-N$_3$ **13** (3.0 × 10^{-3} g, 1.92 x 10^{-7} mol), c-PSTY-(≡)OH **7** (M_n = 2920, Đ = 1.05) (8.24 × 10^{-4} g, 2.13 x 10^{-7} mol) and PMDETA (1.2 × 10^{-3} mL, 5.77 × 10^{-6} mol) were placed in a Schlenk flask and dissolved in toluene (0.3 mL). Oxygen was removed from the solution by purging with argon (30 min). CuBr (0.83 × 10^{-3} g, 5.77 × 10^{-6} mol) was added under a positive argon flow and the reaction vessel was sealed and placed in a water bath at 25 ºC with stirring for 30 min. Linear PSTY calibrated SEC (M_n = 12160, Đ = 1.03).

"Feeding" synthesis of oligomer of cyclic PSTY blocks

*6.2.2.17. Synthesis of ≡(HO)-PSTY$_{27}$-Br (**2f**)*

Styrene (20.78 g, 0.20 mol), PMDETA (0.340 mL, 1.63 x 10^{-3} mol), initiator **1** (1.0 g, 3.25 x 10^{-3} mol) were added to a 50 mL flask sealed with rubber septum and purged by bubbling with argon for 30 min. A 50 mL Schlenk tube was charged with Cu(I)Br (0.234 g, 1.63 x 10^{-3} mol), Cu(II)Br$_2$/PMDETA complex (0.129 g, 3.25 x 10^{-4} mol) and magnetic stirrer, sealed with rubber septum and purged with argon for 30 min. The solution was transferred to the Schlenk flask via cannula. The reaction vessel was placed in an oil bath at 80 ºC, and the reaction mixture was stirred for 6h. The reaction was quenched by cooling the reaction mixture to 0 °C, exposed to air, and diluted with THF (ca. 3 fold to the reaction mixture volume). The copper salts were removed by passage through an activated neutral alumina column. The solution was concentrated by rotary evaporator and the polymer was recovered by precipitation into large volume of MeOH (20 fold excess to polymer solution) and then vacuum filtration. The polymer was dried *in vacuo* for 24 h at 25 °C and characterized by linear PSTY calibrated SEC (M_n = 3080, Đ = 1.09).

*6.2.2.18. Synthesis of ≡(HO)-PSTY$_{27}$-N$_3$ (**3f**)*

≡(HO)-PSTY$_{27}$-Br **2f**: (4.0 g, 1.26 x 10^{-3} mol) was dissolved in 40 mL of DMF in a 50 mL round bottom flask equipped with magnetic stirrer. To this solution, NaN_3 (0.82 g, 1.26 x 10^{-2} mol) was added and the mixture stirred for 24 h at 25 °C. Product was precipitated into a mixture of methanol and water (95/5 v/v%), filtered, washed exhaustively with MeOH and dried *in vacuo* for 24h. Linear PSTY calibrated SEC (M_n = 3380, Đ = 1.07).

*6.2.2.19. Synthesis of c-PSTY$_{27}$-OH (**4f**)*

A solution of ≡(HO)-PSTY$_{27}$-N$_3$ **3f** (2.0 g, 6.06 × 10^{-4} mol) in toluene (110 mL) was purged with argon for 90 min to remove oxygen. CuBr/PMDETA complex was prepared by cannula transfer of PMDETA (6.33 mL, 3.03 × 10^{-2} mol) solution in toluene (110mL) to a 250 mL Schlenk flask charged with CuBr (4.35 g, 3.03 × 10^{-2} mol), equipped with magnetic stirrer and purged with Ar for 90 minutes. Polymer solution was added to the Schlenk flask via syringe pump at a flow rate of 1.240 mL/min by argon feeding procedure. After the addition of the polymer solution the reaction mixture was stirred for additional 3 h. At the end of this period, toluene was evaporated by air flow. Polymer was dissolved in 200 mL of THF, and copper salts were removed by passage through activated neutral alumina column. Polymer was recovered by exhaustive wash with THF (4 × 400 mL). THF was evaporated, and polymer was recovered by precipitation into MeOH (20 fold excess to polymer solution) and then by filtration. The polymer was dried *in vacuo* for 24 h at 25 °C.

(Purity by SEC =78%). The crude products were fractionated by preparative SEC and fractions combined and precipitated in MeOH. Linear PSTY calibrated SEC (M_n =2470, Đ =1.06).

*6.2.2.20. Synthesis of c-PSTY$_{27}$-Br (**5f**)*

c-PSTY$_{27}$-OH **4f** (0.878 g, 2.59 × 10^{-4} mol), TEA (0.36 mL, 2.59 × 10^{-3} mol) and 10 mL of dry THF were added under an argon blanket to a dry 50 mL deoxygenated Schlenk flask. The reaction was then cooled on ice. To this stirred mixture, a solution of BPB (0.27 mL, 2.51 × 10^{-3} mol) in dry THF (4 mL) was added drop-wise under argon via an air-tight syringe over 30 min. After stirring the reaction mixture for 48 h at RT under argon pressure, the polymer was precipitated in MeOH, filtered and washed two times with MeOH. The polymer was dried for 24 h *in vacuo* at 25 °C. Linear PSTY calibrated SEC (M_n = 2730, Đ = 1.08).

*6.2.2.21. Synthesis of c-PSTY$_{27}$-N$_3$ (**6f**)*

c-PSTY$_{26}$-Br **5f** (0.826 g, 2.34×10^{-4} mol), NaN_3 (0.152 g, 2.34×10^{-3} mol) and 9 mL DMF were placed into the 20 mL glass vial equipped with magnetic stirrer. The reaction was carried out for 24 h. The polymer solution was precipitated into MeOH/H_2O (95/5 v/v) (20 fold excess to polymer solution) from DMF, recovered by vacuum filtration and washed exhaustively with water and MeOH. The polymer was dried *in vacuo* for 24 h at 25 °C. Linear PSTY calibrated SEC (M_n = 2530, Đ = 1.06).

*6.2.2.22. Synthesis of c-PSTY$_{27}$-(≡)OH (**7f**)*

c-PSTY$_{27}$-N_3 **6f** (0.55g, 1.69 × 10^{-4} mol), (3,5-bis(prop-2-yn-1-yloxy)phenyl)methanol (0.733g, 3.39 × 10^{-4} mol) and PMDETA (3.5 × 10^{-2} mL, 1.69 × 10^{-4} mol) in 5 mL toluene + 0.5 mL DMSO mixture were added to a 20 mL glass vial, sealed and bubbled with Ar for 30 min. A 20 mL Schlenk flask charged with CuBr (0.0243g, 1.69 × 10^{-4} mol) and equipped with a magnetic stirrer was purged with argon for 30 min to remove oxygen. The polymer solution was then cannula transferred to the Schlenk tube and reaction mixture allowed stirring at RT for 1 h. The reaction was quenched by dilution with THF (ca. 3 fold to the reaction mixture volume) and the copper salts removed by passage through an activated neutral alumina column. The solution was concentrated by rotary evaporator and the polymer recovered by precipitation into MeOH (20 fold excess to polymer solution) and vacuum filtration. The product was also purified by preparative SEC to remove the remove the minimal amount of 2-arm PSTY formed. The polymer was dried *in vacuo* for 24 h at 25 °C. Linear PSTY calibrated SEC (M_n = 2570, Đ = 1.06).

*6.2.2.23. Synthesis of c-PSTY$_{27}$-(≡)N$_3$ (**15f**)*

c-PSTY$_{27}$-(≡)OH **7f** (0.29 g, 8.81 x 10^{-5} mol), DPPA (0.19 mL, 8.81 x 10^{-4} mol) and DBU (0.131 mL, 8.81 x 10^{-4} mol) were added to dry toluene (3 mL) at 0 ºC under Argon flow. The flask was wrapped in aluminium foil to avoid light, and the solution stirred for 24 h. After stirring the toluene was evaporated via nitrogen flow and the contents dissolved in minimal amount of acetone, then precipitated into MeOH/H_2O (80/20 v/v) (10 fold excess to polymer solution) and recovered via vacuum filtration. Linear PSTY calibrated SEC (M_n = 2870, Đ = 1.11).

*6.2.2.24. Synthesis of (c-PSTY)$_n$-N$_3$ (1:50 equivalents) (**17f**)*

CuBr (3.19×10^{-4} g, 2.23×10^{-6} mol) was placed into a 5 mL Schlenk flask equipped with magnetic stirrer, sealed with rubber septum and purged with Ar for 30 min. c-PSTY-N_3 **6f** (1.50×10^{-2} g, 4.45×10^{-6} mol) and PMDETA (4.65×10^{-3} mL, 2.23×10^{-5} mol) were dissolved in 0.4 mL of toluene, put into a sealed 5 mL glass vial and bubbled with Ar for 20 min at a 1-2 bubbles/sec rate. c-PSTY(≡)N_3 **15f** (7.97×10^{-2} g, $2.22\text{x}10^{-5}$ mol) was dissolved in 0.3 mL of toluene, sealed in 4 mL vial and purged with Ar for 30 min. The solution of **6f** and PMDETA was cannula transferred into the Schlenk flask. Then the solution of **15f** in toluene was transferred to the Schlenk flask via syringe pump over 120 min. Reaction was allowed to stir for 30 min. Solvent was evaporated, the contents dissolved in minimal amount of THF, passed through neutral alumina column. Solution was concentrated, and the crude product was fractionated by preparative SEC. Fractions were precipitated into methanol and dried *in vacuo* for 24 h.

*6.2.2.25. Synthesis of (c-PSTY)$_n$-N$_3$ (1:50 equivalents) (**18f**)*

CuBr (3.19×10^{-4} g, 2.23×10^{-6} mol) was placed into a 5 mL Schlenk flask equipped with magnetic stirrer, sealed with rubber septum and purged with Ar for 30 min. c-PSTY-N_3 **6f** ($1.50\text{x}10^{-3}$ g, $4.45\text{x}10^{-7}$ mol) and PMDETA ($4.65\text{x}10^{-4}$ mL, $2.23\text{x}10^{-6}$ mol) were dissolved in 0.4 mL of toluene, put into a sealed 5 mL glass vial and bubbled with Ar for 20 min at a 1-2 bubbles/sec rate. c-PSTY(≡)N_3 **15f** ($7.97\text{x}10^{-2}$ g, $2.22\text{x}10^{-5}$ mol) was dissolved in 0.3 mL of toluene, sealed in 4 mL vial and purged with Ar for 30 min. The solution of **6f** and PMDETA was cannula transferred into the Schlenk flask. Then the solution of **15f** in toluene was transferred to the Schlenk flask via syringe pump over 120 min. Reaction was allowed to stir for 30 min. Solvent was evaporated, the contents dissolved in minimal amount of THF, passed through neutral alumina column. Solution was concentrated, and the crude product was fractionated by preparative SEC. Fractions were precipitated into methanol and dried *in vacuo* for 24 h.

6.2.3. Analytical Methodologies

Size Exclusion Chromatography (SEC)

The dried polymers were dissolved in THF to a concentration of 1 mg/mL and filtered through a 450 nm PTFE syringe filter prior to an injection. Analysis of the molecular weight distributions of the polymers was performed on a Waters 2695 separations module, fitted with a Waters 410 refractive index detector maintained at 35 °C, a Waters 996 photodiode array detector, and two Ultrastyragel linear columns (7.8 x 300 mm) arranged in series. The columns maintained at 40 °C for all analyses are capable of separating polymers in the molecular weight range of 500 – 4 million g/mol with high resolution. Prior to the analysis all polymer samples were dried in a vacuum oven for 24 hours at 25 °C. All samples were eluted at a flow rate of 1.0 mL/min. Narrow molecular weight PSTY standards ($Đ \leq 1.1$) ranging from 500 to 2 million g/mol were used for calibration. Data acquisition was performed using Empower software, and molecular weights were calculated relative to polystyrene standards.

Preparative Size Exclusion Chromatography (Prep-SEC)

Crude polymers were purified using a Varian ProStar preparative SEC system equipped with a manual injector, differential refractive index detector and single wavelength ultraviolet-visible detector. HPLC grade tetrahydrofuran was used as eluent at flow rate of 10 mL/min. Separations were achieved using a PLgel 10 μm 10E3Å, 300 x 25 mm preparative SEC column held at 25 °C. The dried impure polymer was dissolved in THF to a concentration of 100 mg/mL. The solution was filtered through a 0.45 um PTFE syringe filter prior to injection. Fractions were collected manually and the composition of each was determined using the Polymer Labs GPC50 Plus equipped with triple detection as described above.

^{1}H Nuclear Magnetic Resonance (NMR)

All NMR spectra were recorded using one of the following spectrometers: Bruker DRX 500, 400 or 300 MHz at 25 °C using an external lock ($CDCl_3$) and referenced to the residual non-deuterated solvent ($CHCl_3$). DOSY experiments were performed to acquire spectra presented herein by increasing the pulse gradient from 2 to 95 % of the maximum gradient strength and increasing gradient pulse length (*p30*) from 1 ms to 2 ms, using 32 to 256 scans.

Attenuated Total Reflectance Fourier Transform Spectroscopy (ATR-FTIR)

ATR-FTIR spectra were obtained using a single, horizontal bounce, diamond ATR accessory on a Nicolet Nexus 870 FT-IR. Spectra were recorded between 4000 and 500 cm^{-1} for 64 scans at 4 cm^{-1} resolution with an OPD velocity of 0.6289 cm/s. Solids were pressed directly onto the diamond internal reflection element of the ATR without further sample preparation.

Matrix-Assisted Laser Desorption Ionization – Time-of-Flight (MALDI-ToF) Mass Spectrometry

MALDI-ToF MS spectra were obtained using a Bruker MALDI-ToF autoflex III smartbeam equipped with a nitrogen laser (337 nm, 200 Hz maximum firing rate) with a mass range of 600 – 400,000 Da. All spectra were recorded in either reflectron (1500 – 5000 Da) or linear mode (5000 – 400,000 Da) using trans-2-[3-(4-*tert*-butylphenyl)-2-methyl-propenylidene] malononitrile (DCTB; 20 mg/mL in THF) as the matrix and $Ag(CF_3COO)$ (2 mg/mL in THF) as the cation source. The polymers were dissolved to a concentration of 1mg/mL. The matrix (20 μL), Ag(CF3COO) (2 μL) and polymer (20 μL) solutions were mixed together and spotted on the target plate via drying droplet method. Ca. 5000 shots randomly distributed over a sample spot were averaged.

Differential Scanning Calorimetry

Polymers were analysed by differential scanning calorimetry (DSC) using a Mettler Toledo DSC1 STARe System calorimeter. The following temperature profile was used with 5°C/min heating/cooling rate: samples of 3−5 mg were first heated from 20 to 150 °C under nitrogen atmosphere, kept isothermally at 150 °C for 3 min, cooled to 20 °C, heated second time up to 150 °C and finally cooled down to 20°C. The glass-transition temperature was determined as a mid-point of inflection of the obtained DSC curves within the second heating cycle.

Absolute Molecular Weight Determination by DMAc Triple Detection SEC

10-20 mg polymer samples were prepared in HPLC grade N,N-dimethylacetamide (DMAc, containing 0.03 wt % LiCl) and passed through a 0.45 μm PTFE filter membrane prior to injection. Analysis of the molecular weight distributions of the polymers were determined using a Polymer Laboratories GPC50 Plus equipped with differential refractive index detector. DMAc + 0.03 wt % LiCl was used as eluent at a flow rate of 1.0 mL/min. Separations were achieved using two PLGel Mixed B (7.8 x 300 mm) SEC columns connected in series and held at a constant temperature of 50 °C.

Preparative Size Exclusion Chromatography

Varian Pro-Star preparative SEC machine equipped with manual injector, RI and UV detectors was used for purification or fractionation of crude polymers. Prior to analysis polymers were dissolved in THF to 100 mg/mL concentration and passed through 0.45μm PTFE membrane filter. Fractionation was achieved using a PL Gel 10 μm 10 x 10^3 Å, 300 x 25 mm preparative SEC column at 25 °C. HPLC grade THF was used as an eluent, flow rate was maintained at10 mL/min.

LND simulation

Molecular weight distribution of a polymer synthesized by living radical polymerization can be fitted with Gaussian function

$$w(M) = \frac{1}{\mathrm{M}\sqrt{2\pi\sigma^2}}\exp\left(-\frac{(\ln \mathrm{M} - \ln \bar{\mathrm{M}})^2}{2\sigma^2}\right) \qquad (6.3)$$

in which mean $\bar{M}$ is defined by formula:

$$\bar{\mathrm{M}} = \sqrt{\mathrm{M_n M_w}} \qquad (6.4)$$

and variance σ^2 is calculated as follows:

$$\sigma^2 = \left(\ln\left(\frac{M_w}{M_n}\right)\right)^2 \qquad (6.5)$$

where M_n is number-average molecular weight of a polymer and M_w is weight-average molecular weight.[20]

6.3. Results and Discussion

6.3.1. Sequential Approach

The methodology for the synthesis of multicyclic PSTY involves the addition of difunctional c-PSTY-(≡)OH to c-PSTY$_i$-N$_3$ species. The proximity of alkyne and alcohol within the c-PSTY-(≡)OH molecule insures increasing compactness of the growing multicyclic architecture. The nature of the hydroxyl group allowed us to use one step azidation of c-PSTY$_i$-OH species with DPPA/DBU, which reduces the number of synthetic steps substantially. The synthetic methodology to produce a multicyclic polymer sequentially from 1 to 5 cyclic units is given in Scheme 6.1.

Scheme 6.1. Synthetic methodology for the synthesis of multicyclic polystyrene by sequential route[a]

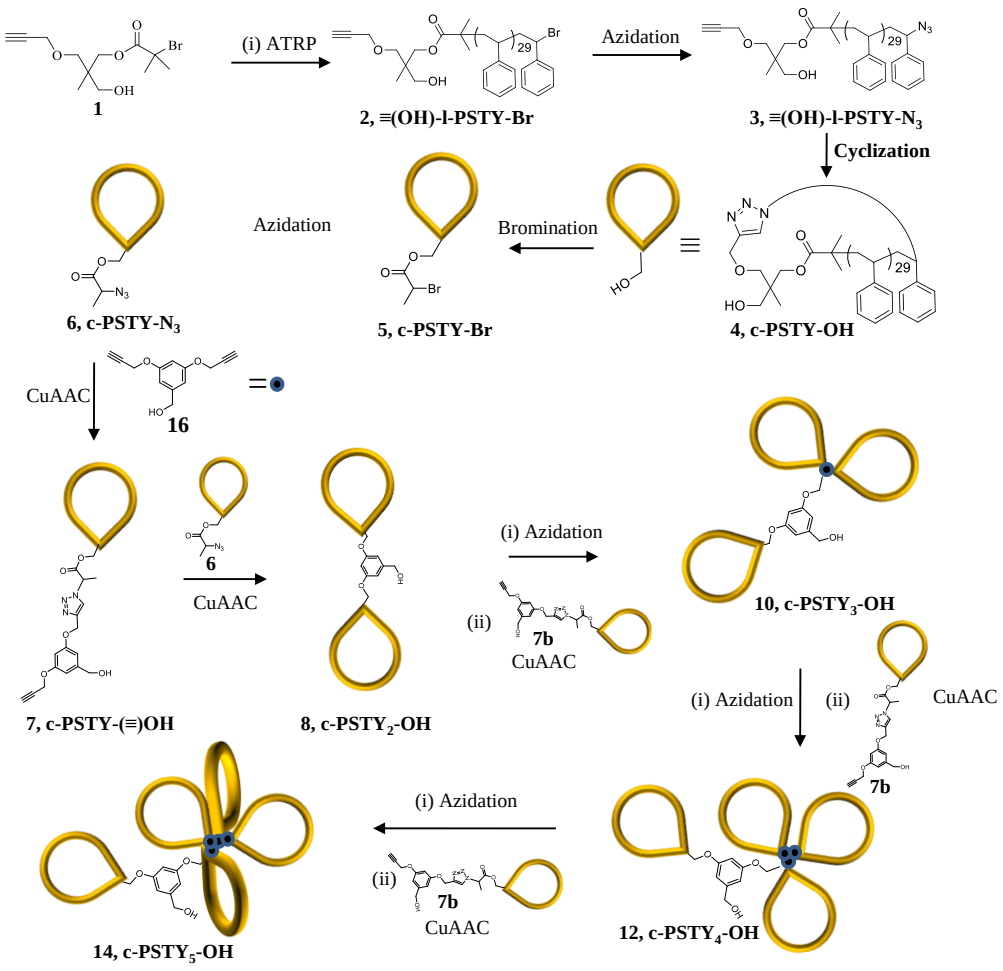

[a]Conditions. ATRP: STY, PMDETA, CuBr, CuBr$_2$/PMDETA. Azidation. NaN$_3$, DMF at 25°C. Cyclization: CuBr, PMDETA in toluene by feed at 25 °C. Bromination: 2-bromopropionyl bromide, TEA in THF; 0 °C – 25°C. CuAAC: CuBr, PMDETA in toluene at 25 °C.

Linear PSTY **2** with a number-average molecular weight (M_n) of 3840 and dispersity ($Đ$) of 1.05 was synthesized using ATRP of styrene with an alkyne initiator **1**. The bromine chain-end functionality determined by diffusion ordered spectroscopy (DOSY) NMR (Figure A6.4 in Appendix) was 97. Azidation of the Br-groups of **2** gave an azide **3** with 96% functionality (Figure A6.7). Cyclization of **3** to form **4** was carried out by feeding **3** at a flow rate of 1.24 mL/min to a solution of CuBr and PMDETA ligand in accordance with our previous procedures. By using the LND simulation, we determined that 91% of the linear **3** was directly converted to the monocyclic **4**, and after fractionation by preparative SEC the purity of cyclic increased to > 99% with a M_h value of 0.765. The OH-group on **4** was converted to an azide **6**, which was further coupled with a large excess of dialkyne linker (**16**) via CuAAC to produce **7**. The addition of **7** to **6** with direct azidation of the benzyl alcohol with DPPA/DBU allowed the sequential growth of a multicyclic polymer with up to 5 units (Scheme 6.1). The purity of the multicyclic after preparative SEC was greater than 99% for 2 units, and decreased to 96% for units 3 and 4 (Table 6.1).

Table 6.1. Log Normal Distribution (LND) simulation and change in hydrodynamic volume (M_h) data for the synthesis of multicyclic polymeric structures.

Polymer N°	Polymer Code	Purity by LND (%)		Coupling efficiency by LND (%)[a]	RI-SEC MWD parameters by LND[b]		Absolute MWD parameters by LND[c]		$V_{h,cyc}$[d] (nm)	$V_{h,abs}$[e] (nm)	M_h[f]
		Crude	Prepped		$M_{n,RI}$	Đ	$M_{n,abs}$	Đ			
3	≡(OH)-PSTY$_{30}$-N$_3$						3470	1.06		9.78	
4	c-PSTY$_{30}$-OH	91	> 99	92.3	2654	1.058	3470	1.058	6.20	9.78	0.765
6	c-PSTY$_{30}$ –N$_3$		> 99		2781	1.052	3636	1.052	6.72	10.58	
7	c-PSTY$_{30}$-(≡)OH	85	> 99		2877	1.038	3761	1.038	7.11	11.21	
8	c-PSTY$_2$-OH	94	> 99	> 99	5920	1.029	7555	1.029	24.25	36.70	0.77
9	c-PSTY$_2$-N$_3$	> 99			5912	1.027					
10	c-PSTY$_3$-OH	85	96	87	8590	1.023	11440	1.023	45.65	74.30	0.739
11	c-PSTY$_3$-N$_3$	96			8698	1.023					
12	c-PSTY$_4$-OH	90	96		10751	1.022	15530	1.022	66.86	124.93	0.69
13	c-PSTY$_4$-N$_3$	> 99			10751	1.022					
14	c-PSTY$_5$-OH	83		85	12688	1.023	1934	1.023	88.59	181.44	0.656

[a]CuAAC coupling efficiency was determined from the RI traces of SEC. Coupling efficiency calculated as follows: purity (LND)/max. purity by theory×100.

[b]Experimental refractive index detector SEC (RI-SEC) traces were fit using the LND model by fitting M_n and Đ.

[c]Calculated using corresponding $M_h(i)$ and $M_{n,cyc}(i)_{LND}$ values.

[d]Calculated using eq. 6.1 and apparent $M_{n,RI}$ determined by LND simulation.

[e]Calculated using eq. 6.1 and absolute $M_{n,abs}$ determined by LND simulation.

[f]M_h was determined by LND simulation .

Multicyclic **14** (with 5 monomer units) was produced with 83% purity immediately after the reaction. Taking into account that the reaction scheme consisted of 13 steps with increasing difficulties in separation of high molecular weight polymers which have very similar hydrodynamic radii, it can be considered that the purity of **14** was high. The purity of all purified c-PSTY$_i$-OH (i = 1-4) was additionally supported by MALDI-ToF (see Appendix). The final product **14** was not purified further by preparative SEC due to the small amount of polymer available (< 7 mg) as a result of the loss of polymer following the many previous purification steps. The SEC chromatograms given in Figure 6.1A showed an increase in molecular weight with addition of each cyclic monomer unit. The molecular weight distributions for the multicyclic polymers after preparative SEC were narrow with the dispersity values all below 1.04 and symmetrical bell shape indicating high purity.

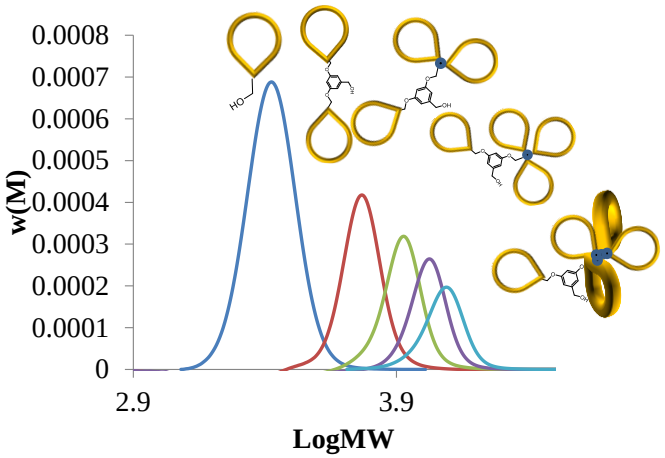

Figure 6.1. Molecular weight distributions (MWDs) of c-PSTY$_i$-OH with i = 1-5 obtained from SEC-RI based on a polystyrene calibration curve.

Cyclic polymers demonstrate lower hydrodynamic volume ($V_{h,cyc}$) and, as a consequence of eq. 6.1, lower apparent molecular weight ($M_{n,cyc}$) compared to the linear analogues as was previously mentioned. In order to quantify the ratio between apparent and absolute molecular weights of cyclic molecules and their linear analogues we used LND simulation. As the absolute molecular weight of monocyclic PSTY **4** is simply the molecular weight of linear **3**, the M_h value of monocyclic PSTY is equal to:

$$M_{h,1} = \frac{M_{cyc}(1)_{LND}}{M_{n,abs}(1)} \qquad (6.6)$$

where $M_{cyc}(1)_{LND}$ is apparent molecular weight of **4** obtained by changing M_n and Đ parameters of LND function to fit the SEC trace of **4**, and $M_{n,abs}(1)$ is an analogical LND fit of **3**. $M_{h,2}$ for the

diblock PSTY **8** formed through coupling reaction between c-PSTY$_{30}$–N$_3$ (**6**) and c-PSTY$_{30}$-(≡)OH (**7**) was calculated as follows:

$$\mathrm{M_{h,2}} = \frac{\mathrm{M_{cyc}(2)}_{LND}}{\mathrm{M_{n,abs}(2)}} \qquad (6.7)$$

where $M_{cyc}(2)_{LND}$ is calculated analogically to $M_{cyc}(1)_{LND}$, and the only unknown $M_{n,abs}(2)$ can be found by

$$\mathrm{M_{n,abs}(2)} = \frac{\mathrm{M_{n,cyc}(1)_{LND,azide}}}{\mathrm{M_h(1)}} + \frac{\mathrm{M_{n,cyc}(1)_{LND,alkyne}}}{\mathrm{M_h(1)}} \qquad (6.8)$$

In this equation $M_{n,abs}(2)$ is basically an addition of the absolute molecular weights of **6** and **7**. Cyclic blocks were added sequentially and a general equation was used iteratively to calculate $M_{h,i}$ for cyclic species with the number of cyclic units i>1 is similar to eq. 6.6 and 6.7:

$$\mathrm{M_h(i)} = \frac{\mathrm{M_{n,cyc(i)_{LND}}}}{\mathrm{M_{n,abs}(i)}} \qquad (6.9)$$

where the only unknown absolute molecular weight of polystyrene $M_{n,abs}(i)$ with i cyclic units was found using eq. 6.8:

$$\mathrm{M_{n,abs}(i)} = \frac{\mathrm{M_{n,cyc(i-1)_{LND}}}}{\mathrm{M_h(i-1)}} + \frac{\mathrm{M_{n,cyc}(1)_{LND}}}{\mathrm{M_h(1)}} \qquad (6.10)$$

in which $M_h(i\text{-}1)$ is taken from i-1 iteration and $\mathrm{M_{n,cyc}(i\text{-}1)_{LND}}$ is found by LND simulation. An example is given in Figure 6.2A for determining $M_{h,i}$ values for an oligomer with i>2. First, we fitted SEC traces of **7** prepped, **9** and **10** by changing M_n and Đ of the Gaussian distribution to find corresponding $M_{n,cyc}(i)_{LND}$ values. After that $M_{n,abs}(3)$ is calculated using eq 6.10. Its substitution into eq. 6.9 gives $M_h(3)$. Substantial contraction of molecule size of **10** is demonstrated on the Figure 6.2A by changing $M_{n,cyc}(3)_{LND}$ to $M_{n,abs}(3)$ in the LND function. Using iteratively equations 6.9 and 6.10 we obtained $M_{h,i}$ values for all c-PSTY$_i$-OH species (Table 6.1). Many polymers were purified using preparative SEC, thus, eq. 6.10 cannot be directly used to calculate $M_{n,abs}(i)$ of the purified polymers as the MWDs of polymers can shift. However these values can be calculated from eq. 6.9 as both $M_{n,cyc}(i)_{LND}$ and $M_h(i)$ are known (Table 6.1). The M_h value decreased significantly from 0.76 to 0.66 for **4** and **14** respectively but the contraction in hydrodynamic volume was even more substantial due to the power law dependence of V_h from M_n.

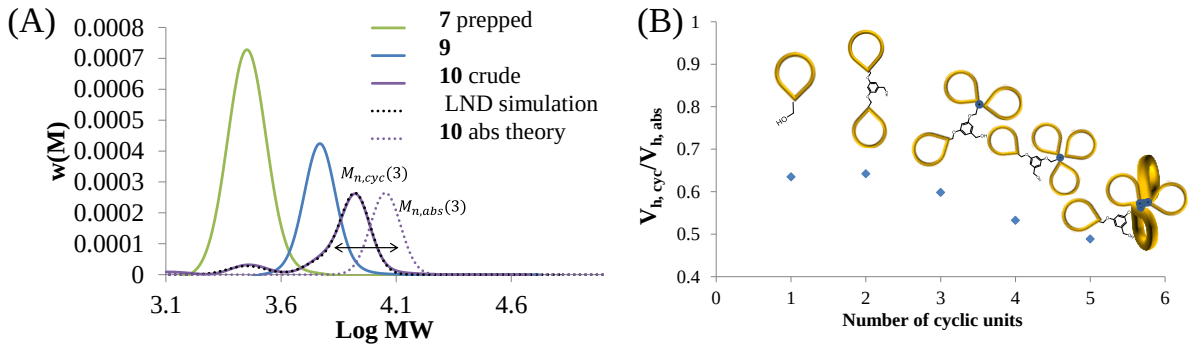

Figure 6.2. LND simulation of **10** and hydrodynamic volume contraction of multicyclic PSTY. (A) Click reaction between **7** and **9**, LND simulation of their conjugate **10** and comparison to theoretical curve of linear analogue. (B) Relationship between number of cyclic units and parameter $V_{h,cyc}/V_{h,abs}$. $V_{h,cyc}$ is a hydrodynamic volume of n-mer, $V_{h,abs}$ is a theoretical hydrodynamic volume of a linear polymer with molecular weight equivalent to that of cyclic n-mer calculated using eq 6.1.

The ratio $V_{h,cyc}/V_{h,abs}$ shown in Figure 6.2B was calculated using eq. 6.1 where the molecular weights of c-PSTY$_i$-OH are $M_{n,cyc}(i)_{LND}$ and absolute molecular weights of linear analogues are $M_{n,abs}(i)$. For monocyclic species the ratio $V_{h,cyc}/V_{h,abs}$ was 0.63, which as was previously mentioned is close to the corresponding published values of g_h. For dicyclic species the ratio remained close to 0.63 as there is no steric hindrance in coupling two cyclic molecules together. The ratio then decreased upon each addition of cyclic units with a final value of 0.49 for **14**. Such a contraction indicates that the chosen topological constraint indeed causes significant changes in the conformation of the multicyclic architecture. Although linking the cyclic units adjacent to each other resulted in a substantial decrease in the coil dimensions, the question we wanted to answer was whether the steric bulk of the cyclic units restrict further addition of cyclics to produce higher molecular weight multicyclic polymers.

6.3.2. Feeding Approach

To address this issue, we used a modified feeding approach. Here, a cyclic monomer (**15f**) with both an azide and alkyne group was prepared by direct azidation of **7f** (see Scheme 6.2A). (The notation of **7f** represents a new batch of polymer with a slightly different molecular weight). Cyclic **15f** was fed slowly (0.0025 mL/min) into a mixture of **6f**, CuBr and PMDETA. The reason for addition of **6f** in the solution was to allow the greatest probability for sequential growth as **6f** has only one chain growth functionality. Two reactions were carried out at a **6f**:**15f** ratio of 1:5 and 1:50. The SEC chromatograms in Figure 6.3A show that both ratio conditions produced multicyclic polymers with broad molecular weight distributions (MWDs).

Scheme 6.2. (A) Synthetic methodology for the synthesis of multicyclic polystyrene by feeding approach[a]. (B) Side 'click' cyclization of n-mers.

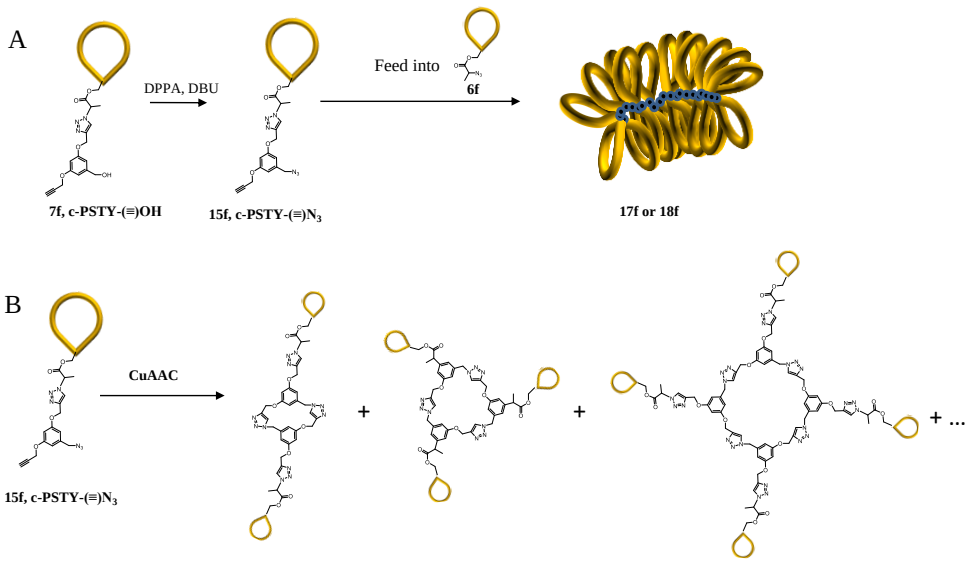

[a]Conditions. ATRP: STY, PMDETA, CuBr, $CuBr_2$/PMDETA. Azidation: NaN_3, DMF at 25°C. Cyclization: CuBr, PMDETA in toluene by feed at 25 °C. Bromination: 2-bromopropionyl bromide, TEA in THF; 0 °C – 25°C. CuAAC : CuBr, PMDETA in toluene at 25 °C.

Significantly higher molecular weights were observed for the 1:50 ratio, demonstrating that the steric bulk of the cyclic side chains did not restrict the formation of high molecular weight multicyclic polymers. The reason for this could be a result of a change in conformation of the polymer coil with an increase in the number of cyclic units. We analyzed the change in coil dimensions as a function of molecular weight by fractionation of **17f** and **18f** (Figure 6.3A). After preparative SEC, the fractions were isolated (see Figures 6.3B and 6.3C, for clarity not all fractions are included in the graphs) and further characterized by LND simulation (Figure 6.4). The $M_h(i)$ values from the sequential approach were used as non-adjustable parameters in LND simulation to fit the low molecular weight region of the fraction **F1** of **17f** which contained lowest molecular weight polymers. The residual high molecular weight tail of the SEC curve was fitted with species consisting of higher number of cyclic units; their $M_{n,cyc}$ values were calculated using eq. 6.9 and fitting was achieved by adjusting $M_h(i)$ and Đ values. It was found that **F1** contained oligomers of 6-9 cyclic units ($\log M > 3.6$).

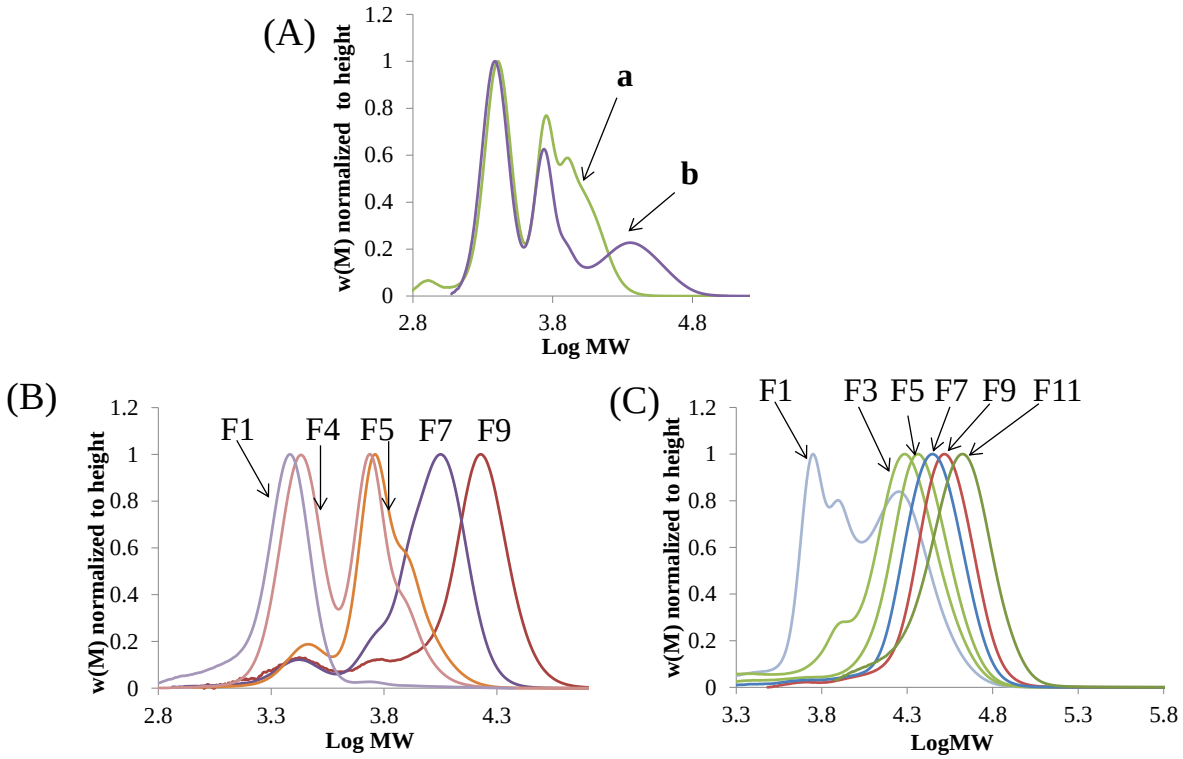

Figure 6.3. (A) SEC traces of multiblock polystyrene prepared by feeding synthesis. (a) SEC trace of **17f** crude, synthesized using 5 to 1 ratio between **15f** and **6f,** (b) SEC trace of **18f** crude, synthesized using 50 to 1 ratio between **15f** and **6f**. (B) SEC traces of fractions **F1**, **F4**, **F5**, **F7** and **F9** of **17f** obtained by preparative SEC and normalized to height. (C) SEC traces of fractions **F1**, **F3**, **F5**, **F7**, **F9** and **F11** of **18f** obtained by preparative SEC and normalized to height.

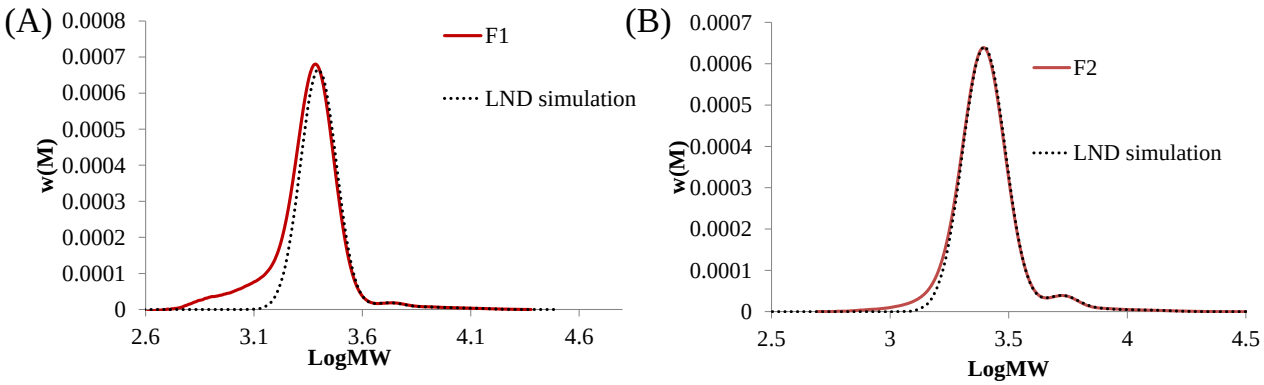

Figure 6.4. LND simulation of fractionated **17f**. (A) Full SEC trace of **F1** fraction of **17f** and its LND simulation. (B) Expanded high molecular weight region of **F1** fraction of **17f** and its LND simulation using fixed $M_h(i)$, where i = 1-5 (green area) and adjustable $M_h(i)$ parameters, for i = 6-9 (blue area).

The M_h values of the oligomers with 1-9 cyclic units were used as fixed parameters in the further LND simulation of higher molecular weight fraction **F2** of **17f**. Residual high molecular weight tail of **F2** was fitted with additional oligomer species with i = 10. The procedure was repeated to fit all

residual fractions **F3** to **F11** of **17f** and **F1** to **F12** of **18f**. The resulting correlation between M_h and the number of cyclic monomer units is given in Figure 6.5.

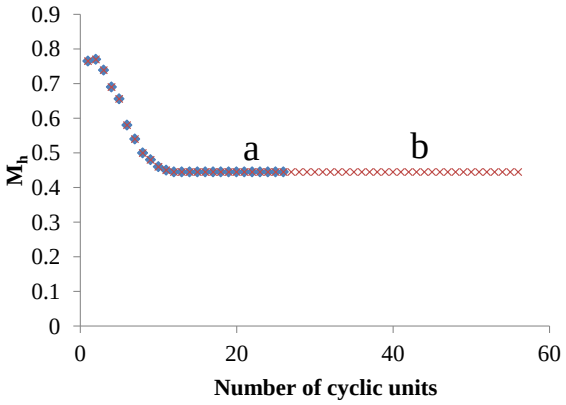

Figure 6.5. (A) Relationship between M_h acquired using iterative LND simulation and number of cyclic units for **17f** (a) and **18f** (b).

It can be seen that M_h decreased from 0.77 to 0.445 from 1 to 12 cyclic units, remaining constant at 0.445 to high cyclic units (~50). In order to demonstrate that the M_h values were determined correctly we used them to fit the MWDs of crude **17f** and **18f** (Figure 6.6A and 6.6C). The fit with the SEC chromatograms using these parameters was excellent suggesting that the LND method was accurate.

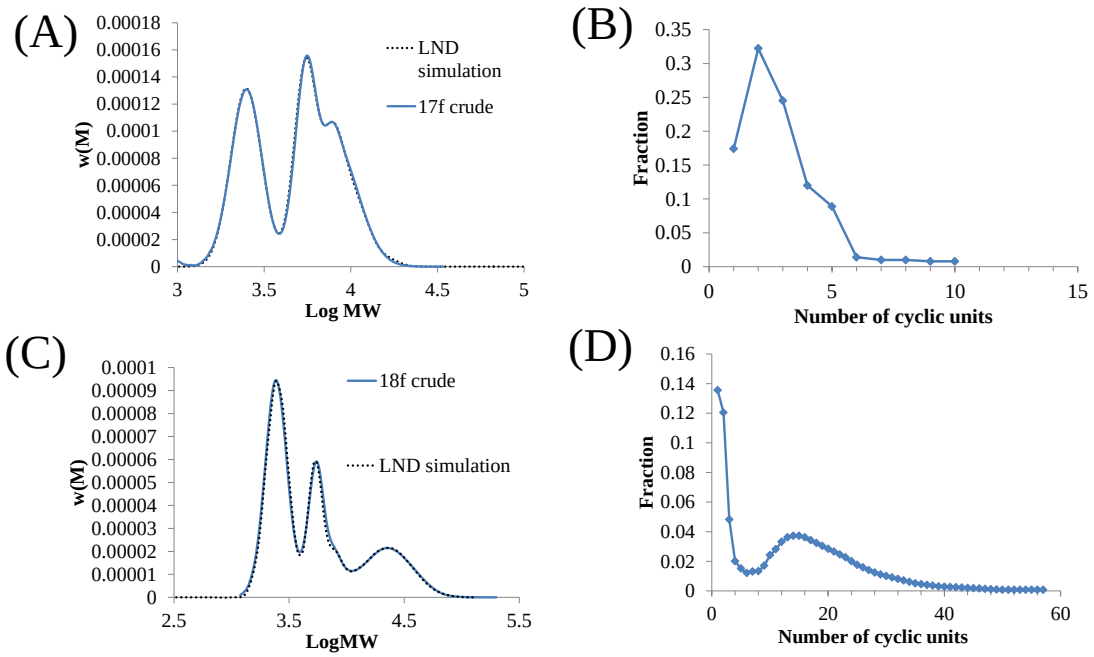

Figure 6.6. (A) SEC trace of **17f** crude (blue curve) and its LND simulation using M_hs acquired from **F1-10** of **17f**. (B) Weight fraction of each n-mer in **17f** crude obtained using LND fit to GPC trace. (C) SEC trace of **18f** crude (blue curve) and its LND simulation using ΔHDVs acquired from **F1-10** of **17f**. (D) Weight fraction of each n-mer in **18f** obtained using LND fit to GPC traces of crude **18f**.

The weight fraction of cyclic units in **17f** (before fractionation) from the 1:5 ratio experiment (Figure 6.6B) showed high weight fractions for 1 and 2 cyclic units, which decreased to 6 units. The much higher fractions of 1 and 2 units suggested that **15f** (Scheme 6.2B) could undergo intramolecular coupling to form an unreactive 1 unit cyclic, and that the 2 cyclic units could also couple to form an unreactive dicyclic species. This was further exemplified for the 1:50 experiment (Figure 6.6D) where the fraction of 1 cyclic was the greatest followed by 2 and 3 cyclic units. The secondary distribution centered at 14 units was formed through a condensation polymerization, although a cyclic polymer containing cyclic side chains was also possible (Scheme 6.2B).

The ratio of $V_{h,cyc}/V_{h,abs}$ given in Figure 6.7 showed that the hydrodynamic volume ratio decreased from 0.63 (1 cyclic unit) to 0.25 (12 cyclic units). Such a volume contraction of ~75% above 12 units from its linear coil volume was remarkable. The theoretical volume contraction going from a good to a theta solvent is based on Eq. 6.1 when a = 0.7 for THF and a = 0.5 under theta conditions (i.e. where solvent is excluded from the coil):

$$\frac{V_{h,\theta}}{V_{h,THF}} = M_n^{-0.2} \qquad (6.9)$$

The ratio was approximately 0.12 or an 88% contraction at a molecular weight of 12 cyclic units. The contraction to 0.25 for multicyclic polymers greater than 12 units suggested that these coils contained little solvent (Figure 6.7).

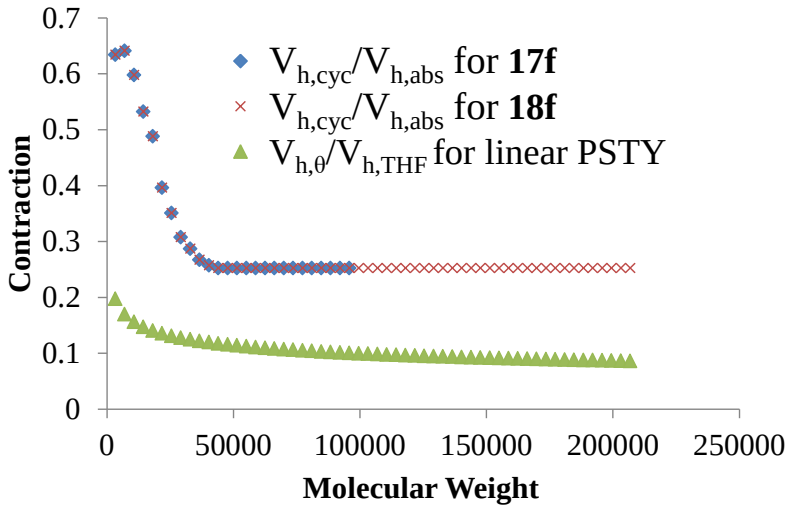

Figure 6.7. Contraction of polystyrene coils due to topological constraints and at theta conditions for various molecular weights. The contraction due to the multicyclic nature ($V_{h,cyc}/V_{h,abs}$) was acquired using M_h values from iterative LND simulation and eq. 6.1 and 6.9. The contraction at theta conditions ($V_{h,\theta}/V_{h,THF}$) was calculated using eq. 6.9.

Such a hydrodynamic volume collapse can further be explained by the Daoud-Cotton model,[35] in which the styrene units on the cyclic side chains attached close to the backbone have a significantly higher styrene concentration. The greater compactness of the multicyclic backbone will drive the

styrene density of the blobs close to that of theta conditions. It was previously reported for bottlebrush polystyrene that the number of attached units must exceed 120 in order to alter from spherical shape,[36] so we presume that the shape of the architectures made in our work is spherical and therefore it is correct to compare hydrodynamic volumes of multicyclic species and their linear analogues up to the highest molecular weights obtained in this work.

6.3.3. Differential Scanning Calorimetry

The change in compactness and topology of the multicyclic polystyrene polymers will also result in a loss of conformational entropy, which will be maintained under bulk conditions. A possible way to characterize these changes can be found from observing changes in glass transition temperature (T_g). We performed Differential Scanning Calorimetry (DSC) on the pure oligomers (with 1 to 4 units) and the fractions (**F1**, **F3**, **F5** and **F7**) from **18f**. Curve a in Figure 6.8A showed that the T_g increased with the number of cyclic units (or M_n) in the multicyclic.

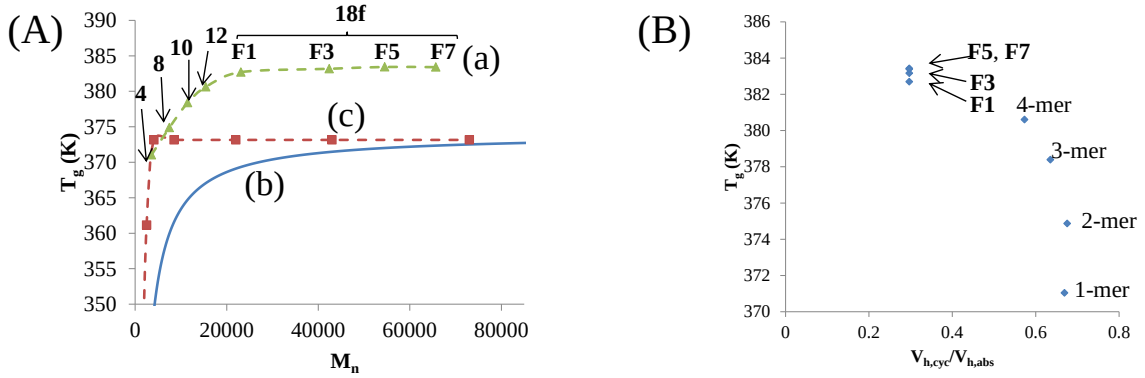

Figure 6.8. (A) Relationship between glass transition temperature of a polymer and its molecular weight for linear polystyrene obtained using the Kanig-Ueberreiter equation (a), experimental data from Gan et al.[37] (b) and T_gs of **4**, **8**, **10** and **12** and fractionated **18f** (c)**.** (B) The influence of $V_{h,cyc}/V_{h,lin}$ of pure n-mers and fractions **F1**, **3**, **5** and **7** of **18f** in θ-solvent on their glass transition temperature.

The T_g values for multicyclic polymers (curve a in Fig 6.8A) were much greater than for their linear analogues (curve b in Fig 6.8A), which were calculated from the Kanig-Ueberreiter equation. It was also found that these values were even greater than T_gs of monocyclic polystyrene chains.[37] It can be seen that the T_g values for the linear and monocyclic chains converge to ~ 373 K at high molecular weights. This was not the case for our multicyclic chains, which plateaued at 383 K, 10 degrees higher than for either the monocyclic or linear polystyrene chains. One can consider the linkages between each cyclic side chain as irreversible knots, resulting in lower conformational entropy of the coil and, therefore, a higher value of T_g. To indicate whether this conformational change was due solely to the compactness of the coil, we plotted the ratio of the hydrodynamic

volume of the multicyclic to that of its linear equivalents in a theta solvent ($V_{h\theta,cyc}/V_{h\theta,abs}$) as shown in Figure 6.8B. A theta solvent should represent the coil dimensions in the bulk. As the ratio of $V_{h\theta,cyc}/V_{h\theta,abs}$ decreased the T_g increased in a non-linear fashion. This suggested that the compactness of the coil, an indication of free volume, was not the sole determinant for the increase in T_g, but that the loss of conformational entropy due to the high styrene density located at the backbone of the multicyclic plays a more dominant role. Once this density becomes uniform through relaxation in the backbone there is no further decrease in the conformational entropy and thus no further increase in T_g.

6.4. Conclusion

In summary, a new iterative synthetic methodology was introduced to make compact multicyclic polystyrene architectures and study how topological constraints affect the properties of the polymers. In the first synthetic scheme, pure oligomers were obtained and precise M_h values determined for each n-mer up to i = 5. A continuous increase in molecule compactness with addition of cyclic units was observed. A feeding approach was then used to study whether the maximum topological compactness could be achieved. Using this method a distribution of oligomers with different number of cyclic units was obtained, and the polymers were fractionated using preparative SEC to give narrow molecular weight distributions. The LND application (described in Chapter 2) was broadened by characterizing these polymer fractions and showed that even narrow MWDs can consist of multiple polymer species. Simulation of the polymer fractions showed that compactness of multicyclic polystyrene is 4 times lower than the theoretically calculated hydrodynamic volume for linear species. Polymer compactness does not change when number of cyclic units exceeds 10, suggesting the formation of stable compact structure. This may result from a lack of chain ends, and internal irreversible entanglements decrease the configurational entropy of the polymer, causing an increase of T_g values for multicyclic polystyrene above that of linear polystyrene with infinite molecular weight.

6.5. References

1. Chen, B.; Jerger, K.; Fréchet, J. M. J.; Szoka Jr, F. C. *Journal of Controlled Release* **2009,** 140, (3), 203-209.

2. McLeish, T. *Science* **2002,** 297, (5589), 2005-2006.

3. Yamamoto, T.; Tezuka, Y. *Soft Matter* **2015,** 11, (38), 7458-7468.

4. Clarson, S. J.; Dodgson, K.; Semlyen, J. A. *Polymer* **1985,** 26, (6), 930-934.

5. Hadziioannou, G.; Cotts, P. M.; ten Brinke, G.; Han, C. C.; Lutz, P.; Strazielle, C.; Rempp, P.; Kovacs, A. J. *Macromolecules* **1987,** 20, (3), 493-497.

6. Ragnetti, M.; Geiser, D.; Höcker, H.; Oberthür, R. C. *Die Makromolekulare Chemie* **1985,** 186, (8), 1701-1709.

7. Hossain, M. D.; Jia, Z.; Monteiro, M. J. *Macromolecules* **2014,** 47, (15), 4955-4970.

8. Benoit, H.; Grubisic, Z.; Rempp, P.; Decker, D.; Zilliox, J. G. *J Chim Phys* **1966,** 63, (11-1), 1507-&.

9. Jia, Z. F.; Monteiro, M. J. *Journal of Polymer Science Part a-Polymer Chemistry* **2012,** 50, (11), 2085-2097.

10. Laurent, B. A.; Grayson, S. M. *Chemical Society Reviews* **2009,** 38, (8), 2202-2213.

11. Kricheldorf, H. R. *J. Polym. Sci., Part A Polym. Chem.* **2010,** 48, (2), 251-284.

12. Bielawski, C. W.; Benitez, D.; Grubbs, R. H. *Science* **2002,** 297, (5589), 2041-2044.

13. Laurent, B. A.; Grayson, S. M. *Journal of the American Chemical Society* **2006,** 128, (13), 4238-4239.

14. Lonsdale, D. E.; Bell, C. A.; Monteiro, M. J. *Macromolecules* **2010,** 43, (7), 3331-3339.

15. Kapnistos, M.; Lang, M.; Vlassopoulos, D.; Pyckhout-Hintzen, W.; Richter, D.; Cho, D.; Chang, T.; Rubinstein, M. *Nat. Mater.* **2008,** 7, (12), 997-1002.

16. Geiser, D.; Höcker, H. *Macromolecules* **1980,** 13, (3), 653-656.

17. Hild, G.; Kohler, A.; Rempp, P. *European Polymer Journal* **1980,** 16, (6), 525-527.

18. Vollmert, B.; Huang, J.-x. *Die Makromolekulare Chemie, Rapid Communications* **1980,** 1, (5), 333-339.

19. Gavrilov, M.; Monteiro, M. J. *European Polymer Journal* **2015,** 65, 191-196.

20. Monteiro, M. J. *European Polymer Journal* **2015,** 65, (0), 197-201.

21. Tezuka, Y.; Komiya, R.; Washizuka, M. *Macromolecules* **2003,** 36, (1), 12-17.

22. Tezuka, Y.; Oike, H. *Journal of the American Chemical Society* **2001,** 123, (47), 11570-11576.

23. Sugai, N.; Heguri, H.; Ohta, K.; Meng, Q.; Yamamoto, T.; Tezuka, Y. *Journal of the American Chemical Society* **2010,** 132, (42), 14790-14802.

24. Kulis, J.; Jia, Z.; Monteiro, M. J. *Macromolecules* **2012,** 45, (15), 5956-5966.

25. Lonsdale, D. E.; Monteiro, M. J. *Chemical Communications* **2010,** 46, (42), 7945-7947.

26. Roovers, J.; Toporowski, P. M. *Macromolecules* **1983,** 16, (6), 843-849.

27. Moore, R. E. *Journal of Industrial Microbiology* **1996,** 16, (2), 134-143.

28. Lambert, J. N.; Mitchell, J. P.; Roberts, K. D. *Journal of the Chemical Society, Perkin Transactions 1* **2001**, (5), 471-484.

29. Abel-Santos, E.; Scott, C. P.; Benkovic, S. J., Use of Inteins for the In Vivo Production of Stable Cyclic Peptide Libraries in E. coli. In *E. coliGene Expression Protocols*, Vaillancourt, P. E., Ed. Humana Press: Totowa, NJ, 2003; pp 281-294.

30. Conibear, A. C.; Wang, C. K.; Bi, T.; Rosengren, K. J.; Camarero, J. A.; Craik, D. J. *J Phys Chem B* **2014,** 118, (49), 14257-14266.

31. Sumners, D. W. *The Mathematical Intelligencer* **1990,** 12, (3), 71-80.

32. Hossain, M. D.; Lu, D.; Jia, Z.; Monteiro, M. J. *ACS Macro Letters* **2014,** 3, (12), 1254-1257.

33. Lonsdale, D. E.; Whittaker, M. R.; Monteiro, M. J. *Journal of Polymer Science Part A: Polymer Chemistry* **2009,** 47, (22), 6292-6303.

34. Jia, Z.; Lonsdale, D. E.; Kulis, J.; Monteiro, M. J. *ACS Macro Letters* **2012,** 1, (6), 780-783.

35. Daoud, M.; Cotton, J. *Journal de Physique* **1982,** 43, (3), 531-538.

36. Pesek, S. L.; Li, X.; Hammouda, B.; Hong, K.; Verduzco, R. *Macromolecules* **2013,** 46, (17), 6998-7005.

37. Gan, Y.; Dong, D.; Hogen-Esch, T. E. *Macromolecules* **1995,** 28, (1), 383-385.

Chapter 7

Summary

The objective of this thesis was to introduce a methodology to correctly interpret SEC data, study the mechanism of copper-catalyzed LRP and apply the acquired knowledge to conjugational polymer chemistry and to the investigation of new polymer topologies. As modern polymer structures become more complex, it is important to characterize them properly. We demonstrated that some aspects of SEC data may be overlooked during conventional analysis, including low molecular weight tailing, insufficient SEC trace shift for cyclic polymers and different d*n*/d*c* of heteropolymers in polymer mixtures. This leads to incorrect characterization of polymer purity and composition. We demonstrated that these problems can be solved by using appropriate weight distribution functions and by LND simulation. Further, we developed a new catalyst for aqueous SET-LRP of NIPAM and studied molecular weight distributions and chain-end functionality of the obtained polymers using LND simulation and 'click' chemistry. Finally, the obtained knowledge was applied to study new compact multicyclic polystyrene in a good solvent and at theta conditions using LND simulation and DSC. It was shown that the introduction of topological constraints leads to significant decrease in hydrodynamic volume and increase in T_g of multicyclic species compared to that of linear analogues.

7.2. Derivation of the Molecular Weight Distributions from Size Exclusion Chromatography and Log-Normal Distribution Simulation

In the beginning of this thesis we demonstrated the derivation of differential log*M* (*x(M)*), weight (*w(M)*) and number (*n(M)*) distribution functions from raw RI-SEC response *vs* elution volume. M_w, and M_n were directly derived from these distributions as normalized integrals of the corresponding functions. These values are essential for LND simulation which uses a two-parameter Gaussian function. We highlighted the importance of using proper MWD functions for plotting SEC data and showed the utility of the LND simulation in two typical reactions. In the first example, dead chains in RAFT polymerization were detected when plotting weight distribution function scaled to conversion *vs* molecular weight indicating that the reaction was not a true living radical polymerization. In the second example, we performed cyclization of heterodifunctional PSTY through ring-closure method and used LND simulation to determine the purity of the obtained polymer. Gaussian fit showed that there was no detectable linear polymer left after cyclization.

Additionally, all the polymer species in the resulting crude product consisting of monocyclic PSTY and multiblocks were quantified.

7.3. Characterization of Hetero-Block Copolymers by the Log-Normal Distribution Model

The derivation of MWDs coupled with LND simulation shown in Chapter 2 demonstrated the usefulness of these methods for polymer characterization. However, often mixtures consisting of two or more different polymers are used in polymer science. Such mixtures contain polymers with different d*n*/d*c* values and, therefore, traditional SEC analysis will result in incorrect results as RI-SEC response is d*n*/d*c* dependent. In this chapter this dependence was taken into account in a modified LND simulation, and the method was tested on mixtures of heteropolymers with known concentrations. PSTY, PNIPAM, P*t*-BA and PEG were used as model polymers because they have significantly different d*n*/d*c* values. Weight fractions (w_p) determined by LND fit gave an excellent match with true weight fractions. w_ps were calculated from d*n*/d*c* values taken from literature and apparent weight fractions of polymers obtained via unmodified LND simulation. Gaussian simulation was further used to determine the efficiencies of 'click' reactions for diblock heteropolymers. It was shown that if d*n*/d*c* is not taken into consideration 'click' efficiency can be considerably over- or underestimated.

7.4. SET-LRP of NIPAM in Water via in situ Reduction of Cu(II) to Cu(0) with $NaBH_4$

In this chapter we introduced a new catalyst for the aqueous SET-LRP of NIPAM. The catalyst was made through reduction of $CuBr_2$/Me_6TREN complex with $NaBH_4$. The reduction is quantitative and, as was shown by UV-vis, does not produce any detectable Cu(I) species, therefore, the polymerization can be considered as a SET-LRP. In addition, no Cu(I) species were detected after the polymerizations were complete indicating that, at the chosen reaction conditions, no comproportionation occurs, supporting a SET-LRP pathway. The polymerizations were well-controlled and for the optimized conditions, resulted in polymers with low dispersity (Đ<1.1). Additionally, control over the polymerization rate was achieved by varying the $CuBr_2$/Me_6TREN to $NaBH_4$ ratio. Polymers of varying degrees of polymerization (DP) were successfully synthesized demonstrating the versatility of the catalytic system (DP = 20-50). End-group functionality (EGF) studies were performed by capping terminal bromide with thiophenol, in the presence of TEA, and characterized by MALDI-ToF spectrometry. It was found when less reducing agent is used EGF

remains near 100%, even for full monomer conversion. Although, for higher amounts of $NaBH_4$ EGF can decrease to ca. 90%, this is a common result for a copper-mediated LRP and, therefore, the proposed catalytic system can be used when control over polymerization rate is required.

7.5. Quantitative End-Group Functionalization of PNIPAM from Aqueous SET-LRP via in situ Reduction of Cu(II) with $NaBH_4$

Terminal halides on polymers made via copper mediated LRP are frequently used for 'click' reactions by converting them into an azide and carrying out CuAAC. However, purification of PNIPAM-Br obtained by aqueous SET-LRP resulted in loss of terminal bromide due to hydrolysis. In this chapter we studied the hydrolysis rate of the bromide chain end and found that it is a relatively slow process and takes approximately 20 h to complete. We attempted to do in situ azidation by adding NaN_3 directly to the reaction media after SET-LRP completion and found that the azidation rate was much higher than that of hydrolysis. MALDI-ToF analysis showed that azidation was complete within 30s and EGF reaches 85-95% depending on SET-LRP conditions. This was an unexpected result as azidation reactions are conventionally considered as a slow process that takes over 10-20 h in organic solvents. However, MALDI-ToF cannot be used for precise EGF quantification and so 'click' chemistry was used as an alternative. The polymers were recovered after SET-LRP using dialysis and freeze-drying and further used in CuAAC with PNIPAM-≡ in DMF at 25°. The coupling efficiencies were determined using LND simulation and the results were quite exceptional: more than 97% of almost all azides reacted indicating extremely high EGF. Therefore, in situ azidation of PNIPAM made via aqueous SET-LRP can be used to produce highly functional PNIPAM-N_3 in a one pot reaction.

7.6. Synthesis of Densely Packed Multicyclic Polystyrene

At the final stage of this thesis we studied the properties of densely packed multicyclic polystyrene. Increased density of the multicyclic PSTY was caused by closely situated linking functionalities. The polymer was synthesized using ATRP and CuAAC via two synthetic approaches. In the first approach, individual multicyclic c-$PSTY_i$-OH species with *i* cyclic blocks (*i* = 1-5) were m by sequential addition of cyclic units. All polymer species were highly pure according to LND simulation. In addition, these polymers demonstrated considerable contraction of hydrodynamic volume ($V_{h,cyc}$) upon addition of successive cyclic units compared to linear analogues of the same mass ($V_{h,abs}$). The ratio $V_{h,cyc}/V_{h,abs}$ decreased from 0.63 for c-PSTY-OH to 0.49 for c-$PSTY_5$-OH. Due to multiple synthetic steps we were unable to add more cyclic units, thus, a feeding approach was employed where difunctional c-PSTY(≡)N_3 was slowly fed into a solution of

c-PSTY-N_3. This resulted in condensation polymerization of cyclic macromonomer c-PSTY(≡)N_3 in which c-PSTY-N_3 acted as an initiator. LND simulation showed that oligomers consisting of up to 60 cyclic units were presented in the crude product. It was also found that the ratio $V_{h,cyc}/V_{h,abs}$ kept decreasing and reached a plateau of 0.25 at i = 12. This was still higher than the hydrodynamic volume of a linear analogue at theta conditions suggesting that the polymer coil behaviour of our multicyclic architectures lies in between a typical behaviour in a good solvent and at theta conditions. The relaxation of polymer backbone must be responsible for the plateau of $V_{h,cyc}/V_{h,abs}$ function. Finally, the properties of the multicyclic PSTY at theta conditions were studied via DSC. Interestingly, glass transition temperature of all multicyclic polymers with i>1 was higher than that of linear and monocyclic polymer. This was caused by the loss of conformational entropy caused by introduced topological constraints.

Appendix A

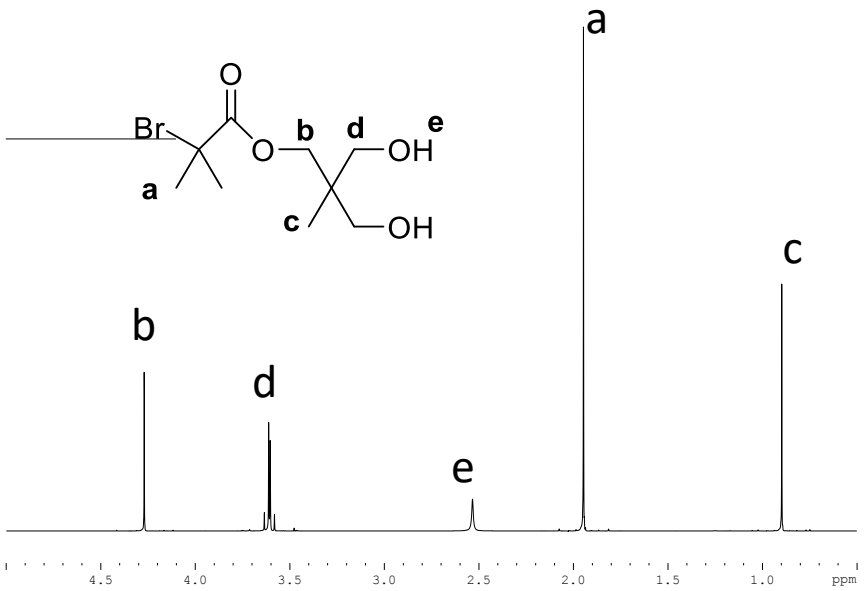

Figure A4.1. ^{1}H NMR of **11** at 298K (500 MHz), recorded in $CDCl_3$.

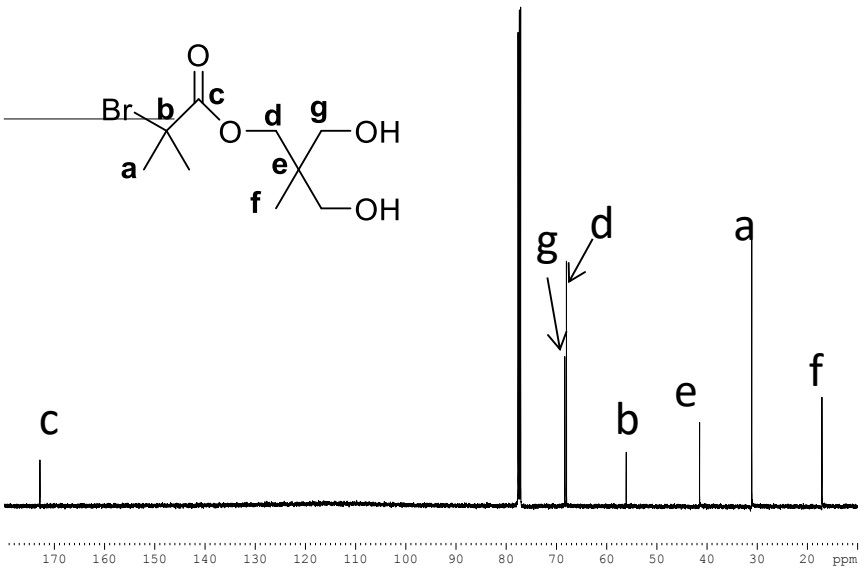

Figure A4.2. ^{13}C NMR of **11** at 298K (500 MHz), recorded in $CDCl_3$.

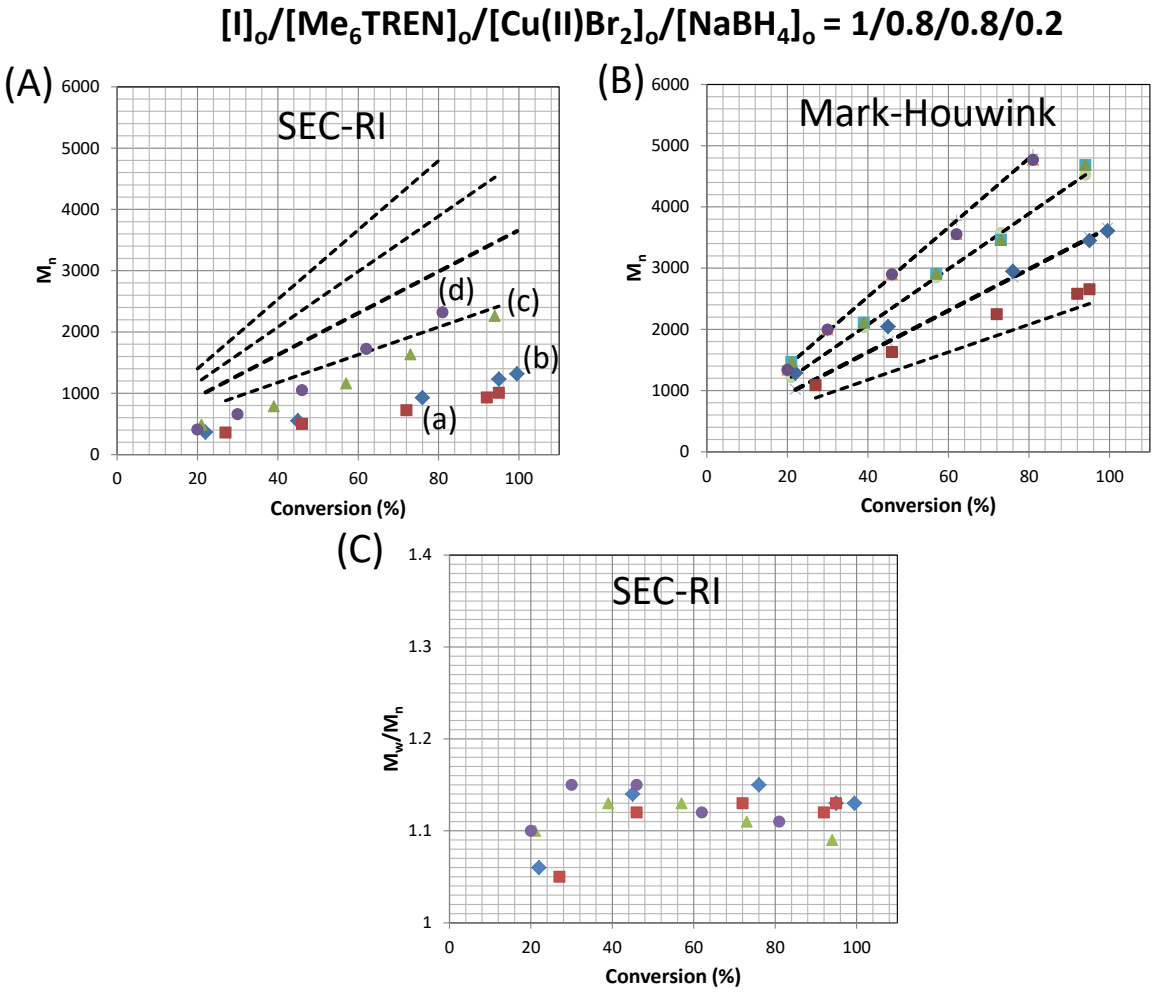

Figure A4.3. Aqueous SET-LRP of NIPAM catalyzed by the in situ generation of Cu(0) from $NaBH_4$ by varying $[NIPAM]_0/[I]_0$ from (a) 20/1 ■, (b) 30/1 ♦ , (c) 40/1 ▲, (d) 50/1 ●. (A) M_n determined from SEC using RI and polystyrene standards (dashed lines represent theoretical M_n values. (B) M_n calculated using Mark-Houwink equation and (C) M_w/M_n values from SEC. Reaction conditions: $[I]_0/[Me_6TREN]_0/[Cu(II)Br_2]_0/[NaBH_4]_0$ = 1/0.8/0.8/0.2. [I] = 0.0267 M in 3.48 mL of water.

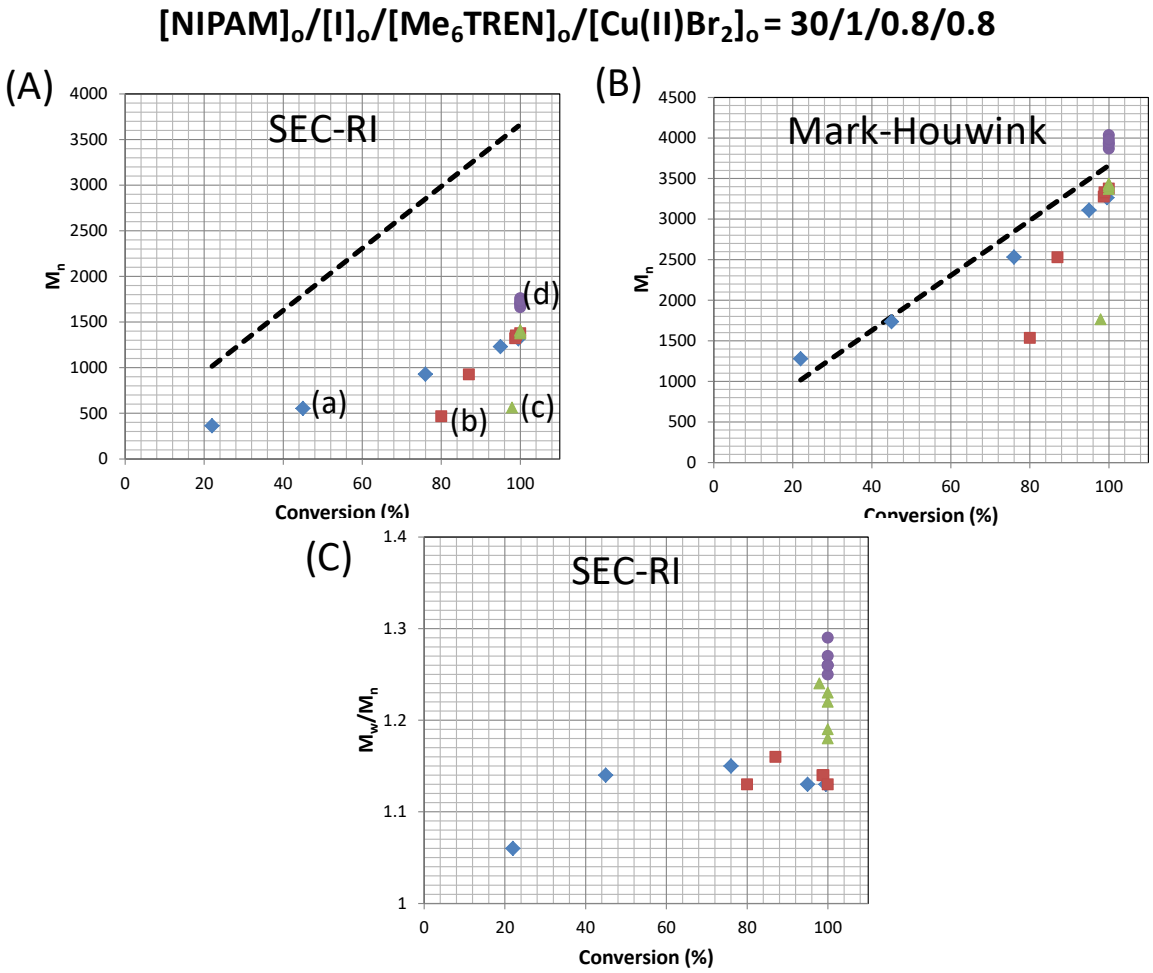

Figure A4.4. Aqueous SET-LRP of NIPAM catalyzed by the in situ generation of Cu(0) from $NaBH_4$ at $[NIPAM]_0/[I]_0$ = 30 and varying $[CuBr_2]_0/[NaBH_4]_0$ from (a) 0.8/0.2 ♦, (b) 0.8/0.4 ■, (c) 0.8/0.6 ▲, (d) 0.8/0.8 ●. (A) M_n determined from SEC using RI and polystyrene standards (dashed lines represent theoretical M_n values, (B) M_n calculated using Mark-Houwink equation and (C) M_w/M_n values from SEC. Reaction conditions: $[NIPAM]_0/[I]_0/[Me_6TREN]_0/[Cu(II)Br_2]_0$ = 30/1/0.8/0.8. [I] = 0.0267 M in 3.48 mL of water.

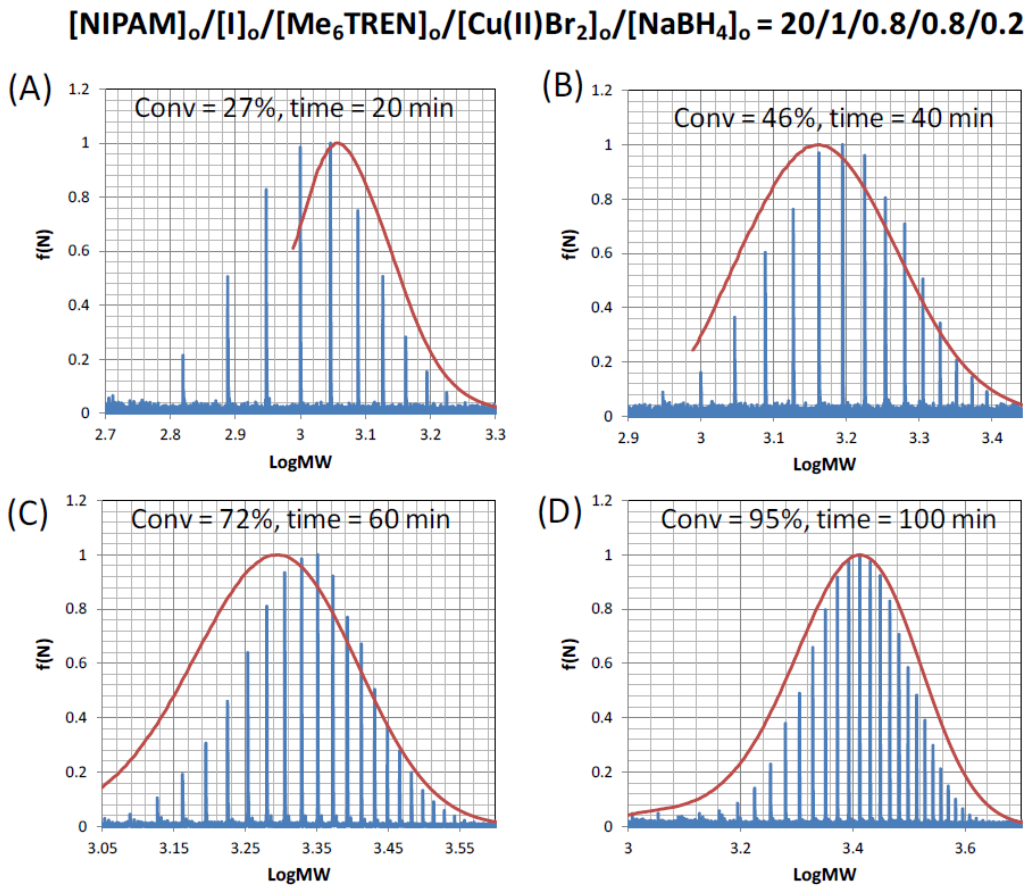

Figure A4.5. MALDI-ToF and SEC (RI using polystyrene standards, red line) for the aqueous SET-LRP of NIPAM over the conversion range. Reaction conditions: $[NIPAM]_0/[I]_0/[Me_6TREN]_0/[Cu(II)Br_2]_0/[NaBH_4]_0$ = 20/1/0.8/0.8/0.2. [I] = 0.0267 M in 3.48 mL of water.

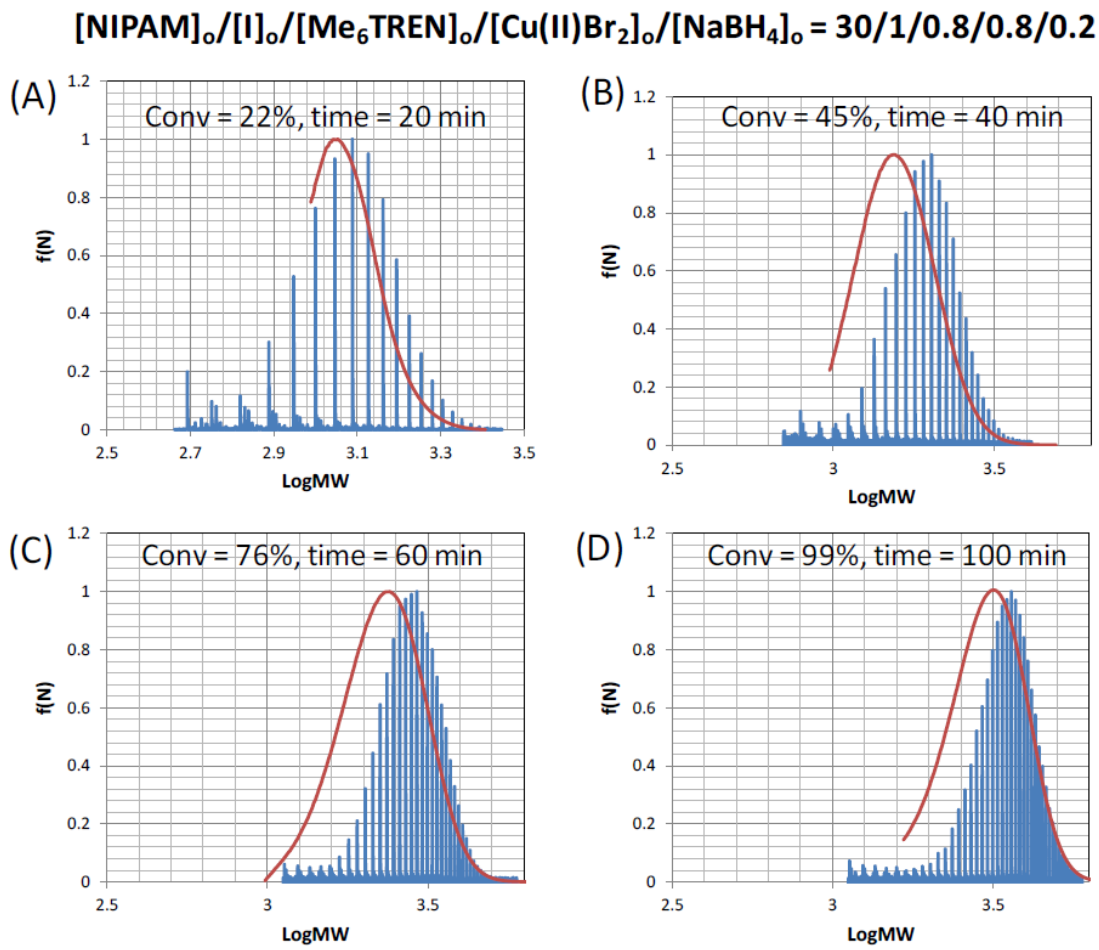

Figure A4.6. MALDI-ToF and SEC (RI using polystyrene standards, red line) for the aqueous SET-LRP of NIPAM over the conversion range. Reaction conditions: $[NIPAM]_0/[I]_0/[Me_6TREN]_0/[Cu(II)Br_2]_0/[NaBH_4]_0$ = 30/1/0.8/0.8/0.2. [I]=0.0267 M in 3.48 mL of water.

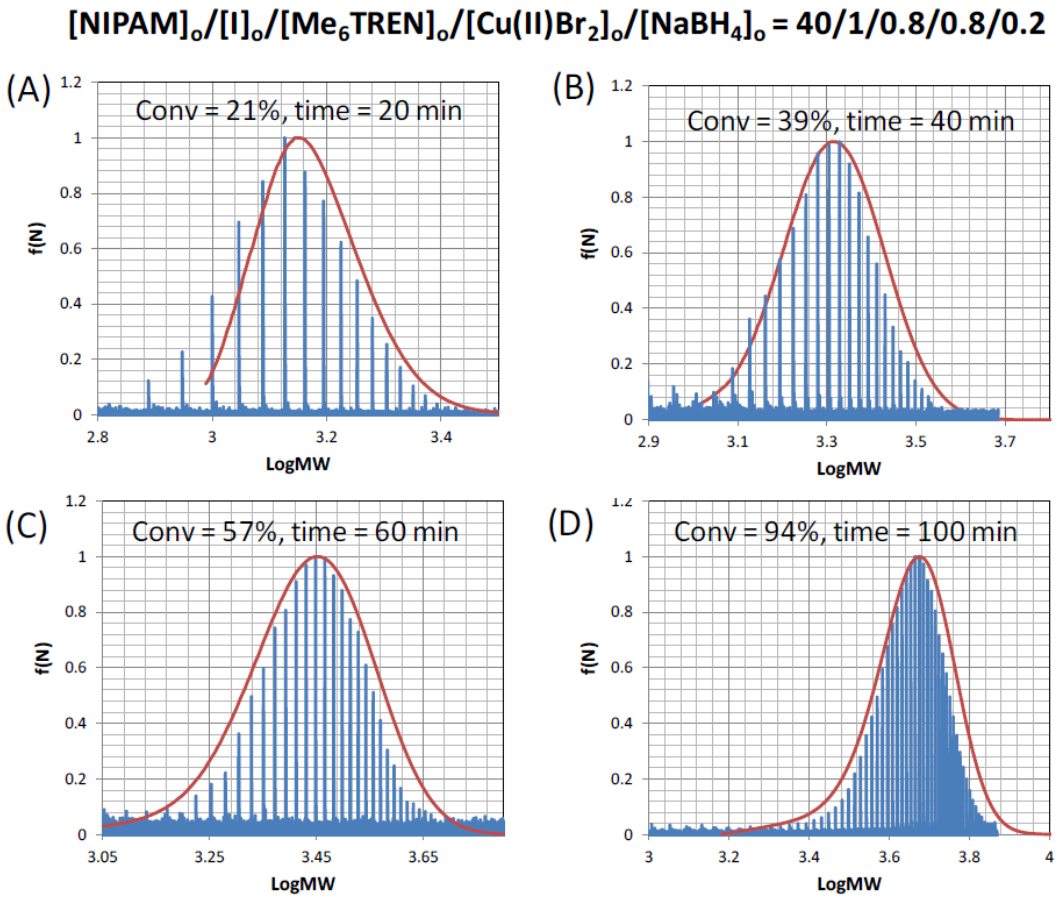

Figure A4.7. MALDI-ToF and SEC (RI using polystyrene standards, red line) for the aqueous SET-LRP of NIPAM over the conversion range. Reaction conditions: $[NIPAM]_0/[I]_0/[Me_6TREN]_0/[Cu(II)Br_2]_0/[NaBH_4]_0$ = 40/1/0.8/0.8/0.2. [I]=0.0267 M in 3.48 mL of water.

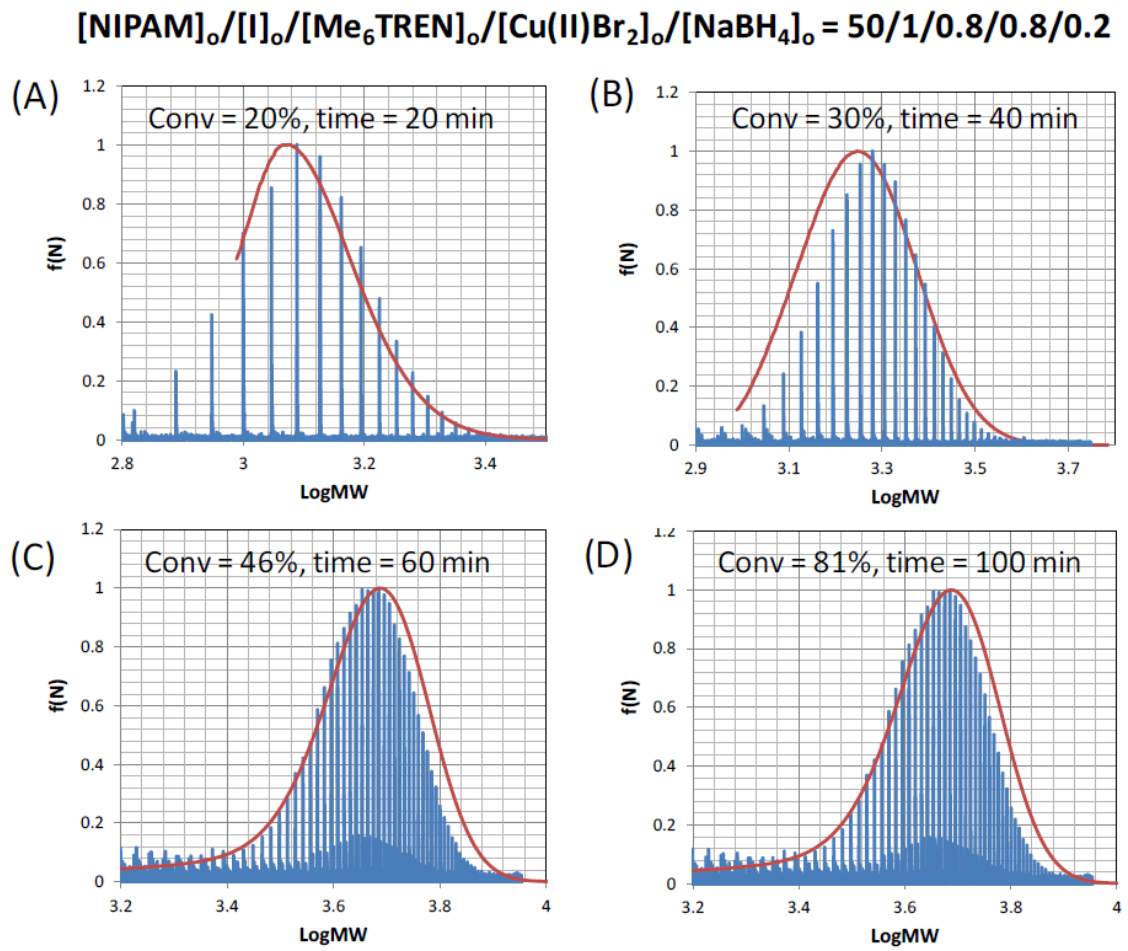

Figure A4.8. MALDI-ToF and SEC (RI using polystyrene standards, red line) for the aqueous SET-LRP of NIPAM over the conversion range. Reaction conditions: $[NIPAM]_0/[I]_0/[Me_6TREN]_0/[Cu(II)Br_2]_0/[NaBH_4]_0$ = 50/1/0.8/0.8/0.2. [I]=0.0267 M in 3.48 mL of water.

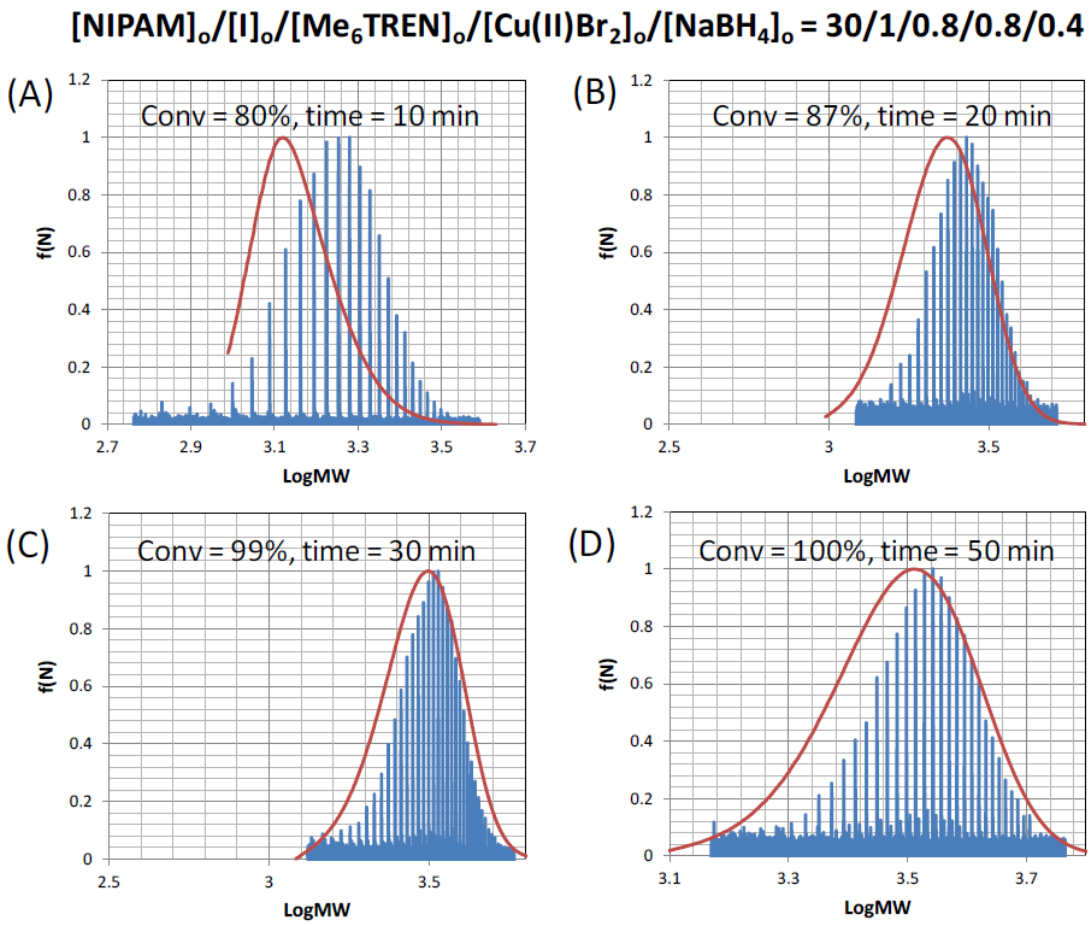

Figure A4.9. MALDI-ToF and SEC (RI using polystyrene standards, red line) for the aqueous SET-LRP of NIPAM over the conversion range. Reaction conditions: $[NIPAM]_0/[I]_0/[Me_6TREN]_0/[Cu(II)Br_2]_0/[NaBH_4]_0$ = 30/1/0.8/0.8/0.4. [I]=0.0267 M in 3.48 mL of water.

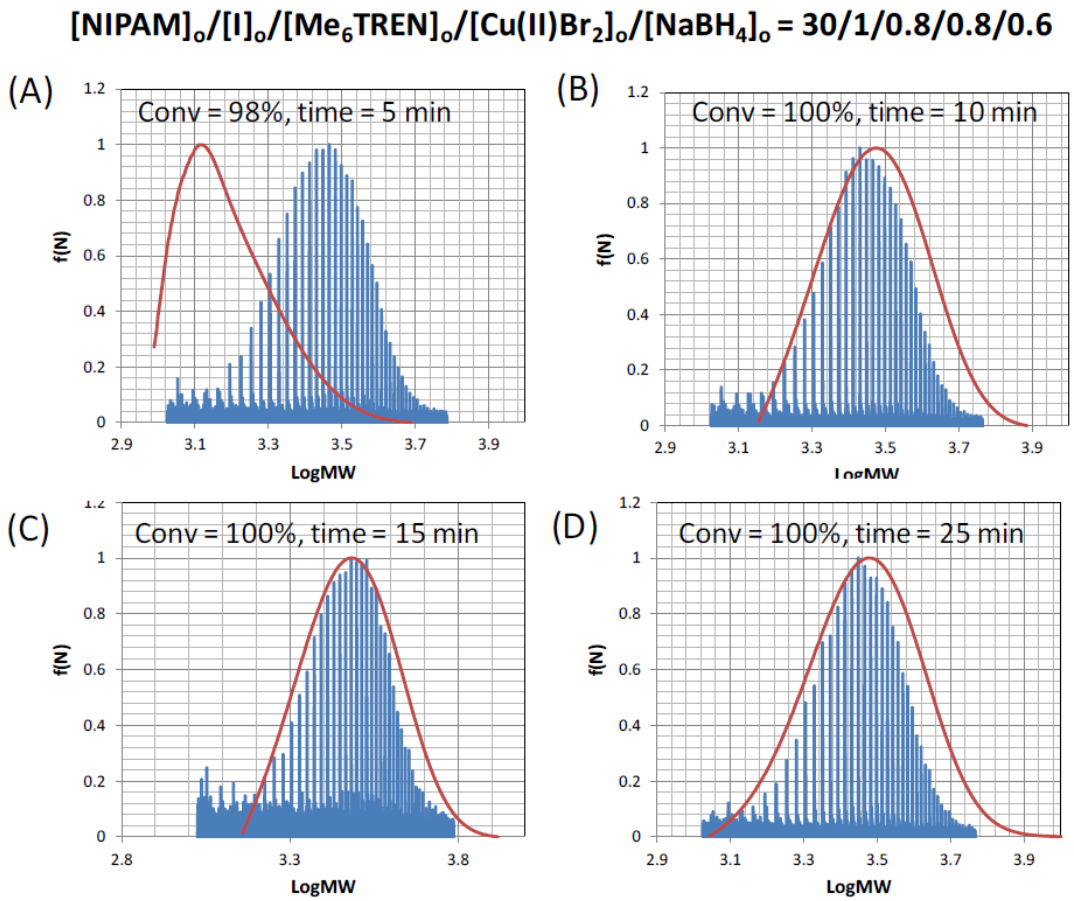

Figure A4.10. MALDI-ToF and SEC (RI using polystyrene standards, red line) for the aqueous SET-LRP of NIPAM over the conversion range. Reaction conditions: $[NIPAM]_0/[I]_0/[Me_6TREN]_0/[Cu(II)Br_2]_0/[NaBH_4]_0$ = 30/1/0.8/0.8/0.6. [I]=0.0267 M in 3.48 mL of water.

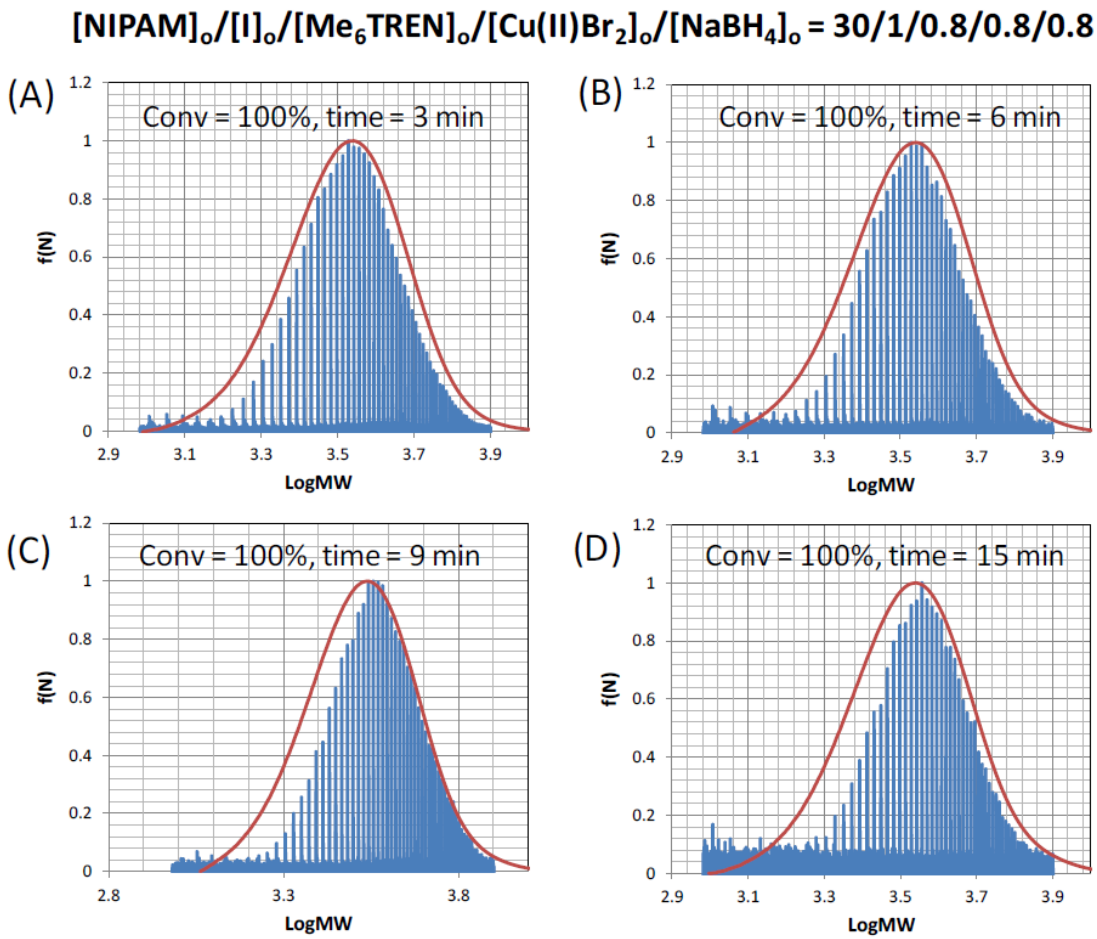

Figure A4.11. MALDI-ToF and SEC (RI using polystyrene standards, red line) for the aqueous SET-LRP of NIPAM over the conversion range. Reaction conditions: $[NIPAM]_0/[I]_0/[Me_6TREN]_0/[Cu(II)Br_2]_0/[NaBH_4]_0$ = 30/1/0.8/0.8/0.8. [I]=0.0267 M in 3.48 mL of water.

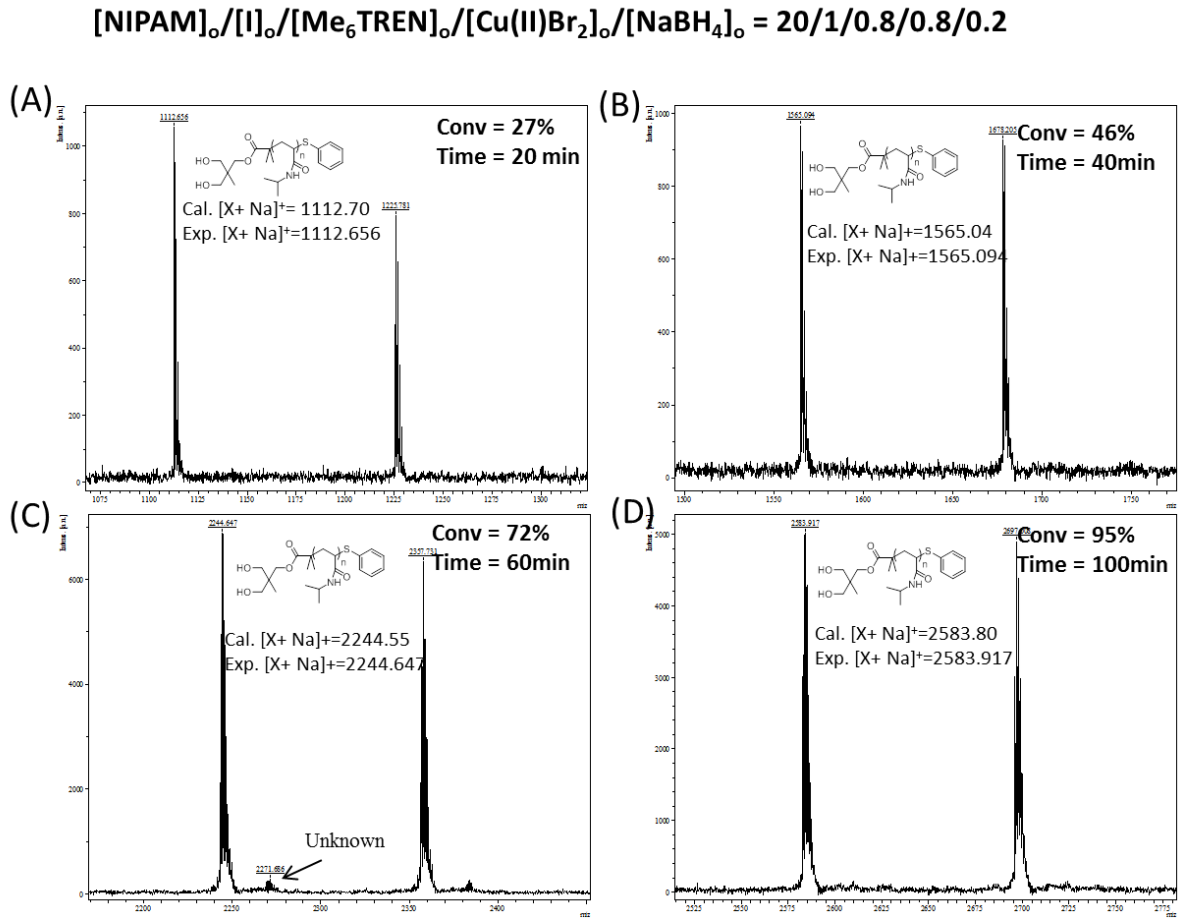

Figure A4.12. MALDI-ToF for the aqueous SET-LRP of NIPAM over the conversion range. Reaction conditions: $[NIPAM]_0/[I]_0/[Me_6TREN]_0/[Cu(II)Br_2]_0/[NaBH_4]_0$ = 20/1/0.8/0.8/0.2. [I]=0.0267 M in 3.48 mL of water.

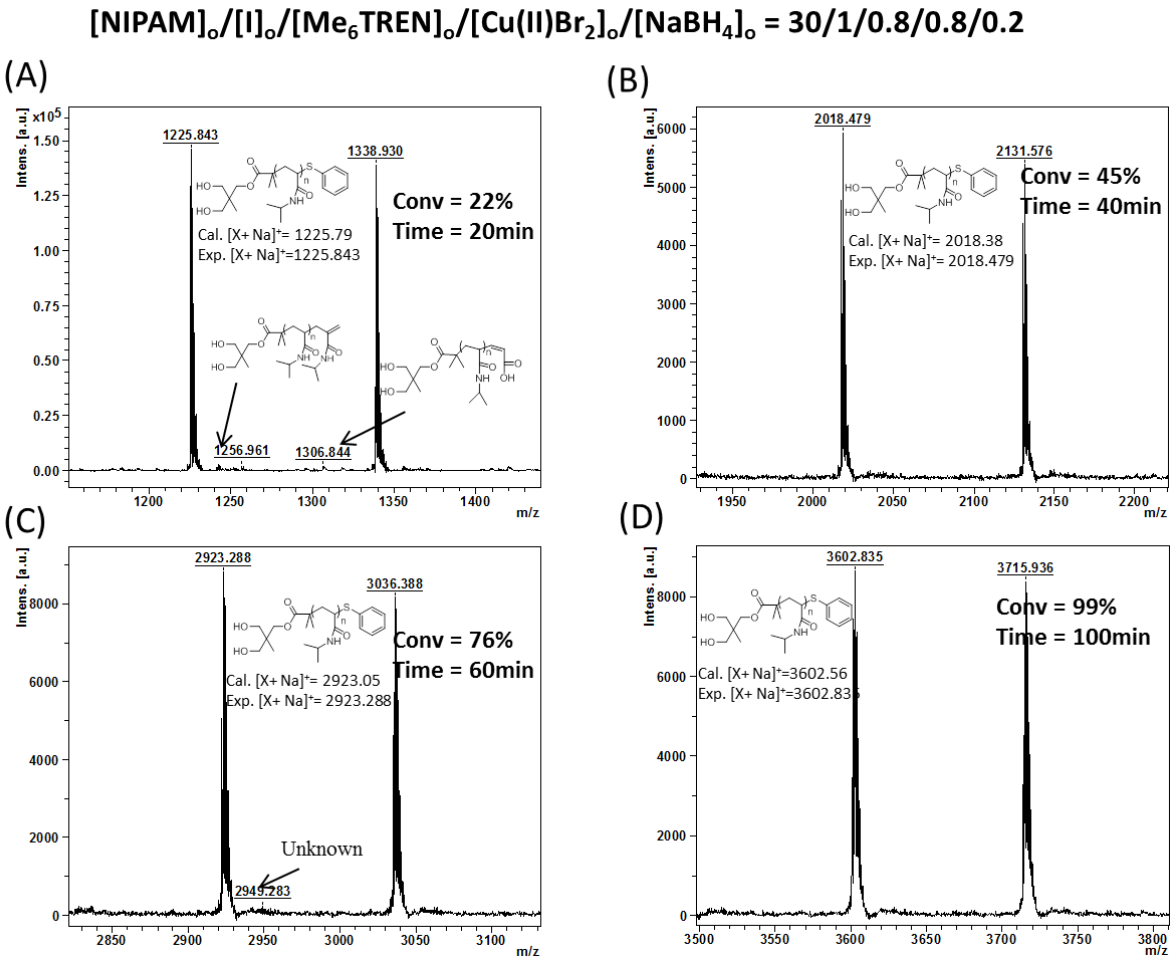

Figure A4.13. MALDI-ToF for the aqueous SET-LRP of NIPAM over the conversion range. Reaction conditions: $[NIPAM]_0/[I]_0/[Me_6TREN]_0/[Cu(II)Br_2]_0/[NaBH_4]_0$ = 30/1/0.8/0.8/0.2. [I]=0.0267 M in 3.48 mL of water.

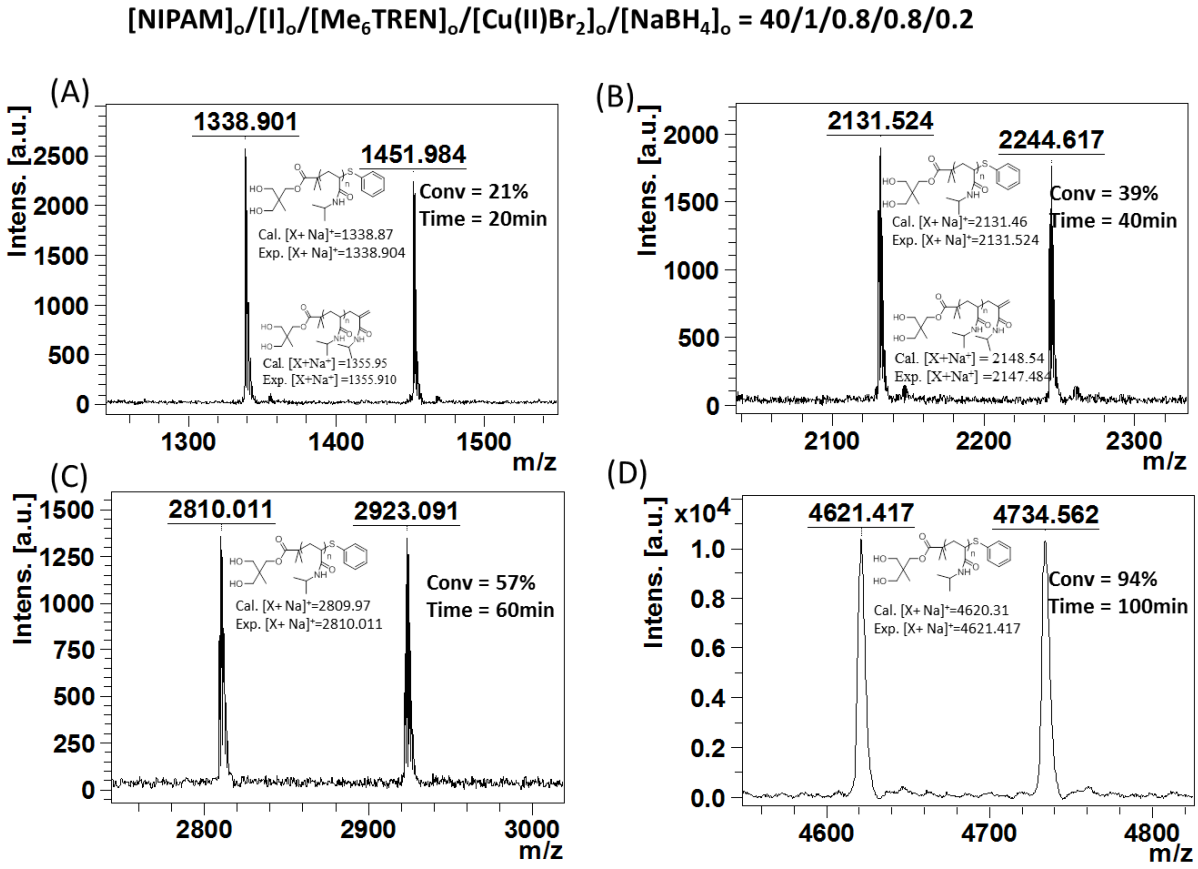

Figure A4.14. MALDI-ToF for the aqueous SET-LRP of NIPAM over the conversion range. Reaction conditions: $[NIPAM]_0/[I]_0/[Me_6TREN]_0/[Cu(II)Br_2]_0/[NaBH_4]_0$ = 40/1/0.8/0.8/0.2. [I]=0.0267 M in 3.48 mL of water.

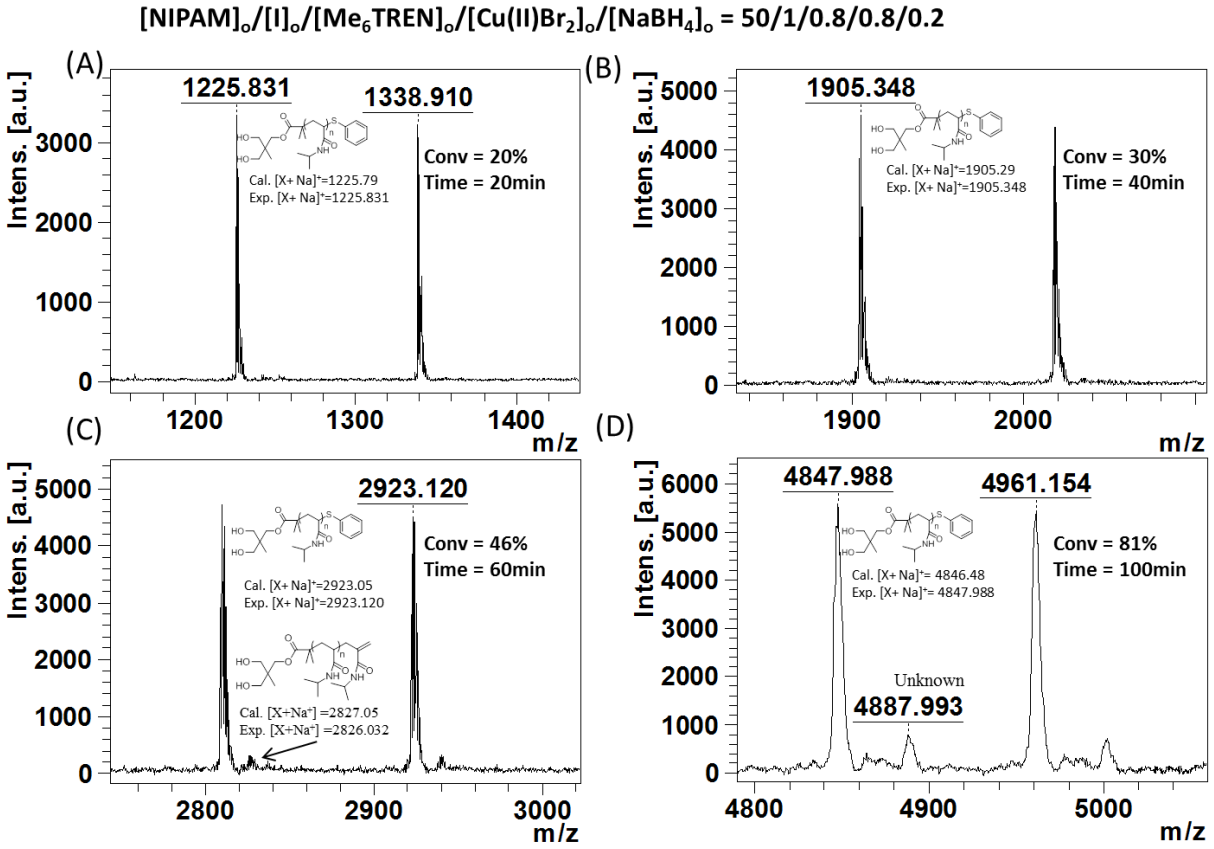

Figure A4.15. MALDI-ToF for the aqueous SET-LRP of NIPAM over the conversion range. Reaction conditions: $[NIPAM]_0/[I]_0/[Me_6TREN]_0/[Cu(II)Br_2]_0/[NaBH_4]_0$ = 50/1/0.8/0.8/0.2. [I]=0.0267 M in 3.48 mL of water.

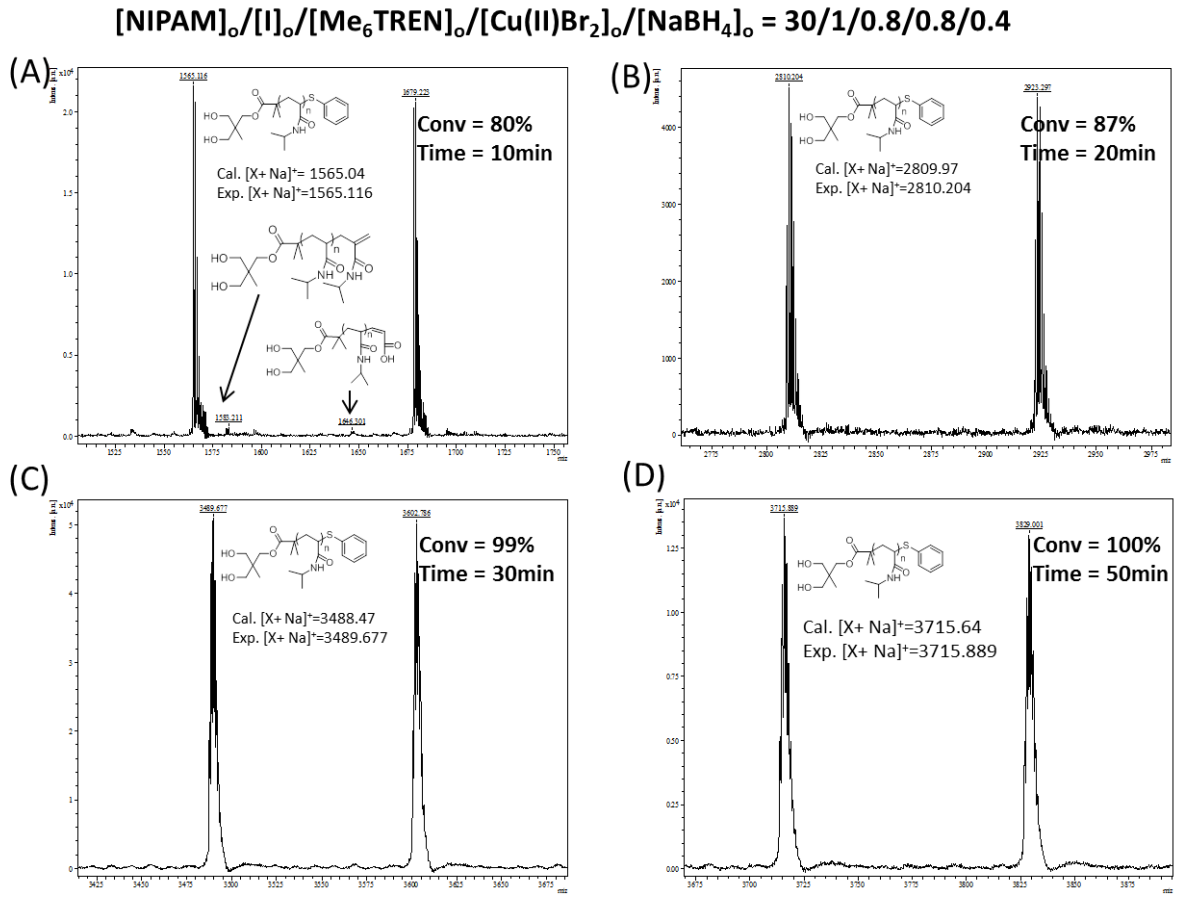

Figure A4.16. MALDI-ToF for the aqueous SET-LRP of NIPAM over the conversion range. Reaction conditions: $[NIPAM]_0/[I]_0/[Me_6TREN]_0/[Cu(II)Br_2]_0/[NaBH_4]_0$ = 30/1/0.8/0.8/0.4. [I]=0.0267 M in 3.48 mL of water.

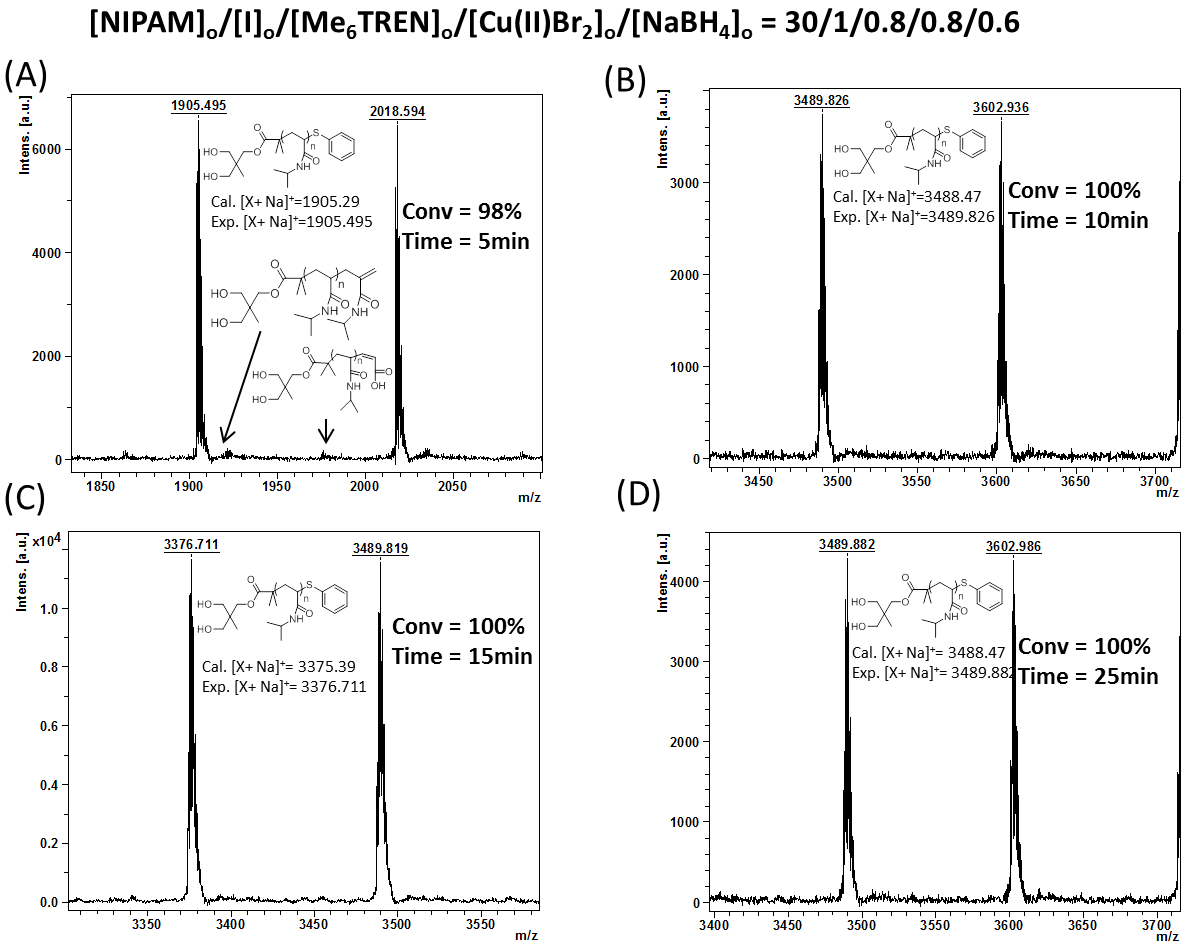

Figure A4.17. MALDI-ToF for the aqueous SET-LRP of NIPAM over the conversion range. Reaction conditions: $[NIPAM]_0/[I]_0/[Me_6TREN]_0/[Cu(II)Br_2]_0/[NaBH_4]_0$ = 30/1/0.8/0.8/0.6. [I]=0.0267 M in 3.48 mL of water.

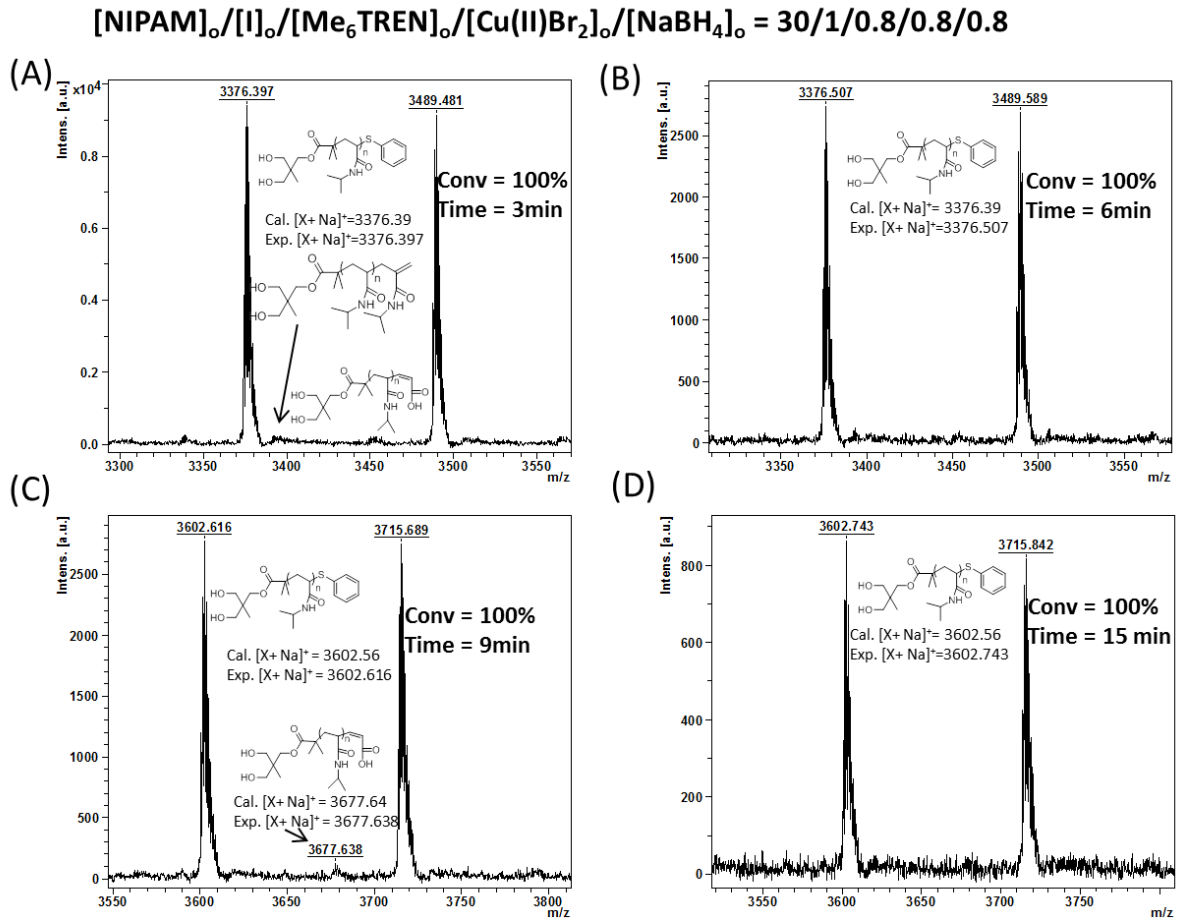

Figure A4.18. MALDI-ToF for the aqueous SET-LRP of NIPAM over the conversion range. Reaction conditions: $[NIPAM]_0/[I]_0/[Me_6TREN]_0/[Cu(II)Br_2]_0/[NaBH_4]_0$ = 30/1/0.8/0.8/0.8. [I] = 0.0267 M in 3.48 mL of water.

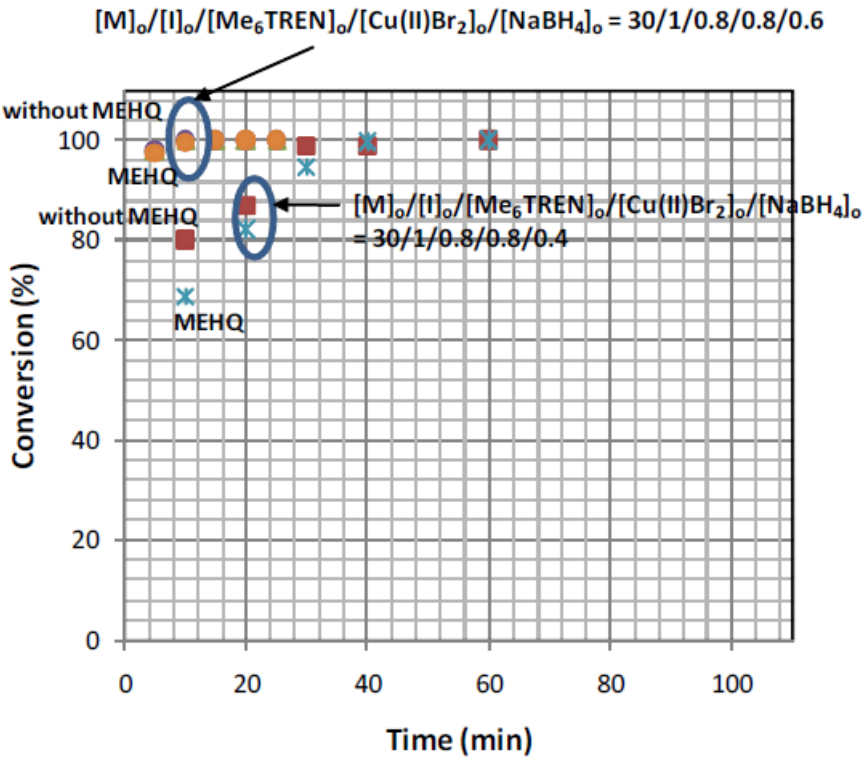

Figure A4.19. Aqueous SET-LRP of NIPAM catalyzed by the in situ generation of Cu(0) from $NaBH_4$ at $[NIPAM]_0/[I]_0$ = 30 in the absence and presence of inhibitor MEHQ added to the polymerization mixture after sampling, and varying $[CuBr_2]_0/[NaBH_4]_0$ from (a) 0.8/0.6 ● without MEHQ, (b) 0.8/0.6 ● with MEHQ, (c) 0.8/0.4 ■ without MEHQ, (d) 0.8/0.4 *. Reaction conditions: $[NIPAM]_0/[I]_0/[Me_6TREN]_0/[Cu(II)Br_2]_0$ = 30/1/0.8/0.8. [I] = 0.0267 M in 3.48 mL of water.

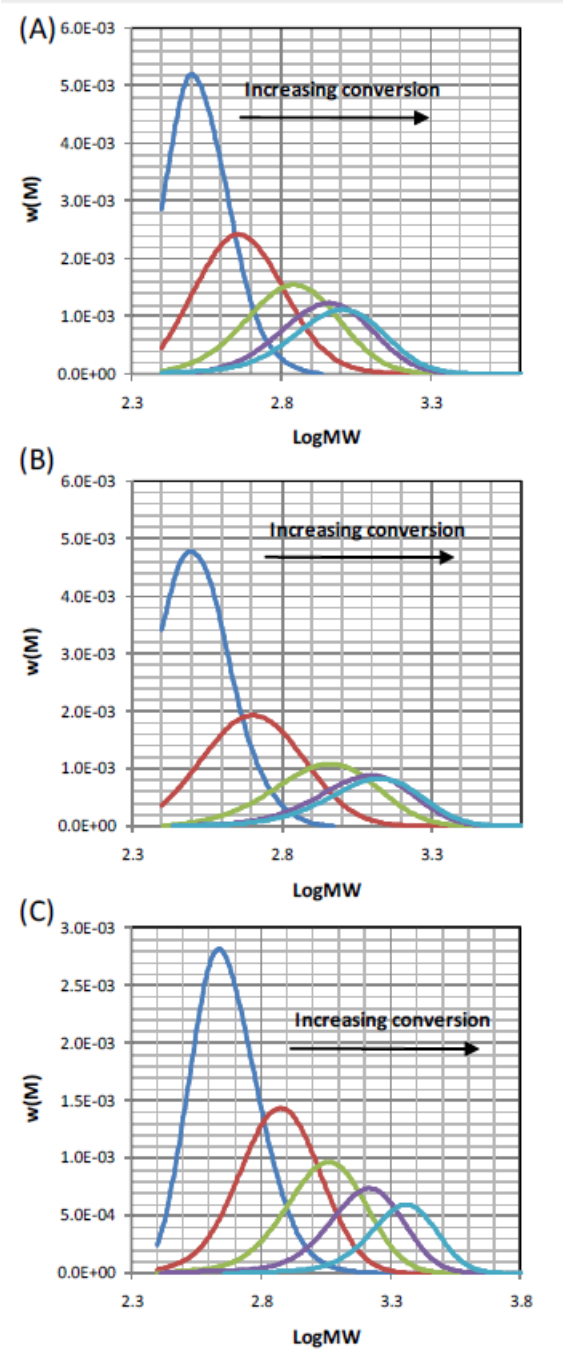

Figure A4.20. SEC chromatograms from aqueous SET-LRP of NIPAM catalyzed by the in situ generation of Cu(0) from $NaBH_4$ by varying $[NIPAM]_0/[I]_0$ from (A) 20/1 , (B) 30/1 , and (C) 40/1. Reaction conditions: $[I]_0/[Me_6TREN]_0/[Cu(II)Br_2]_0/[NaBH_4]_0$ = 1/0.8/0.8/0.2. [I] = 0.0267 M in 3.48 mL of water. These SEC chromatograms are based on a polystyrene calibration curve and have not been adjusted using the Mark-Houwink parameters.

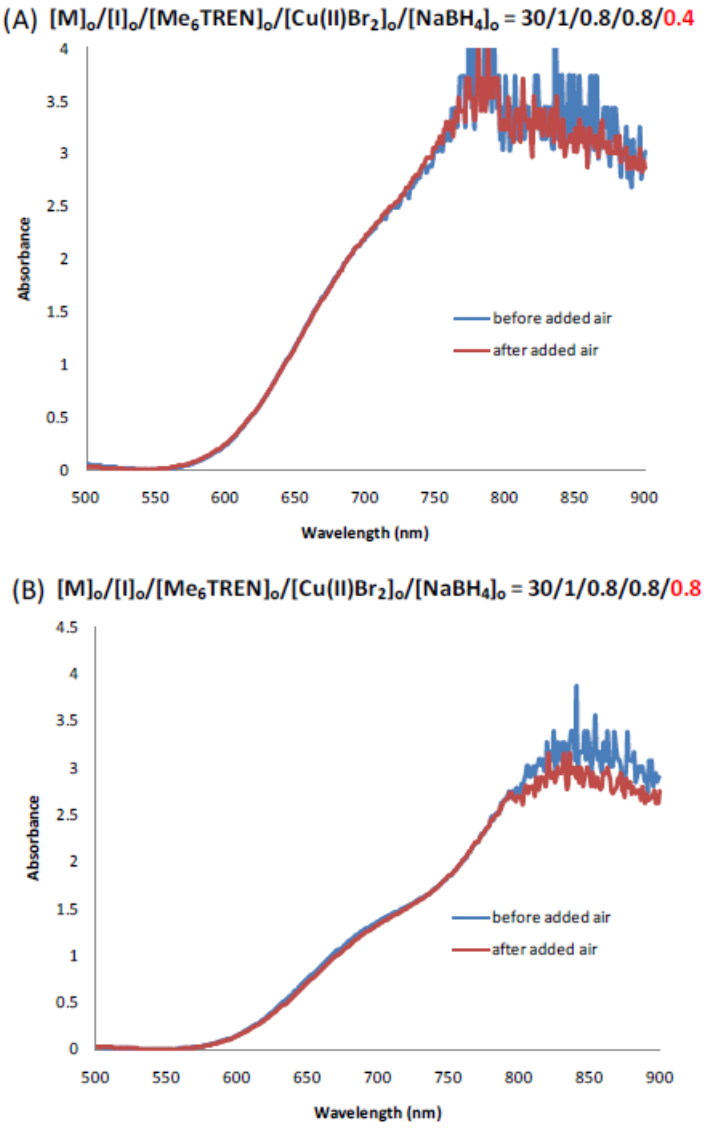

Figure A4.21. UV-vis spectra (measured in the 500-900 nm range) at the end of the aqueous SET-LRP of NIPAM polymerization before and after opening and bubbling with air for 1 min. (A) $[M]_0/[I]_0/[Me_6TREN]_0/[Cu(II)Br_2]_0/[NaBH_4]_0$ = 30/1/0.8/0.8/0.4, and (B) $[M]_0/[I]_0/[Me_6TREN]_0/[Cu(II)Br_2]_0/[NaBH_4]_0$ = 30/1/0.8/0.8/0.8. Reaction conditions: $[I]_0/[Me_6TREN]_0/[Cu(II)Br_2]_0/[NaBH_4]_0$ = 1/0.8/0.8/0.2. [I] = 0.0267 M in 3.48 mL of water.

Appendix B

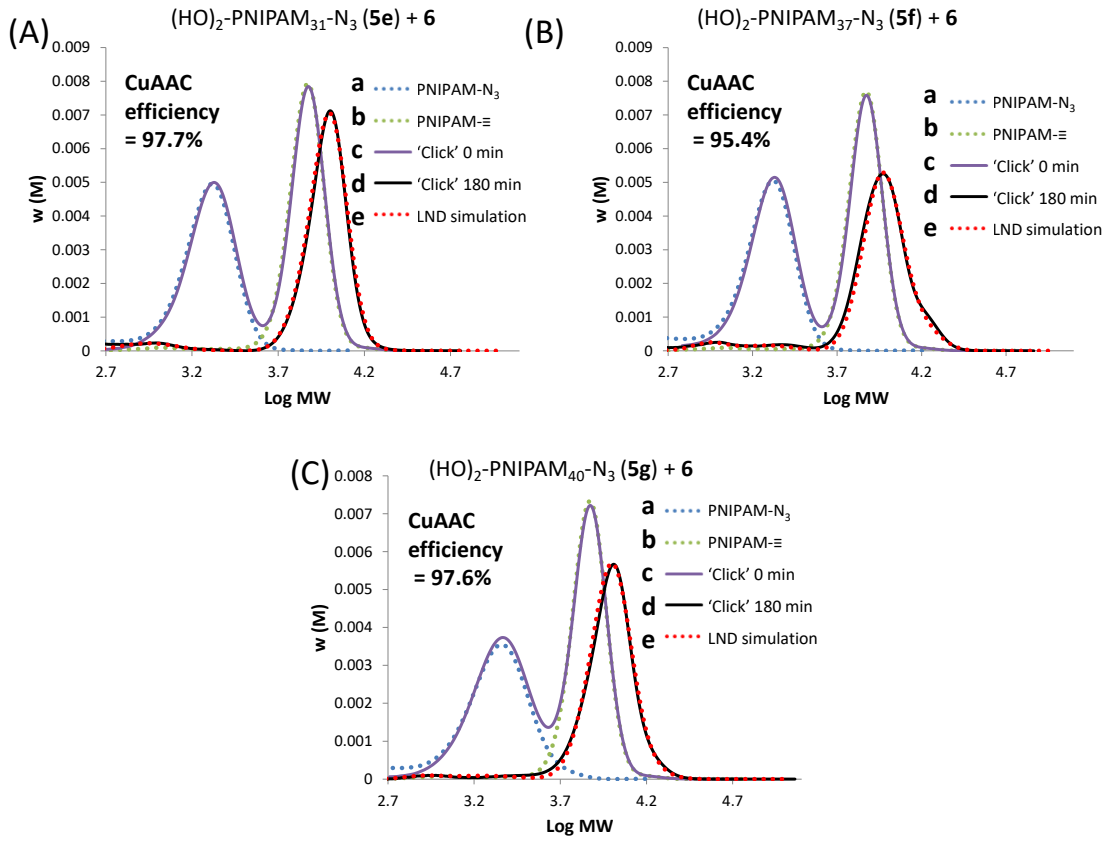

Figure A5.1. Size exclusion chromatograms for the CuAAC 'click' reaction between **5** and **6**. (A) Polymer **5e** + **6**, (B) Polymer **5f** + **6**, (C) Polymer **5g** + **6**. Curves (a) **5**, (b) **6**, (c) at time = 0 min for CuAAC, (d) at time = 180 min for CuAAC, and (e) LND model simulation of curve d.

Table A5.1. Weight fractions of components after the CuAAC reaction determined by LND model simulation of SEC curves.

CuAAC	PNIPAM-N_3 (**5**), %	PNIPAM-≡ (**6**), %	PNIPAM-PNIPAM (**7**), %	Alk-Alk coupling (**8**), %	Unknown 1, %	Unknown 2, %
6+**5a**	0.14	8.59	65.67	25.60		
6+**5b**	0.00	10.77	67.97	21.26		
6+**5c**	0.38	13.13	70.93	15.56		
6+**5d**	0.64	10.70	71.92	16.73		
6+**5e**	0.00	15.66	82.77	1.12	0.00	0.45
6+**5f**	0.53	5.01	80.18	13.78	0.25	0.25
6+**5g**	0.25	12.77	80.53	6.14	0.25	0.07

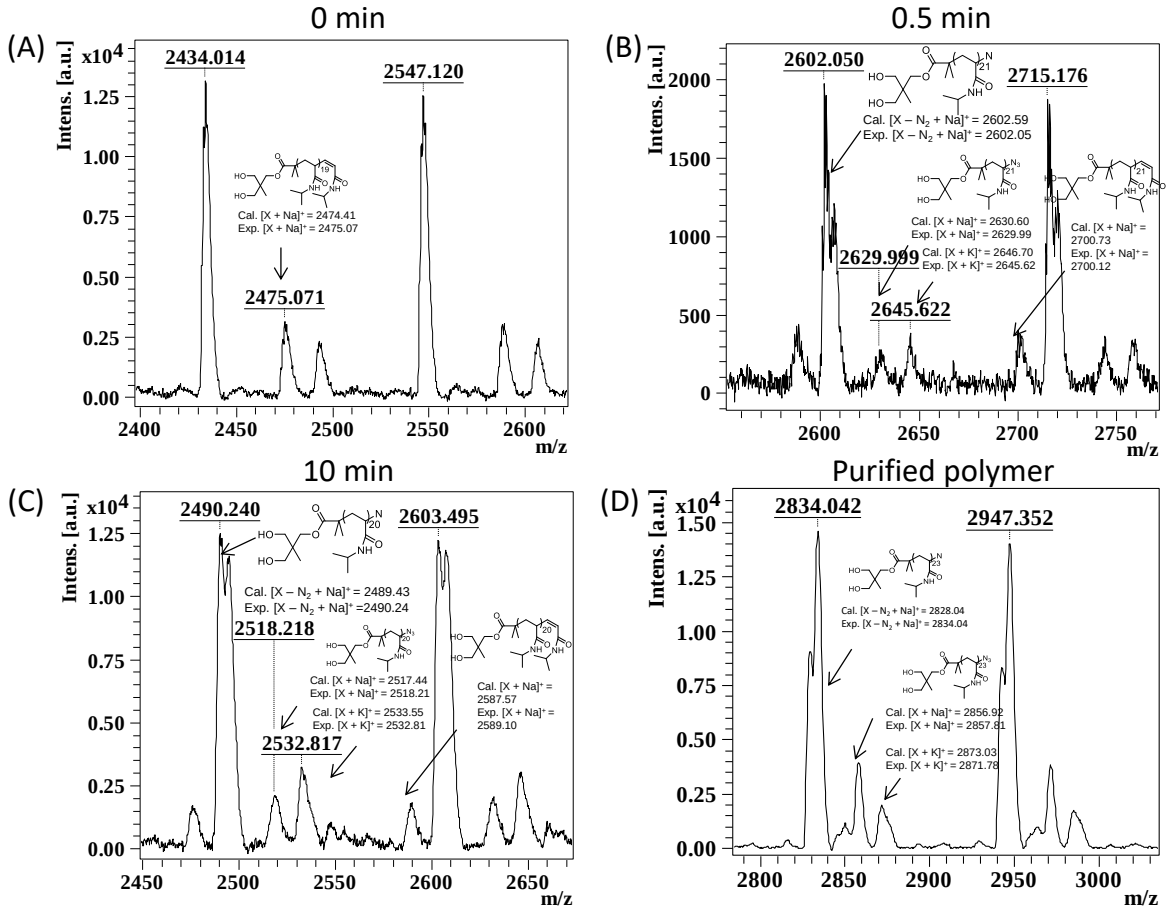

Figure A5.2. Kinetics of in situ azidation of $(HO)_2$-PNIPAM$_n$-Br (**2a**) after 120 min of aqueous SET-LRP at 0°C. MALDI-ToF spectra of (A) at 0 min, (B) 0.5 min, (C) 10min and (D) of purified **5a**.

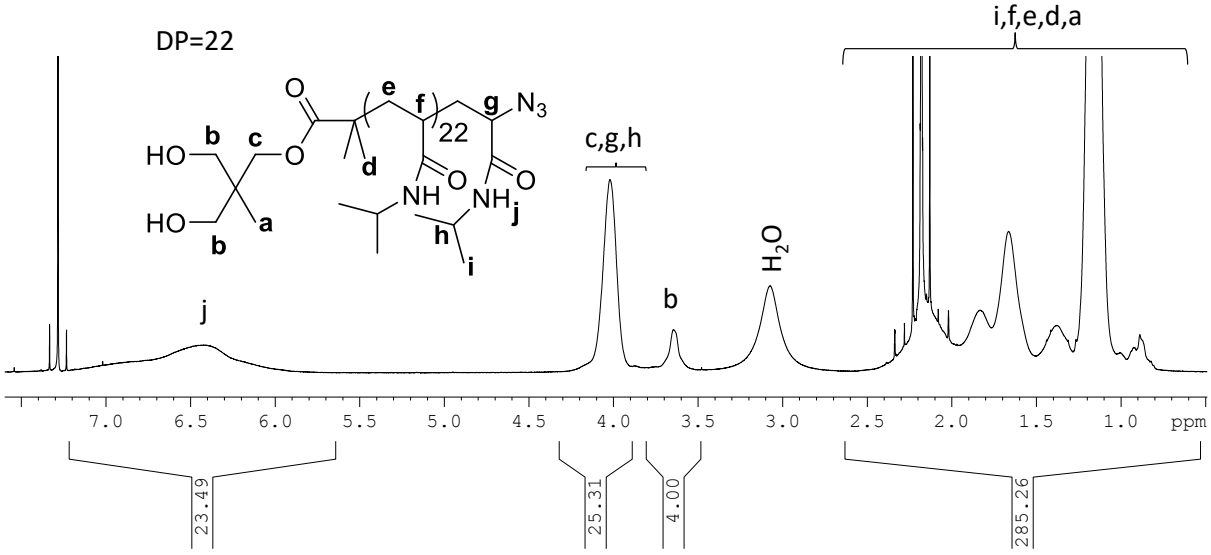

Figure A5.3. ^{1}H NMR spectrum of $(HO)_2$-PNIPAM$_{22}$-N$_3$ (**5a**) recorded in $CDCl_3$ at 298K (400 MHz).

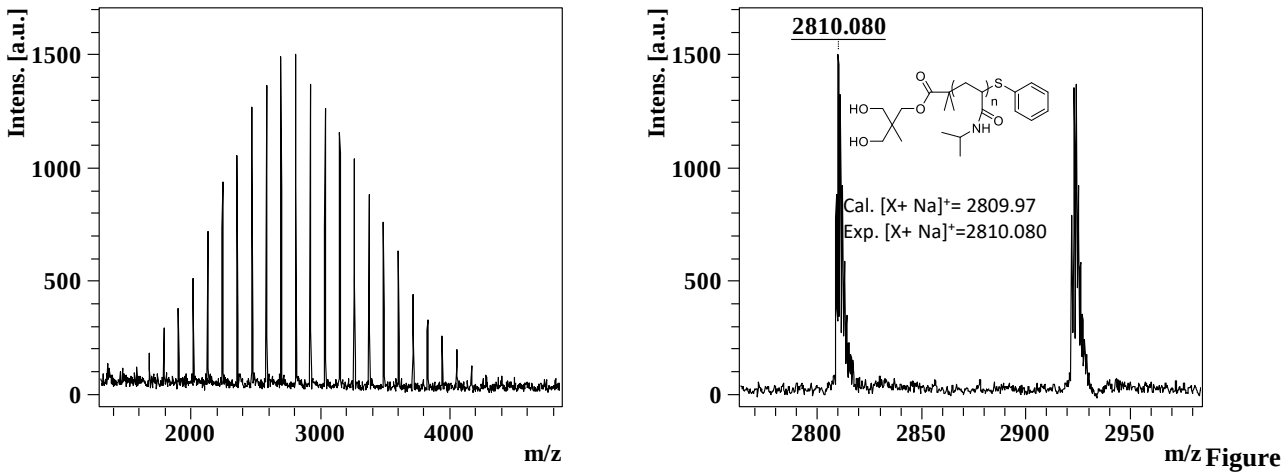

A5.4. Full and expanded MALDI-ToF spectra of $(HO)_2$-PNIPAM$_{24}$-S-Ph (**4a)** acquired in reflectron mode with Na salt as cationizing agent and DCTB matrix.

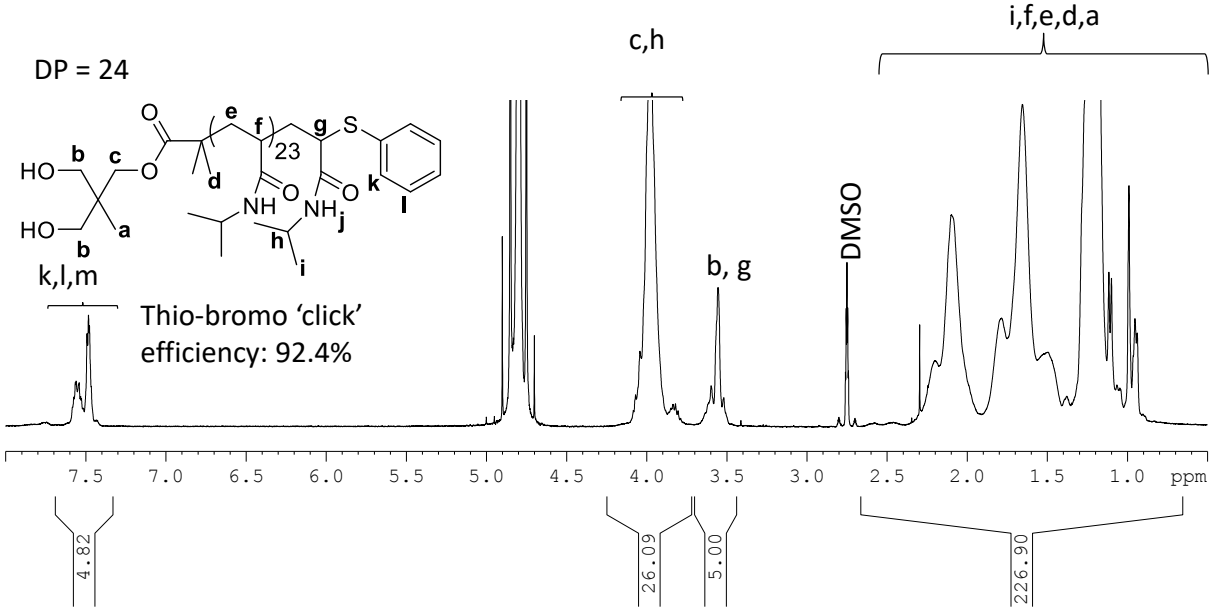

Figure A5.5. ^{1}H NMR spectrum of $(HO)_2$-PNIPAM$_{24}$-S-Ph (**4a**) recorded in D_2O (0.6 mL) + DMSO-d_6 (0.1mL) at 298K (400 MHz).

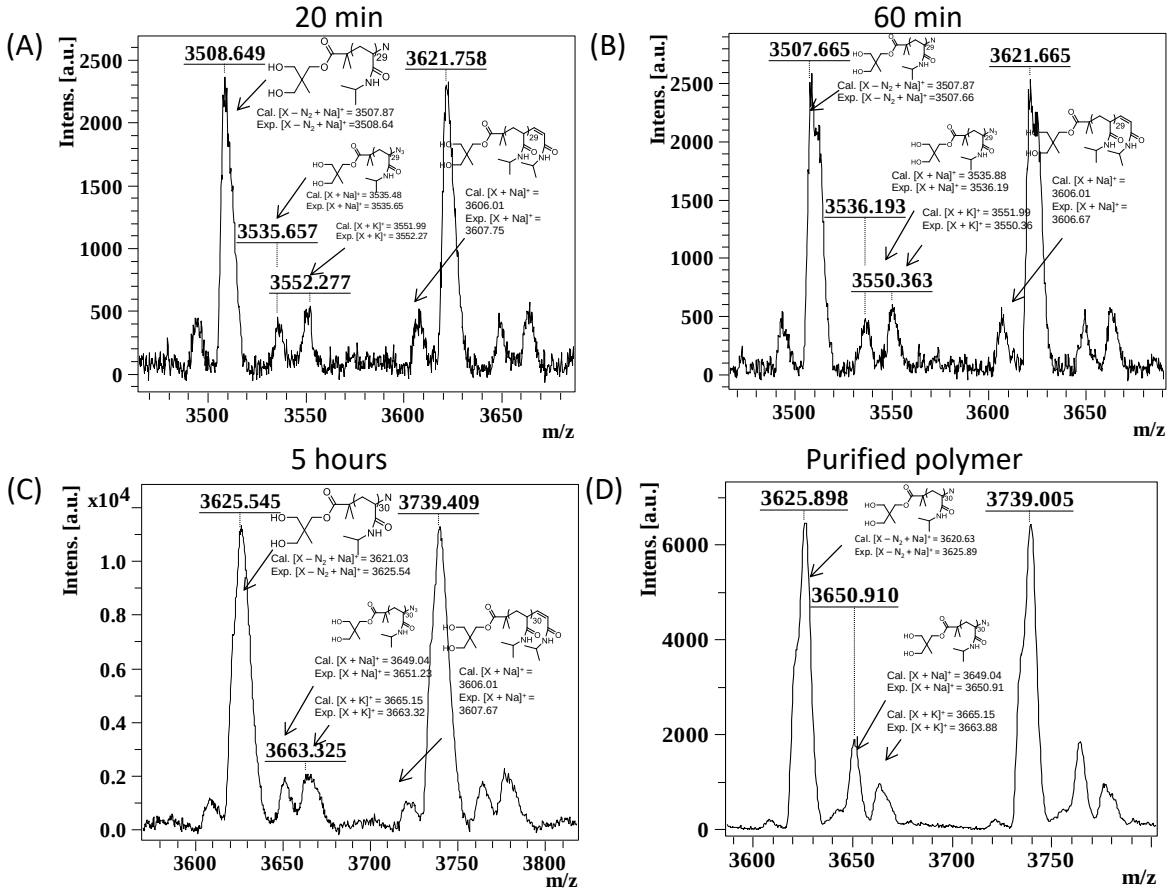

Figure A5.6. Kinetics of in situ azidation of $(HO)_2$-PNIPAM$_n$-Br (**2b**) after 120 min of aqueous SET-LRP at 0°C. MALDI-ToF spectra of (A) at 20 min, (B) 60 min, (C) 5 hours and (D) of purified **5b**.

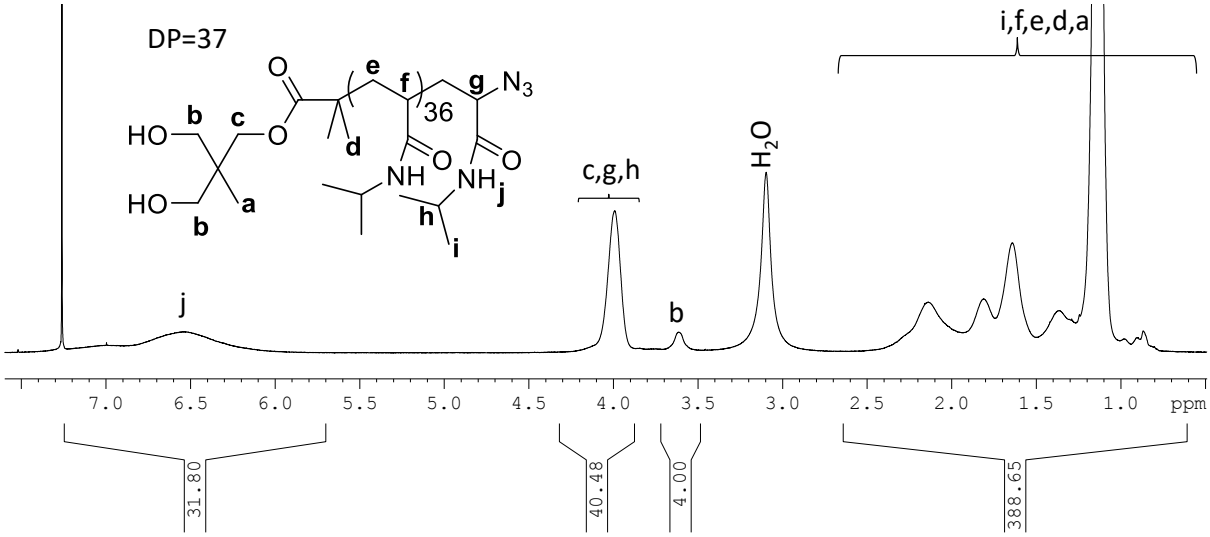

Figure A5.7. ^{1}H NMR spectrum of $(HO)_2$-PNIPAM$_{37}$-N$_3$, **5b** recorded in $CDCl_3$ at 298K (400 MHz).

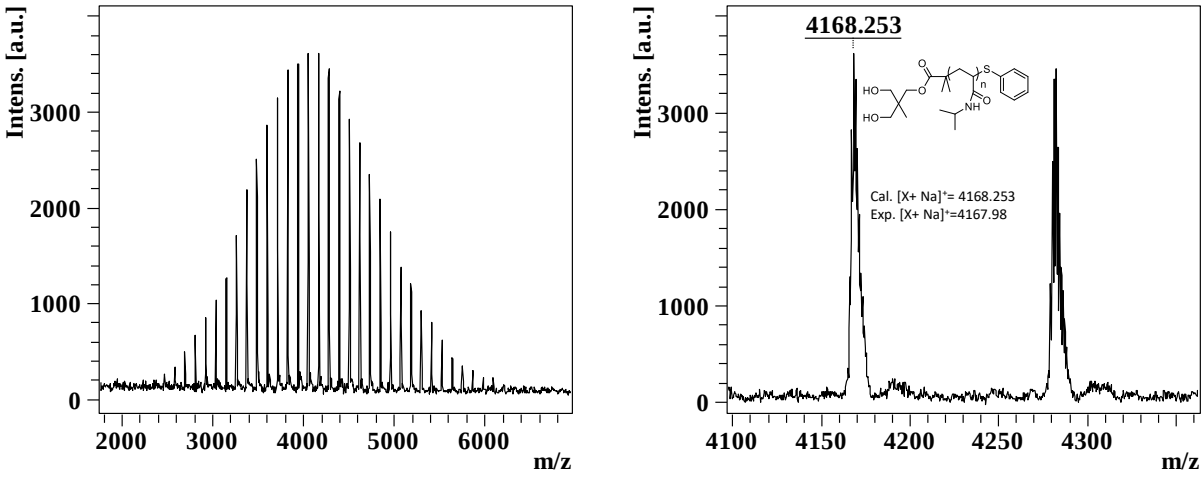

Figure A5.8. Full and expanded MALDI-ToF spectra of $(HO)_2$-PNIPAM$_{36}$-S-Ph (**4b)** acquired in reflectron mode with Na salt as cationizing agent and DCTB matrix.

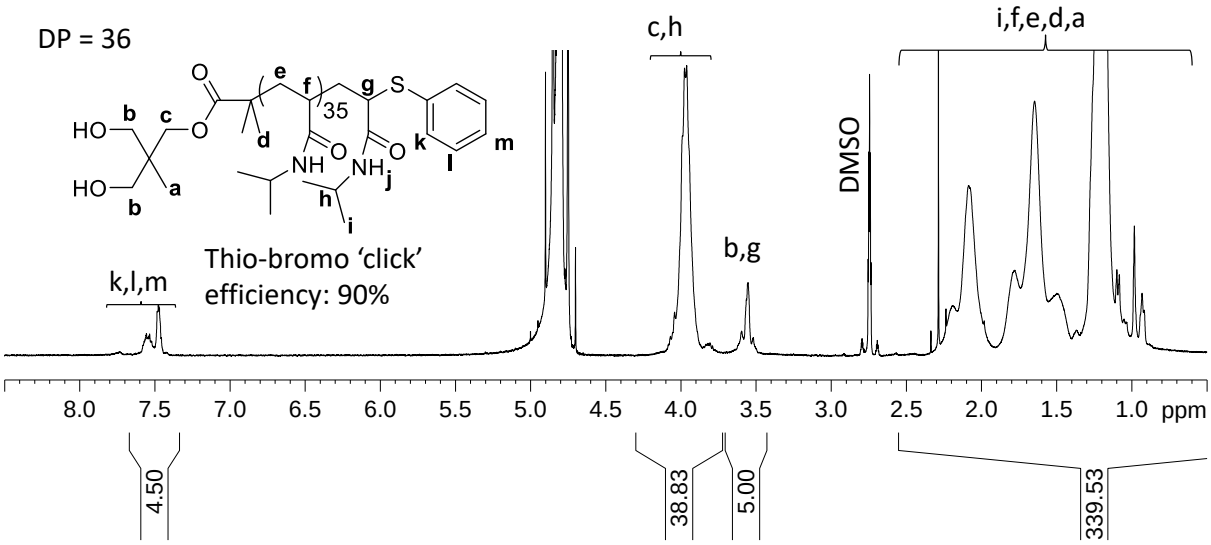

Figure A5.9. ^{1}H NMR spectrum of $(HO)_2$-PNIPAM$_{36}$-S-Ph, **4b** recorded in D_2O (0.6 mL) + DMSO-d_6 (0.1mL) at 298K (400 MHz).

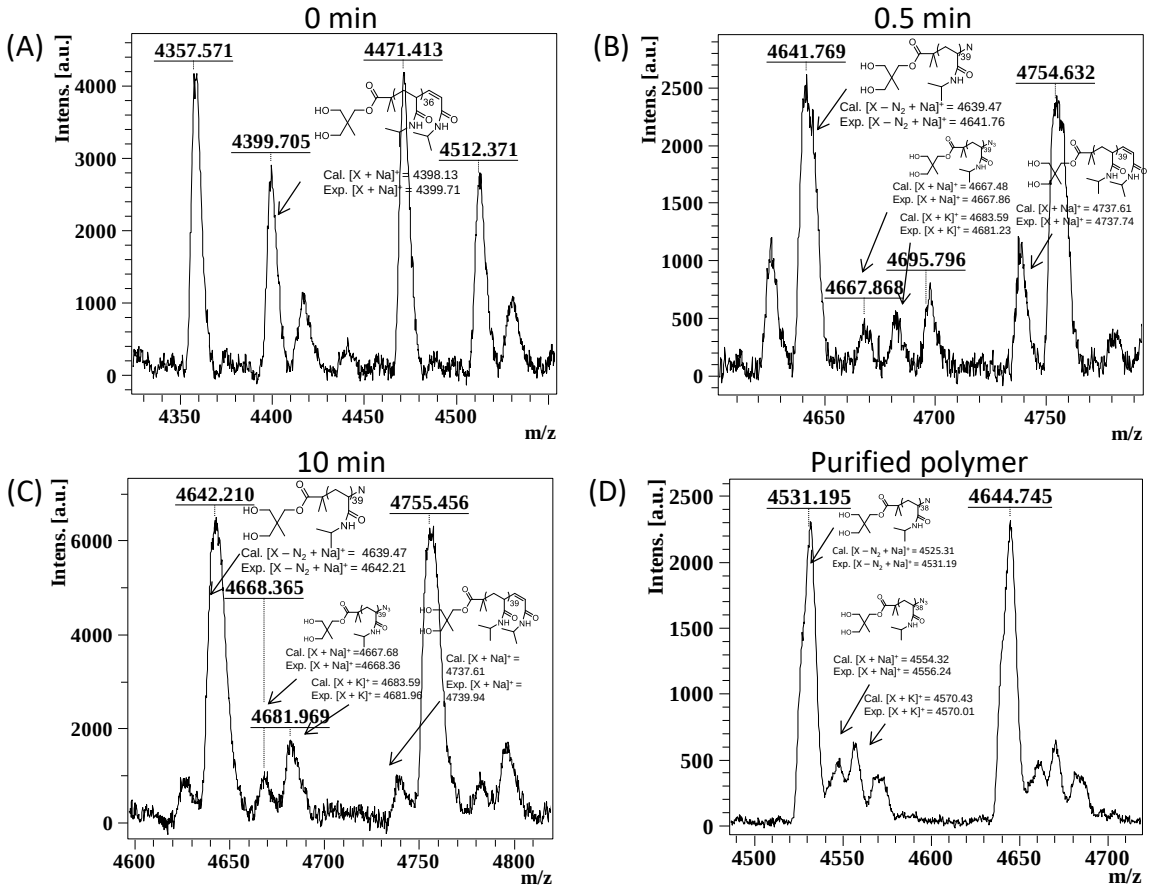

Figure A5.10. Kinetics of in situ azidation of $(HO)_2$-PNIPAM$_n$-Br (**2c**) after 120 min of aqueous SET-LRP at 0°C. MALDI-ToF spectra of (A) at 0 min, (B) 0.5 min, (C) 10min and (D) of purified **5c**.

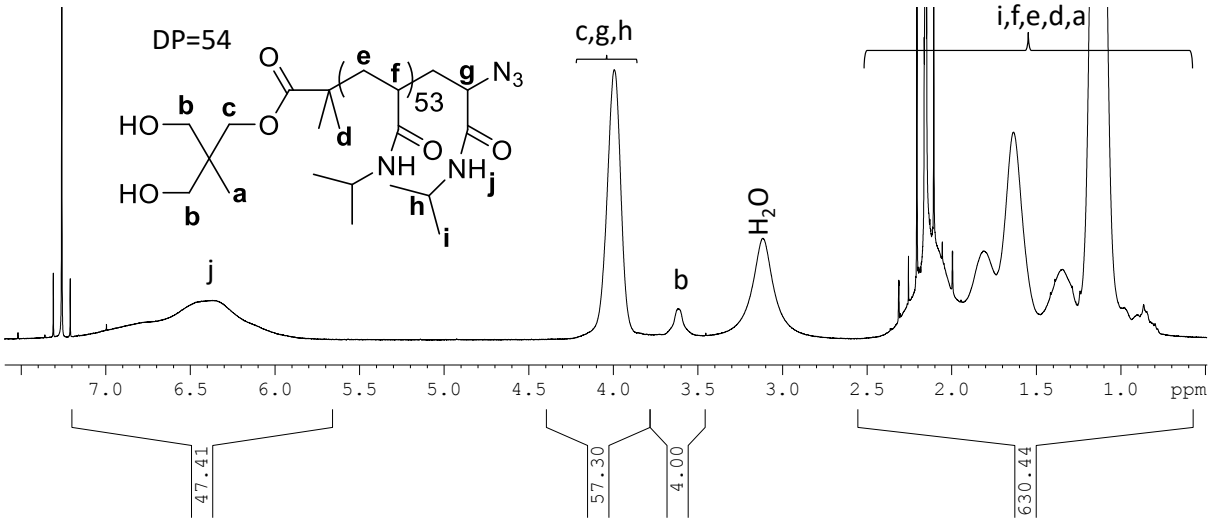

Figure A5.11. ^{1}H NMR spectrum of $(HO)_2$-PNIPAM$_{54}$-N$_3$, **5c** recorded in $CDCl_3$ at 298K (400 MHz).

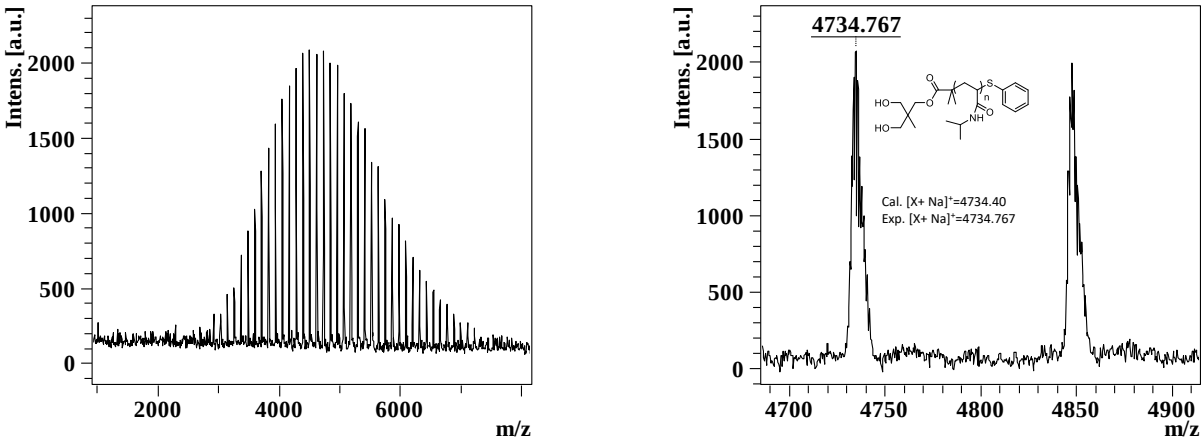

Figure A5.12. Full and expanded MALDI-ToF spectra of $(HO)_2$-PNIPAM$_{44}$-S-Ph (**4c)** acquired in reflectron mode with Na salt as cationizing agent and DCTB matrix.

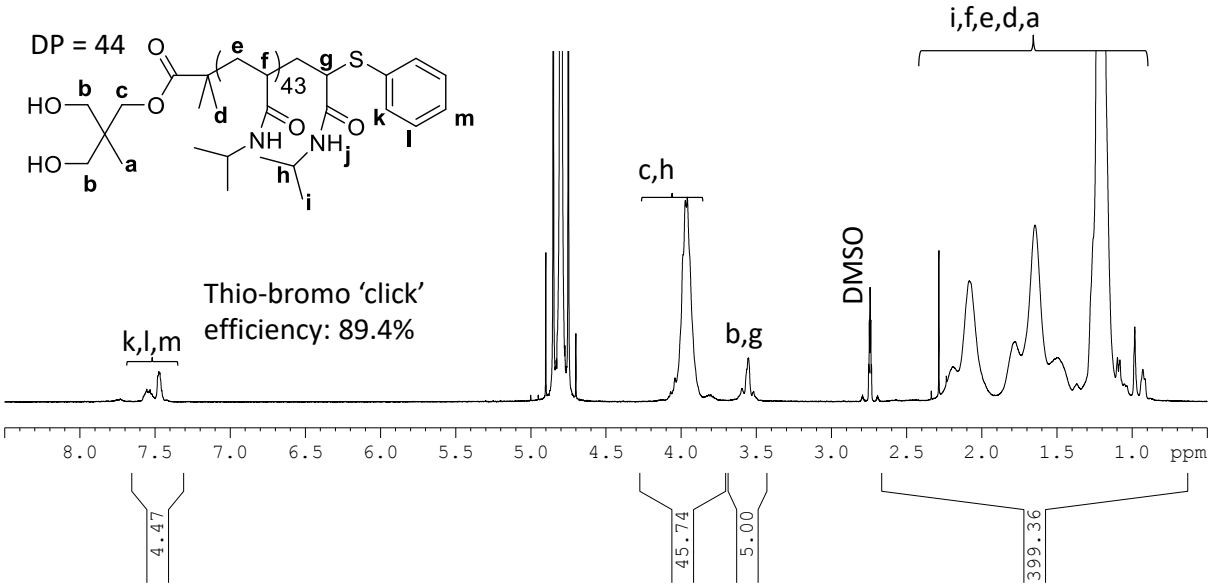

Figure A5.13. ^{1}H NMR spectrum of $(HO)_2$-PNIPAM$_{44}$-S-Ph, **4c** recorded in D_2O (0.6 mL) + DMSO-d_6 (0.1mL) at 298K (400 MHz).

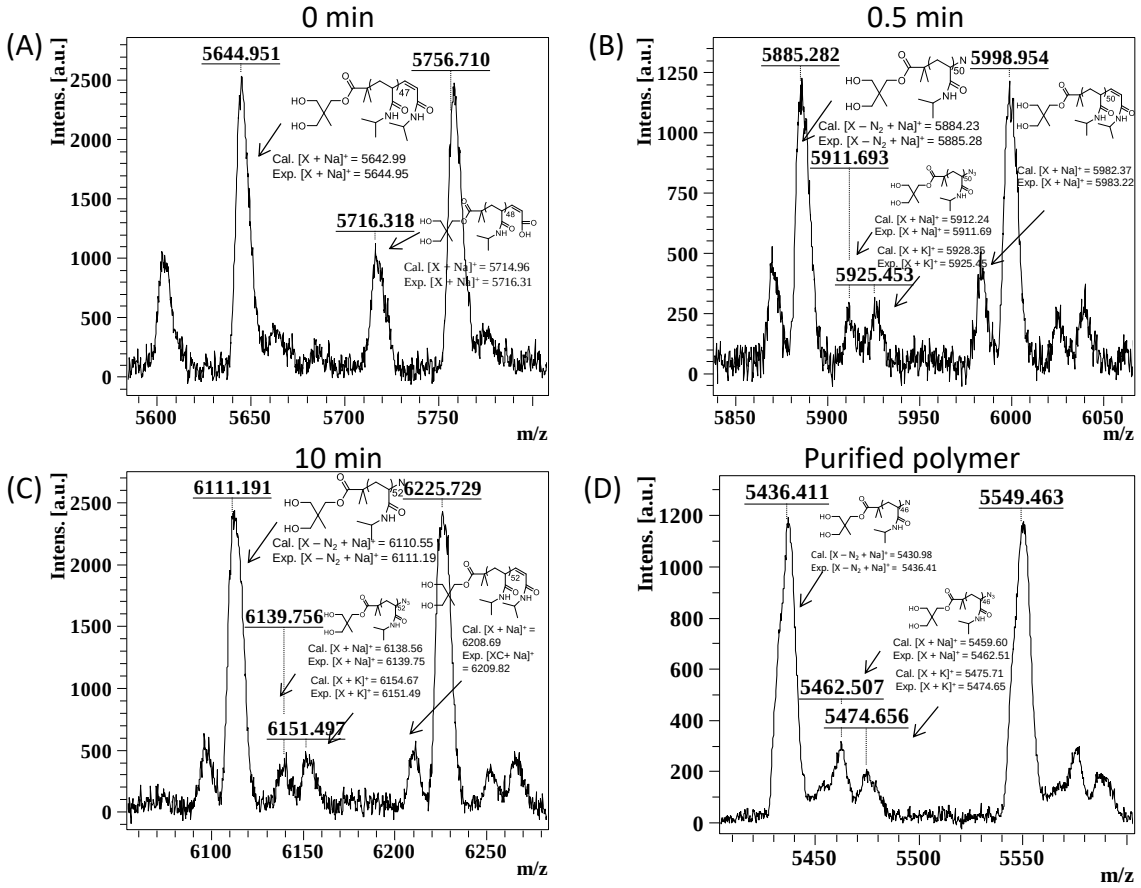

Figure A5.14. Kinetics of in situ azidation of $(HO)_2$-PNIPAM$_n$-Br (**2d**) after 120 min of aqueous SET-LRP at 0°C. MALDI-ToF spectra of (A) at 0 min, (B) 0.5 min, (C) 10min and (D) of purified **5d.**

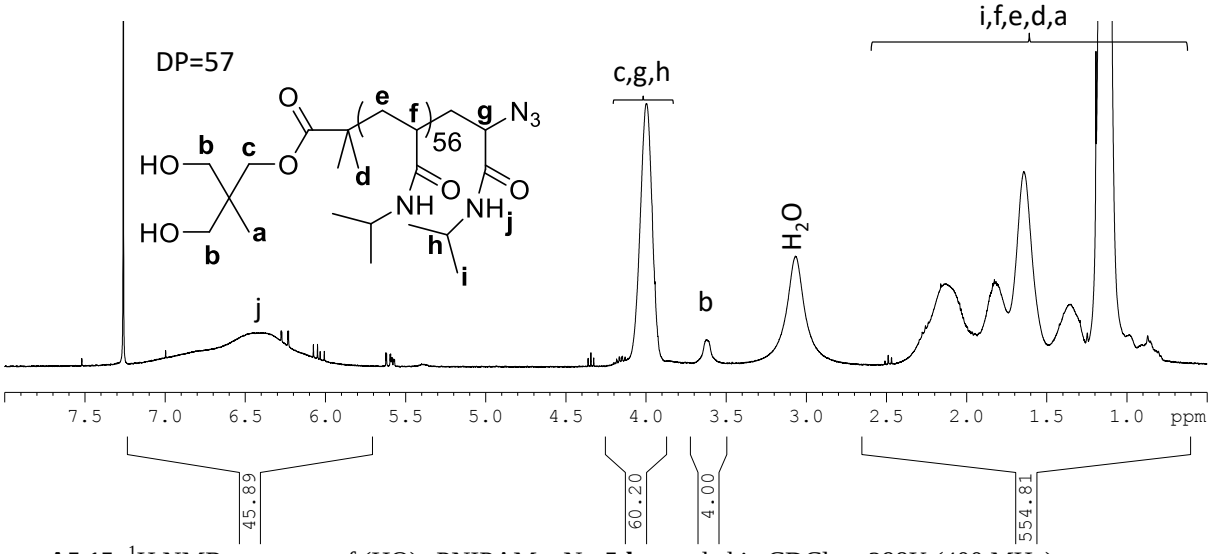

Figure A5.15. ^{1}H NMR spectrum of $(HO)_2$-PNIPAM$_{57}$-N$_3$, **5d** recorded in $CDCl_3$ at 298K (400 MHz).

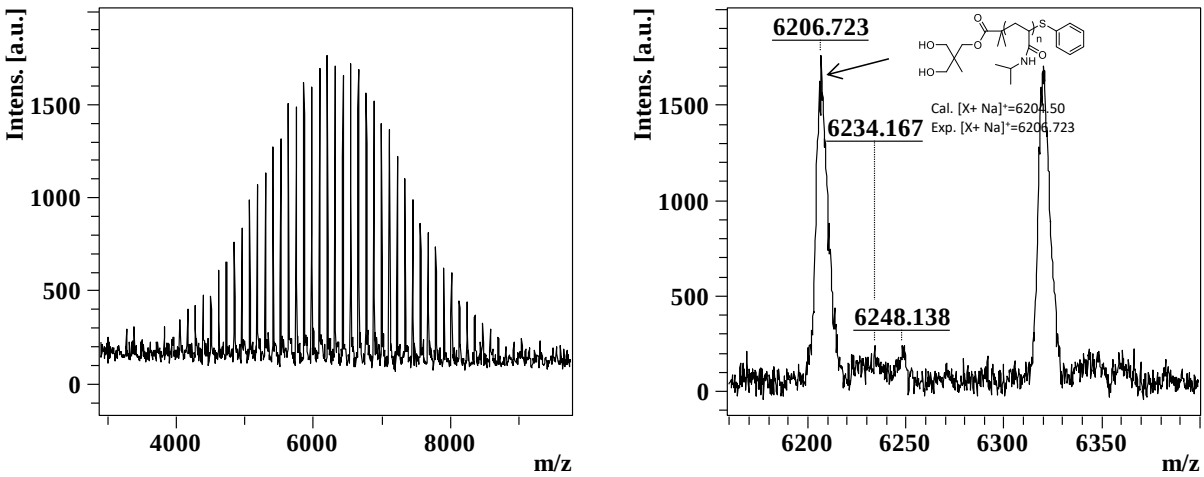

Figure A5.16. Full and expanded MALDI-ToF spectra of $(HO)_2$-PNIPAM$_{55}$-S-Ph (**4d)** acquired in reflectron mode with Na salt as cationizing agent and DCTB matrix.

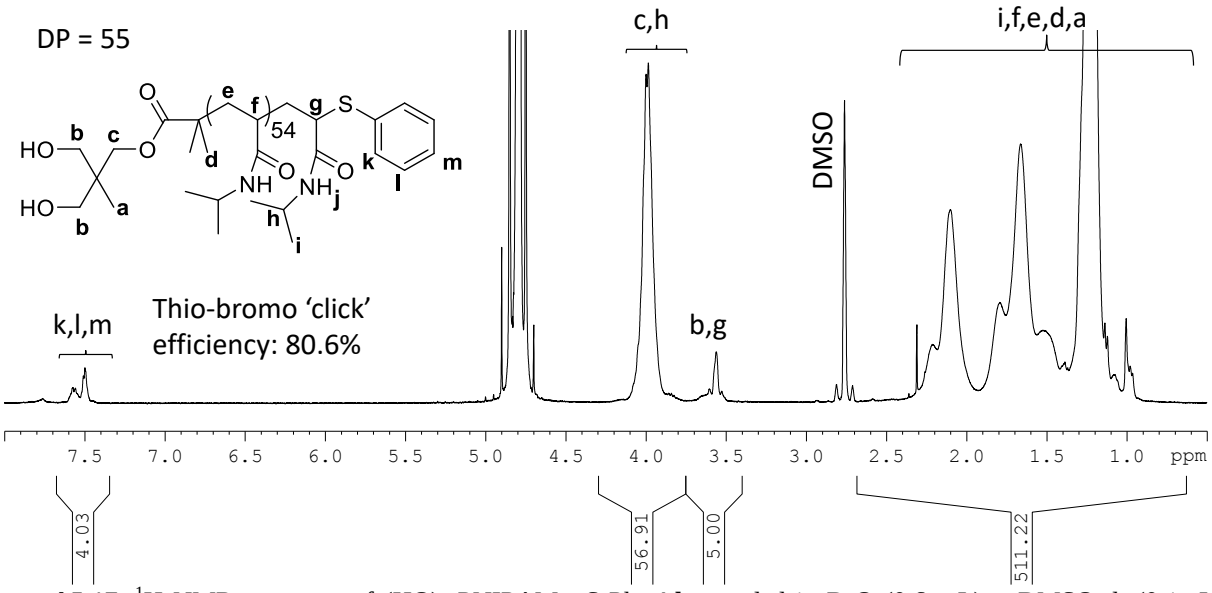

Figure A5.17. ^{1}H NMR spectrum of $(HO)_2$-PNIPAM$_{55}$-S-Ph, **4d** recorded in D_2O (0.6 mL) + DMSO-d_6 (0.1mL) at 298K (400 MHz).

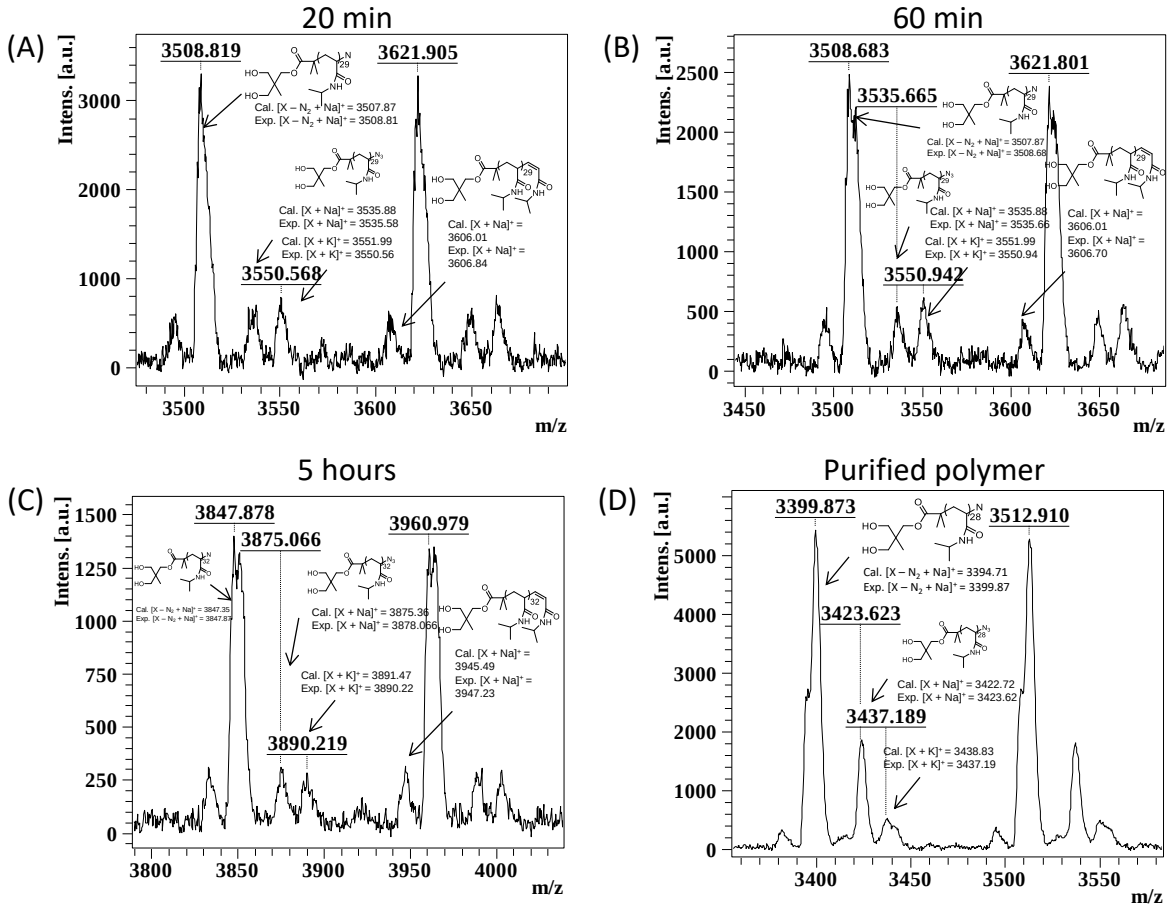

Figure A5.18. Kinetics of in situ azidation of $(HO)_2$-PNIPAM$_n$-Br (**2e**) after 120 min of aqueous SET-LRP at 0°C. MALDI-ToF spectra of (A) at 20 min, (B) 60 min, (C) 5 hours and (D) of purified **5e**.

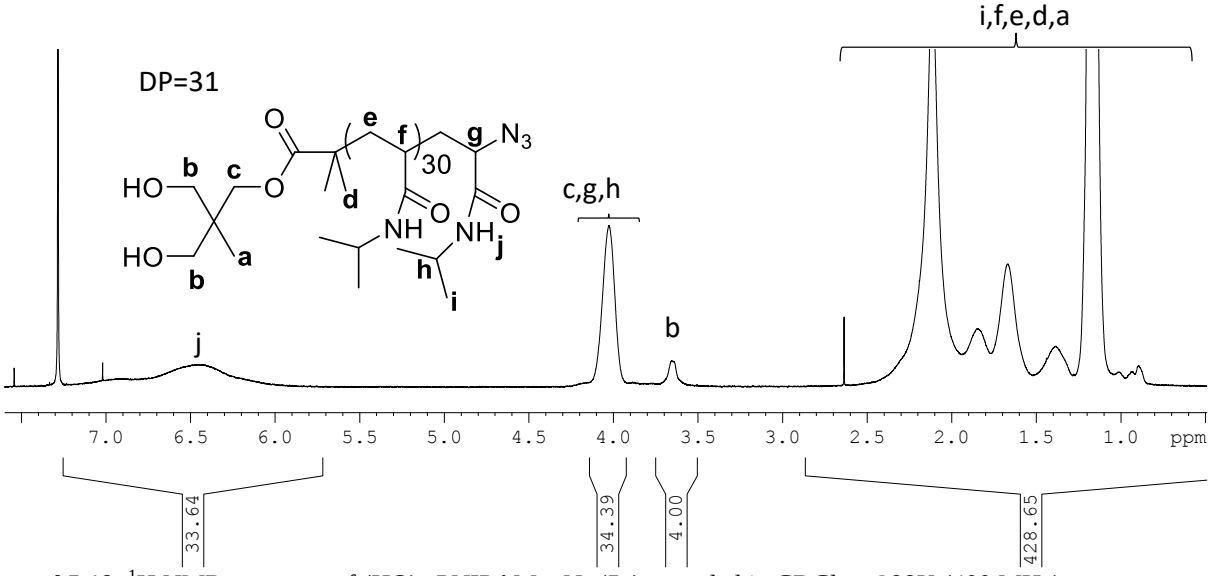

Figure A5.19. ^{1}H NMR spectrum of $(HO)_2$-PNIPAM$_{31}$-N_3 (**5e**) recorded in $CDCl_3$ at 298K (400 MHz).

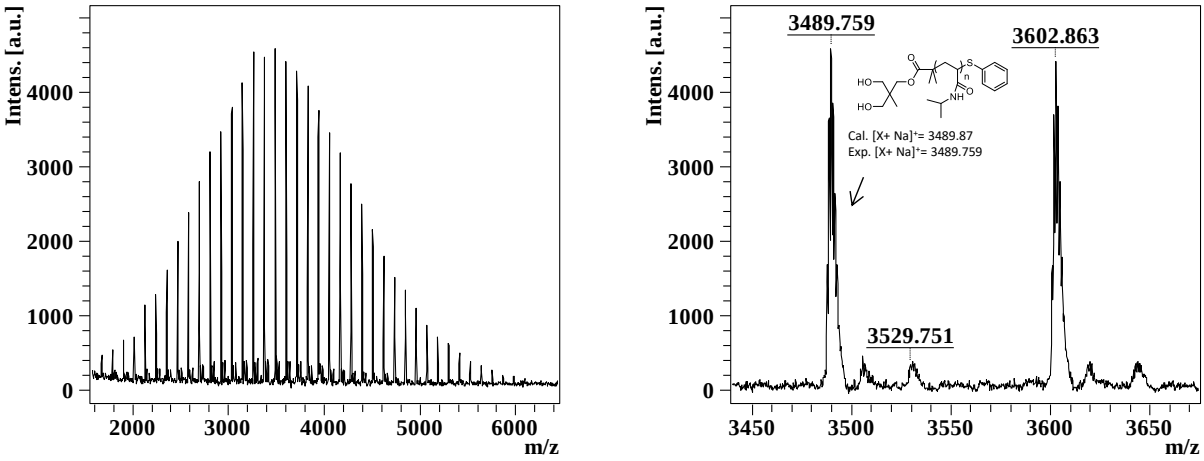

Figure A5.20. Full and expanded MALDI-ToF spectra of $(HO)_2$-PNIPAM$_{34}$-S-Ph (**4e)** acquired in reflectron mode with Na salt as cationizing agent and DCTB matrix.

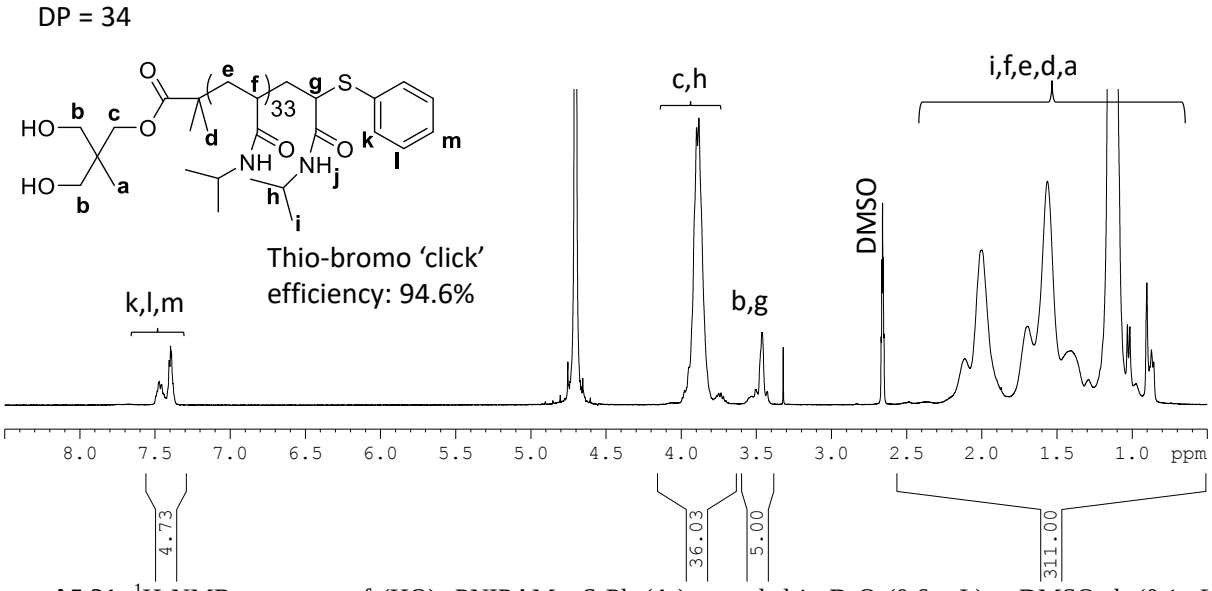

Figure A5.21. ^{1}H NMR spectrum of $(HO)_2$-PNIPAM$_{34}$-S-Ph (**4e**) recorded in D_2O (0.6 mL) + DMSO-d_6 (0.1mL) at 298K (400 MHz).

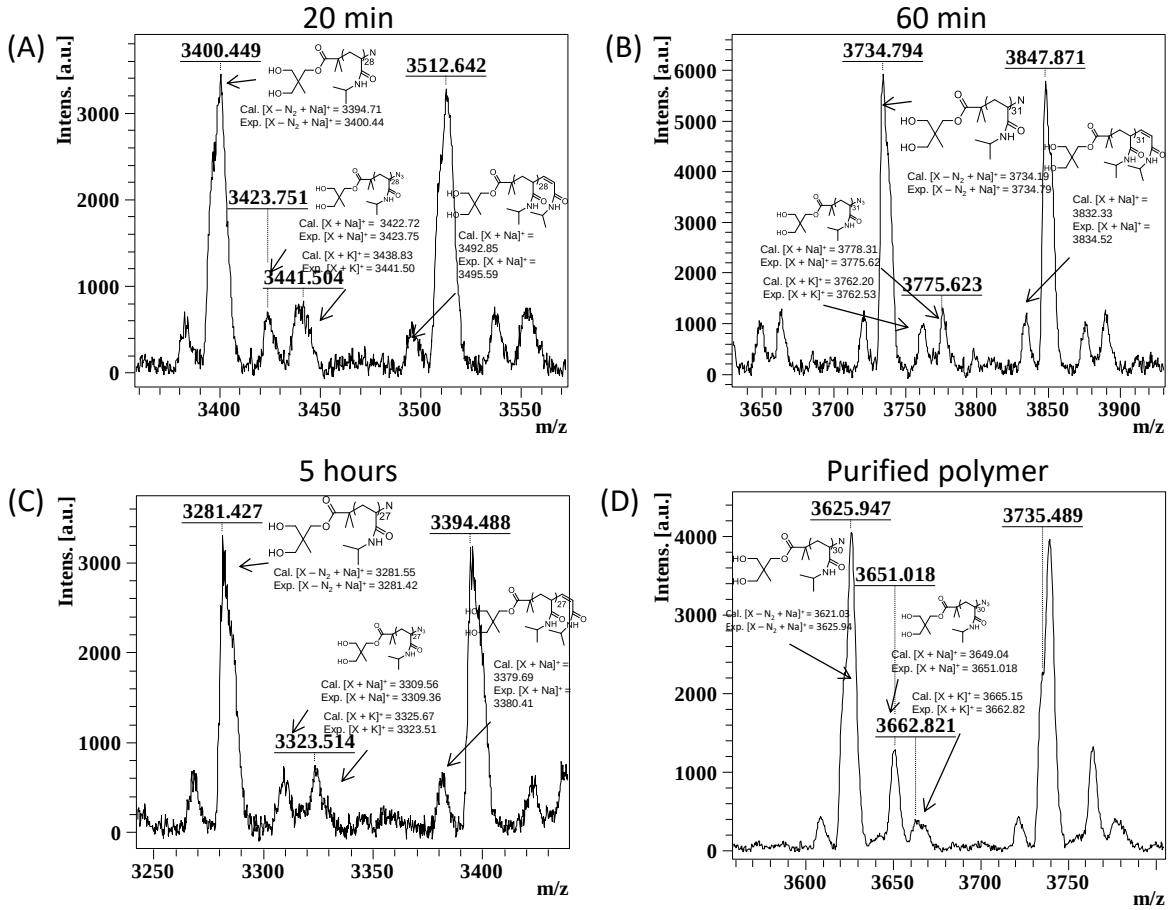

Figure A5.22. Kinetics of in situ azidation of $(HO)_2$-$PNIPAM_n$-Br (**2f**) after 120 min of aqueous SET-LRP at 0°C. MALDI-ToF spectra of (A) at 20 min, (B) 60 min, (C) 5 hours and (D) of purified **5f**.

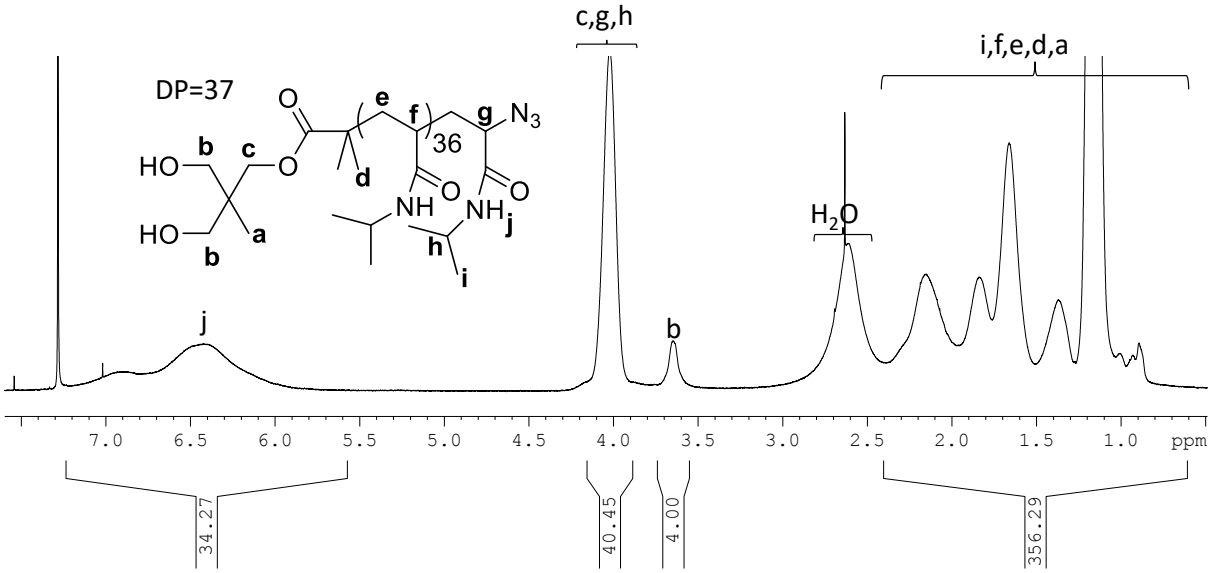

Figure A5.23. ^{1}H NMR spectrum of $(HO)_2$-$PNIPAM_{37}$-N_3 (**5f**) recorded in $CDCl_3$ at 298K (400 MHz).

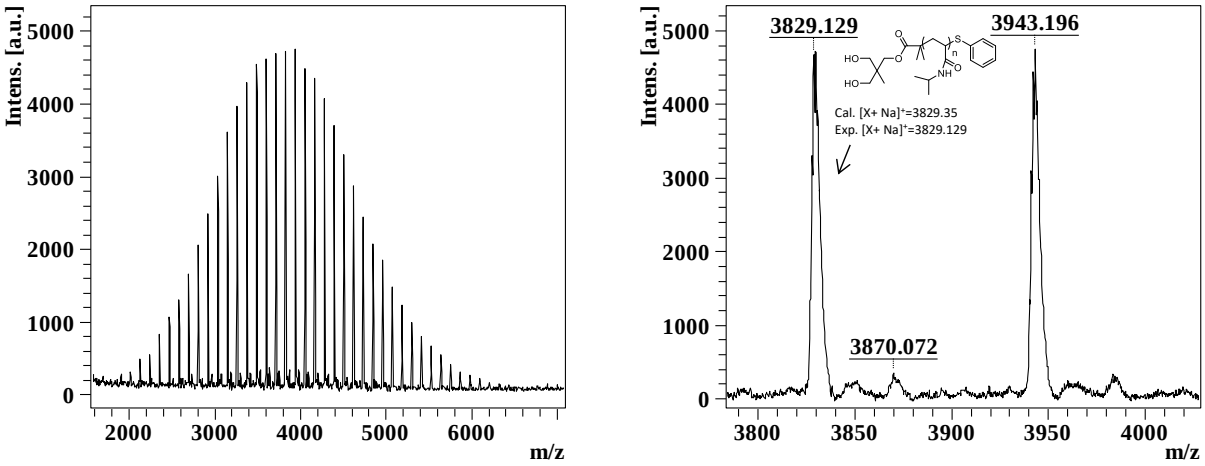

Figure A5.24. Full and expanded MALDI-ToF spectra of $(HO)_2$-$PNIPAM_{31}$-S-Ph (**4f)** acquired in reflectron mode with Na salt as cationizing agent and DCTB matrix.

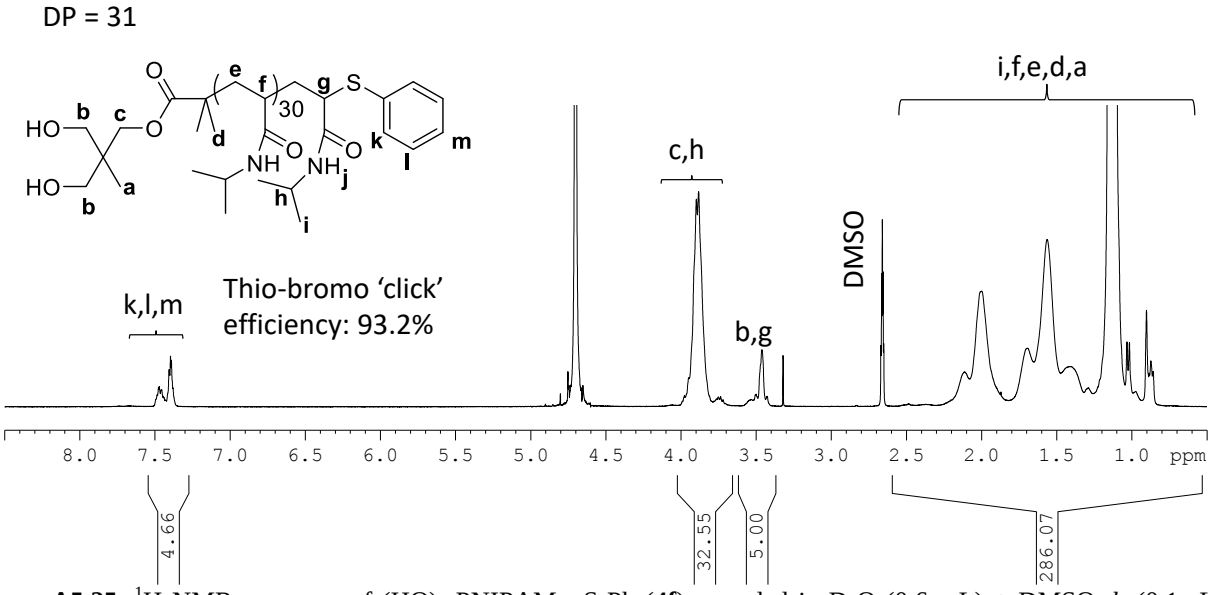

Figure A5.25. ^{1}H NMR spectrum of $(HO)_2$-$PNIPAM_{31}$-S-Ph (**4f**) recorded in D_2O (0.6 mL) + DMSO-d_6 (0.1mL) at 298K (400 MHz).

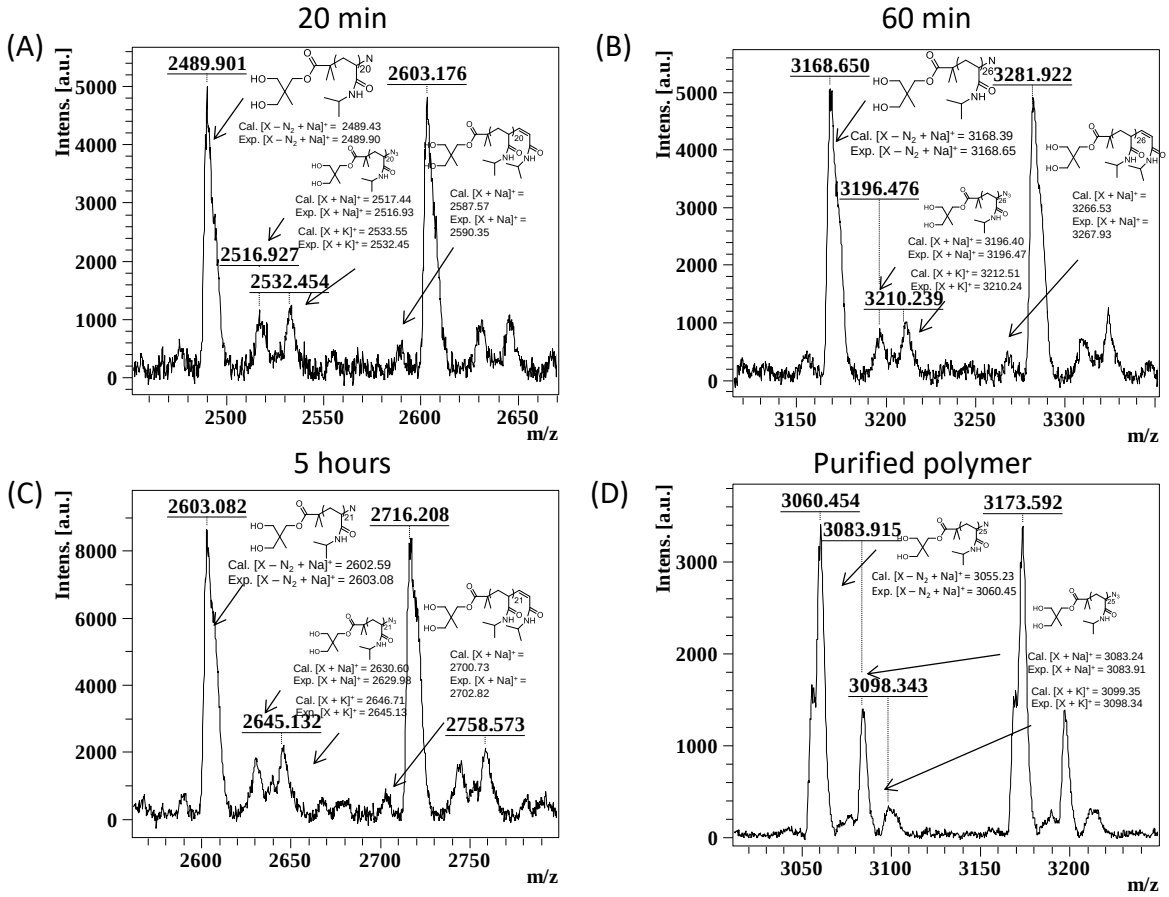

Figure A5.26. Kinetics of in situ azidation of $(HO)_2$-PNIPAM$_n$-Br (**2g**) after 120 min of aqueous SET-LRP at 0°C. MALDI-ToF spectra of (A) at 20 min, (B) 60 min, (C) 5 hours and (D) of purified **5g**.

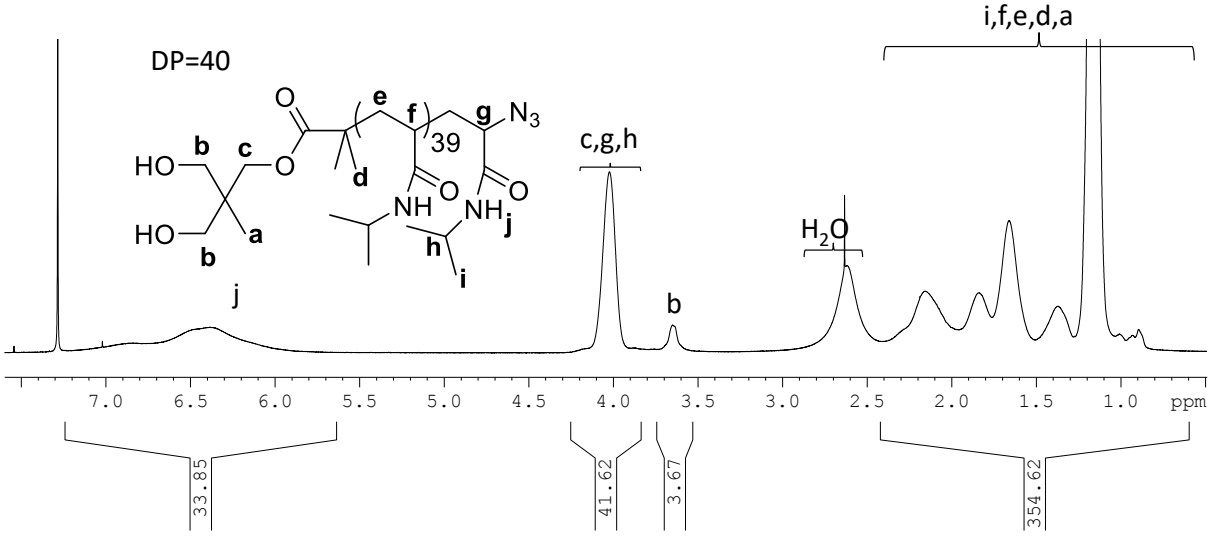

Figure A5.27. ^{1}H NMR spectrum of $(HO)_2$-PNIPAM$_{40}$-N_3 (**5g**) recorded in $CDCl_3$ at 298K (400 MHz).

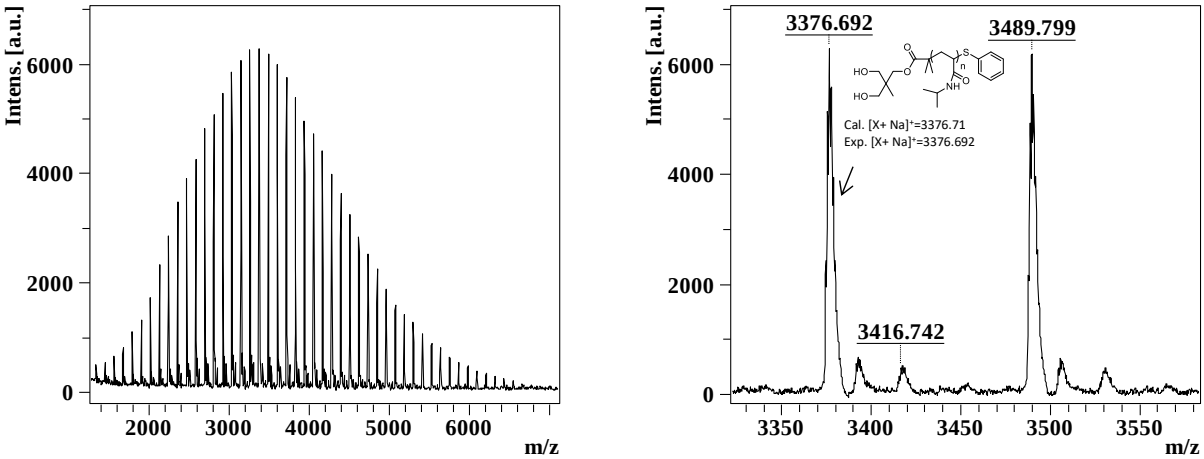

Figure A5.28. Full and expanded MALDI-ToF spectra of $(HO)_2$-PNIPAM$_{34}$-S-Ph (**4g)** acquired in reflectron mode with Na salt as cationizing agent and DCTB matrix.

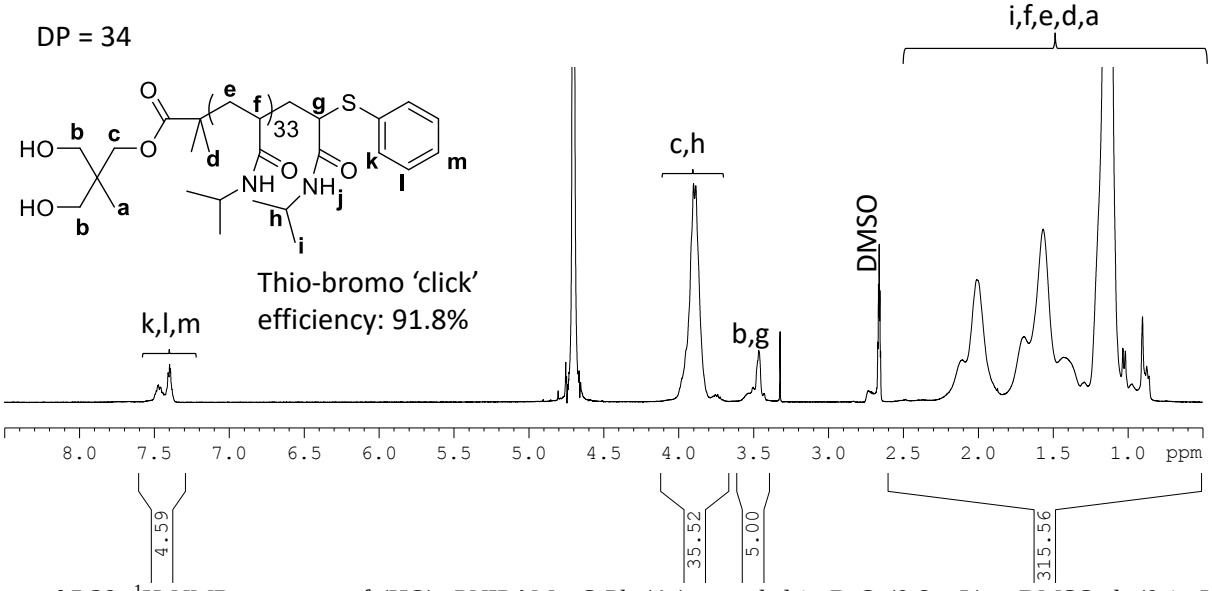

Figure A5.29. ^{1}H NMR spectrum of $(HO)_2$-PNIPAM$_{34}$-S-Ph (**4g**) recorded in D_2O (0.6 mL) + DMSO-d_6 (0.1mL) at 298K (400 MHz).

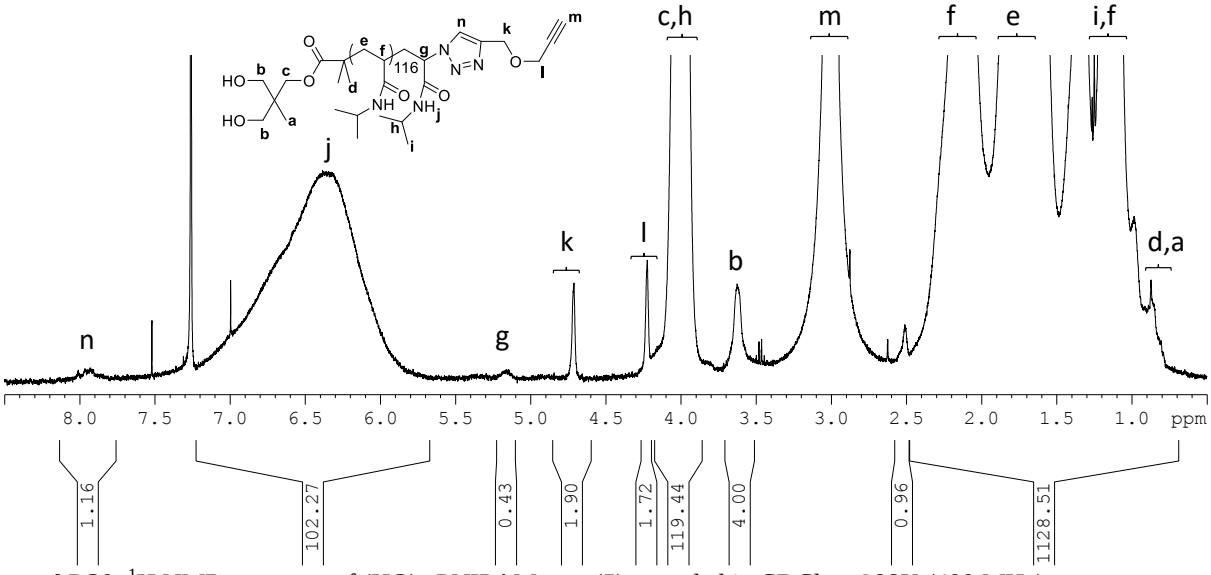

Figure A5.30. ^{1}H NMR spectrum of $(HO)_2$-PNIPAM$_{117}$-≡ (**5**) recorded in $CDCl_3$ at 298K (400 MHz).

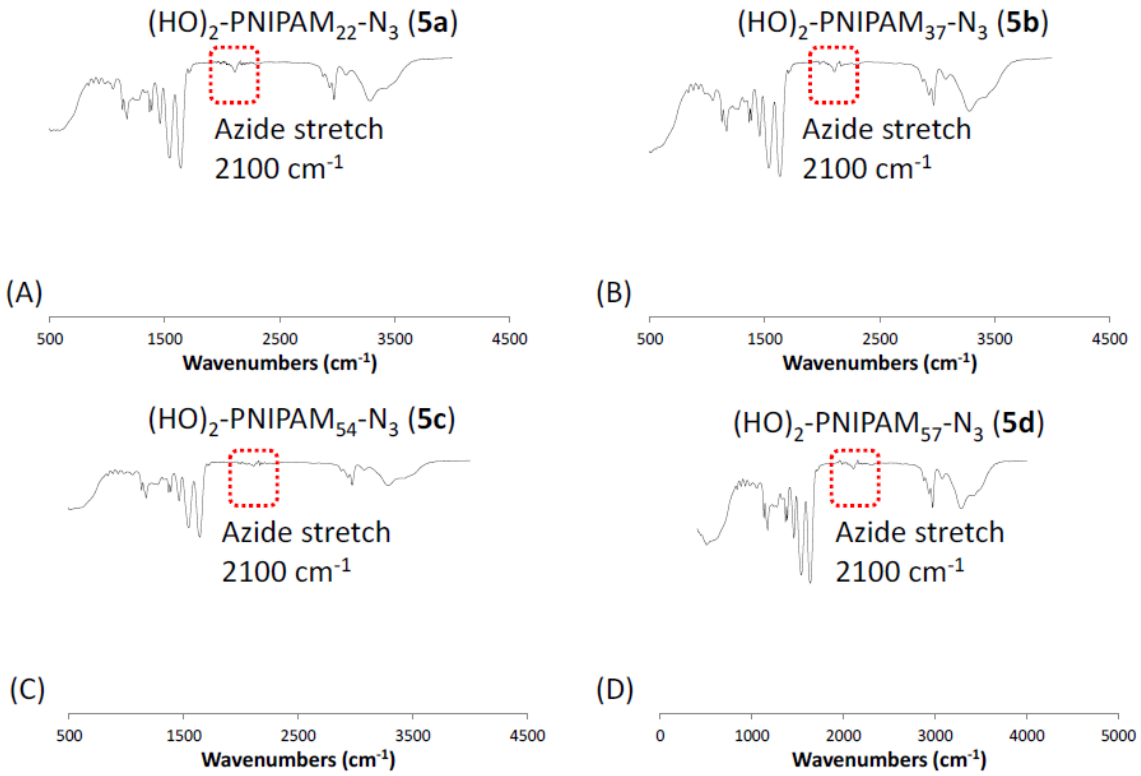

Figure A5.31: ATR-FTIR of spectra of (A) $(HO)_2$-PNIPAM$_{22}$-N_3 (**5a**), (B) $(HO)_2$-PNIPAM$_{37}$-N_3 (**5b**), (C) $(HO)_2$-PNIPAM$_{54}$-N_3 (**5c**) and (D) $(HO)_2$-PNIPAM$_{57}$-N_3 (**5d**).

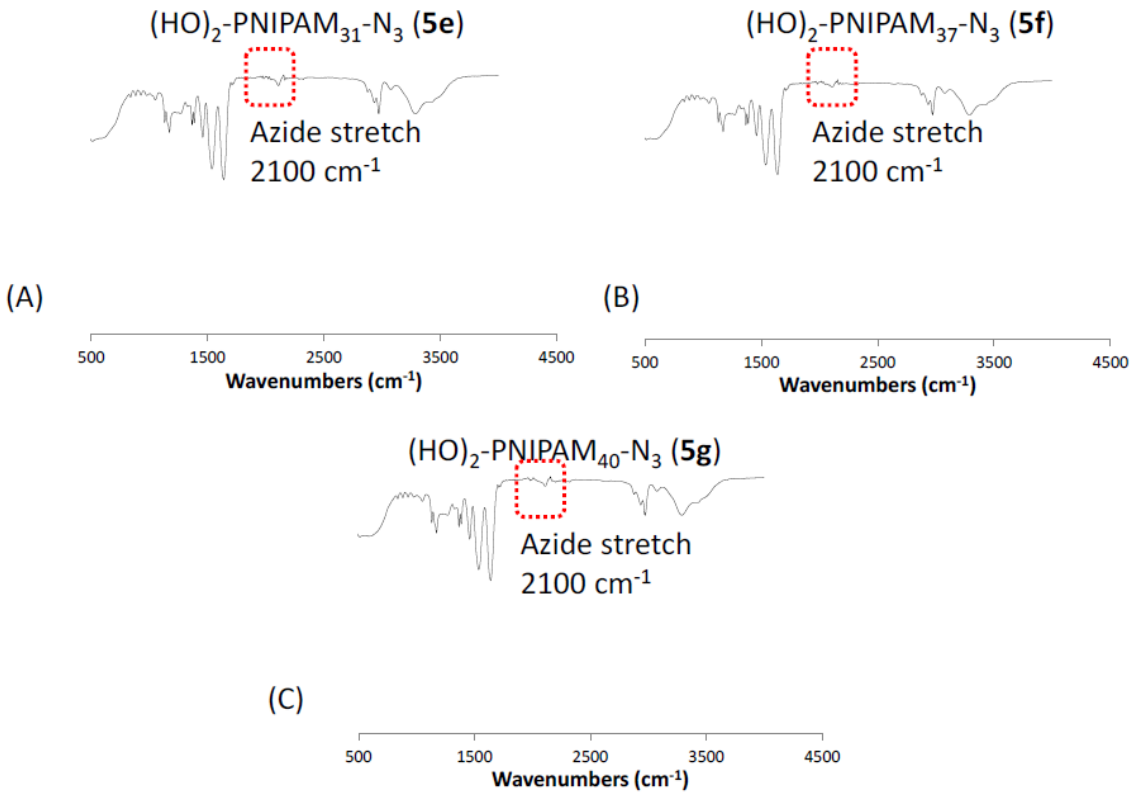

Figure A5.32: ATR-FTIR of spectra of (A) $(HO)_2$-$PNIPAM_{31}$-N_3 (**5e**), (B) $(HO)_2$-$PNIPAM_{37}$-N_3 (**5f**) and (C) $(HO)_2$-$PNIPAM_{40}$-N_3 (**5g**).

Appendix C

Table A6.1. Molecular weight data for the synthesis of polymeric structures.

Polymer N^{o}	Polymer Code	RI detection [a]			Triple detection [b]			M_n by NMR
		M_n	M_p	PDI	M_n	M_p	PDI	
2	≡(OH)-PSTY$_{30}$-Br	3480	3580	1.05	3690	3830	1.02	3740
3	≡(OH)-PSTY$_{30}$-N$_3$	3550	3560	1.08	3910	3980	1.03	3810
4	c-PSTY$_{30}$-OH	2730	2760	1.05	3740	3830	1.01	4020
5	c-PSTY$_{30}$-Br	2760	2820	1.05				4050
6	c-PSTY$_{30}$ –N$_3$	2930	2820	1.24	3790	3900	1.01	4010
7	c-PSTY$_{30}$-(≡)OH	2920	2920	1.05	4010	4150	1.01	4230
8	c-PSTY$_2$-OH	5750	5820	1.03	7880	8050	1.003	8240
9	c-PSTY$_2$-N$_3$	5980	6010	1.03	8010	8560	1.02	8270
10	c-PSTY$_3$-OH	8480	8640	1.03	12490	12730	1.003	12490
11	c-PSTY$_3$-N$_3$	8550	8740	1.04	12320	12750	1.01	12520
12	c-PSTY$_4$-OH	10650	10830	1.03	16850	17060	1.001	17160
13	c-PSTY$_4$-N$_3$	10720	10850	1.02	15970	16550	1.01	16670
14	c-PSTY$_5$-OH	12160	12590	1.03				

[a]SEC (RI detector) based on PSTY calibration curve. [b]The data was acquired using DMAc Triple Detection SEC with 0.03 wt% of LiCl as eluent.

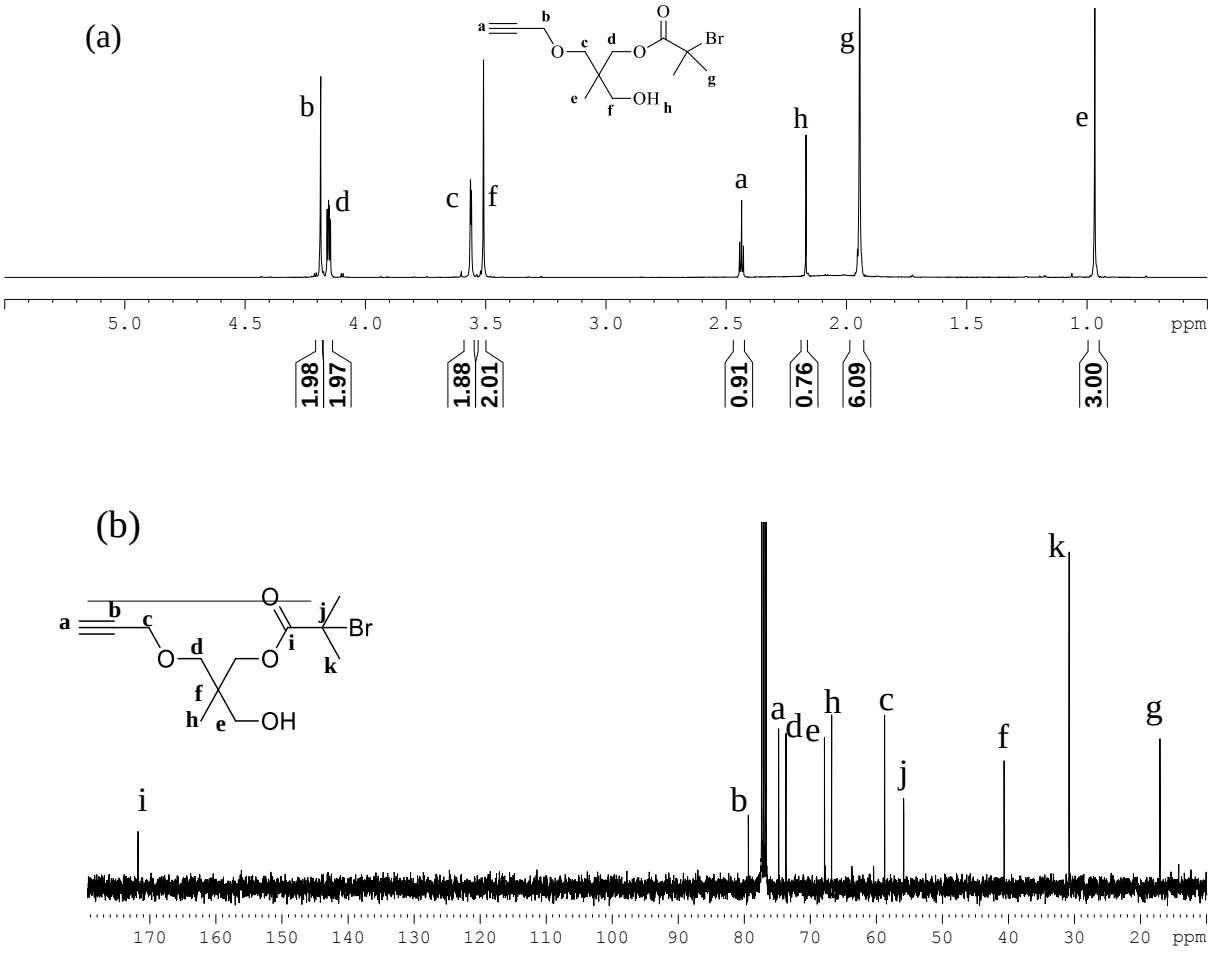

Figure A6.1: (a) ^{1}H NMR of **1**, recorded in $CDCl_3$ at 298K (300 MHz) and (b) ^{13}C NMR recorded in $CDCl_3$ at 298K (400 MHz)**.**

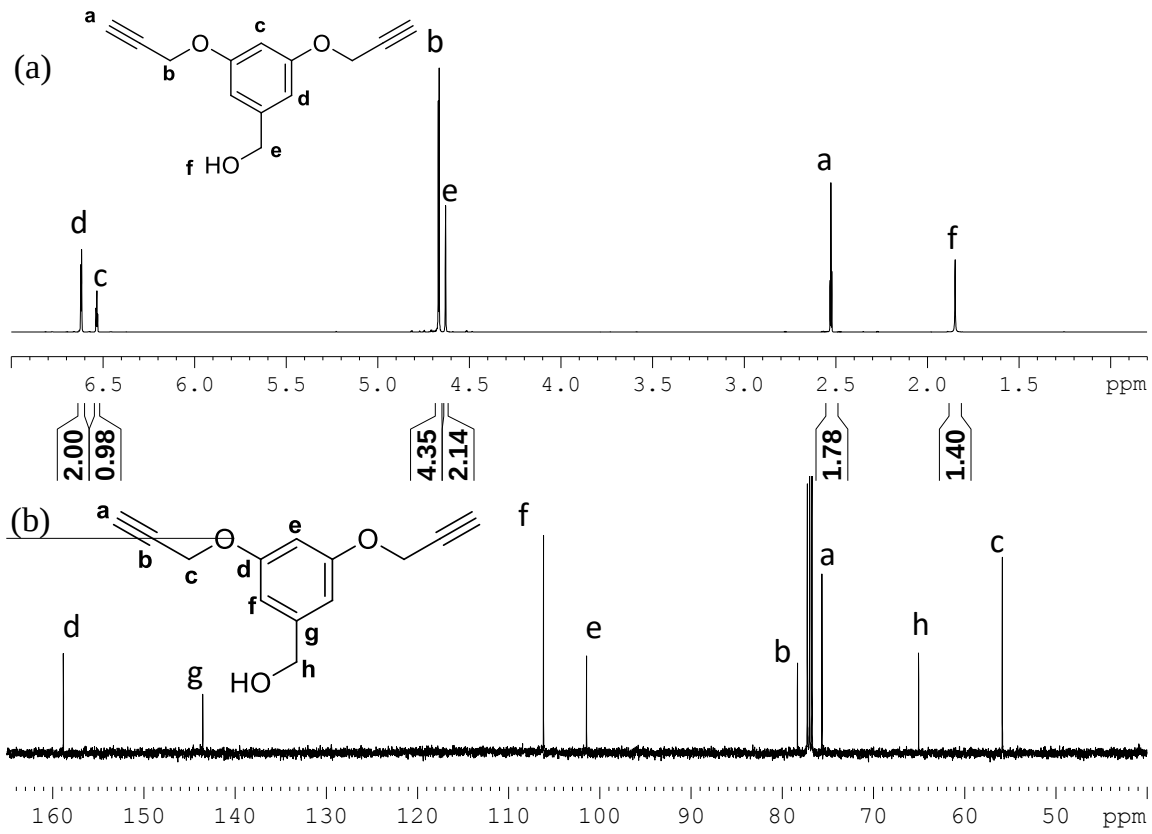

Figure A6.2: (a) ^{1}H and (b) ^{13}C 400 MHz NMR spectra of (3,5-bis(prop-2-yn-1-yloxy)phenyl)methanol (**16**) in $CDCl_3$.

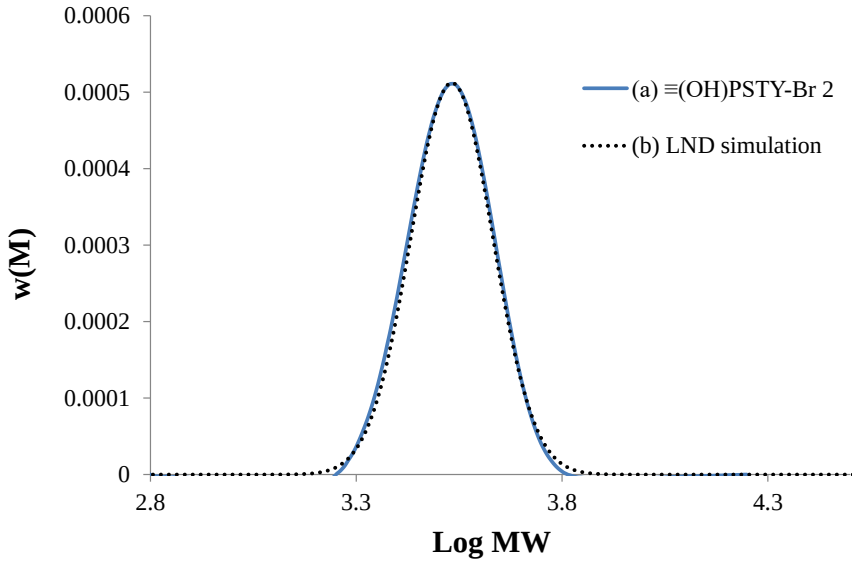

Figure A6.3: SEC chromatograms of (a) ≡(OH)-$PSTY_{30}$-Br (**2)** and (b) LND simulation of **2**. SEC chromatogram is based on PSTY calibration curve.

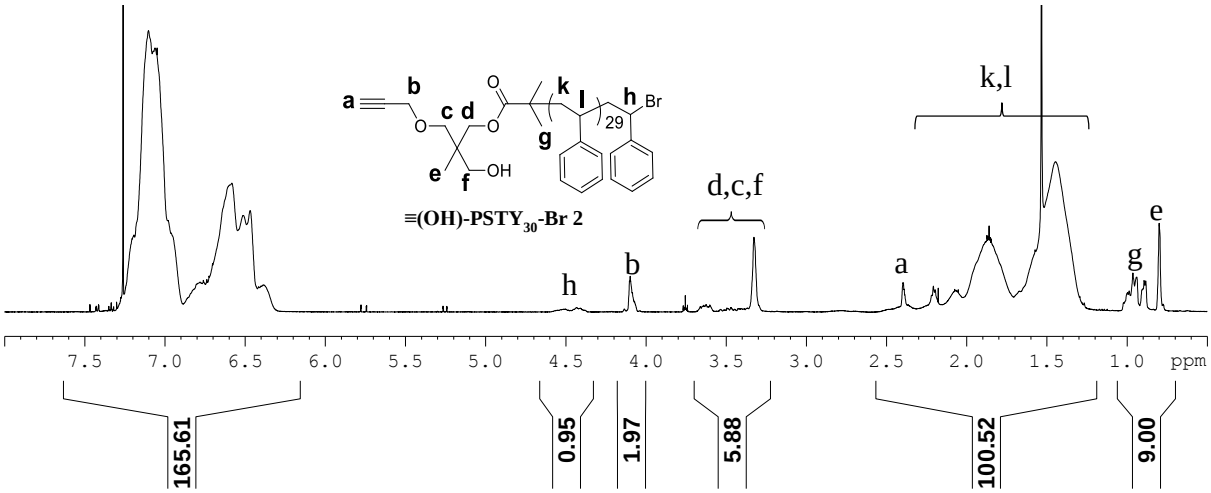

Figure A6.4. 500 MHz ^{1}H NMR spectrum in $CDCl_3$ of ≡(OH)-PSTY$_{30}$-Br, (**2**).

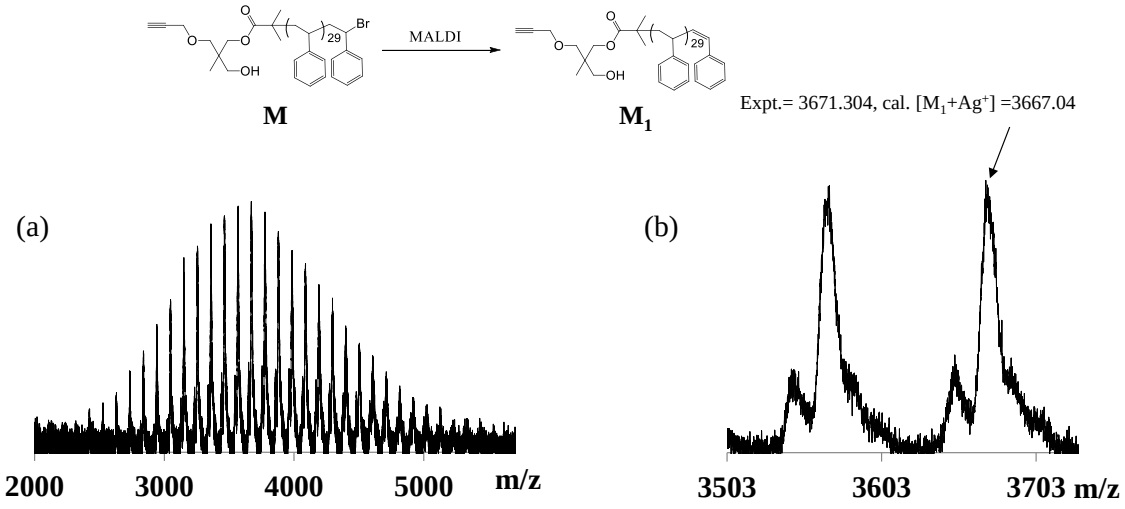

Figure A6.5: MALDI-ToF mass spectrum acquired in reflectron mode with Ag salt as cationizing agent and DCTB matrix. The full (a) and expanded (b) spectra correspond to ≡(HO)-PSTY$_{30}$-Br (**2**).

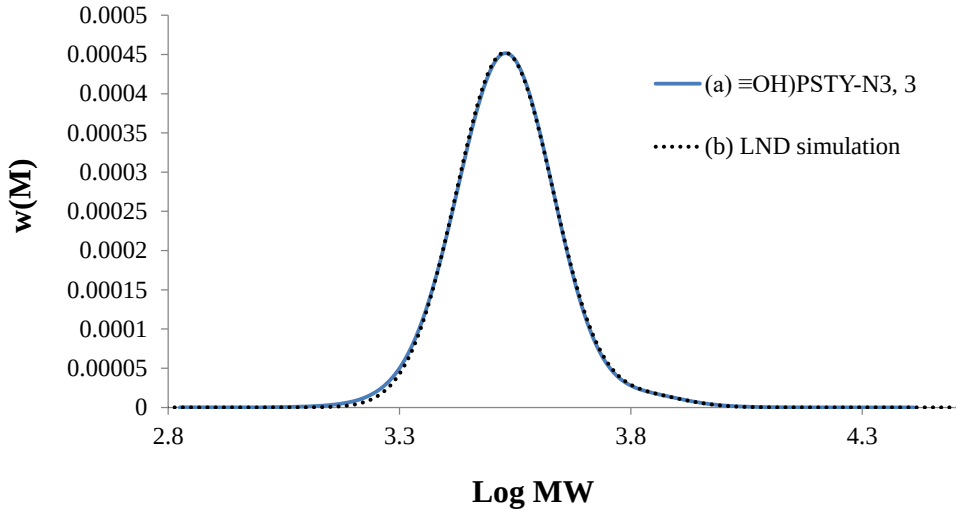

Figure A6.6: SEC chromatograms of (a) ≡(OH)-PSTY$_{30}$-N$_3$ (**3**) and (b) LND simulation of **3**. SEC chromatogram is based on PSTY calibration curve.

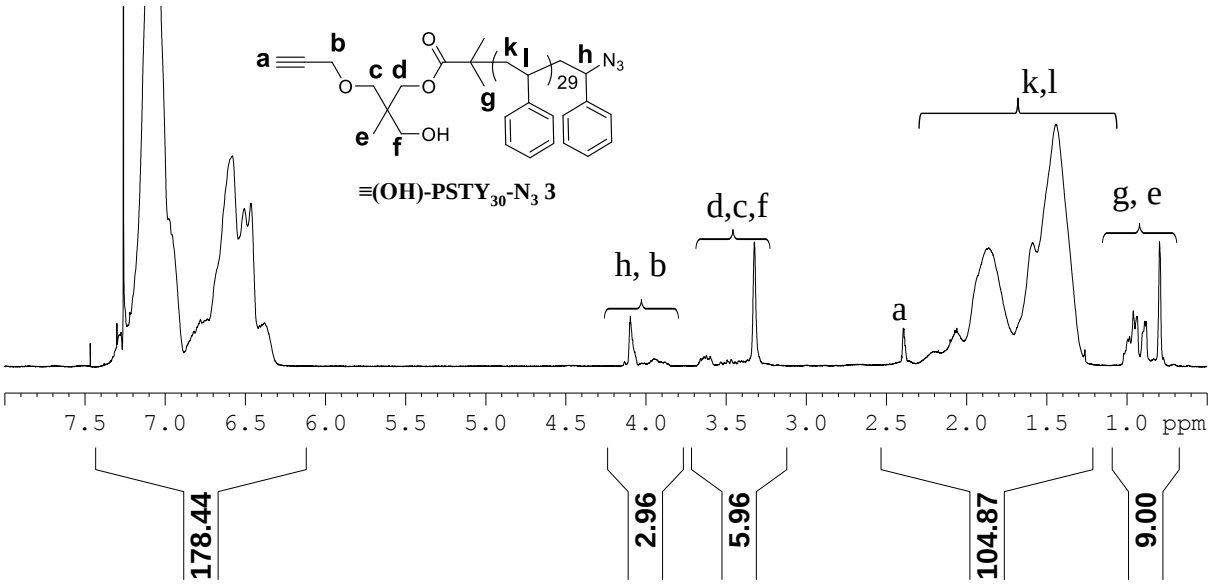

Figure A6.7. 500 MHz ^{1}H NMR spectrum in $CDCl_3$ of ≡(OH)-PSTY$_{30}$-N$_3$ (**3**).

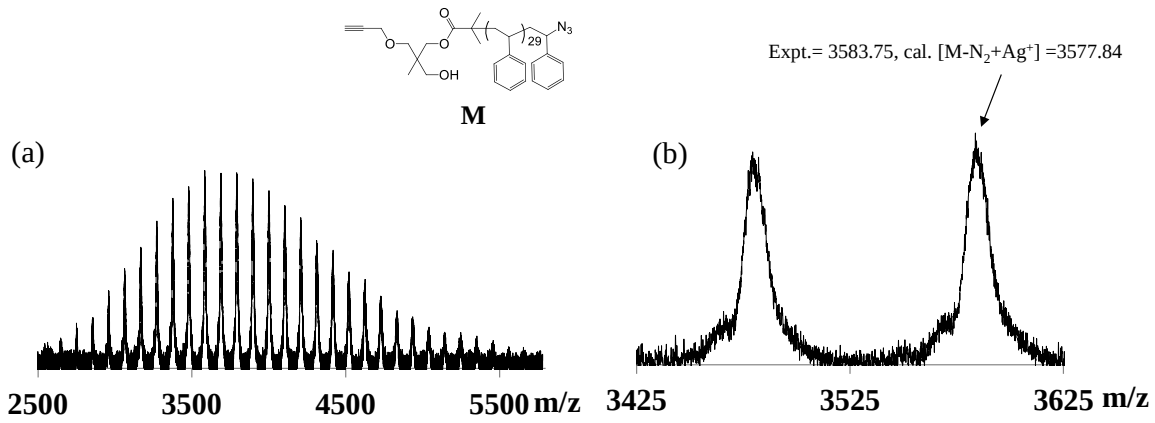

Figure A6.8: MALDI-ToF mass spectrum acquired in reflectron mode with Ag salt as cationizing agent and DCTB matrix. The full (a) and expanded (b) spectra correspond to ≡(HO)-PSTY$_{30}$-N$_3$ (**3**).

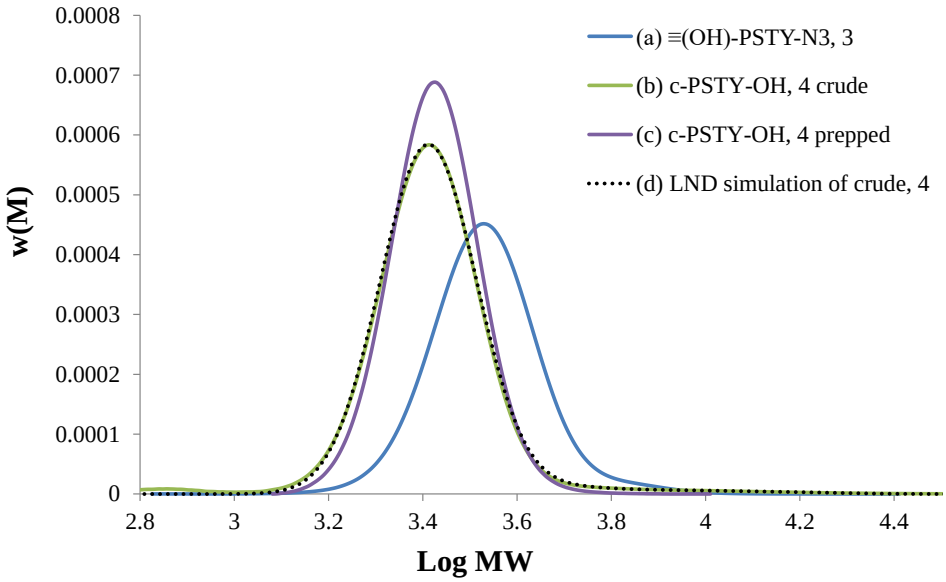

Figure A6.9: SEC traces for cyclization of linear polymer. (a) ≡(OH)-PSTY$_{30}$-N$_3$ (**3**), (b) c-PSTY$_{30}$-OH (**4**) crude, (c) **4** purified by preparative SEC and (d) Log-Normal distribution (LND) simulation of **4** with hydrodynamic volume change of 0.77. SEC analysis based on polystyrene calibration curve.

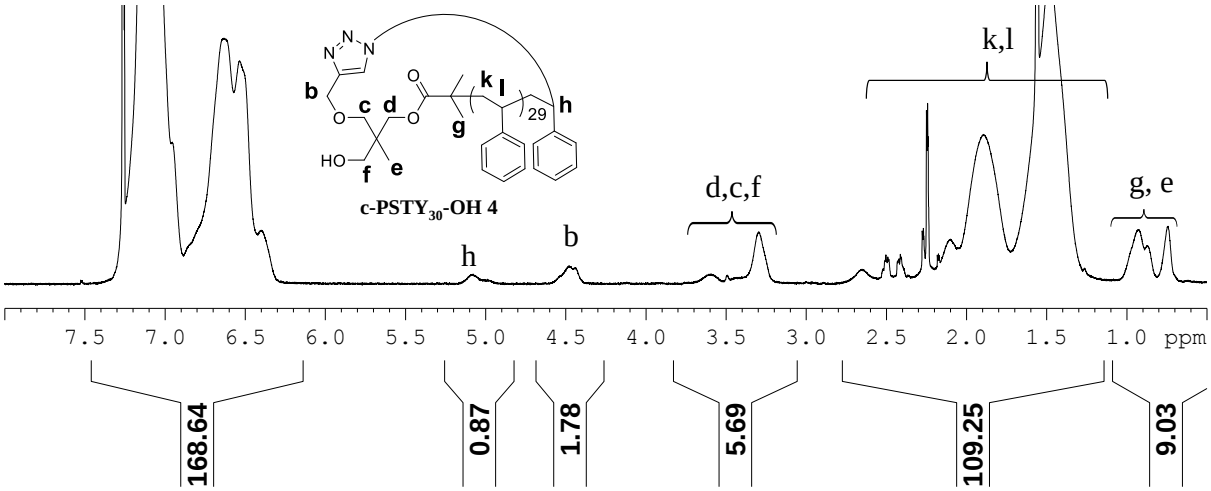

Figure A6.10. 500 MHz ^{1}H NMR spectrum in $CDCl_3$ of c-PSTY$_{30}$-OH (**4**).

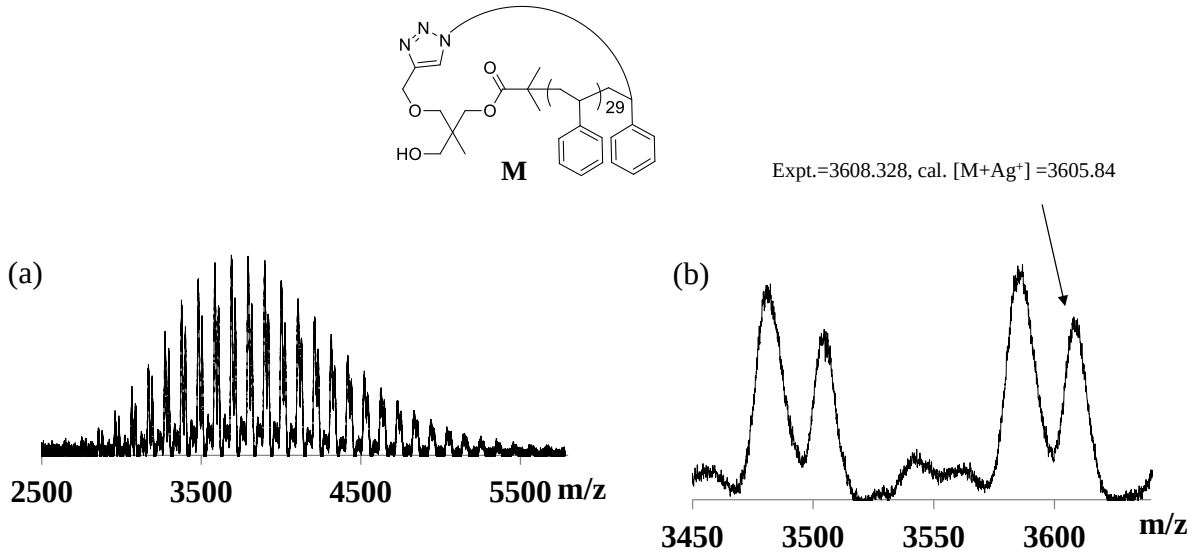

Figure A6.11: MALDI-ToF mass spectrum acquired in reflectron mode with Ag salt as cationizing agent and DCTB matrix. The full (a) and expanded (b) spectra correspond to c-PSTY$_{30}$-OH (**4**).

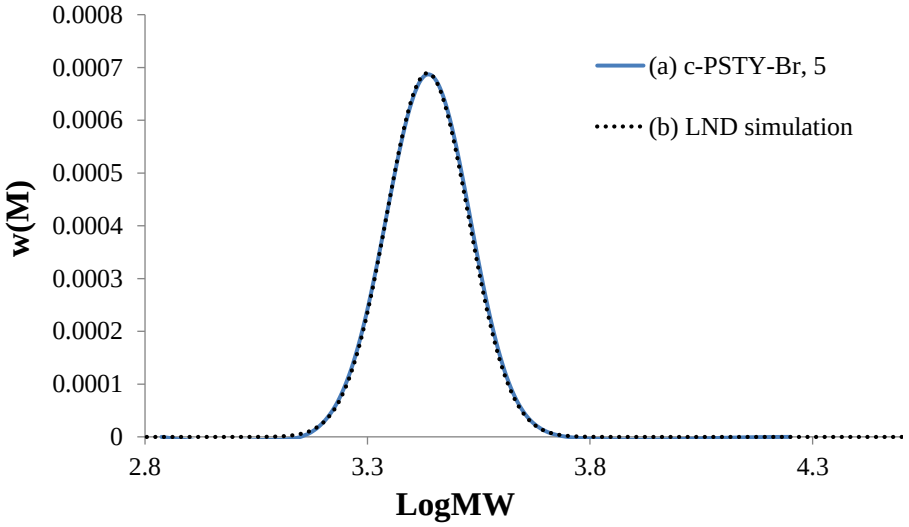

Figure A6.12: SEC chromatogram of (a) c-PSTY$_{30}$-Br (**5**) and (b) LND simulation of **5**. SEC chromatogram is based on PSTY calibration curve.

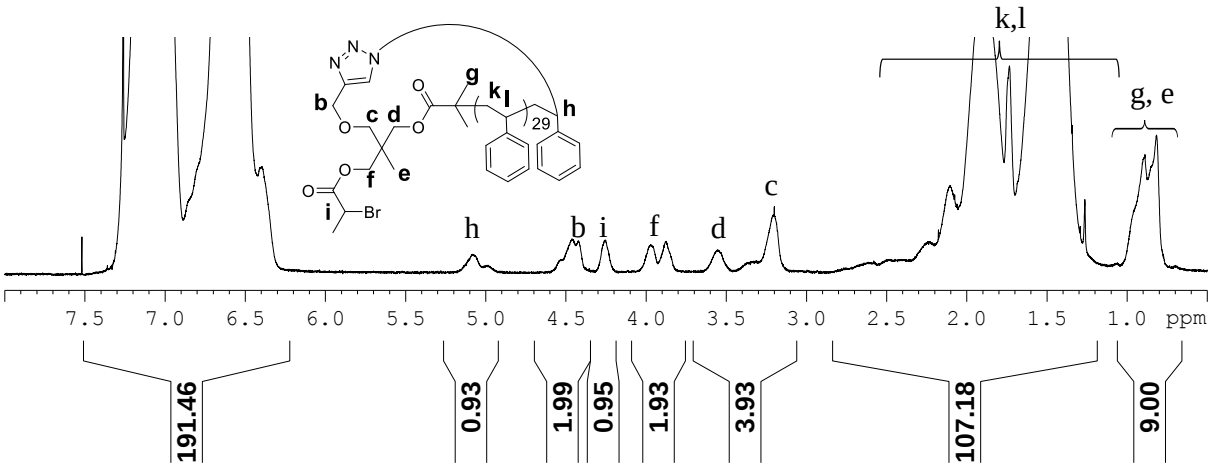

Figure A6.13. 500 MHz ^{1}H NMR spectrum in $CDCl_3$ of c-PSTY$_{30}$-Br (**5**).

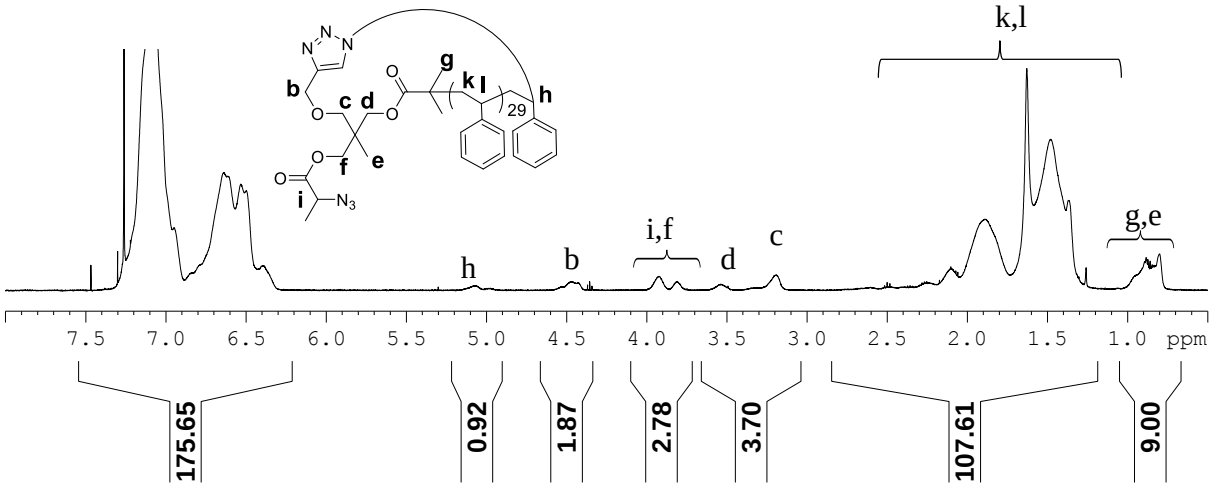

Figure A6.14. 500 MHz ^{1}H NMR spectrum in $CDCl_3$ of c-PSTY$_{30}$-N$_3$ (**6**).

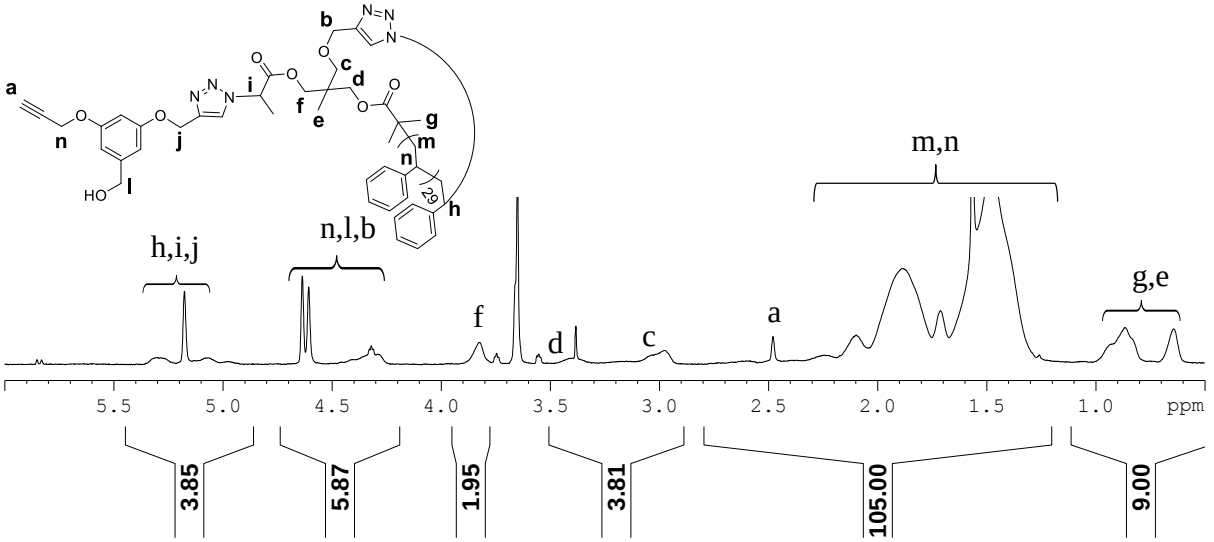

Figure A6.15. 500 MHz ^{1}H 1D DOSY spectrum in $CDCl_3$ of c-PSTY$_{30}$ (≡)OH (**7**).

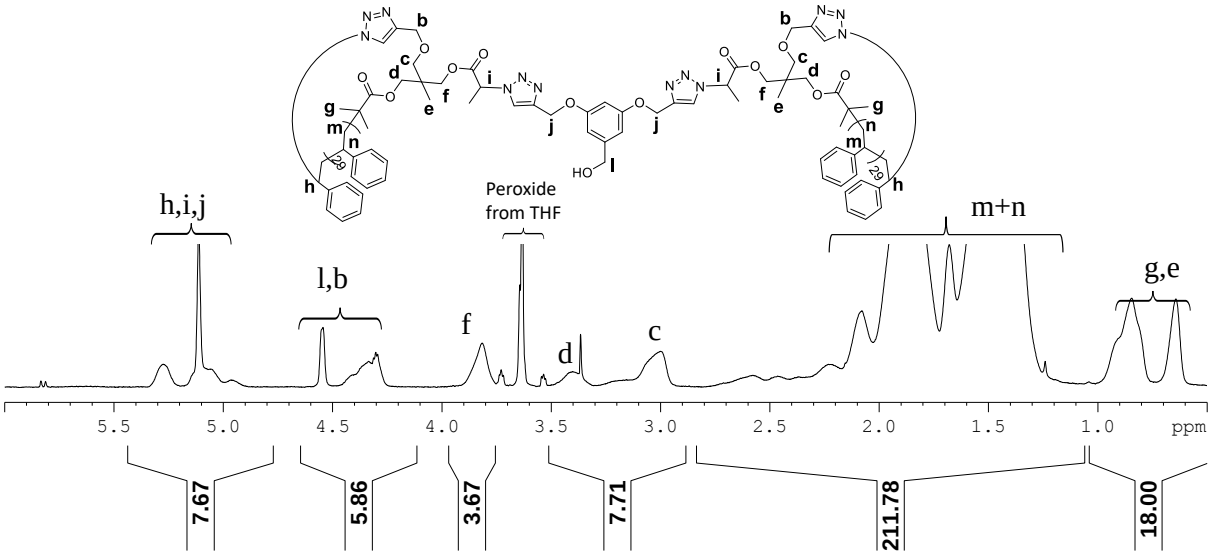

Figure A6.16. 500 MHz ^{1}H 1D DOSY spectrum in $CDCl_3$ of c-PSTY$_2$OH (**8**).

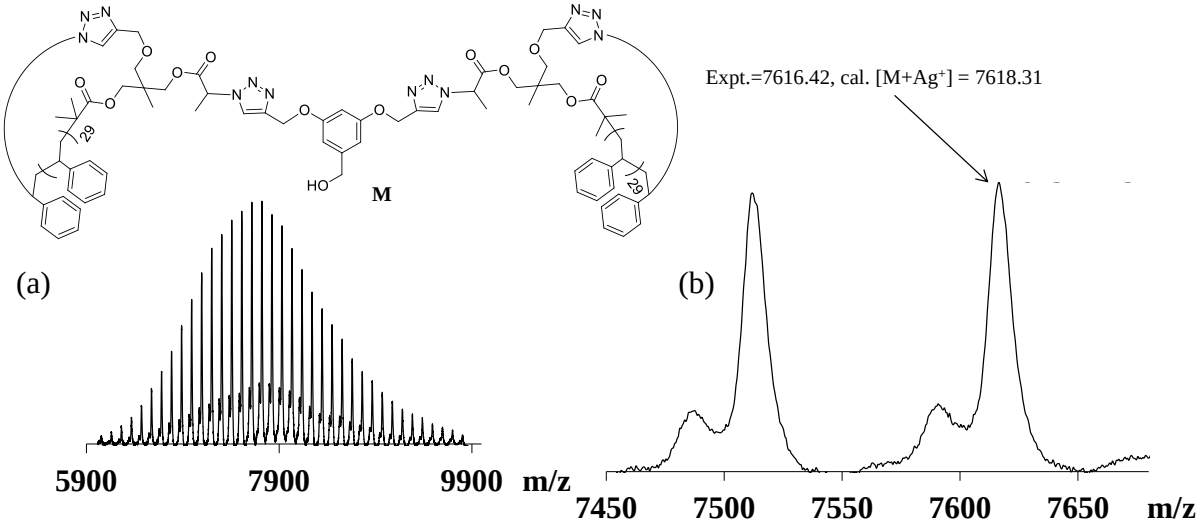

Figure A6.17: MALDI-ToF mass spectrum acquired in linear mode with Ag salt as cationizing agent and DCTB matrix. The full (a) and expanded (b) spectra correspond to c-PSTY$_2$-OH (**8**).

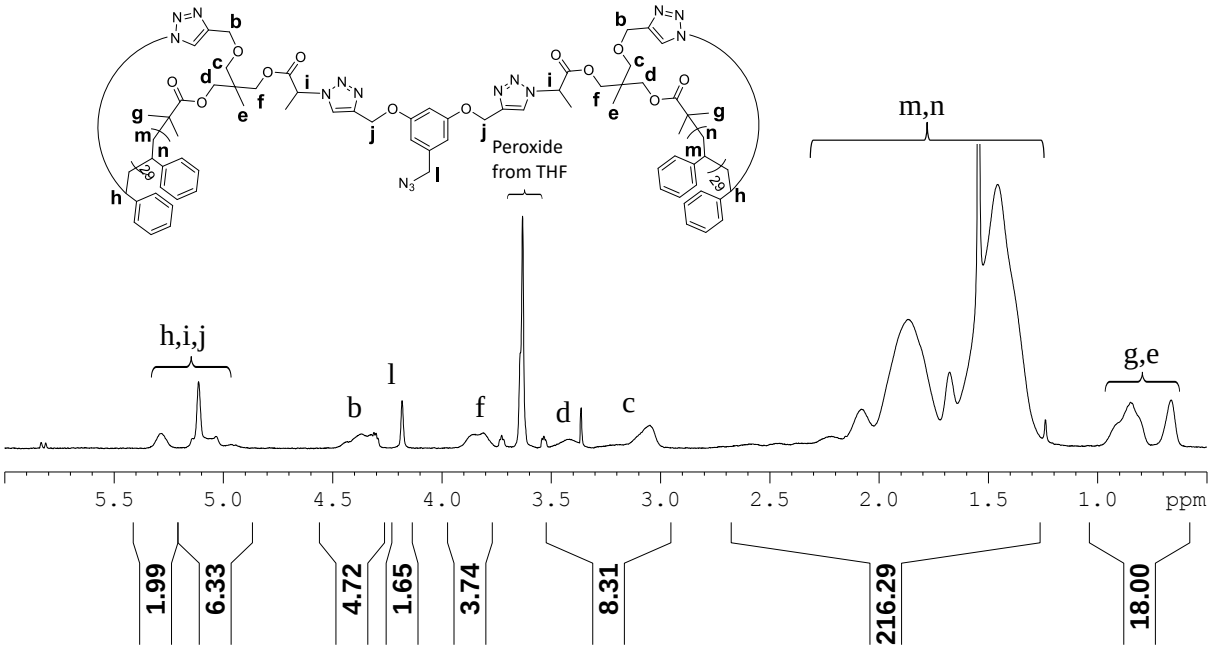

Figure A6.18. 500 MHz ^{1}H 1D DOSY spectrum in $CDCl_3$ of c-PSTY$_2$-N$_3$ (**9**).

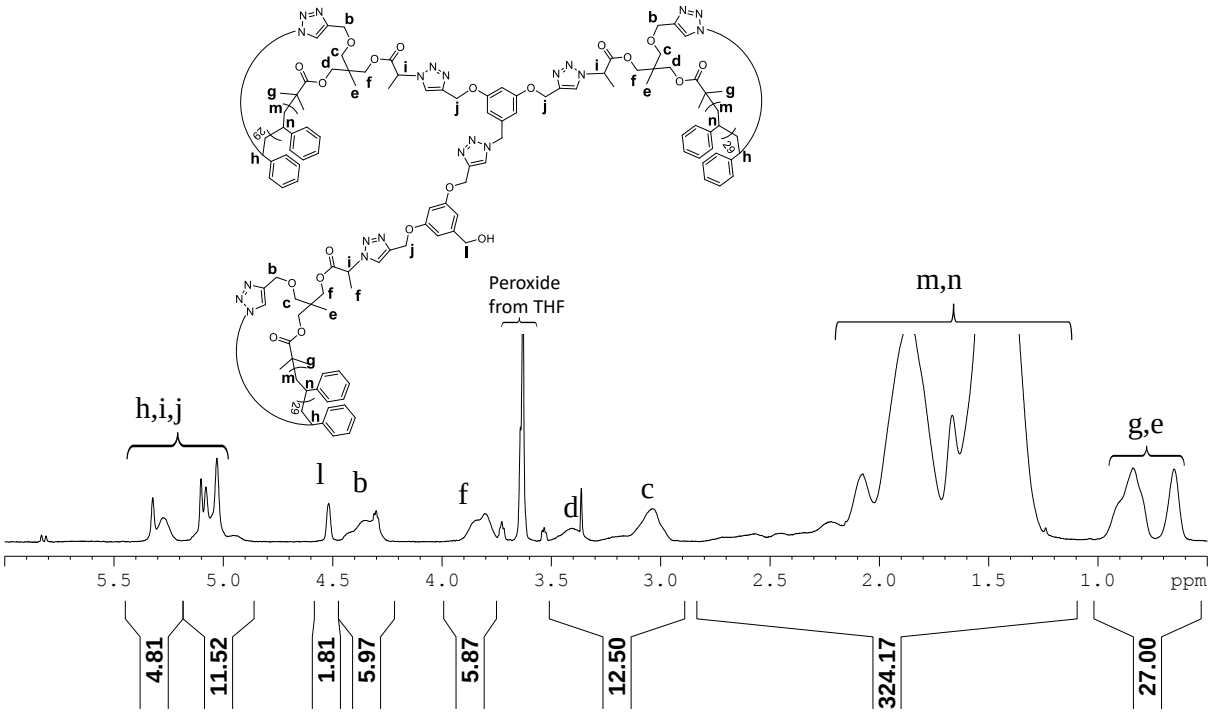

Figure A6.19. 500 MHz ^{1}H 1D DOSY spectrum in $CDCl_3$ of c-PSTY$_3$-OH (**10**).

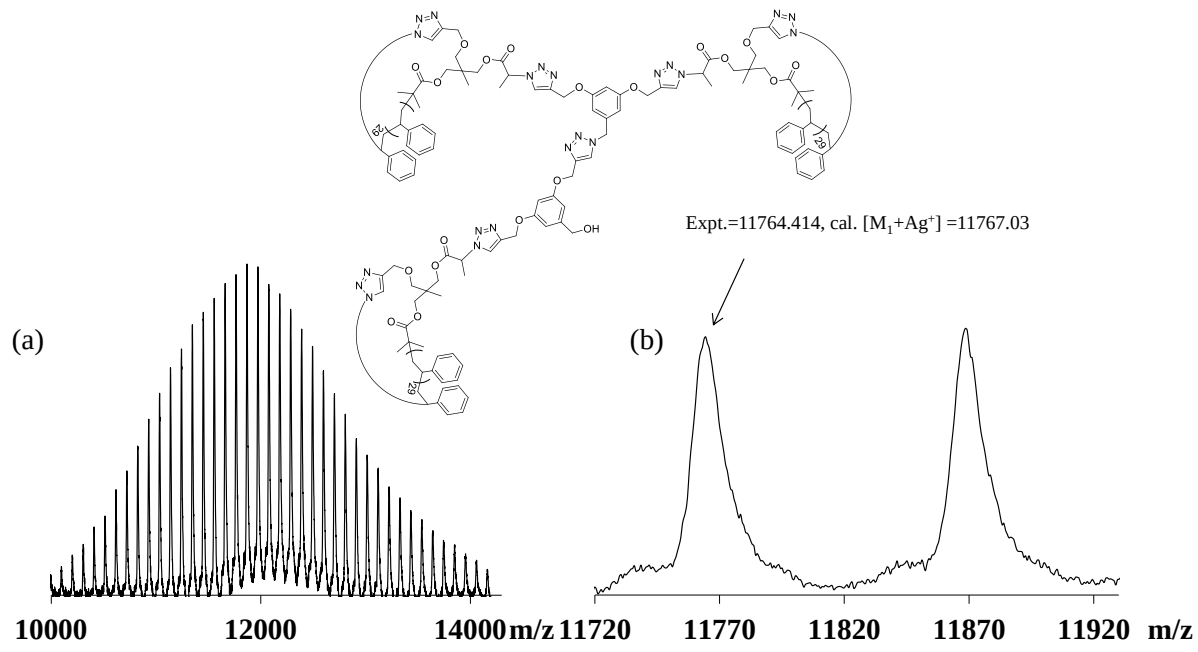

Figure A6.20: MALDI-ToF mass spectrum acquired in linear mode with Ag salt as cationizing agent and DCTB matrix. The full (a) and expanded (b) spectra correspond to c-PSTY$_3$-OH (**10**).

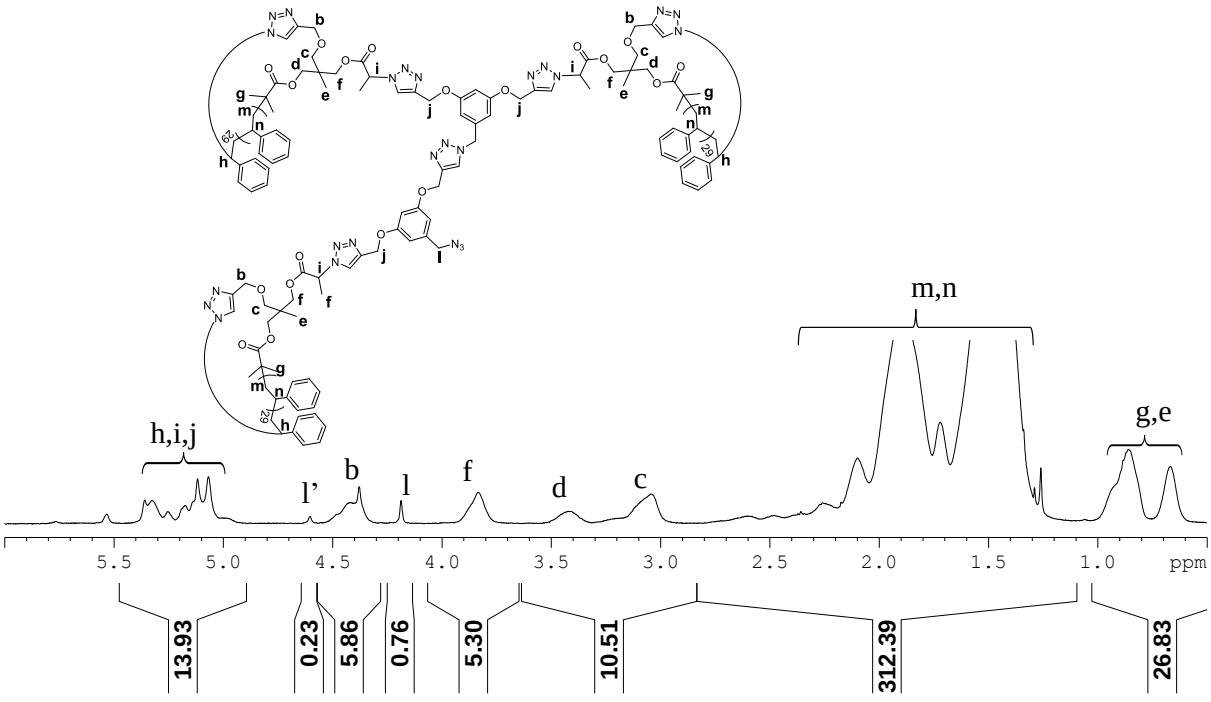

Figure A6.21. 500 MHz ^{1}H 1D DOSY spectrum in $CDCl_3$ of c-PSTY$_3$-N$_3$ (**11**).

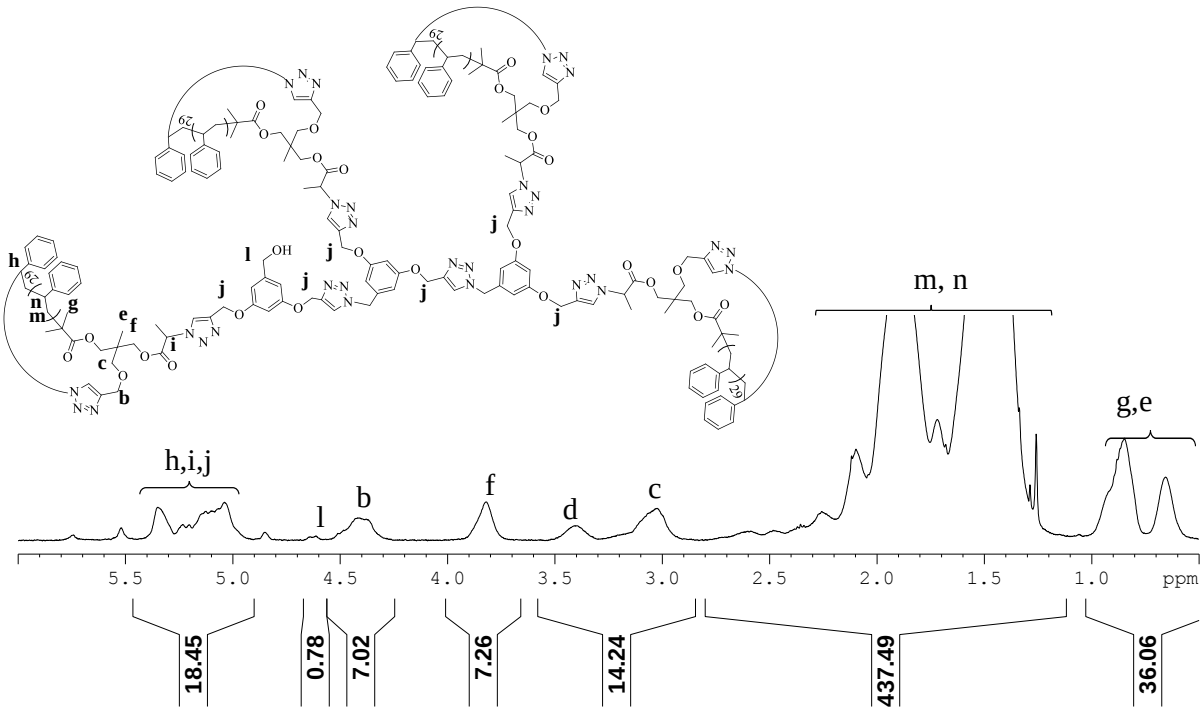

Figure A6.22. 500 MHz ^{1}H 1D DOSY spectrum in $CDCl_3$ of c-PSTY$_4$-OH (**12**).

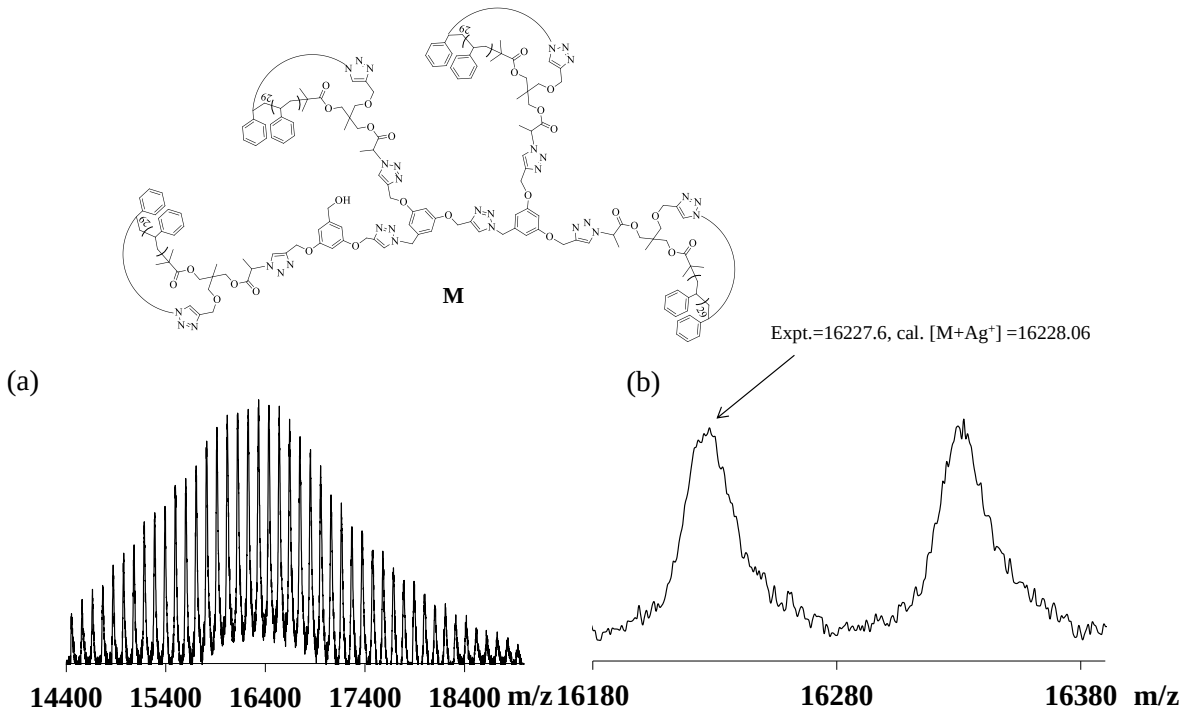

Figure A6.23: MALDI-ToF mass spectrum acquired in linear mode with Ag salt as cationizing agent and DCTB matrix. The full (a) and expanded (b) spectra correspond to c-PSTY$_4$-OH (**12**).

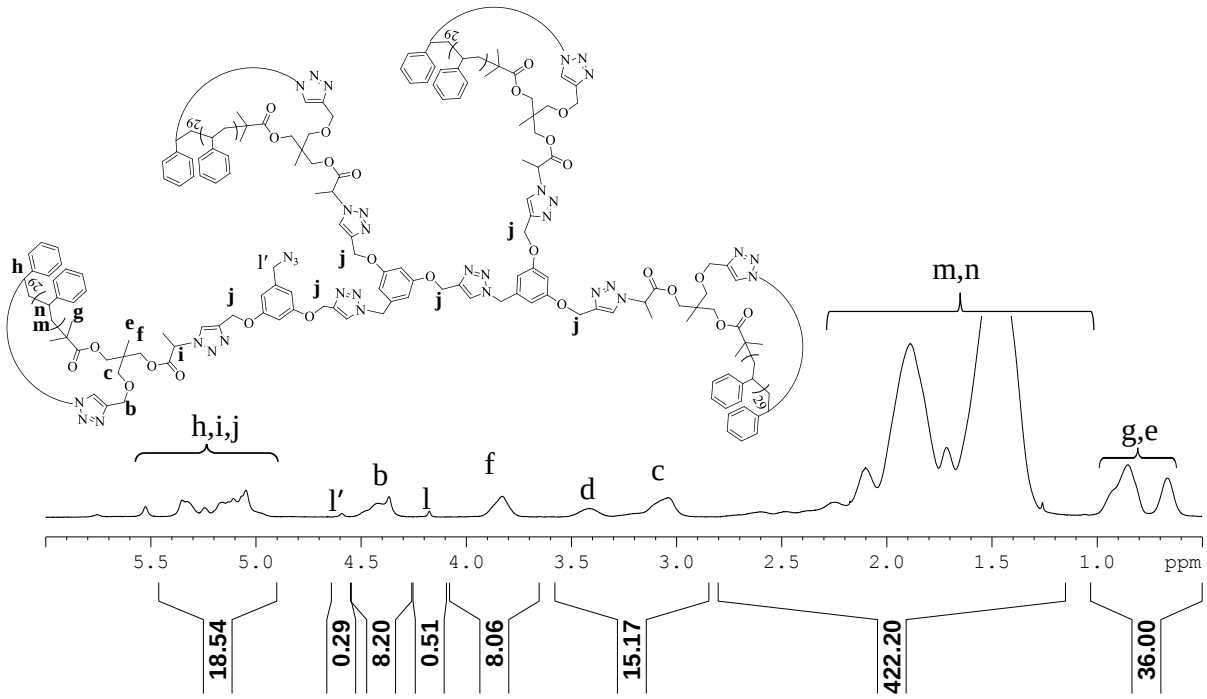

Figure A6.24. 500 MHz ^{1}H 1D DOSY spectrum in $CDCl_3$ of c-PSTY$_4$-OH (**13**).

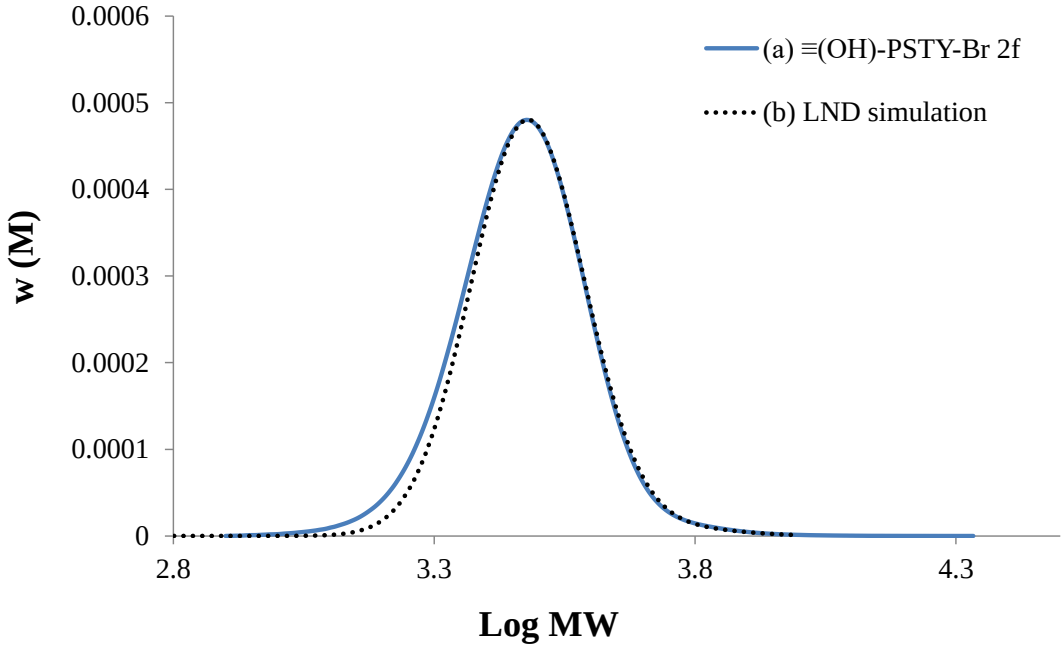

Figure A6.25: SEC chromatograms of (a) ≡(OH)-PSTY$_{27}$-Br (**2f**) and (b) LND simulation of **2f**. SEC chromatogram is based on PSTY calibration curve.

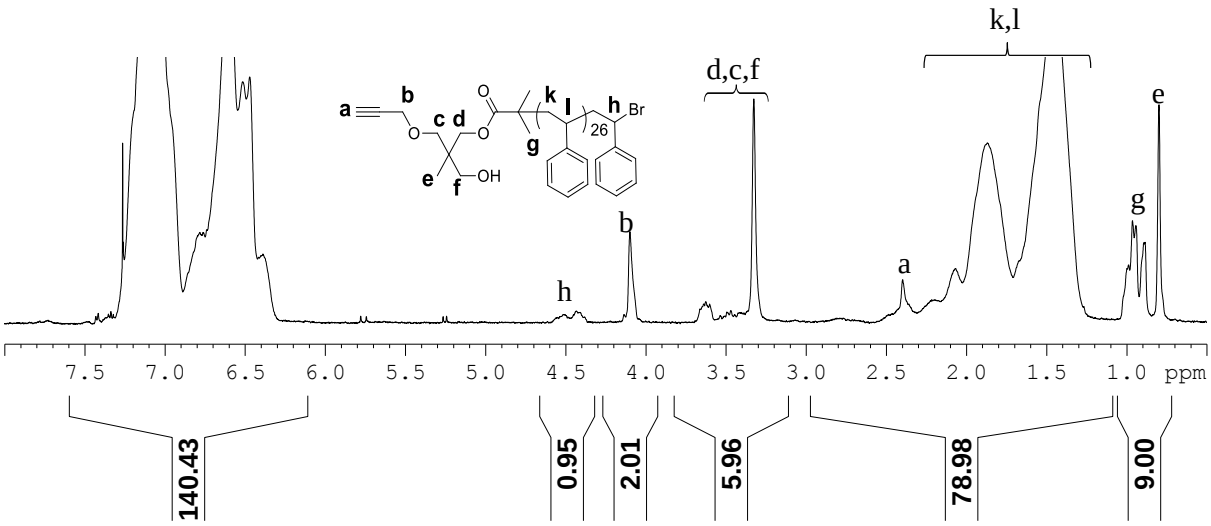

Figure A6.26. 500 MHz ^{1}H NMR spectrum in $CDCl_3$ of ≡(OH)-PSTY$_{27}$-Br (**2f**).

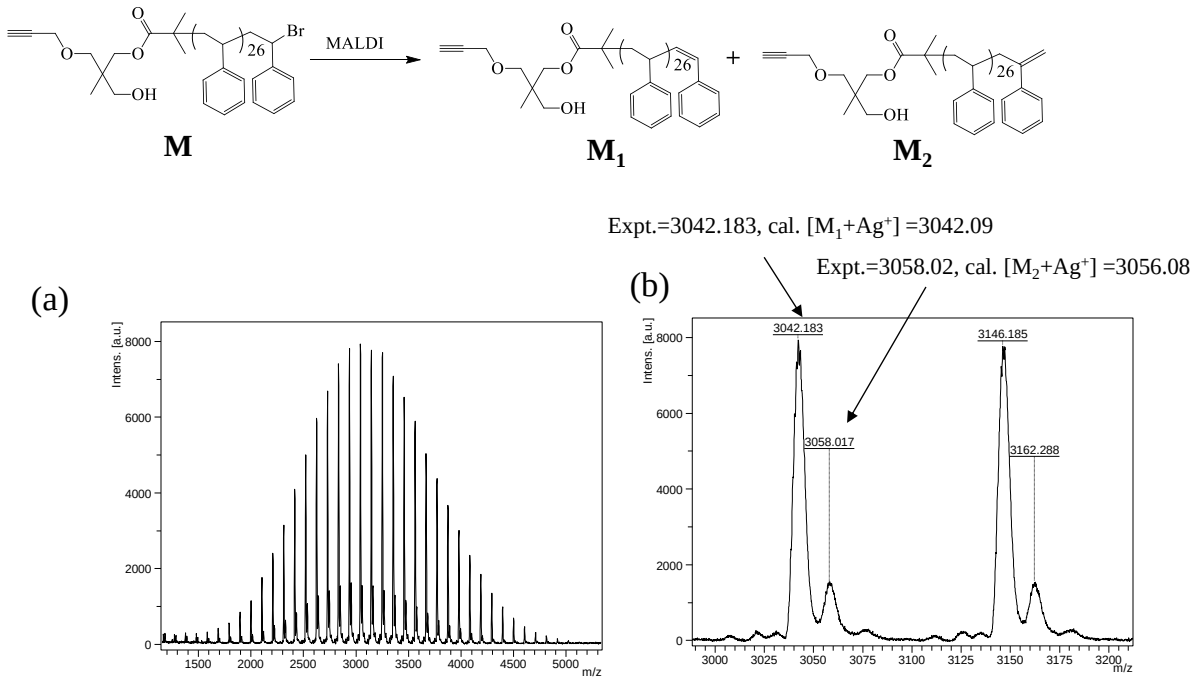

Figure A6.27: MALDI-ToF mass spectrum acquired in reflectron mode with Ag salt as cationizing agent and DCTB matrix. The full (a) and expanded (b) spectra correspond to ≡(HO)-PSTY$_{27}$-Br (**2f**).

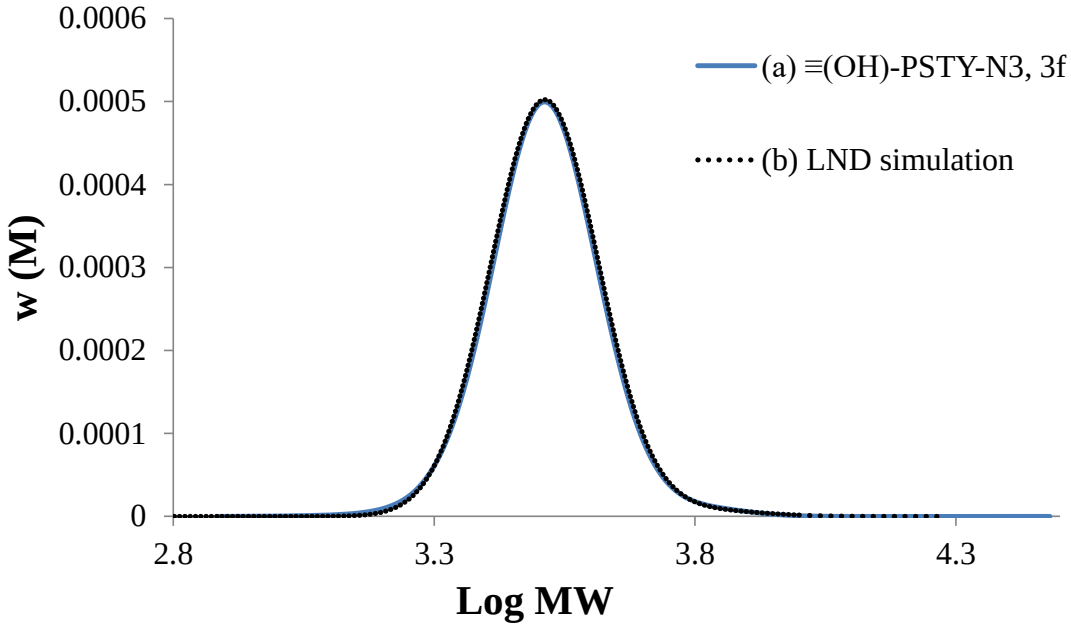

Figure A6.28: SEC chromatograms of (a) ≡(OH)-PSTY$_{27}$-N$_3$ (**3f**) and (b) LND simulation of **3f**. SEC chromatogram is based on PSTY calibration curve.

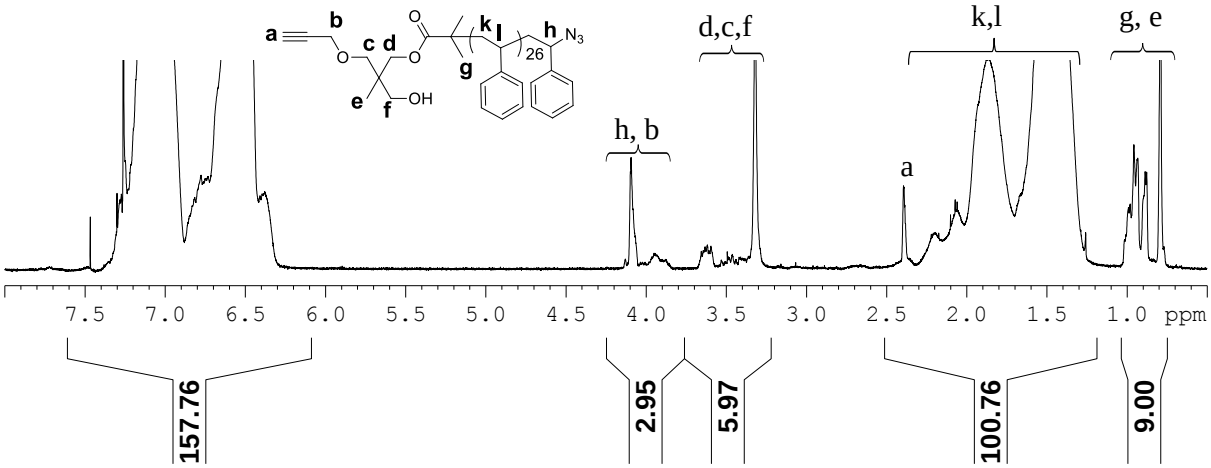

Figure A6.29. 500 MHz ^{1}H NMR spectrum in $CDCl_3$ of ≡(OH)-PSTY$_{27}$-N_3 (**3f**).

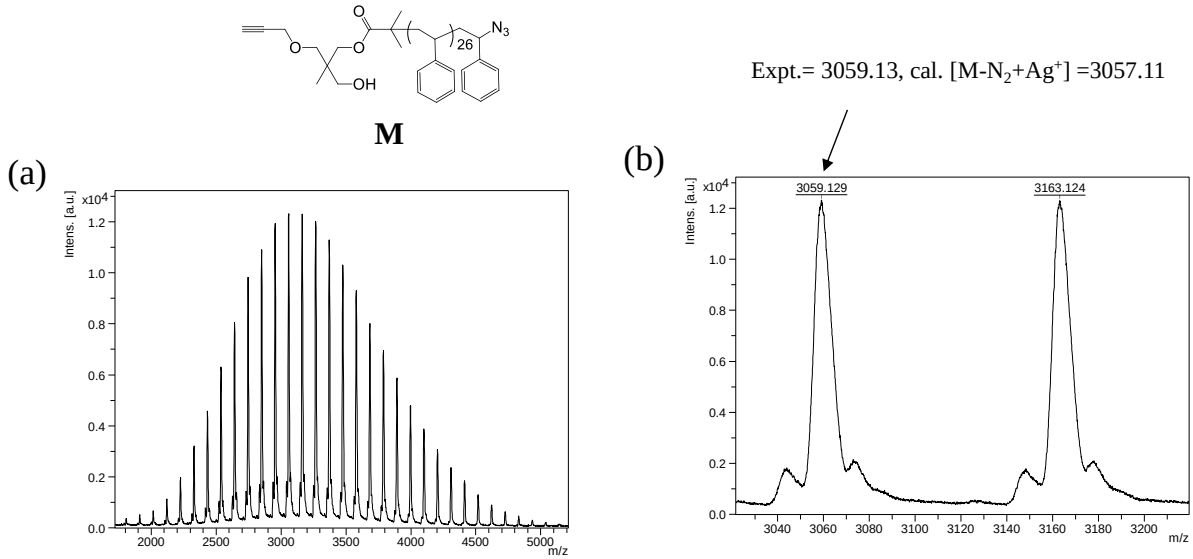

Figure A6.30: MALDI-ToF mass spectrum acquired in reflectron mode with Ag salt as cationizing agent and DCTB matrix. The full (a) and expanded (b) spectra correspond to ≡(HO)-PSTY$_{27}$-N_3 (**3f**).

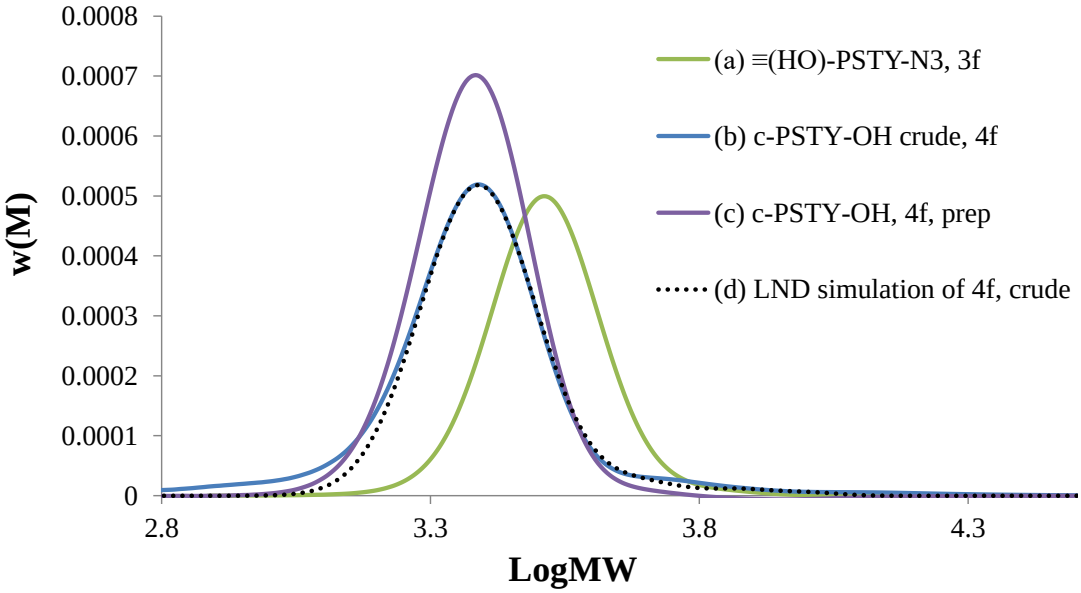

Figure A6.31: SEC traces for cyclization of linear polymer. (a) ≡(OH)-PSTY$_{27}$-N$_3$ (**3f**), (b) c-PSTY$_{27}$-OH (**4f**) crude, (c) **4f** purified by preparative SEC and (d) Log-Normal distribution (LND) simulation of **4f** with hydrodynamic volume change of 0.755. SEC analysis based on polystyrene calibration curve.

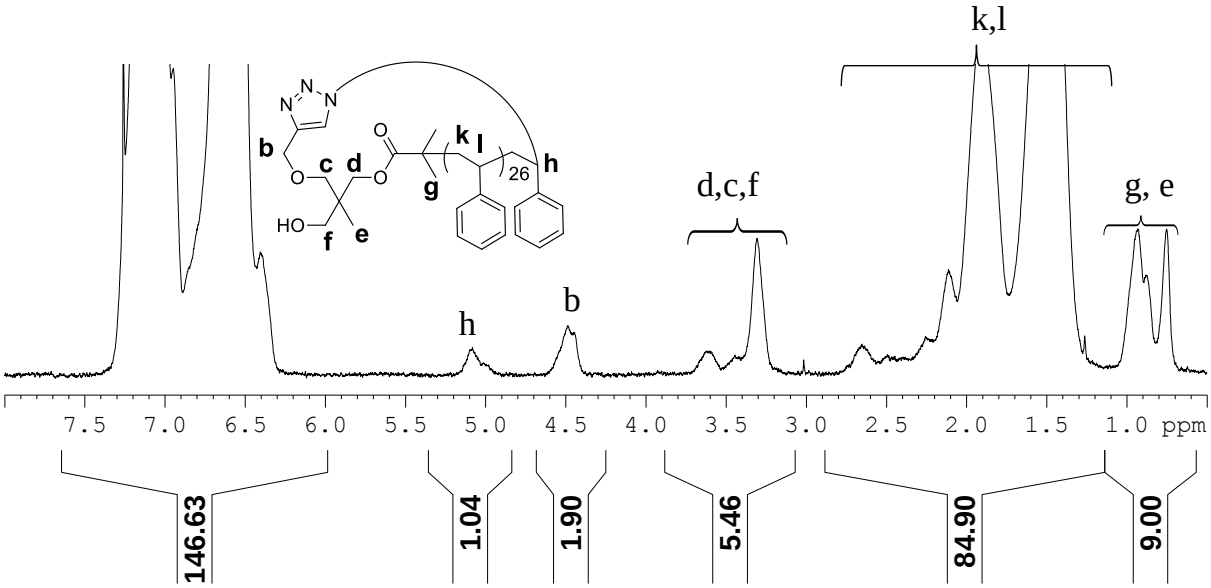

Figure A6.32. 500 MHz ^{1}H NMR spectrum in $CDCl_3$ of c-PSTY$_{27}$-OH (**4f**).

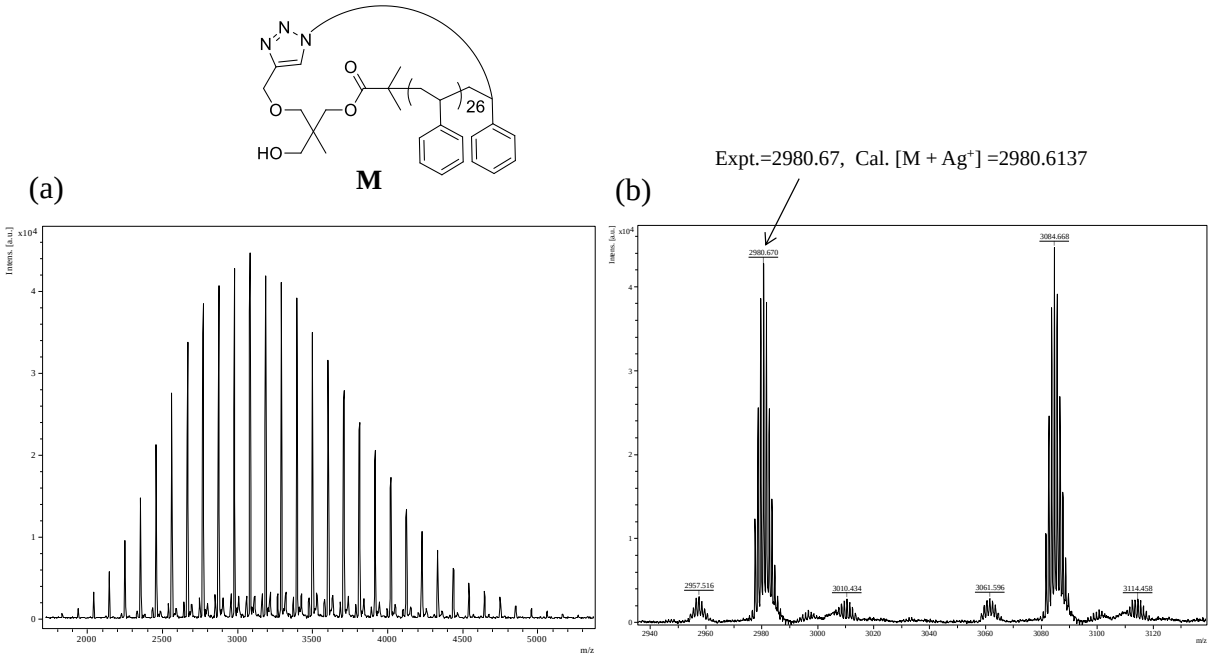

Figure A6.33: MALDI-ToF mass spectrum acquired in reflectron mode with Ag salt as cationizing agent and DCTB matrix. The full (a) and expanded (b) spectra correspond to c-PSTY$_{27}$-OH (**4f**).

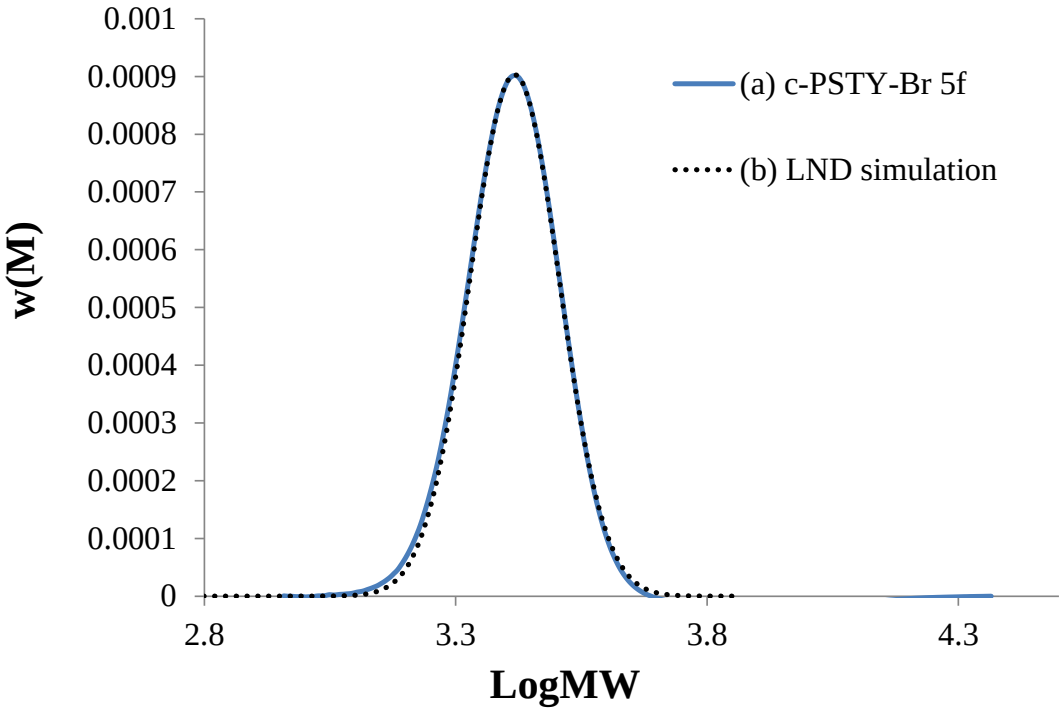

Figure A6.34: SEC chromatograms of (a) c-PSTY$_{27}$-Br, (**5f)** and (b) LND simulation of **5f**. SEC chromatogram is based on PSTY calibration curve.

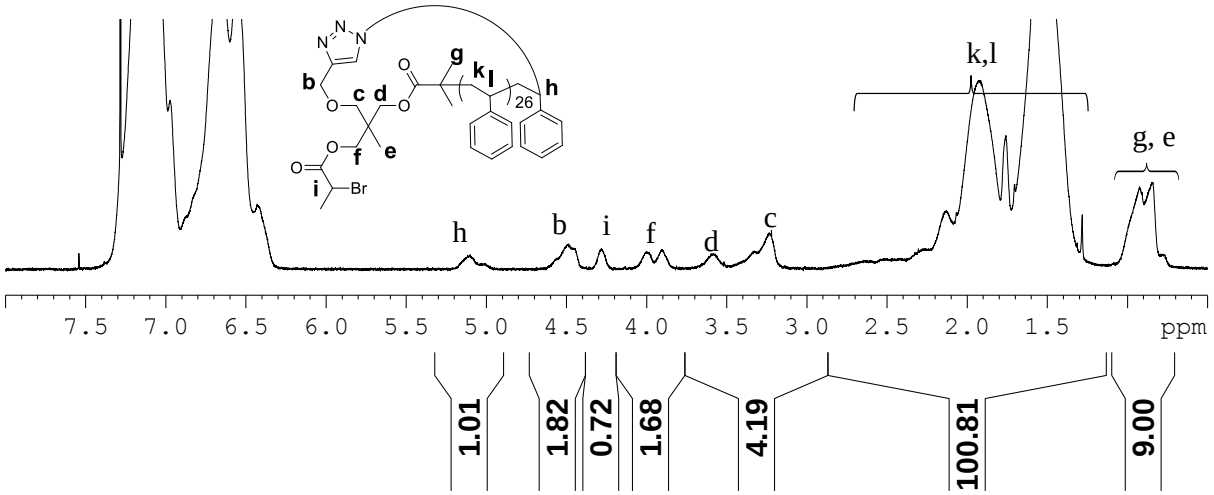

Figure A6.35. 400 MHz ^{1}H NMR spectrum in $CDCl_3$ of c-$PSTY_{27}$-Br (**5f**).

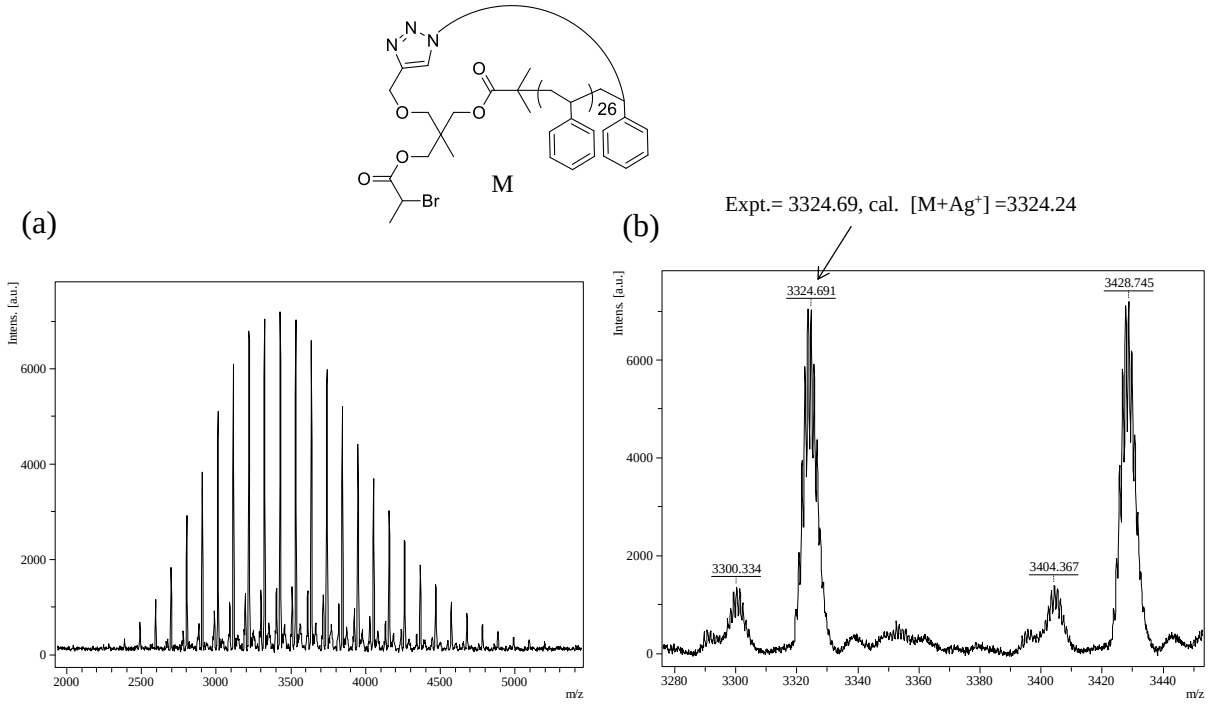

Figure A6.36: MALDI-ToF mass spectrum acquired in reflectron mode with Ag salt as cationizing agent and DCTB matrix. The full (a) and expanded (b) spectra correspond to c-$PSTY_{27}$-Br, (**5f**).

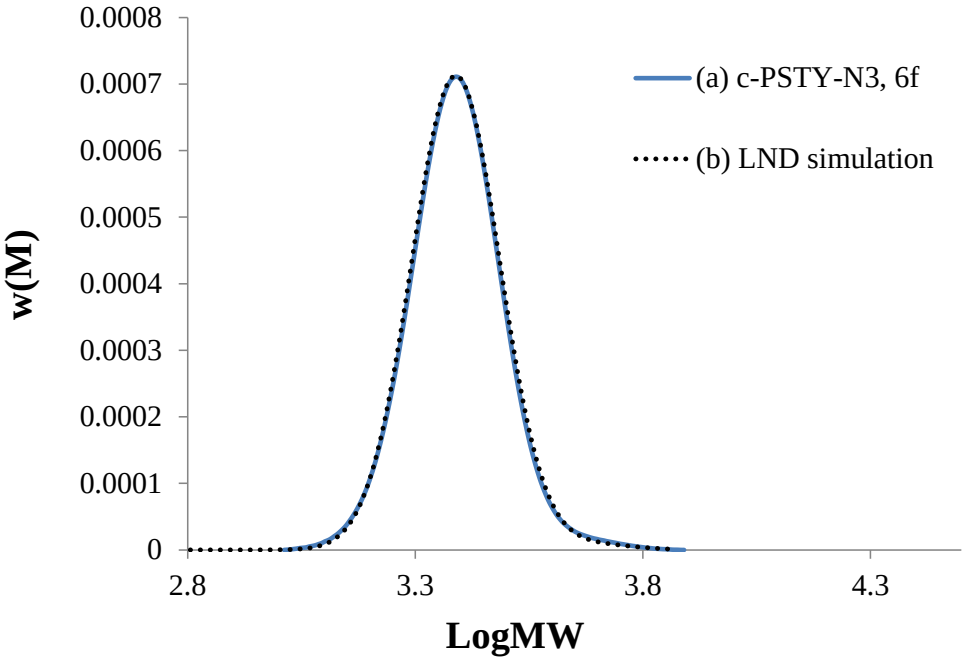

Figure A6.37: SEC chromatograms of (a) c-PSTY$_{27}$-N$_3$ (**6f**) and (b) LND simulation of **6f**. SEC chromatogram is based on PSTY calibration curve.

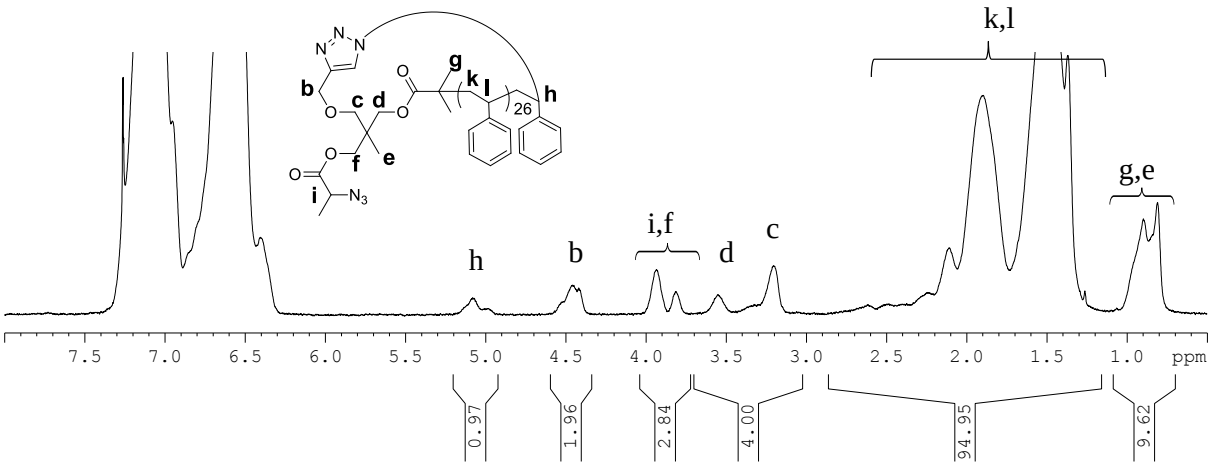

Figure A6.38. 500 MHz ^{1}H NMR spectrum in $CDCl_3$ of c-PSTY$_{27}$-N$_3$, (**6f**).

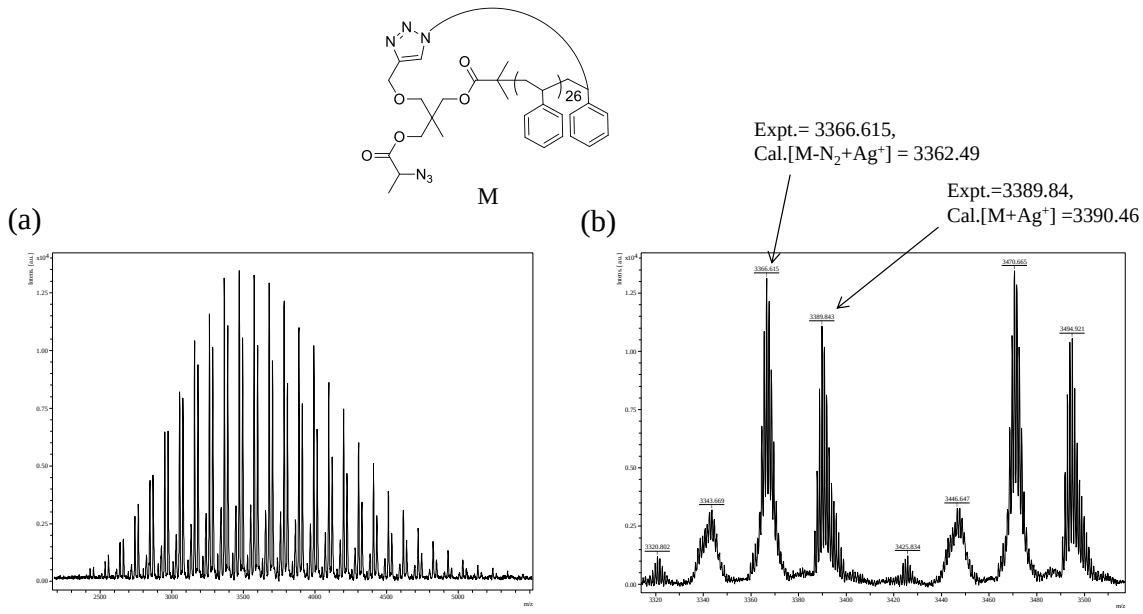

Figure A6.39: MALDI-ToF mass spectrum acquired in reflectron mode with Ag salt as cationizing agent and DCTB matrix. The full (a) and expanded (b) spectra correspond to c-PSTY$_{27}$-N$_3$, (**6f**).

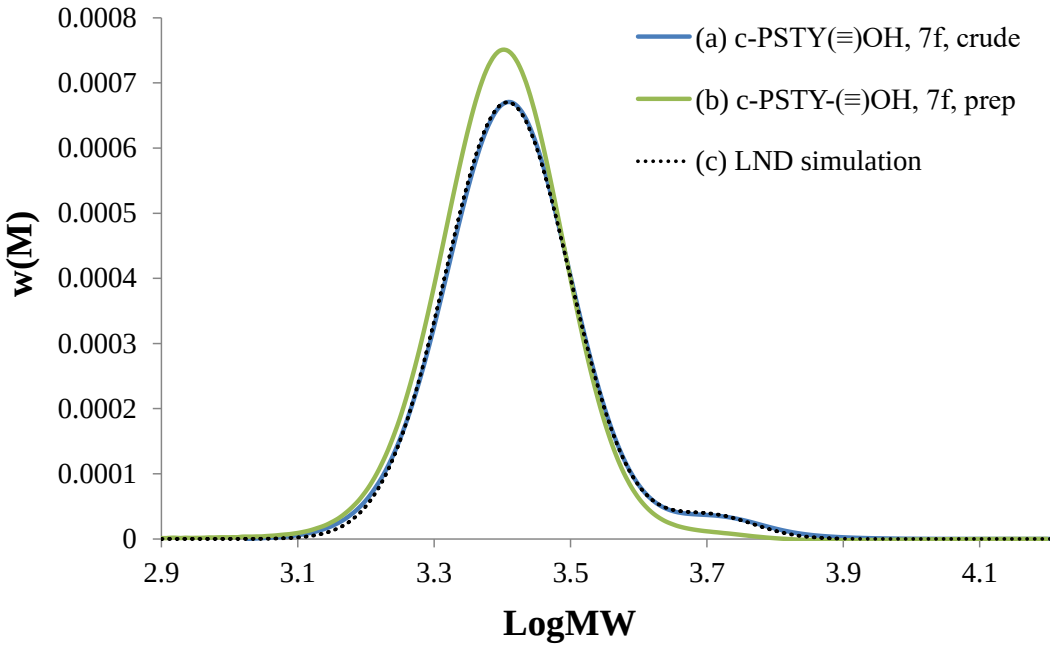

Figure A6.40: SEC chromatograms of (a) c-PSTY$_{27}$(≡)OH (**7f**) crude and (b) **7f** purified by preparative SEC (c) LND simulation of **7f**, crude. SEC chromatogram is based on PSTY calibration curve.

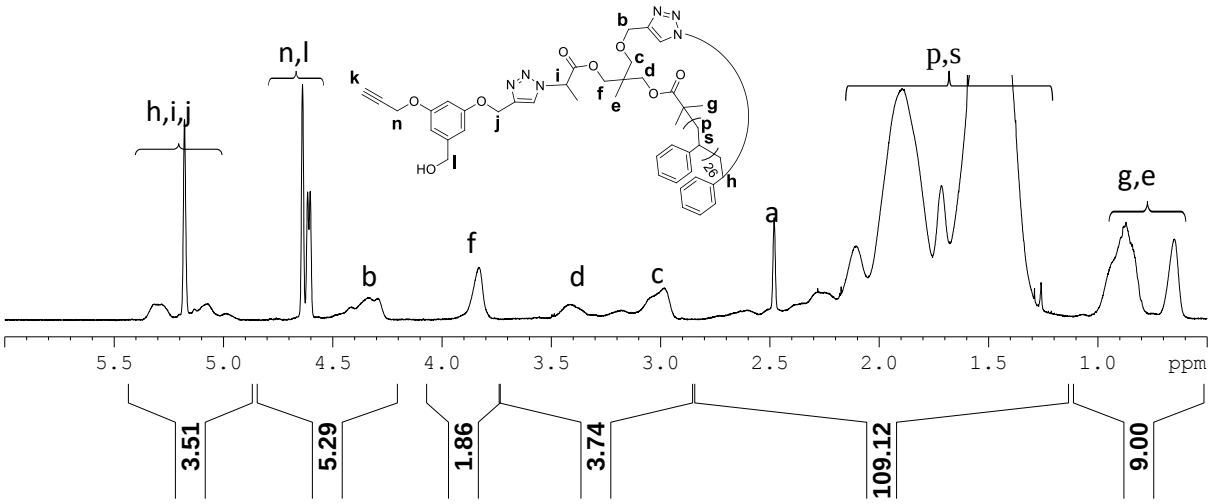

Figure A6.41. 500 MHz ^{1}H NMR spectrum in $CDCl_3$ of c-PSTY$_{27}$(≡)OH (**7f**).

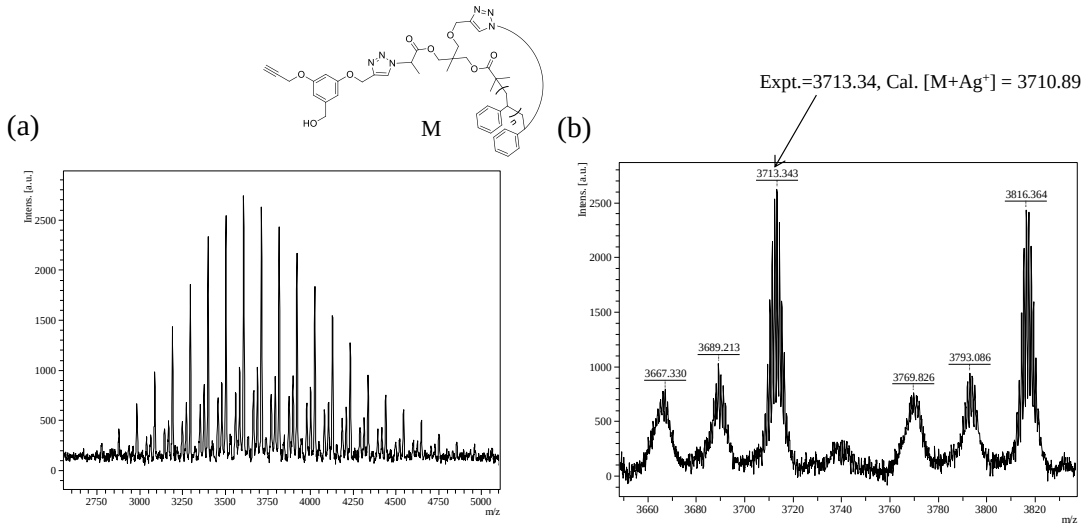

Figure A6.42: MALDI-ToF mass spectrum acquired in reflectron mode with Ag salt as cationizing agent and DCTB matrix. The full (a) and expanded (b) spectra correspond to c-PSTY$_{27}$(≡)OH (**7f**).

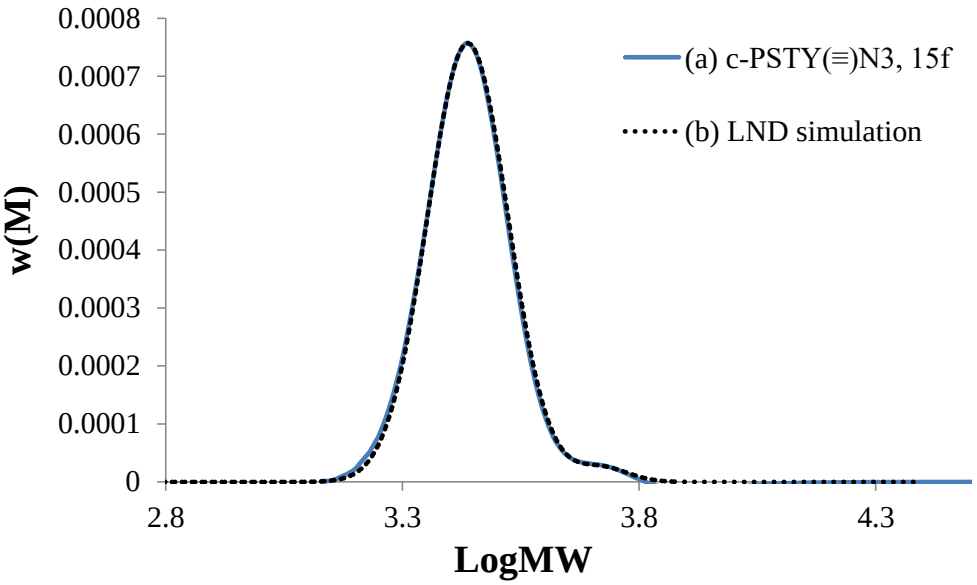

Figure A6.43: SEC chromatograms of (a) c-PSTY$_{27}$(≡)N$_3$ (**15f**) and (b) LND simulation of **15f**. SEC chromatogram is based on PSTY calibration curve.

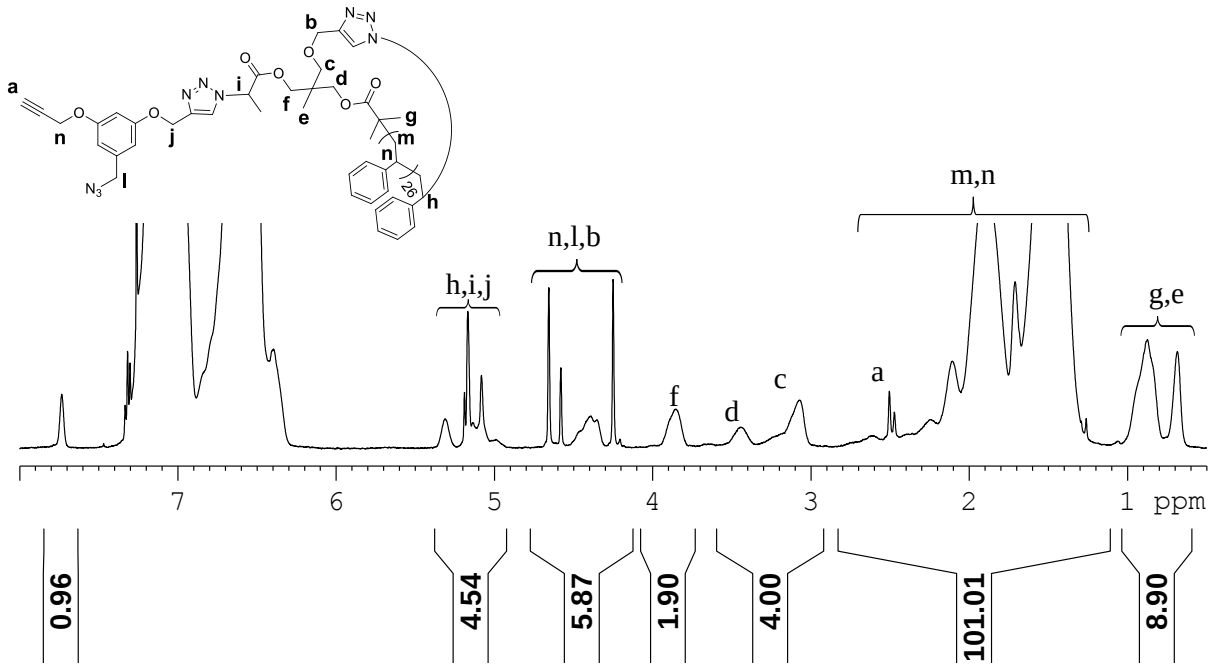

Figure A6.44. 500 MHz ^{1}H NMR spectrum in CDCl$_3$ of c-PSTY$_{27}$(≡)N$_3$ (**15f**).

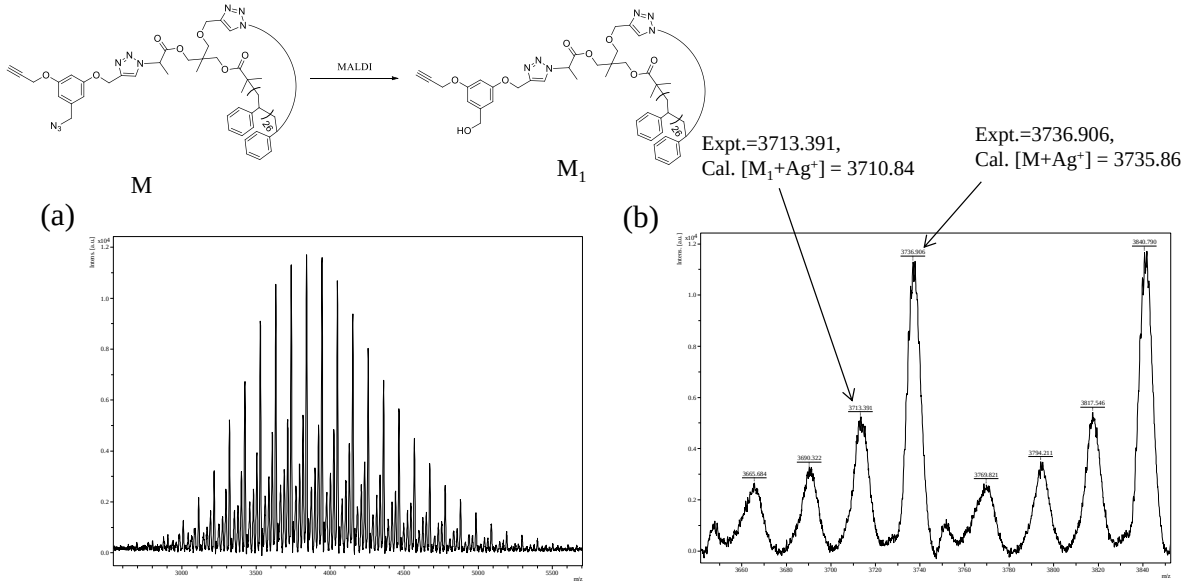

Figure A6.45: MALDI-ToF mass spectrum acquired in reflectron mode with Ag salt as cationizing agent and DCTB matrix. The full (a) and expanded (b) spectra correspond to c-PSTY$_{27}$(≡)N$_3$ (**15f**).